

**Faculty of Science and Engineering**  
**Department of Exploration Geophysics**

**Geophysics in the Search for Diamonds in the Kimberley  
Region of Western Australia**

**Paul Graeme Wilkes**

**This thesis is presented for the Degree of**

**Doctor of Philosophy**

**of**

**Curtin University**

**February 2013**

## **Declaration**

To the best of my knowledge and belief this thesis contains no material previously published by any other person except where due acknowledgment has been made.

This thesis contains no material which has been accepted for the award of any other degree or diploma in any university.

Signature: *P. G. Wilkes*

Date: 1 September 2016

## **ACKNOWLEDGEMENTS**

The author is grateful to Striker Resources N.L. (now North Australian Diamonds Ltd) for collaboration and funding of the geophysical fieldwork done in the North Kimberley region of WA in the period 1997 to 2000.

Particular thanks go to Dr Robert Ramsay – former Technical Director of Striker Resources - with whom the field project was conceived and whose wisdom and enthusiasm contributed so much to the project. Thanks also to company geologists Luke Kerr and Justin Robins who also contributed greatly to the project.

My thanks also go to the four Curtin University honours geophysics students who worked with me in the earlier phases of this project: Jon Sumner, Russell McChesney, Dave Carter and Geoff Garton.

I thank Dr Jayson Meyers and A/Prof Brett Harris, of Exploration Geophysics Department, Curtin University for their input into this project.

Thanks to my wife Margaret for her patience and support whilst I have been away for long periods working on this project and thesis.

## Contents

ACKNOWLEDGEMENTS .....	3
ABSTRACT.....	21
1 INTRODUCTION .....	24
2 EXPLORATION MODELS AND AREA SELECTION .....	26
3 GEOLOGY AND PHYSICAL PROPERTIES OF KIMBERLITES AND LAMPROITES, GEOPHYSICAL MODELS .....	32
3.1    Geology of kimberlites .....	32
3.2    Geology of lamproites .....	34
3.3    Physical properties.....	34
3.3.1    Density.....	34
3.3.2    Magnetic susceptibility.....	35
3.4    Geophysical models.....	35
4 PREVIOUS RESEARCH.....	46
4.1    Review of worldwide use of geophysics in the exploration for diamonds.....	46
4.2    Brief history of diamond exploration in the Kimberley region.. .....	48
5 REGIONAL DATASETS AND DIAMOND OCCURRENCE IN THE KIMBERLEY REGION – GEOLOGY, SEISMIC, AEROMAGNETIC DATA, GRAVITY, DIGITAL ELEVATION DATA.....	51
5.1    Regional geology.....	51
5.2    SKIPPY seismic tomography studies.....	58
5.3    Digital elevation data.....	59
5.4    Regional aeromagnetic data .....	63
5.5    Regional gravity data.....	70

5.6	Regional airborne radiometric data .....	74
5.7	Structures at cratonic scale .....	77
5.7.1	Reconstructions of Rodinia. ....	78
5.7.2	Mohorovicic discontinuity geometry .....	82
5.7.3	Isostatic Residual Gravity.....	87
5.7.4	Euler deconvolution.....	88
5.7.5	Multiscale edge detection applied to Isostatic Residual Gravity .....	90
5.7.6	Total horizontal gradient computation on upward continued reduced to pole aeromagnetic data .....	101
5.7.7	Multiscale edge detection using aeromagnetic data.....	103
5.7.8	Texture analysis and trend detection from aeromagnetic data .....	109
5.7.9	Discussion of regional datasets for cratonic studies.....	112
6	EXPLORATION AT ASHMORE .....	115
6.1	Geology .....	115
6.2	Previous exploration.....	115
6.3	Ground elevation data at Ashmore .....	118
6.4	Low level aeromagnetic survey at Ashmore .....	118
6.5	Heliborne DIGHEM frequency domain electromagnetic surveys .....	121
6.6	Ground gravity at Ashmore .....	125
6.7	Ground magnetic survey at Ashmore .....	127
6.8	Ground electromagnetic survey at Ashmore .....	130
6.9	Discussion on integrated datasets.....	132
7	EXPLORATION OVER SEPPELT PROSPECTS.....	133
7.1	Geology .....	133

7.2	Previous exploration.....	134
7.3	Digital elevation data for Seppelt prospects.....	137
7.4	Helicopter electromagnetic survey of Seppelt areas .....	141
7.5	Aeromagnetic surveys .....	144
7.6	Ground magnetic surveys at Seppelt 1 and Seppelt 2 .....	144
7.7	Ground gravity at Seppelt 1, 2, 4, 5, and 6.....	149
7.8	Ground electromagnetic surveys at Seppelt 1 and 2 .....	156
7.9	Discussion on integrated datasets for Seppelt areas.....	160
8	EXPLORATION AT PTEROPUS.....	162
8.1	Geology .....	162
8.2	Previous exploration.....	164
8.3	Elevation data .....	165
8.4	Airborne gravity gradiometry using the Falcon system .....	165
8.5	Discussion on integrated datasets at Pteropus .....	173
9	EXPLORATION AT ARIES .....	174
9.1	Geology.....	174
9.2	Previous exploration.....	175
9.3	Elevation data.....	176
9.4	Aeromagnetic data.....	177
9.5	Gravity data .....	180
9.6	Discussion on integrated datasets at Aries .....	180
10	EXPLORATION AT ELLENDALE.....	181
10.1	Geology .....	181
10.2	Previous exploration and mining.....	183
10.3	Elevation data .....	185
10.4	Aeromagnetic data.....	186

10.5	Gravity data .....	189
10.6	Discussion on integrated datasets at Ellendale.....	192
11	DISCUSSION.....	193
12	CONCLUSIONS AND RECOMMENDATIONS.....	200
13	REFERENCES .....	206
	APPENDIX: PAPER SUBMITTED TO GEOPHYSICAL RESEARCH LETTERS.....	216

## List of Figures

Figure 2-1: Summary diagram of tectonic and structural controls on the formation of primary diamond deposits Reproduced from Helmstaedt and Gurney (1995). .....	27
Figure 2-2: Simplified model of a diamondiferous lithospheric or mantle root. Reproduced from Haggerty (1986). .....	28
Figure 2-3: Worldwide ages of kimberlite, lamproite and carbonatite emplacement. Reproduced from Pidgeon et al (1989). This figure shows how the ages of the West Kimberley, North Kimberley and Argyle intrusions correlate with other diamond-bearing intrusions around the world. ....	31
Figure 3-1: Idealised kimberlite magmatic system reproduced from Jaques (1998) and modified from Mitchell (1986). This shows the different facies which may be recognised in the study areas. ....	33
Figure 3-2: Computed gravity response for a tapering vertical cylindrical pipe model and weathered cap. This shows that the gravity anomaly due to the weathered cap can dominate in the combined effect of cap plus pipe. ....	37
Figure 3-3: Computed plan view of magnetic response for a tapering vertical cylindrical pipe model. For induced magnetisation only, we see characteristic magnetic high over northern end of pipe and low to the south of the pipe. Susceptibility contrast for the pipe with respect to host rocks is 0.01 SI units. ....	40
Figure 3-4: Computed north-south profile of magnetic response for a tapering vertical cylindrical pipe. For the modelling parameters used here, the maximum anomaly is 8 nT and the minimum -3 nT.....	41
Figure 3-5: Computed variation of magnetic anomaly response for a range of pipe radii. Depth to unweathered top of pipe is 100 metres.....	42
Figure 3-6: Computed variation of magnetic amplitude with flying height over a pipe of radius 50 metres and depth of 100 metres to top of unweathered pipe. Anomaly amplitude reduces markedly with increasing flying height. ....	43
Figure 3-7: Kimberlite models used in Raiche (2000) model study of the effect of conductivity variations on airborne electromagnetic measurements.....	45

Figure 4-1: Kimberley Craton and diamond occurrences. This is reproduced from the northwest corner of an Australia-wide map by Jaques (2006b).....	50
Figure 5-1: Map showing locations of Australian cratons. Reproduced from Betts and Giles (2006).....	52
Figure 5-2: Time-space plot of Proterozoic events related to the North Australian Craton reproduced from Johnson (2013).....	53
Figure 5-3: Schematic section of the Kimberley Basin geology. Modified from Griffin and Grey, (1990) .....	54
Figure 5-4: Structural controls on Diamond occurrence in the Kimberley region reproduced from Jaques et al. (1986).....	55
Figure 5-5: Location of kimberlites and lamproites in the East Kimberley province reproduced from Jaques et al., (1986) page 35. ....	56
Figure 5-6: Location of kimberlites in the North Kimberley Province, showing locations of diamondiferous and non-diamondiferous kimberlite intrusions. Reproduced from Jaques (2002). ....	57
Figure 5-7: Location of lamproites in the West Kimberley province. Reproduced from Jaques et al. (1986) page 74.....	58
Figure 5-8: Image showing locations of study pipes with regional digital elevation data for the Kimberley region using SRTM data. Sun illumination from NW with 45 degree elevation.....	60
Figure 5-9: Digital elevation image for the Kimberley region using Shuttle Radar (SRTM) data with histogram equalisation colour stretch. Locations of study pipes are also shown on this image. ....	61
Figure 5-10: Digital elevation image using Shuttle Radar (SRTM) data for the NE Kimberley region including the Ashmore, Seppelt and Pteropus prospects. Histogram equalisation colour stretch.....	62
Figure 5-11: Total magnetic intensity (TMI) image for the Kimberley region using GSWA gridded data and NW sun illumination and elevation of 45 degrees.....	64
Figure 5-12 Aeromagnetic RTP image for the Kimberley region using GSWA gridded data and NW sun illumination with 45 degree elevation.....	65

Figure 5-13: Aeromagnetic RTP image for the Kimberley region using GSWA gridded data and NE sun illumination with 45 degree elevation. ....	66
Figure 5-14: Regional aeromagnetic and gravity interpretation by Gunn and Meixner (1998) with locations added for Argyle, Aries, Ashmore, Ellendale, Pteropus and Seppelt. ....	68
Figure 5-15: Total magnetic intensity (TMI) image with regional aeromagnetic and gravity interpretation for the Kimberley region. The white polygons show the major units interpreted from this study. This is an extension of the interpretation of Gunn and Meixner (1998). Sun illumination from NW with 45 degree elevation. ....	69
Figure 5-16: RTP aeromagnetic image with regional aeromagnetic and gravity interpretation for the Kimberley region. The white polygons show the major units interpreted from this study. This is an extension of the interpretation of Gunn and Meixner (1998). Sun illumination from NW with 45 degree elevation. ....	70
Figure 5-17: Bouguer Anomaly image for Kimberley region using GA datasets. Density used is 2.67 g/cc. All of the studied pipes are located close to major gradients in the Bouguer gravity image. Sun illumination from NW with 45 degree elevation. ....	72
Figure 5-18: GA gravity stations map for Kimberley region. This shows a regular 11 x 11 km coverage supplemented by road traverses with approx. 400 m station spacing and 800 m spaced traverses and stations close to Ellendale. ....	73
Figure 5-19: Bouguer gravity image with regional interpretation The white polygons show the major units interpreted from this study. This is an extension of the interpretation of Gunn and Meixner (1998). Sun illumination from NW with 45 degree elevation. ....	74
Figure 5-20: Kimberley region ternary radiometric image RGB for K, U, Th on total count. 100 metre gridded data from NT Geological Survey. Locations of the study kimberlites and lamproites are shown with black symbols. The radiometric image is useful for assisting surface geological mapping. ....	76

Figure 5-21: Kimberley region. RGB radiometric image with regional aeromagnetic and gravity interpretation. The white polygons show the major units interpreted from this study. This is an extension of the interpretation of Gunn and Meixner (1998). ..... 77

Figure 5-22: Reconstructions of Rodinia from 1100 Ma to 1000 Ma, after Li et al (2008) ..... 80

Figure 5-23: Reconstructions of Rodinia from 900 Ma to 750 Ma, after Li et al (2008) ..... 81

Figure 5-24: Alternative reconstructions of Rodinia, Blewett (2012) ..... 82

Figure 5-25: Depth to Moho for the Kimberley Block and surrounding region. Computed from data supplied by Aitken (2010). All the study pipes are located close to marked changes in slope of the Moho surface. .... 85

Figure 5-26: Magnitude of slope (in degrees) of Moho surface. All the study pipes are located close to marked changes in slope of the Moho surface. Image has been sun illuminated from the east with 45 degree elevation. .... 86

Figure 5-27: 3D view of Moho surface. Top surface is digital elevation data from Shuttle Radar Topographic Mission (SRTM) data. The six vertical black lines shows the Argyle, Aries, Ashmore, Ellendale 4, Pteropus and Seppelt pipes projected vertically down from known positions at surface. Moho depth scale is in metres relative to sea level. All the study pipes are located close to marked changes in slope of the Moho surface. .... 87

Figure 5-28: Isostatic Residual Gravity image for the Kimberley region. The black diamond symbols show location of the study pipes. Sun illumination from the NW with 45 degree elevation. .... 92

Figure 5-29: Isostatic Residual Gravity with interpretation. The white polygons show the major units interpreted from this study. This is an extension of the interpretation of Gunn and Meixner (1998). Sun illumination from NW with 45 degree elevation. .... 93

Figure 5-30: Vertical gradient of Isostatic Residual Gravity image for the Kimberley Region. The study pipes are located close to significant horizontal changes in the vertical gradient of the Isostatic Residual Gravity. Sun illumination from the north with 45 degree elevation. .... 94

Figure 5-31: Vertical gradient of Isostatic Residual Gravity image with interpretation. The white polygons show the major units interpreted from this study. This is an extension of the interpretation of Gunn and Meixner (1998). Sun illumination from NW with 45 degree elevation. .... 95

Figure 5-32: Analytic Signal of Isostatic Residual Gravity image for Kimberley Region. Sun illumination from north with 45 degree elevation. .... 96

Figure 5-33: Euler solution locations for structural index of 0.05, shown as white triangles, on analytic signal image computed from Isostatic Residual Gravity data. Sun illumination from north with 45 degree elevation. .... 97

Figure 5-34: Euler depths image for structural index of 0.05 computed from Isostatic Residual Gravity. .... 98

Figure 5-35: Worms computed from Isostatic Residual Gravity. The study pipes are all located along structures highlighted by the worming processing. .... 99

Figure 5-36: Worms computed from Isostatic Residual Gravity and shown superimposed on an image of the Isostatic Residual Gravity. .... 100

Figure 5-37: NE Kimberley total horizontal gradient of RTP aeromagnetic data upward continued by 1600 m. Red symbols show locations of kimberlite and lamproite intrusions. Sun illumination from north with 45 degree elevation. .... 102

Figure 5-38: Magnetic worms as 3D voxel (2 x 2 x 2 km) image, view to the NW. View from right hand side of page. .... 104

Figure 5-39: Level plan through magnetic worms at 5 km elevation. .... 105

Figure 5-40: Level plan through magnetic worms at 10 km elevation. .... 106

Figure 5-41: Level plan through magnetic worms at 15 km elevation. .... 107

Figure 5-42: Level plan through magnetic worms at 20 km elevation. .... 108

Figure 5-43: RTP aeromagnetic image of North Kimberley region. Locations of pipes at Ashmore, Seppelt 1 and Pteropus 1 are also shown. Sun illumination from NW with 45 degree elevation. .... 110

Figure 5-44: Lineations computed from RTP aeromagnetic grid for North Kimberley region. Locations of pipes at Ashmore, Seppelt 1 and Pteropus 1 are also shown. Sun illumination from NW with 45 degree elevation. .... 111

Figure 5-45: Zoomed in version of part of Figure 5-43 with post 1990 kimberlite discoveries added and shown by blue diamonds. .... 112

Figure 5-46 Isostatic Residual Gravity worms and 100 mGal contour. This is combined with Moho slope sun illuminated colour image. Sun illumination is from the east with 45 degree elevation. Note that the six study pipes are all located close to the margins of major gravity highs and also close to gravity worm locations. .... 114

Figure 6-1: Ashmore regional geology reproduced from mapping of the Drysdale 1:250,000 scale map sheet by Gellatly and Sofoulis (1969). Czv is Cainozoic volcanic derived soil, Czs are soil and colluvium, PkC (in orange) are Carson Volcanics, Pke is Elgee Siltstone, Pkw is Warton Sandstone and Tp is ferruginous laterite. Locations of various pipes in the vicinity of Ashmore are also included as red symbols. .... 116

Figure 6-2: Cross section through Ashmore 1, reproduced from Ramsay (1997). .... 117

Figure 6-3: Selected diamonds above 0.5 ct from Ashmore (Striker Resources Annual Report Year 1999). .... 118

Figure 6-4: Ashmore ground elevation data acquired by total station surveying for 1997 and 1998 gravity surveys. Pipe outlines and labels are shown in white. The Ashmore pipes are just downslope from a small topographic high. .... 119

Figure 6-5: Total magnetic intensity image of Ashmore area from DIGHEM helicopter electromagnetic and magnetic survey. Ashmore pipes 1 to 4 are shown labelled in black on the image. The pipes 1, 2 and 3 are associated with a positive magnetic anomaly. Ashmore 4 does not appear to have a magnetic signature. .... 120

Figure 6-6: Dighem 56 KHz Apparent resistivity image for Ashmore and surrounding area. Ashmore pipes 1 to 4 are shown labelled in black text on the image as A1 to A4. The pipes are located in relatively more conductive ground than surrounding areas but are not sufficiently distinctive to be detectable from their conductivity signature. 56 KHz is the highest frequency used on this survey and emphasises near surface conductivity. .... 123

Figure 6-7: Dighem 5.5 KHz Apparent resistivity image for Ashmore and surrounding area. Ashmore pipes 1 to 4 are shown labelled in black on the image. .... 124

Figure 6-8: Ashmore Bouguer gravity map for density 2.4 g/cc. All four pipes are well defined by the gravity results which show gravity lows over all these pipes. .... 126

Figure 6-9: Ashmore ground total magnetic intensity map. The Ashmore pipes 1, 2 and 3 are all magnetic but due to surface magnetic sources are not as clearly seen without reduction to pole and upward continuation. The results following those two additional processing steps are shown in Figure 6-10. Sun illumination from NE with 45 degree elevation. .... 128

Figure 6-10: Ashmore ground magnetic data upward continued by 10 m and reduced to pole. Pipe outlines are shown in white. Contours are of Bouguer gravity. Pipes A1, A2 and A3 are well seen in the ground magnetic data of this image. The Ashmore 4 does not appear to be magnetic. Reduction to pole and upward continuation have clarified the magnetic response over Ashmore 1, 2 and 3 pipes. .... 129

Figure 6-11: Ashmore ground conductivity map from Geonics EM34 1600 Hz frequency domain survey. Ashmore pipes 1 to 4 are shown labelled in white. Note that pipes A1, A2, and A3 are well defined by the conductivity results. A4 area is less conductive but more conductive than its surrounding area. 131

Figure 7-1: Surface geology of the Seppelt areas reproduced from GSWA 1:250 000 Drysdale map sheet by Gellatly and Sofoulis (1969). Pkpm is Pentecost Sandstone (middle unit), Pkpl is Pentecost Sandstone (lower unit), Czs is Cainozoic sand, Czl is Cainozoic laterite and Qa is Quaternary alluvium. Black polygons show the locations of ground geophysical survey areas Seppelt 1 and Seppelt 2. .... 134

Figure 7-2: Seppelt location map showing the main prospects, reproduced from announcement by Striker Resources to the ASX on 2002 ..... 136

Figure 7-3: Seppelt area SRTM digital elevation image. Seppelt 1 and 2 appear to be close to NNW striking faults. .... 138

Figure 7-4: Seppelt 1 detailed digital elevation image from gravity survey height data. Seppelt 1 is located close to and down slope from an east west topographic ridge. .... 139

Figure 7-5: Seppelt 2 digital elevation image from gravity survey height data. Seppelt 2 is located in a shallow gradient area between higher ground to the south east and north west. .... 140

Figure 7-6: Seppelt areas digital terrain image from Hummingbird HEM survey. A regional structure trending about 315 degrees is seen in the topography of the Seppelt 1 area. Topographic control is not evident for the other Seppelt prospects. Topographic control is better seen in the SRTM image which is shown as Figure 7-3. Sun illumination from NE with 45 degree elevation. .... 142

Figure 7-7: Seppelt areas 34 kHz apparent resistivity image. Pipe outlines for Seppelt 1 and 2 are shown in black. Seppelt 1, 2, 4 and 6 are located in ground of lower resistivity than surrounding areas. Seppelt 5 is in ground of higher resistivity. .... 143

Figure 7-8: Detailed total magnetic intensity aeromagnetic image over Seppelt 1 using gridded data from Stockdale Prospecting. Seppelt 1 has an associated aeromagnetic anomaly of about 14 nT. .... 145

Figure 7-9: Regional total magnetic intensity aeromagnetic image for Seppelt and Pteropus areas. Seppelt 1 is located in a regional aeromagnetic low which is associated with a circular positive magnetic feature to the north. Seppelt 2 and the Pteropus pipes are not seen in the regional aeromagnetic data. Sun illumination from north with 45 degree elevation. .... 146

Figure 7-10: Seppelt 1 ground magnetic image. Data have been upward continued by 10 m and reduced to pole. Kimberlitic areas are shown outlined in white. Seppelt 1 has associated ground magnetic anomalies as seen in this image. Sun illumination from NE with 45 degree elevation. .... 147

Figure 7-11: Seppelt 2 ground magnetic image. Data upward continued by 10 m and reduced to pole. Seppelt 2 location is shown outlined in white. Seppelt 2 does not appear to be magnetic but is close to magnetic features. Sun illumination from NE with 45 degree elevation. .... 148

Figure 7-12: Seppelt areas 1, 2, 4, 5 and 6. Bouguer gravity image with 0.2 mGal contours. Regional residual separation is required to clearly show the gravity over pipes in this area. The result of this separation is shown as Figure 7-13. .... 150

Figure 7-13: Seppelt areas 3rd order residual Bouguer gravity image. Note the important north east trending structure that links through from Seppelt 2 to Seppelt 1..... 151

Figure 7-14: Seppelt 1 Bouguer gravity for density 2.3 g/cc. Pipe locations are outlined in white. Regional residual separation is required to better define the location of Seppelt 1. The result of this separation is shown as Figure 7-15. .... 152

Figure 7-15: Seppelt 1 3rd order residual Bouguer gravity image for density 2.3 g/cc. Seppelt 1 has a small residual negative gravity anomaly associated with weathering over this pipe. Pipe outlines shown in white..... 153

Figure 7-16: Seppelt 2 Bouguer gravity image for density 2.3 g/cc. Seppelt 2 is not obvious in this image..... 154

Figure 7-17: Seppelt 2 3rd order residual Bouguer gravity for density 2.3 g/cc. Seppelt 2 is located in a small residual gravity low along a major structure trending about 040 degrees. .... 155

Figure 7-18: Seppelt 1 ground conductivity image from Geonics EM 34 survey using vertical coplanar (VCP) coils at 1600 Hz with 40 m line spacing and 20 m station spacing. Pipes outlines are shown in white. Ground conductivity contour interval 1 mS/m. The pipes have clear conductivity responses due to conductive weathering caps. More potential pipes are evident in this image. .... 157

Figure 7-19: Seppelt 1 ground conductivity map from Geonics EM 34 survey using horizontal coplanar (HCP) coils at 1600 Hz with 40 m line spacing and 20 m station spacing. Pipe outlines are shown in white. Ground conductivity contour interval is 1 mS/m. This image contrasts with Figure 7-18. The difference is due to the different orientation of the coils. .... 158

Figure 7-20: Seppelt 2 ground conductivity map from Geonics EM 34 survey using vertical coplanar coils at 1600 Hz, with line spacing of 80 m and station

spacing of 20 m. Pipe outline is shown in white. South western end of pipe is seen in ground of elevated conductivity but there is higher conductivity to the north of the pipe which appears not to be related to Seppelt 2. Ground conductivity contour interval is 0.5 mS/m. .... 159

Figure 8-1: Geology of Pteropus area from GSWA 1:250 000 Drysdale map sheet mapped by Gellatly and Sofoulis (1969). Pke is Elgee Sandstone, Pkw is Warton Sandstone, Pkpm is Pentecost Sandstone (middle unit), Pkpl is Pentecost Sandstone (lower unit), and Qa is Quaternary alluvium. Pteropus 1 and 2 pipes are outlined and labelled in red. .... 163

Figure 8-2: Surface geology and ground gravity contours, with 0.2 mGal intervals at Pteropus 1 breccia pipe. Reproduced from Jaques et al. (1986) page 29. A gravity low of about – 0.6 mGal is seen over the pipe. .... 164

Figure 8-3: Pteropus digital elevation image from Falcon gravity gradiometry survey. This shows the pipes are located in low lying ground close to the base of steep cliffs. Sun illumination from NE with 45 degree elevation. .... 167

Figure 8-4: Pteropus calculated Bouguer gravity ( $G_z$ ) image from Falcon survey. The pipes are located in areas of gravity lows but the lows are more extensive than the known pipes. .... 168

Figure 8-5: Pteropus calculated Bouguer gravity gradient ( $G_{zz}$ ) image from Falcon survey. The pipes are located in areas of gravity gradient lows but the lows are more extensive than the known pipes. .... 169

Figure 8-6: Pteropus aeromagnetic image from Falcon survey. Pteropus 2 is seen to have a small aeromagnetic anomaly associated with the pipe but Pteropus 1 is not seen directly in the aeromagnetic data. The low to the north east of Pteropus 1 is related to the high to the north of Pteropus 1. Sun illumination from NE with 45 degree elevation. .... 170

Figure 8-7: Pteropus calculated first vertical gradient aeromagnetic image from Falcon survey. Pteropus 2 has a small gradient feature at the north western end but Pteropus 1 is not seen in this image. Sun illumination from NE with 45 degree elevation. .... 171

Figure 8-8: Pteropus 34 kHz apparent resistivity from Hummingbird HEM survey with terrain contours overlain. The pipes are located in areas of low resistivity but these are more extensive than the pipes. .... 172

Figure 9-1: Geology of the SW part of the Mount Elizabeth 1:250 000 map sheet showing location of the Aries kimberlite. Pdh is Hart Dolerite. Pkc is Carson Volcanics, Pkl is King Leopold Sandstone. Pkw is Warton Sandstone. Reproduced from GSWA geological mapping of Mount Elizabeth mapsheet. .... 174

Figure 9-2: Aries interpreted geology from aeromagnetic and airborne gravity datasets. After Isles and Moody (2004a)..... 175

Figure 9-3: Shuttle Radar Topographic Mission (SRTM) digital elevation model (DEM) image for Aries area. The Aries pipe is located just north of high ground in the southern part of the image. Sun illumination from NW with 45 degree elevation. .... 176

Figure 9-4: Aries area total magnetic intensity image. The Aries pipe has a small positive magnetic anomaly associated with the pipe. Sun illumination from NW with 45 degree elevation..... 177

Figure 9-5: Aries area reduction to pole (RTP) aeromagnetic image. The Aries pipe has a small positive magnetic anomaly associated with the pipe. Sun illumination from NW with 45 degree elevation. .... 178

Figure 9-6: Aries area vertical gradient of RTP image. Sun illumination from NW with 45 degree elevation..... 179

Figure 9-7: Aries area vertical gravity gradient (Gzz) image from Falcon airborne gravity gradiometry. Contour interval 10 eotvos. Map reproduced from Isles and Moody (2004b). The various pipes are associated with lows on the vertical gradient of the gravity. .... 180

Figure 10-1: Ellendale geology from GSWA cdrom of 1:250 000 geology sheets. Legend is shown in Figure 10-2..... 181

Figure 10-2: Legend for West Kimberley geology map shown in Figure 10.1. After Hassan (2004) ..... 182

Figure 10-3: Geological map of Ellendale 4 with four cross sections. After Jaques et al (1986), page 103 ..... 184

Figure 10-4: Ellendale SRTM DEM image. Black dots indicate locations of lamproite intrusions. Ellendale 4 is indicated with a black cross. Ellendale 4 is aligned with a NW trend in the DEM image. Sun illumination from NE with 45 degree elevation. .... 185

Figure 10-5: Ellendale region. TMI aeromagnetic image. Black dots indicate locations of lamproite intrusions. Ellendale 4 location is indicated with a black cross. Sun illumination from NE with 45 degree elevation. .... 186

Figure 10-6: Ellendale region. RTP aeromagnetic image. Black dots indicate locations of lamproite intrusions. Ellendale 4 is indicated with a black cross. Sun illumination from NE with 45 degree elevation. .... 187

Figure 10-7: Ellendale aeromagnetic contours with 10 nT intervals. Thick black lines indicate interpreted faults. Lamproite pipes are shown numbered. After Jenke and Cowan (1994) ..... 188

Figure 10-8: Ellendale regional Bouguer gravity image using GA data. Black dots indicate locations of lamproite intrusions. Ellendale 4 location is marked with a black cross. Ellendale 4 is located on a prominent gravity high feature. Sun illumination from NE with 45 degree elevation. .... 189

Figure 10-9: Ellendale ground gravity contours with 2 mGal contour intervals. Thick black lines indicate faults. Numbers refer to pipe numbers. After Jenke and Cowan (1994). .... 190

Figure 10-10: Ellendale region. Isostatic Residual Gravity image. Black dots indicate locations of lamproite intrusions. Ellendale 4 location is marked with a black cross. Ellendale 4 is located on a prominent gravity high feature. Sun illumination from NE with 45 degree elevation. .... 191

Figure 10-11: Ellendale. Falcon gravity gradiometry (Gzz) image with known pipes. 5 eotvos contour interval. After Isles and Moody (2004b). Ellendale pipes here are coincident with positive and negative Gzz features. .... 192

## **List of Tables**

Table 6-1: Coils and frequencies used in the DIGHEM surveys.....	121
Table 6-2: Established absolute values for the Striker Resources gravity bases. .....	125
Table 7-1: Coils and frequencies used in the Hummingbird survey.....	141
Table 11-1: Summary results for individual study areas .....	194

## **ABSTRACT**

This thesis presents an analysis of the use of geophysical methods for diamond exploration in the Kimberley region of Western Australia. Airborne and ground geophysical surveys for the Ashmore, Pteropus and Seppelt areas were designed by the author in collaboration with, and funded by, Striker Resources (now North Australian Diamonds Limited) between 1997 and 2000. The research was extended by analysing newly acquired open file government funded aeromagnetic, gravity and radiometric datasets, and company funded Falcon airborne gravity gradiometry data at Pteropus, Aries and Ellendale.

Recent interpretation of gravity data with seismic control has led to some new insights in the geometry of the Moho in the Kimberley region. I demonstrate that the six study areas: Argyle, Aries, Ashmore, Ellendale 4, Pteropus and Seppelt 1 - used as examples in this thesis, occur within 15 km of local maxima in the slope of the Moho surface, probably reflecting deep crustal structures that have facilitated kimberlite and lamproite intrusion.

The age of emplacement of diamond bearing pipes in the Kimberley region fit into the worldwide age distribution of pipes and for the 800 to 825 Ma pipes at Aries, Ashmore, Pteropus and Seppelt are close in age to significant periods of mantle plume hot spot activity at 780, 800 and 825 Ma.

The use of Isostatic Residual Gravity has been helpful in defining local gravity highs, and shows how the onshore data relates to the offshore data extending into the Bonaparte Basin in the north. The diamondiferous intrusions at Argyle, Aries, Ashmore, Ellendale, Pteropus and Seppelt areas are all located on the flanks of significant, positive gravity anomalies in the Isostatic Residual Gravity data.

Various methods of processing and interpreting regional potential field data are presented, which include multiscale edge detection ('worming') to provide useful 3D visualisation of gravity and aeromagnetic data and their gradients to reveal structures down to about 50 km. These are likely to be important in defining suitable areas for location of kimberlite and lamproite pipes and dykes.

Texture analysis and trend detection has also been tested to highlight structural trends.

Three detailed field study areas in the North Kimberley region – Ashmore, Seppelt and Pteropus – have been used to test the effectiveness of various detailed airborne and ground geophysical methods. These areas are remote and were accessed by flying in from Kununurra to a local airstrip at Geebung in the NE Kimberley region and then driving by 4WD to a field camp established close to the Ashmore pipes. Seppelt was reached by a further drive of several hours from the Ashmore camp to a temporary field camp close to the Seppelt 1 and 2 pipes.

The ground geophysical field work was done in the winter months of four field seasons. Results are also presented from the Aries and Ellendale areas in the southern part of the Kimberley. No fieldwork was done by the author in these areas as part of this thesis project.

Physical property contrasts exist between the kimberlite and lamproite rocks, their overlying weathering products, and the surrounding country rocks. These include density, electrical conductivity and magnetic contrasts. The properties of kimberlite weathered to clays overlying pipes, are important in providing conductivity and density contrasts, which are exploited using gravity and electromagnetic methods. Examples are presented of high resolution airborne magnetic, electromagnetic and gravity gradiometry surveys.

Airborne gravity gradiometry using the fixed-wing Falcon system was tested at Pteropus, but did not find any more pipes than were already known. The negative Bouguer gravity and vertical gradient anomalies detected over and around Pteropus 1 and 2 were larger in areal extent than the known pipes. With pipes in the Kimberley region being generally small in areal extent (100 metre diameter or less) the current resolution and noise levels of fixed-wing airborne gravity gradiometry are marginal for effective exploration and still need ground gravity follow up. More recently, since about 2006, helicopter versions of gravity gradiometry systems have been developed and with lower flying speed

and height are better suited for diamond exploration than the fixed-wing systems. Fixed-wing Falcon gravity gradiometry results from Ellendale are included in this thesis.

Helicopter frequency domain electromagnetic methods have been used at Ashmore, Seppelt and Pteropus. They were flown at low level – typically bird height of 30 metres above ground level and also included magnetic measurements. Whilst they showed conductive surface areas over Ashmore, Seppelt 1 and 2 and Pteropus 1 and 2, the results were not of sufficient resolution to be fully effective for targeting.

Ground geophysical results are presented using frequency domain electromagnetic, gravity and magnetic methods. The most effective ground geophysical methods have proved to be close spaced gravity and also frequency domain electromagnetic methods. These two methods respond well to the weathered clay caps which often form over the top of kimberlite pipes. Ground magnetic methods are rapid and cheap to conduct, but suffer from the disadvantage that not all pipes are magnetic. Ground gravity was rapidly shown to be effective by producing some new target kimberlite locations at Ashmore which were followed up and confirmed by drilling.

The thesis includes a review of diamond exploration models and geophysical methods used over 50 years. It also shows how geophysics can help to provide exploration guidelines and strategies for effective exploration.

# 1 INTRODUCTION

This research project set out to investigate the following main questions:

- How are suitable areas for diamond exploration recognised at regional scale?
- How well do geophysical methods work for diamond prospecting in the Kimberley region of Western Australia?
- How can the use of geophysical methods be optimised within selected areas?
- Which advanced processing methods are best for defining suitable geological structures which are important controls for emplacement of kimberlites and lamproites?
- Does the present day topography provide clues to assist diamond exploration beyond catchment analysis of indicator minerals?

The project grew out of work that began with Striker Resources – now North Australian Diamonds Limited (NADL) - in 1997 and led to four honours geophysical projects, which were supervised by the author together with staff from Striker Resources. The honours project results are summarised in theses by Sumner (1997), McChesney (1998), Carter (1999) and Garton (2000).

Striker Resources funded the geophysical fieldwork undertaken in the winters of 1997 to 2000, and also further contract gravity surveys and airborne surveys designed by the author, in collaboration with the staff of Striker Resources. These surveys included: detailed frequency domain low level airborne electromagnetic and magnetic surveys, and an airborne gravity gradiometry survey using the Falcon system, in late 2000.

Exploration for diamonds is expensive and time consuming. Diamonds are not directly detectable by geophysical methods. The primary diamond bearing rocks – kimberlites and lamproites may be detected by geophysical methods, but are often small targets and great care is required to recognise the geophysical signatures of these rocks within the overall regional geophysical background of the host rocks or country rock.

It is usually necessary to employ multiple geophysical methods. Research is required to optimise the use of each method and to produce an optimum sequence for their use within an overall exploration strategy for the location of kimberlite fields, which also includes geological and geochemical components. Successful exploration requires a careful interplay of all the different parts of the exploration program.

Geophysics can be used at a regional and crustal scale as well as at more local scales within selected areas e.g. Macnae (1995). Geophysics is widely used by companies exploring for diamonds, but with widely varying strategies. Some companies use aeromagnetic surveys very extensively and rely heavily on this technique mainly because they can cover large areas quickly and inexpensively to produce a magnetic anomaly “bedrock” map. However this ignores the fact that some of the host kimberlites and lamproites are non-magnetic or only very weakly magnetic and can be very small or have complex shapes. Some host environments are significantly magnetic, e.g. volcanic areas and this makes it difficult to detect weak magnetic signatures from the host kimberlites and lamproites in the presence of larger amplitude and sometimes complex magnetic environments.

Very detailed gravity surveys are useful at a local scale for detecting weathering over kimberlites. It is important to integrate regional gravity data from Geoscience Australia (GA) with company data. This requires that the data are tied by means of using GA ‘absolute’ stations that GA has established around the country. In this study a network of local gravity bases were established and tied back to a GA station at Kununurra Airport.

The arrival of airborne gravity gradiometry with the BHP Billiton Falcon and Bell Geospace systems has had considerable impact on diamond exploration, and has accelerated the exploration process by providing gravity coverage at an earlier stage in the exploration sequence than was previously possible, when only ground gravity was available. An important issue here is the effective spatial resolution of this technique. High resolution is required, given the small surface extent of likely targets.

## **2 EXPLORATION MODELS AND AREA SELECTION**

Economically important kimberlite and lamproite intrusions are restricted to cratons which have been stable since the Early Proterozoic and usually contain Archean cores. These cratons have deep lithospheric roots, where the lithosphere-asthenosphere boundary is deeper than 250 km, and the high pressure and relatively low temperatures produce and preserve diamonds. Typically these cratons are older than 2500 Ma, and cratonised provinces are older than 1800 Ma (Jaques, 1998). The correlation with diamondiferous intrusions and ancient cratons is sometimes described as Clifford's Rule (Clifford, 1966). This has been re-affirmed by Janse (1985 and 1991). Mitchell (1986) describes the process of cratonisation as the accretion of mobile belts onto older cores which then act as rigid blocks with respect to younger tectonic events. Helmstaedt and Gurney (1991, 1995) summarise a model for diamond exploration as shown in Figure 2-1. They describe a three step exploration model for the formation of diamond deposits.

1. Predictions of regions under which diamonds have formed.
2. Selection of areas where diamonds may have survived to be sampled by younger kimberlites and lamproites.
3. Establishment of mantle processes controlling kimberlite and lamproite formation and regional tectonic and local structural controls for the emplacement of kimberlites and lamproites.

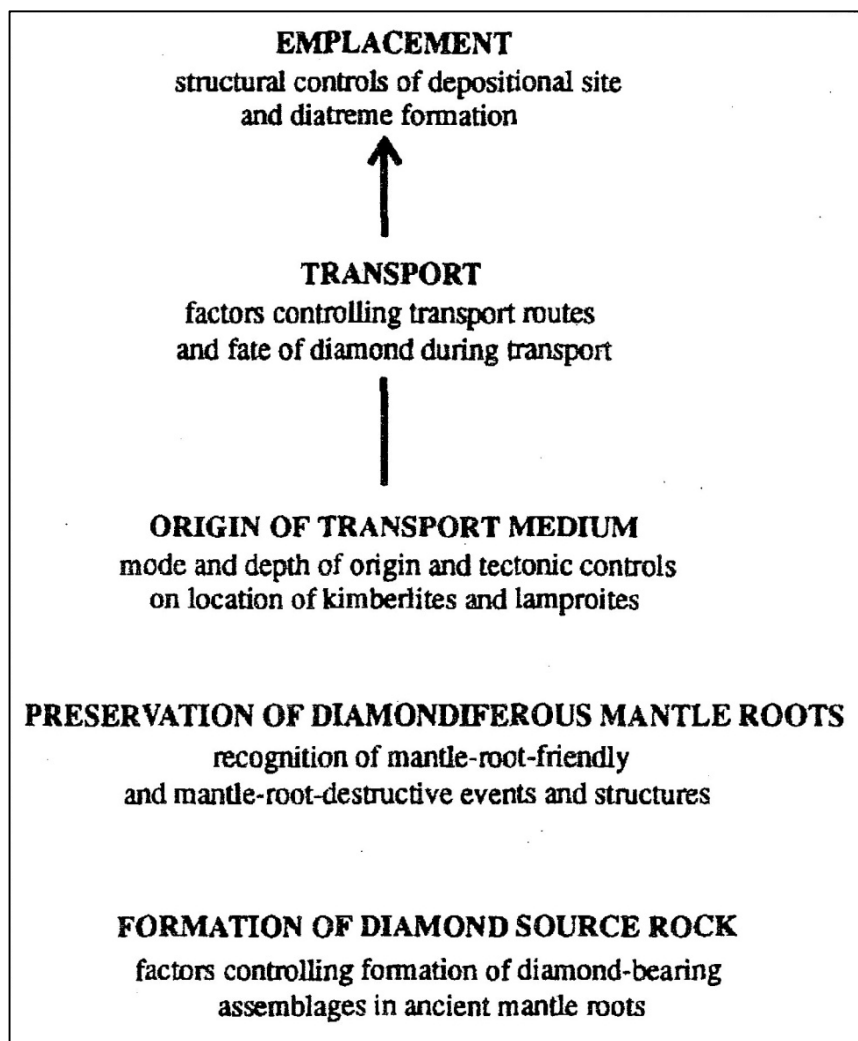


Figure 2-1: Summary diagram of tectonic and structural controls on the formation of primary diamond deposits Reproduced from Helmstaedt and Gurney (1995).

Haggerty (1986) shows a simplified model of a diamondiferous lithosphere or mantle root where the temperature and pressure conditions are optimal for diamond formation and preservation (Figure 2-2). This shows that deep lithospheric roots are required, with depths in excess of about 120 km to sit within the diamond stability curve where diamonds are formed in preference to graphite. This requires particular temperature and pressure conditions. Diamonds are often formed near the boundary between the asthenosphere and the lithosphere in these lithospheric root zones.

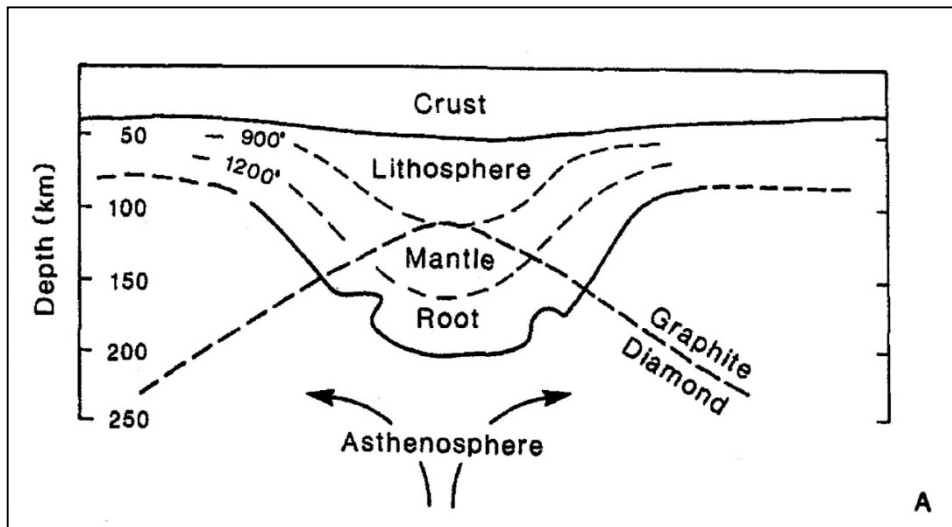


Figure 2-2: Simplified model of a diamondiferous lithospheric or mantle root. Reproduced from Haggerty (1986).

It is now recognised that relatively cool conditions are required to preserve diamonds in the roots of the cratons, and this may be reflected in the low surface heat flow – typically less than  $50 \text{ mW/m}^2$  (Morgan, 1995). The possible correspondence between petrological and geophysical signatures of mantle roots is important for diamond exploration. Studies of teleseismic tomography are providing evidence of anomalous high velocity sheer waves indicating cooler lithosphere (Simons et al., 1999).

Lewis (1990) states that kimberlite and lamproite magmas are melts from a peridotitic parent rock. The presence of diamond in the rocks indicates that the magma is formed in the mantle at depths of 150 to 300 km and is brought to the surface rapidly in volatile rich volcanic eruptions. Suitable pathways are required to bring the kimberlites and lamproites to the surface. In Western Australia the magmatism is closely related to major faults of the Halls Creek and King Leopold Orogens (Lewis, 1990). These faults have been active from the Proterozoic to the Miocene.

Exploration models for diamondiferous intrusions have been well summarised in Cox and Singer (1996), Glover and Harris (1985), Mitchell (1986) and

Pretorius (1979). Glover and Harris (1985) described six main theories to explain the distribution of kimberlites within cratonic terrains. These are:

1. A continent moving across a hotspot. e.g. some kimberlites in Brazil.
2. Extended oceanic transform faults transecting a continent. An example of this is Angola, where transform faults in the Atlantic Ocean extend onshore and kimberlites are clustered along these faults.
3. Subducted oceanic lithosphere extending under a continent, e.g. some South African kimberlites.
4. Flexuring and folding of large blocks within cratons.
5. Domal uplift where kimberlite intrusions are concentrated around a large dome.
6. Large-scale concentric tectonic framework of continents. This was based largely on the nature of concentric gravity anomalies in South African data by Pretorius (1979).

Deep seated structural controls commonly influence the emplacement of kimberlites and lamproites, and these structures may be recognised in regional geophysical datasets, particularly in gravity, magnetic and seismic datasets. White et al. (1995) have described structural controls on the emplacement of kimberlite and lamproite pipes. O'Neill et al. (2005) have described geodynamic controls on diamond deposits and their importance for Australian exploration.

Kimberlite and lamproite intrusions often occur in clusters. Hence once the first intrusions have been found in an area it is useful to do further exploration close by, to discover whether they are part of a cluster. This was true for the Ashmore area in the North Kimberley, where six pipes were discovered within an area of 2 km<sup>2</sup>. More detail about this is provided in Chapter 6 of this thesis. Jaques (1998) states that clusters can occur in fields up to about 50 km across with up to 100 pipes included within this size of area.

Cox and Singer (1986) state that the most productive pipes occur in distinct age ranges through earth history: 80-100 Ma, 250 Ma and 1000–1100 Ma. Gurney et al. (2005) have also studied the distribution of diamond deposits over time and identified particular periods which were more productive for diamond formation.

The following Figure 2-3 is reproduced from Pidgeon et al (1989). This shows the clustering of kimberlite and lamproite intrusions over time in different parts of the world. Included in this figure are various deposits from the Kimberley area. These include Argyle (AK1) at about 1178 Ma and Pteropus at 805 Ma (Pidgeon et al. 1989).

Aries was intruded at about 820 Ma (Towie et al, 1991), Ashmore and Seppelt pipes at approximately 800 Ma (Ramsay pers. comm. 1997) and the Ellendale pipes at about 20 - 22 Ma (Wellman, 1972).

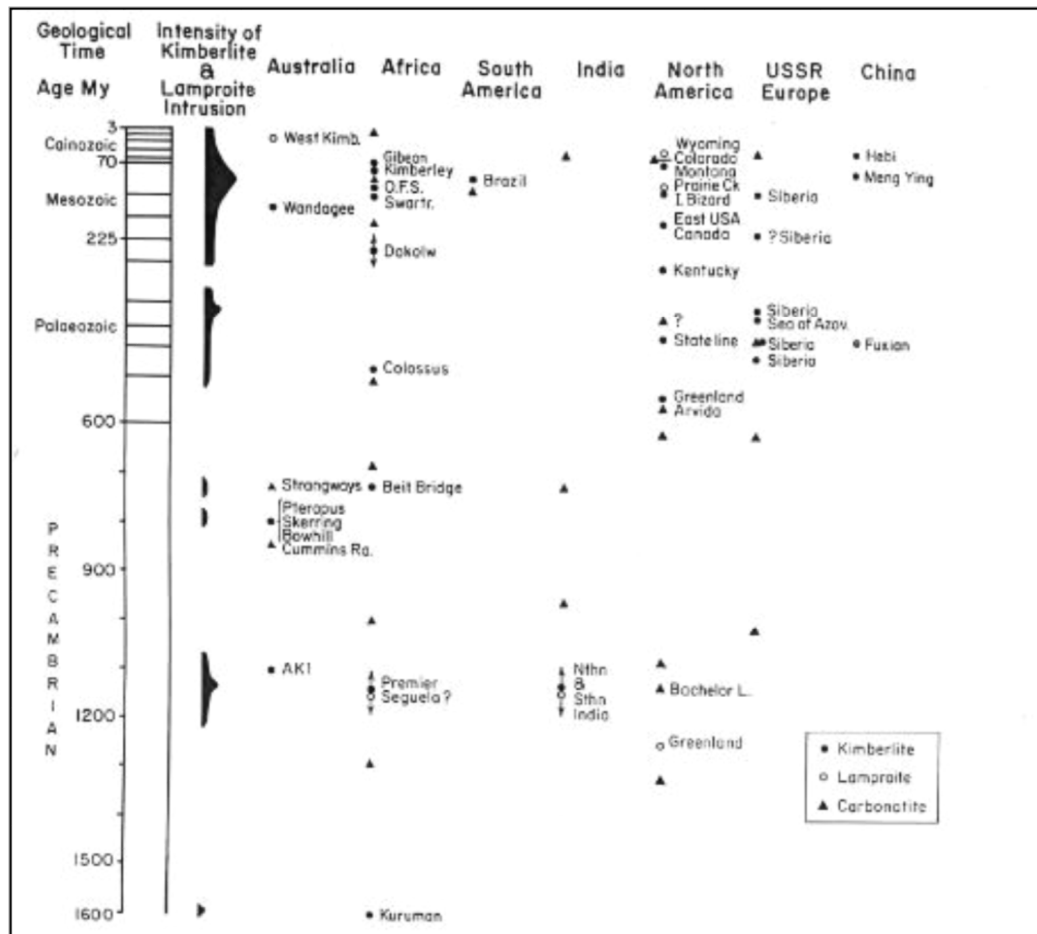


**Figure 2-3: Worldwide ages of kimberlite, lamproite and carbonatite emplacement. Reproduced from Pidgeon et al (1989). This figure shows how the ages of the West Kimberley, North Kimberley and Argyle intrusions correlate with other diamond-bearing intrusions around the world.**

Various methods have been published on diamond field area selection methods. These include papers by Atkinson (1989), Morgan (1995) and Kaminsky et al. (1995). Atkinson (1989) describes the philosophy of the exploration process, including area selection, and states that the discovery of diamonds in lamproites in WA focused more attention on the early Proterozoic mobile belts.

Papers focussing more on geophysical prospecting include those by Macnae (1979 and 1995), Snyder et al. (2004) who describe the use of teleseismic methods for mapping mantle lithosphere, and Jones and Craven (2004) who describe deep probing electromagnetic MT methods.

### **3 GEOLOGY AND PHYSICAL PROPERTIES OF KIMBERLITES AND LAMPROITES, GEOPHYSICAL MODELS**

#### **3.1 Geology of kimberlites**

Kimberlite is an ultrabasic rock which consists chiefly of coarse grained olivine or olivine and phlogopite mica. It occurs as tuff, volcanic breccias and intrusives which are usually serpentinised and often carbonatised. The mineralogical classification proposed by Skinner and Clement (1979) is:

*“ In addition to olivine, any one of five other minerals may be present as a major mineral constituent of kimberlite. These minerals are diopside, monticellite, phlogopite, calcite and serpentine. Accordingly we propose the recognition of five basic subdivisions of kimberlite depending upon (and named after) whichever one is volumetrically more abundant.*

*Further subdivision can be made if one or more of these or any other mineral is present in sufficient abundance for it to qualify as a characterizing accessory or modifier. We have found it useful to accept, as characterizing accessories, those minerals which are present to the extent of, or exceed two thirds of the volumetric abundance of the dominant mineral. In addition to the five minerals listed above, some other mineral may occur as a major constituent of kimberlite. In this event our primary subdivision could be extended ”*

Physical properties depend on mineral composition and weathering. Kimberlite alters to clay minerals nontronite and montmorillonite near the land surface (Gerryts, 1970).

Kimberlite often occurs in pipes and dykes, as illustrated in Figure 3-1, which shows the relationships between crater, diatreme and hypabyssal facies rock (Jaques, 1998). Worldwide, pipes usually have diameters from 50 metres up to about 1500 metres, with surface areas in the range 1 to 150 ha.

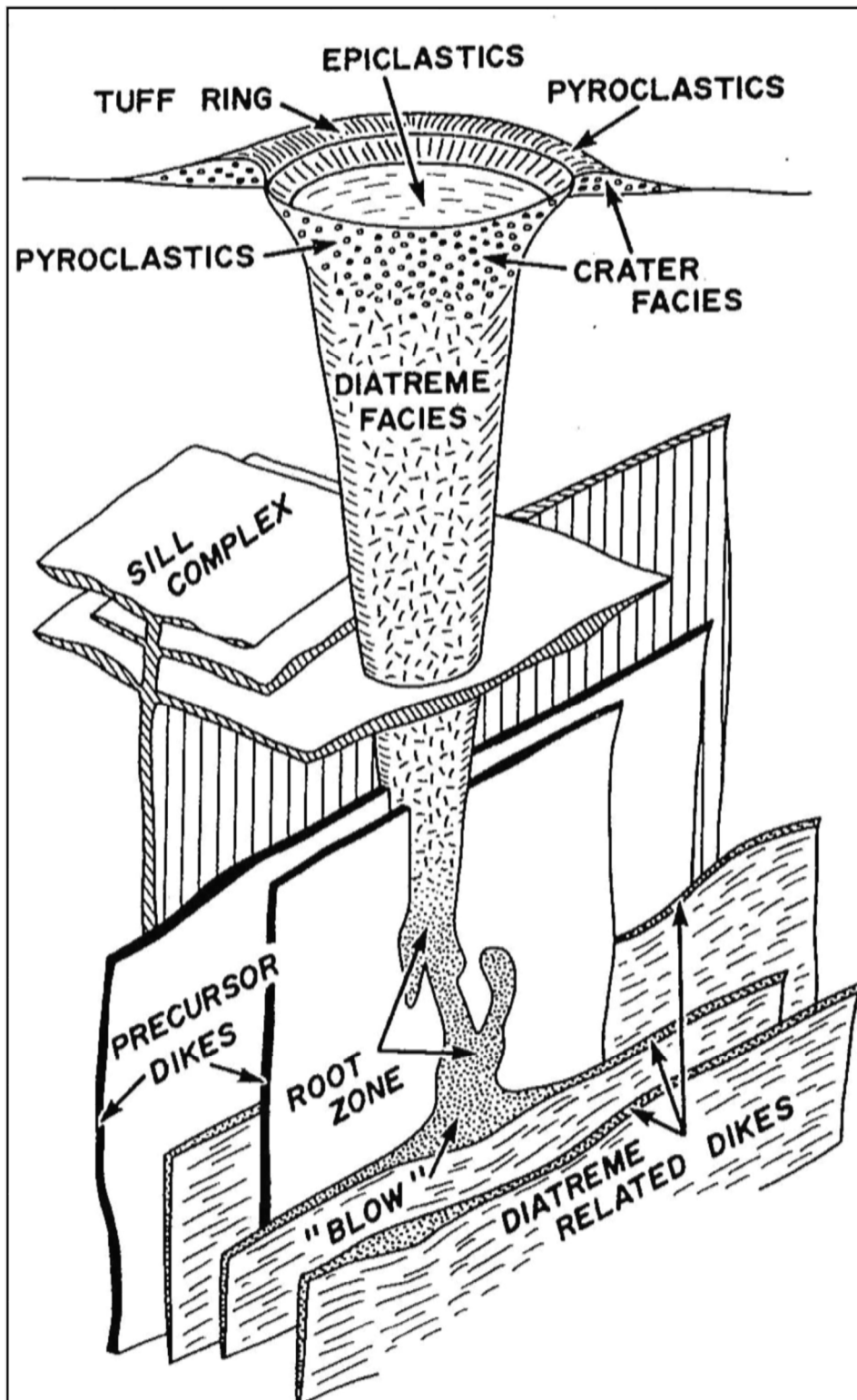


Figure 3-1: Idealised kimberlite magmatic system reproduced from Jaques (1998) and modified from Mitchell (1986). This shows the different facies which may be recognised in the study areas.

## 3.2 Geology of lamproites

Following the style of Clement et al. (1977) in the definition of kimberlites, Jaques et al. (1984) defined lamproite as follows:

- “ *a potash and magnesia-rich lampropyric rock of volcanic or hypabyssal origin belonging to the ultrapotassic rock series. Minerals commonly present as major primary constituents include olivine, clinopyroxene (typically diopside), phlogopite (typically titaniferous), leucite, amphibole (typically potassic richterite), orthopyroxene, sanidine and glass. Accessory minerals may include priderite, apatite, nepheline, spinel, perovskite, wadeite and ilmenite;*
- *Xenoliths and xenocrysts (including olivine, pyroxene, garnet and spinel) of upper mantle origin may be present and diamond as a rare accessory;*
- *Lamproite may be either basic or ultrabasic composition, and is characterized by high  $K_2O / Na_2O$  ratios ( $>3$ ) and high abundances of Rb, Sr, Ba, Ti, Zr, Nb, Pb, Th, U, and light rare earth elements. “*

## 3.3 Physical properties

The physical properties of kimberlites depend markedly on their mineral composition and state of weathering: Gerryts (1970). Kamara (1981) provides a useful table of various physical properties which include magnetic susceptibility, density, resistivity, thermal conductivity and seismic velocities.

### 3.3.1 Density

Gerryts (1970) reported that fresh kimberlites from Sierra Leone have densities in the range 2.71 to 3.12 g/cc and in South Africa kimberlites in diamond mines have densities in the range 2.64 to 2.98 g/cc. McChesney (1998) reported density measurements on kimberlites from the North Kimberley region: *Ashmore 1*: 2.40 and 3.19 g/cc, *Seppelt 1*: 2.61 and 2.65 g/cc. Carter (1999)

reported density measurements from *Seppelt 1*: weathered surface samples had densities of 1.63 – 1.69 g/cc and fresh kimberlite samples had densities of 2.50 – 2.72 g/cc.

It is clear that the degree of weathering has a big influence on the density measurements as well as the abundance of xenoliths and nature of the kimberlite facies.

### **3.3.2 Magnetic susceptibility**

Magnetic properties of kimberlite are highly variable and due mainly to the presence of magnetite and ilmenite. Remanent magnetisation is often important. Some kimberlites are not magnetic.

From our work in the North Kimberley region with Striker Resources, McChesney (1998) reported magnetic susceptibility measurements on kimberlite pipe samples.

Seppelt 1: 120 – 31000 x 10<sup>-6</sup> SI units

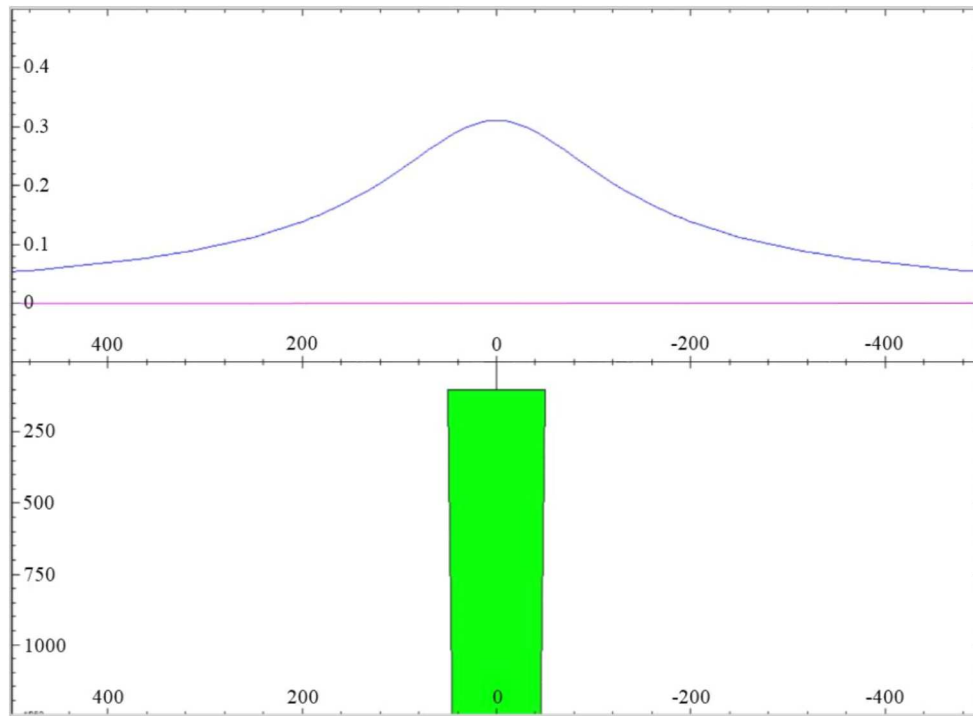
Skerring: 5500 – 20000 x 10<sup>-6</sup> SI units

### **3.4 Geophysical models**

Geophysical models of Kimberlite pipes generally use elliptical or circular plan and taper with depth.

Whilst fresh kimberlite has generally a high density – typically greater than 3 g/cc -where weathering has taken place and there is a weathering cap present, the low density of the weathered material more than counteracts the gravity high from the kimberlite and the resultant anomaly is generally negative. This is illustrated by the central cross section from a computer model shown in Figure 3-2. In this model the country rock has a density of 2.3 g/cc (typical of sandstone), the weathered cap (shown here in blue) has a density of 1.9 g/cc and the pipe (shown in green) has a density of 3.0 g/cc. The top of the pipe has a depth of 100 m below surface and extends down to 10 km. the top radius is 50 m and the radius at 10 km is 10 m. In each half of the figure, the top panel

shows gravity response in mGal and the lower part the depth section in metres below ground level. It can be seen that without the weathering there is a positive anomaly of 0.31 mGal. With weathering present the combined response is  $-0.49$  mGal. The upper part of the figure shows response for pipe only and the lower part pipe plus weathering.



**NORTH**

**horizontal distance (metres)**

**SOUTH**

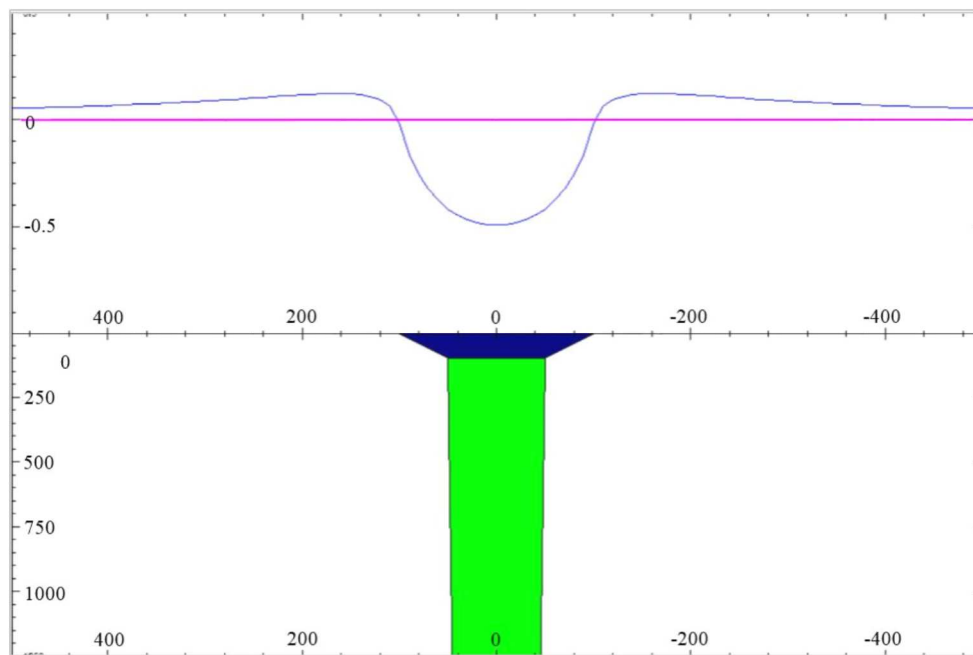


**Figure 3-2: Computed gravity response for a tapering vertical cylindrical pipe model and weathered cap. This shows that the gravity anomaly due to the weathered cap can dominate in the combined effect of cap plus pipe.**

Computer modelling shows that for the pipe dimensions used here, gravity anomalies at 40 metres above ground are reduced to about 50 percent of ground figures and for 80 metre height about 25 percent.

Most of the gravity anomalies observed over kimberlites in the Kimberley region are negative and in the range of -0.05 to -0.5 mGal. It would be expected that some positive anomalies are possible where weathering is either not present or thin, but this has not been seen in this study. There may be some cases where the negative anomaly, due to weathered material, closely balances out the positive gravity anomaly from the higher density kimberlite and leaves virtually no detectable gravity anomaly. No cases of kimberlites detectable by magnetic and/or electromagnetic methods but with no gravity signature have been seen in this study.

Magnetic properties of kimberlite are highly variable, and due mainly to the presence of magnetic and ilmenite, as a primary mineral or formed during serpentinization. Remanent magnetisation is if often present. Some kimberlites are non-magnetic or only weakly magnetised. From the work in the North Kimberley region with Striker Resources, McChesney (1998) reported magnetic susceptibility values for kimberlite pipe samples:

Seppelt 1: 0.00012 – 0.03 SI units

Skerring: 0.055 – 0.02 SI units

The magnetic mineral content of pipes is very variable and controlled by erosion and weathering. Remanence is also commonly present. Some pipes are effectively non-magnetic due to very low iron mineral content.

### **Magnetic modelling**

Forward computer modelling, using ModelVision software, has been used to show the computed magnetic response from a magnetic pipe with circular plan form and tapering with depth. The computed magnetic response is shown in plan form in Figure 3.3 and as a north south central profile in Figure 3.4.

**Model parameters are :**

Flying height: 40 metres

Depth to top of fresh pipe: 100 metres

Depth extent: 10 km

Top radius: 50 metres

Radius at 10 km depth: 10 metres

Susceptibility contrast: 0.01 SI units

Total Magnetic Intensity; 48800 nT

Inclination: - 45.6 degrees

Declination: + 2.8 degrees

Remanent magnetisation: zero

Anomaly maximum is 7.9 nT and minimum -2.9 nT

The field parameters were calculated using the IGRF routine in Geosoft Oasis Montaj software package for the centre of the Kimberley study area.

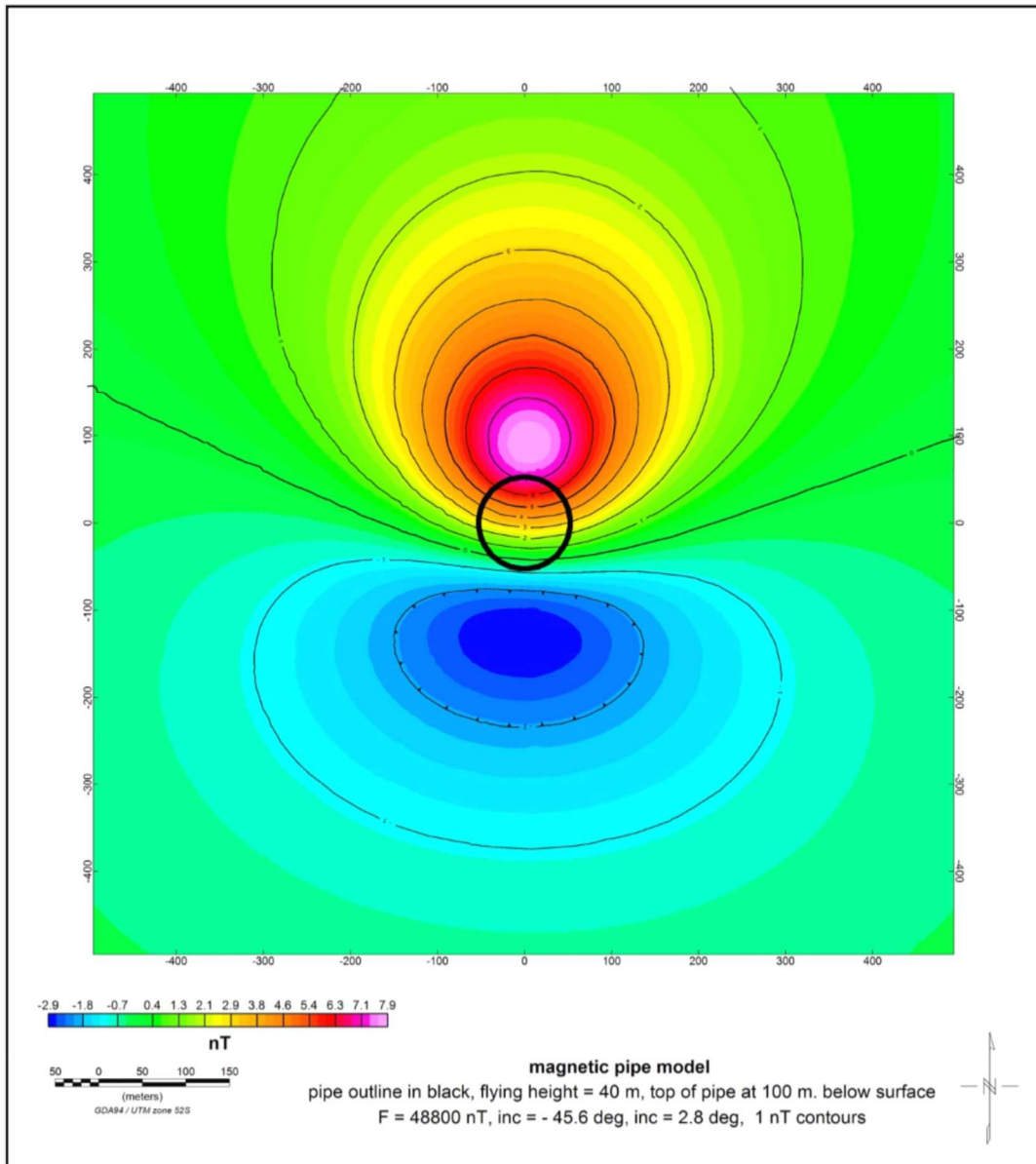
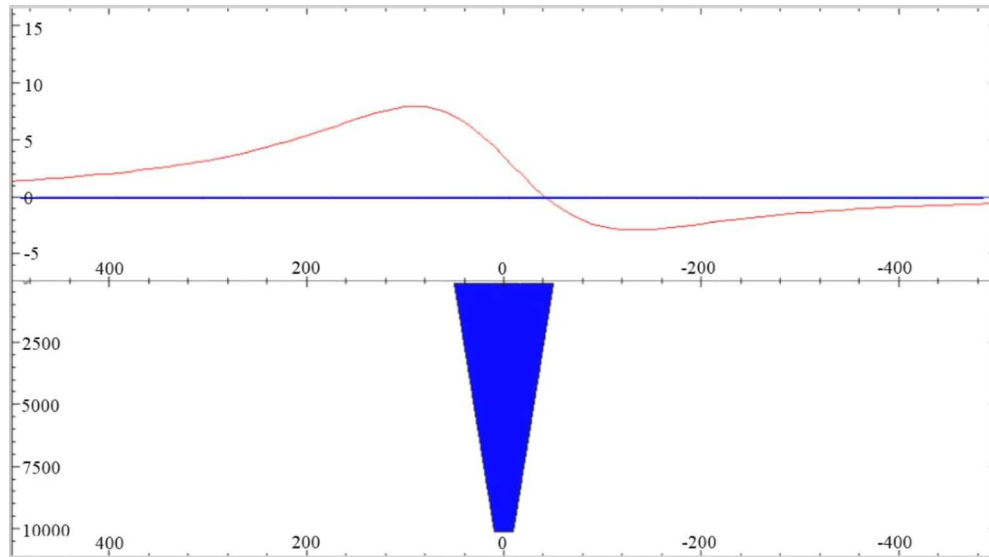


**Figure 3-3: Computed plan view of magnetic response for a tapering vertical cylindrical pipe model. For induced magnetisation only, we see characteristic magnetic high over northern end of pipe and low to the south of the pipe. Susceptibility contrast for the pipe with respect to host rocks is 0.01 SI units.**

NORTH

SOUTH



Horizontal distance (metres)

**Figure 3-4: Computed north-south profile of magnetic response for a tapering vertical cylindrical pipe. For the modelling parameters used here, the maximum anomaly is 8 nT and the minimum -3 nT.**

The top panel shows magnetic response in nanoteslas.

The lower panel shows the depth section in metres down to 10 km with the model cross section in blue.

Modelling shows that for induced magnetisation only, there is a maximum on the northern side of the pipe and a minimum to the south of the pipe. This characteristic shape is often observed in the field examples. It is important to use a flight line direction of north – south or close to that to try to capture this characteristic feature.

Further computation shows the effects of varying pipe model radius from 20 metres to 100 metres, and varying flying heights for a 50 metre radius pipe. The results of these computations are shown in Figures 3-5 and 3-6.

Figure 3-6 illustrates the importance of flying low - typically about 40 metres above ground level if aircraft type and terrain permit this to be done safely. It

can be seen with this model that at 80 m flying height peak amplitudes are about 62 % that observed at 40 metre flying height.

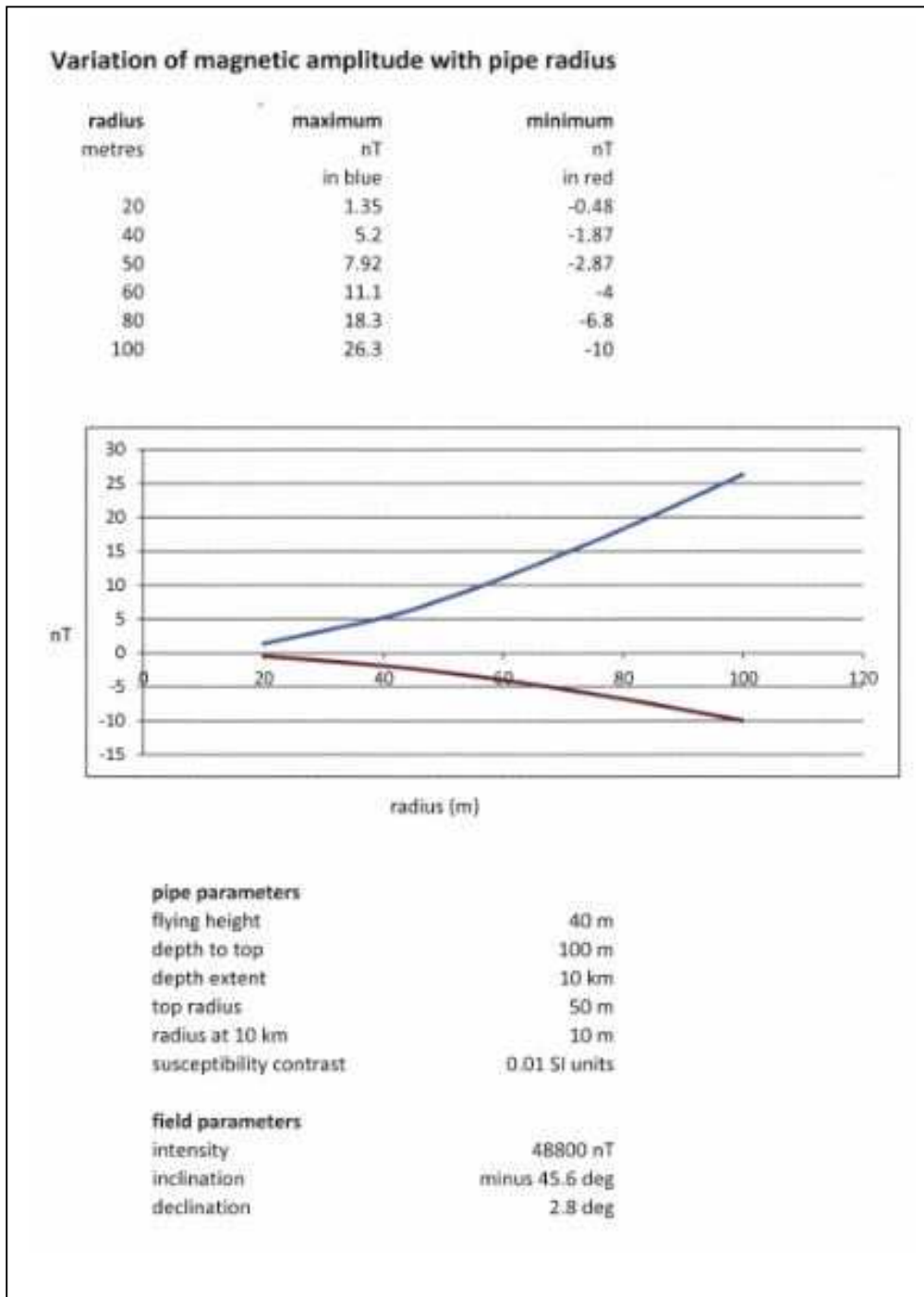
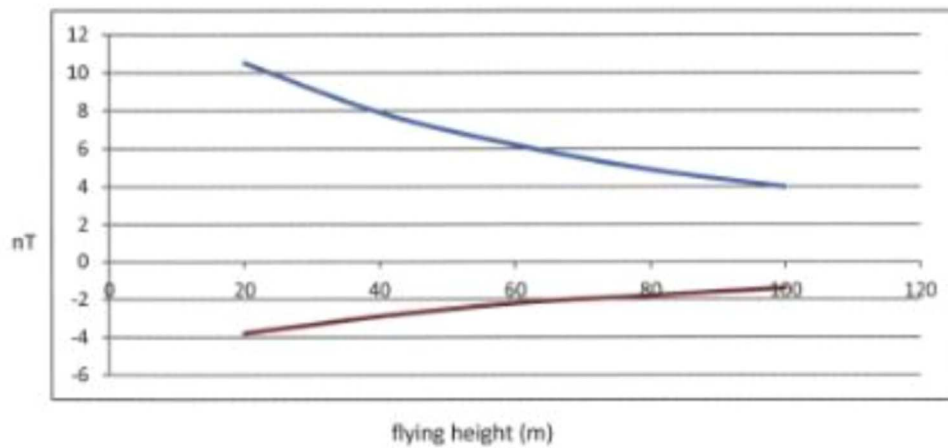


Figure 3-5: Computed variation of magnetic anomaly response for a range of pipe radii. Depth to unweathered top of pipe is 100 metres.

### Variation of magnetic amplitude with flying height

flying ht. metres	maximum nT in blue	minimum nT in red
20	10.5	-3.8
40	7.9	-2.9
60	6.2	-2.2
80	4.9	-1.8
100	4	-1.4



#### pipe parameters

depth to top	100 m
depth extent	10 km
top radius	50 m
radius at 10 km	10 m
susceptibility contrast	0.01 SI units

#### field parameters

intensity	48800 nT
inclination	minus 45.6 deg
declination	2.8 deg

**Figure 3-6: Computed variation of magnetic amplitude with flying height over a pipe of radius 50 metres and depth of 100 metres to top of unweathered pipe. Anomaly amplitude reduces markedly with increasing flying height.**

## **Electromagnetic modelling**

Raiche (2000) describes modelling various airborne EM systems and how to select an airborne EM system for kimberlite exploration. In his study, a 3D integral equation program was used to compute the responses of kimberlite pipe with a weathered clay cap in a resistive environment, for several different airborne EM systems. This included various time domain systems and well as a generic frequency domain helicopter system with five frequencies ranging from 500 Hz to 50,000 Hz. Coplanar and coaxial systems with coil separations of 6 and 8 metres. The results showed that for a resistive environment, such as we have in the North Kimberley study area, helicopter frequency domain systems were the best practical choice. This was followed by using Dighem and Hummingbird helicopter systems in the work designed and recommended by the author for Striker Resources.

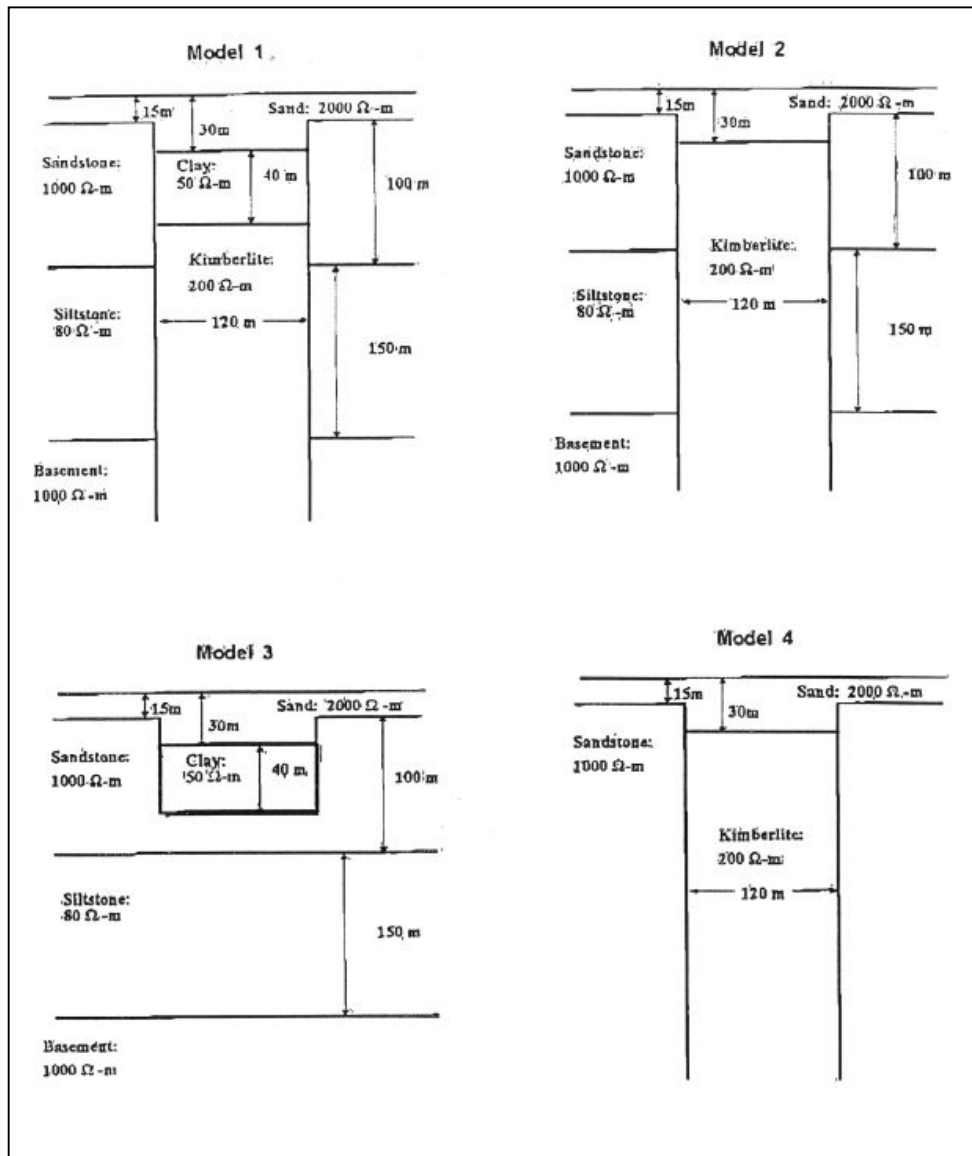


Figure 3-7: Kimberlite models used in Raiche (2000) model study of the effect of conductivity variations on airborne electromagnetic measurements.

## **4 PREVIOUS RESEARCH**

This section reviews previous research on the general use of geophysics in diamond exploration and the specific history of diamond exploration in the Kimberley region.

### **4.1 Review of worldwide use of geophysics in the exploration for diamonds**

Geophysics in the search for diamonds has been summarised in a number of key papers. In time sequence these include Gerryts (1970), Burley and Greenwood (1972), Macnae (1979 and 1995), Kamara (1981), Jaques and Milligan (2004), Jones and Craven (2004), Power et al. (2004), and Reed and Witherly (2007).

Gerryts (1970) provided a review of geophysical methods, mainly magnetic, gravity and electrical techniques that had been used in the search for diamonds in kimberlites up to 1970. His paper includes examples from Mali, Sierra Leone, South Africa and Tanzania, and some descriptions of Russian experience. Gerryts (1970) provides some data on densities and magnetic susceptibility. He reported that many African kimberlites are non-magnetic. This author worked with Gerryts in 1968 and conducted field trials in South Africa of a new ground EM device specifically to detect non-magnetic kimberlites (Wilkes, 1968). This was designed by Wilkes and Scofham at Imperial College, London.

Burley and Greenwood (1972) reported on geophysical surveys over kimberlite pipes in Lesotho. EM, gravity, magnetic, resistivity and seismic methods were used. They concluded that magnetic methods were the most useful whilst EM and seismic methods were not particularly helpful.

Macnae (1979) discussed geophysical prospecting methods for diamonds and presented a simple geological model based on papers by Hawthorn (1975) and Nixon (1973). The physical properties are very much determined by erosion and weathering. Macnae (1979) includes some results of airborne EM using the

Input system and showed examples of the conductive response obtained over weathered kimberlites.

Macnae (1995) reported on the extensive use of airborne EM methods (AEM) in southern Africa, which were used to find weathered, crater facies pipes. Macnae (1995) recommended ground magnetics, EM and resistivity as follow up techniques.

Drew and Cowan (1994) showed some results from the Kimberley region of WA, with the use of magnetic and Euler Deconvolution (Reid et al., 1990) to help interpret aeromagnetic data from the Argyle area. Various other authors have also reported on the use of Euler Deconvolution with aeromagnetic data. More recently Euler Deconvolution has been adapted to work with gravity data. A significant issue here is the choice of appropriate structural indices for this method. Structural indices relate to the rate of fall off of anomaly amplitude with distance from the source.

Milligan et al. (2003a and 2003b) have described the use of potential field datasets and their gradients in mapping crustal architecture.

Le Cheminant et al.(1996) and Katsube and Kjarsgaard (1996) in a useful publication by the Geological Survey of Canada describe diamond exploration methodology used in Canada. Power et al. (2004) describe geophysical methods for kimberlite exploration in the Slave Craton of northern Canada. In 1991, diamondiferous kimberlite was discovered and considerable exploration activity followed so that by 2004 two major diamond mines were in operation - Diavik and Ekati. The exploration methods included geochemical sampling of glacier till material and fluvial channels followed by geophysics – aeromagnetic, helicopter EM and gravity surveys. In the Canadian examples quoted, there are usually good contrasts in physical properties – magnetic susceptibility, conductivity and density – which enable the geophysical methods to work well.

Heliborne Falcon gravity gradiometers have been developed from 2006 and have a number of advantages over the fixed wing gravity gradiometer systems.

These include better ability to follow terrain, lower flying height and lower flying speed. These result in improved spatial resolution. First test results are described in Lee et al (2007). Rajagopalan et al (2008) also describes heliborne results from diamond exploration in Canada.. Dransfield (2010) quotes an accuracy of 3 eotvos and a spatial resolution of 45 metres for the heliborne version of Falcon.

Reed and Witherly (2007) provide a 50 year review of kimberlite geophysics which includes a review of some of the earlier papers and in addition to magnetics, gravity, EM and resistivity. This paper includes some results from airborne gravity, seismic, ground probing radar and advances in geophysical processing techniques.

#### **4.2 Brief history of diamond exploration in the Kimberley region**

Jaques et al. (1986) review the history of diamond exploration in the Kimberley region. The description that follows here is largely based on Ramsay (2000). Smith (1984) summarises the genesis of diamond deposits in the West Kimberley.

In the early 1970's, the Kimberley region of Western Australia was identified by the Tanganyika Joint venture companies (later renamed the Ashton Joint Venture) as having geological similarities with diamondiferous areas in Africa and the Soviet Republic (Ramsay, 2000). The Kimberley Block was targeted as a cratonic nucleus underlain by up to 300 km of depleted lithospheric mantle material which is a preferred host for diamond crystallisation (Haggerty, 1986).

The Tanganyika Joint Venture recovered alluvial diamonds and indicator minerals from the northern Kimberley region by 1972. In the period 1974 to 1976, kimberlites were discovered at Skerring, Pteropus, Hadfields and KGB2 and these were grouped by Jaques et al. (1986) as the North Kimberley Kimberlite Province. These kimberlites have been dated at about 800 Ma (Pidgeon et al., 1989). Of these four occurrences, diamonds were only found at Pteropus.

In 1976, the Ashton Joint Venture discovered the first of more than 100 diamondiferous lamproites in the Ellendale area. These pipes have been dated at 20-22 Ma (Wellman, 1972). These are located in the King Leopold Mobile Zone and Lennard Shelf of the Canning Basin.

After this discovery, exploration was extended to the Halls Creek Mobile belt and in 1979 resulted in the discovery of the Argyle lamproite deposit. The Argyle lamproite pipe has been dated at about 1178 Ma with a range of Rb-Sr and K-Ar methods ranging from 1253 +/- 26 Ma to 1048 +/- 160 Ma (Jaques et al., 1986, and Pidgeon et al., 1989). This deposit has been highly productive and has provided large volumes of rough industrial diamonds and high quality gem diamonds. This deposit is a world class deposit due to the sheer volume of diamonds produced. Jaques (1998) reported that the grade of Argyle is about 650 metric carats (CM) per 100 tonnes.

The Aries, 20 ha kimberlite pipe, was discovered in 1985 in the Phillips Range in the central Kimberley by a Triad-Freeport joint venture using traditional drainage sampling methods. Its discovery and age determination (about 820 Ma) are described by Towie et al. (1991). The surface expression of the kimberlite pipe comprises three depressions of up to 20 m depth which are clearly visible on aerial photography. This is similar to some kimberlite pipes in South Africa where changes in surface topography provide leads to aid in discovery.

The early exploration and discovery of kimberlites and diamonds in the Ashmore, Seppelt and Pteropus areas are described separately in chapters 6, 7, and 8 of this thesis.

A map showing locations of diamond occurrences in the Kimberley region is shown as Figure 4-1. This is the north western section of a map produced by Jaques (2006b). Two insert maps on Figure 4-1 show the North Kimberley province and the Ellendale area in more detail.



## **5 REGIONAL DATASETS AND DIAMOND OCCURRENCE IN THE KIMBERLEY REGION – GEOLOGY, SEISMIC, AEROMAGNETIC DATA, GRAVITY, DIGITAL ELEVATION DATA**

### **5.1 Regional geology**

Regional geology of the Kimberley region of Western Australia is well summarised in Jaques et al. (1986) and Lewis (1990). Mineral occurrences and exploration potential of parts of the Kimberley region are described in Sanders (1999), Hassan (2000), and Ruddock (2003). Digital versions of GSWA 1:250 000 scale geological map sheets have been accessed through a DVD which is available from GSWA.

Further details on Kimberley geology and diamond mineralisation are provided in Atkinson et al. (1990), Shaw et al. (1996 and 2000). Reddicliffe et al. (2003) provide information on the Ashmore and Seppelt areas.

Hillis and Muller (2003) and Hillis and Reynolds (2003) provide useful descriptions of the modern stress field in Australia using various tectonic models. These show a dominant stress direction of SW – NE in the Kimberley region.

Plumb (1979) shows how Australia may be divided into major crustal blocks each of which has its own history and tectonic style. This subdivision shows that the Kimberley Block is part of the North Australian Craton, which extends into the Northern Territory and has been stable for the last 1700 Ma. The eastern boundary of the North Australian Craton is the western side of the Mount Isa Orogen. The North Australia Craton includes the Kimberley Block and the adjoining Halls Creek and King Leopold mobile zones.

Figure 5-1 shows the locations of the Australian Cratons. This has been reproduced from Betts and Giles (2006).

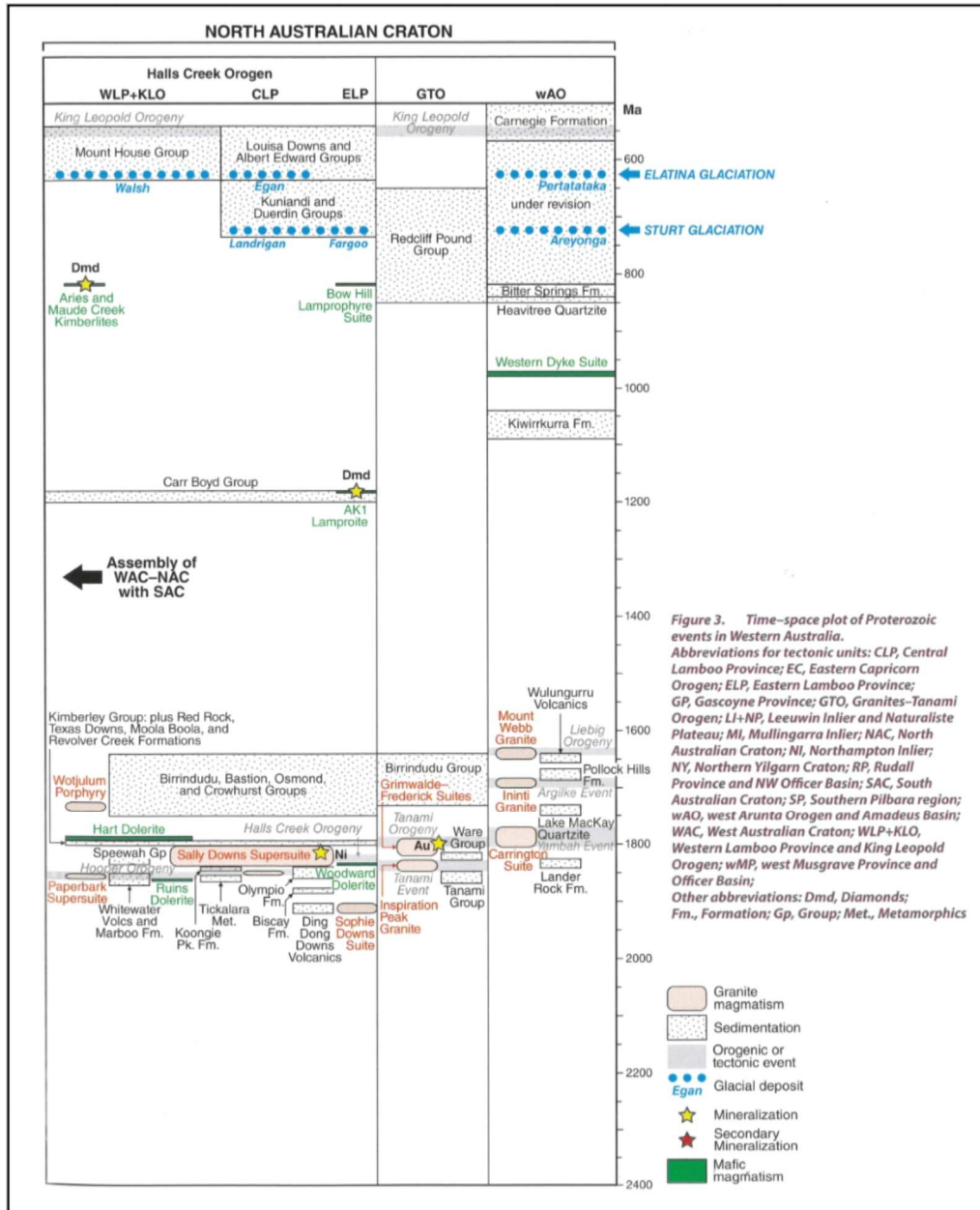


Figure 5-1: Map showing locations of Australian cratons. Reproduced from Betts and Giles (2006).

Figure 5-2 shows a time-space plot of Proterozoic events in the North Australian Craton in Western Australia. This is reproduced from part of a figure by Johnson (2013). The figure includes:

- the assembly of the West Australian, North Australian and South Australian Cratons at about 1300 Ma, as part of the formation of Rodinia.

- The intrusion of the pipes at Argyle, Aries and Maude Creek (near Argyle).
- The Hart Dolerite at about 1800 Ma.



**Figure 5-2: Time-space plot of Proterozoic events related to the North Australian Craton reproduced from Johnson (2013).**

Whether the Kimberley Block has an Archaean core is problematic, as the basement rocks here are covered by up to 5 km of gently folded Proterozoic sediments and basalts and dolerites of the Kimberley Basin succession (Jaques

et al., 1986). Gunn and Meixner (1998) interpreted possible Archaean rocks in their interpretation of aeromagnetic and gravity data for the Kimberley region (see also Figure 5-12).

A stratigraphic column through the Kimberley Basin is shown in Figure 5-1.

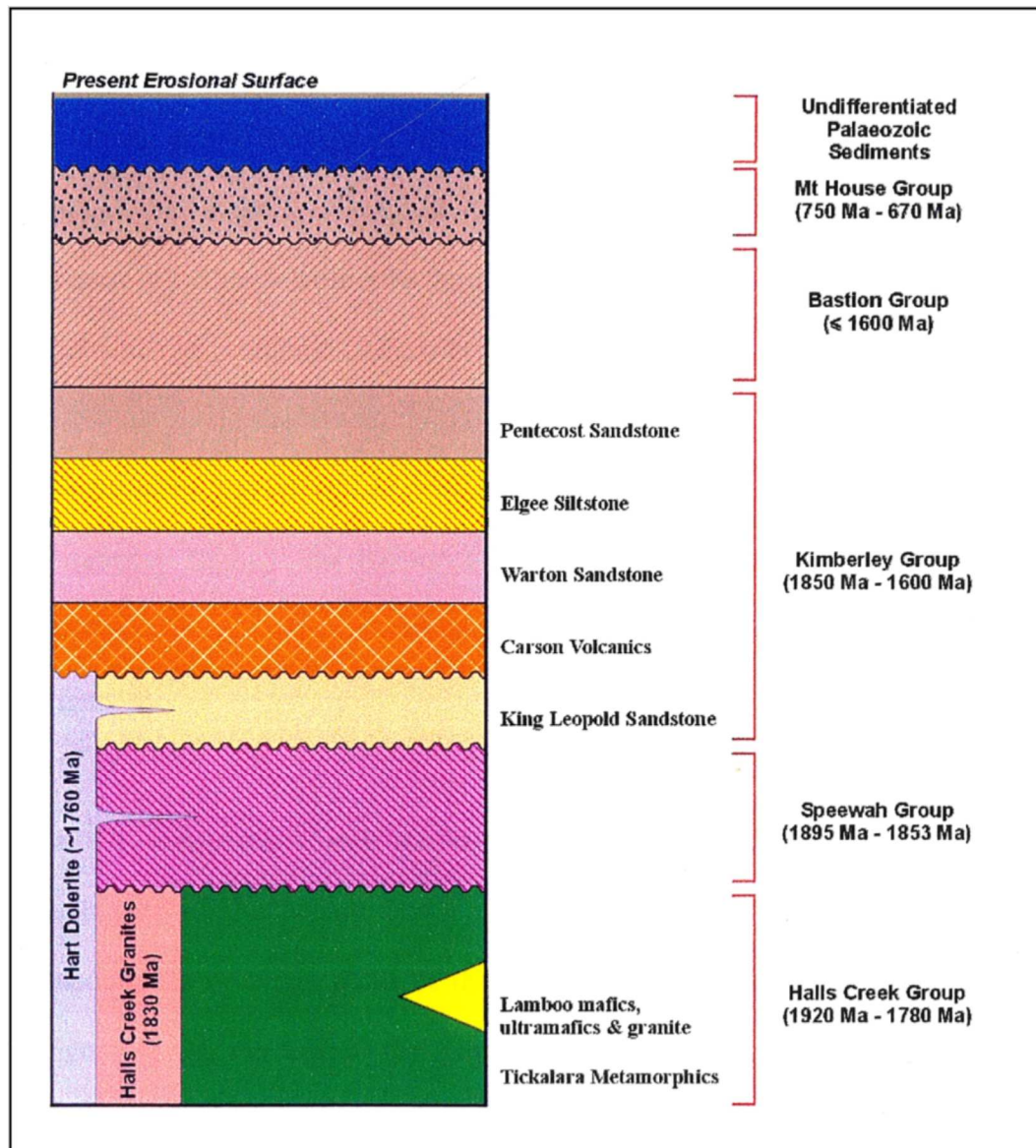


Figure 5-3: Schematic section of the Kimberley Basin geology. Modified from Griffin and Grey, (1990)

Figures 5-4 and 5-5 show locations of diamond occurrences and structural geology.

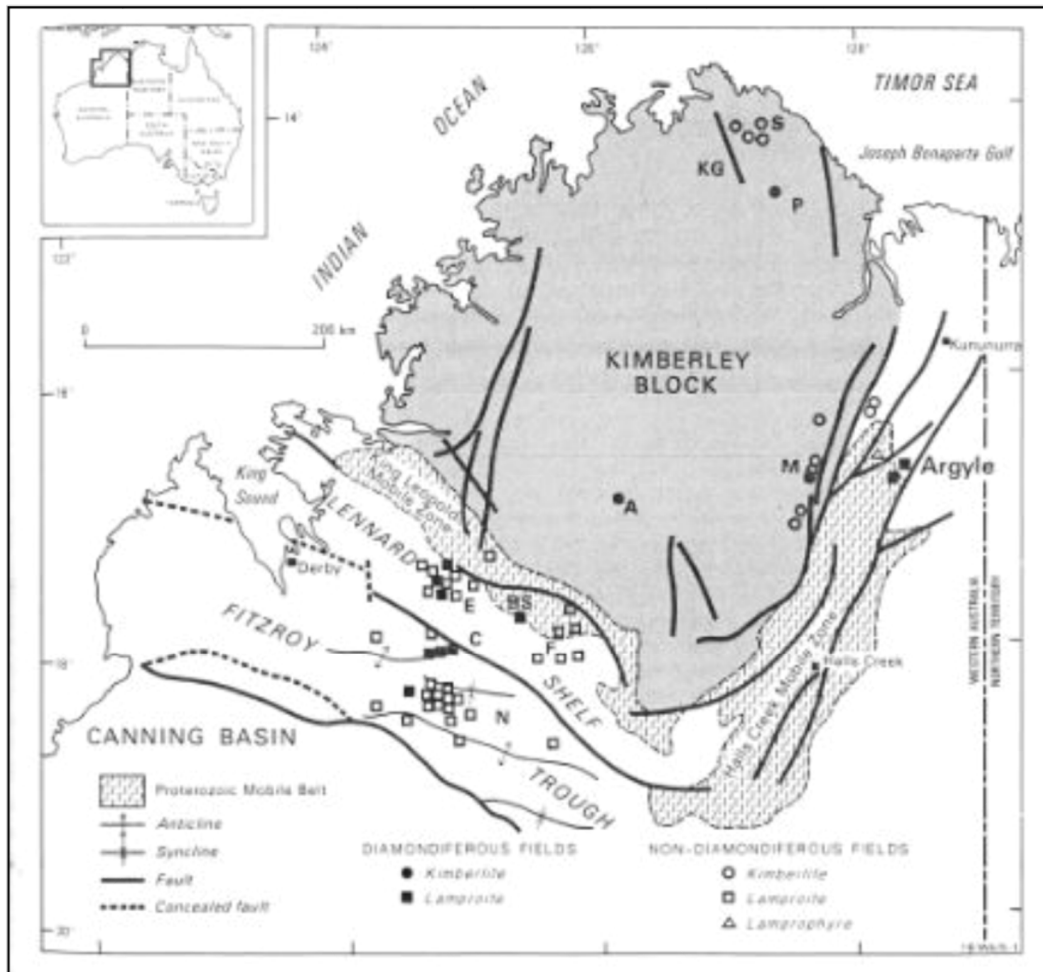
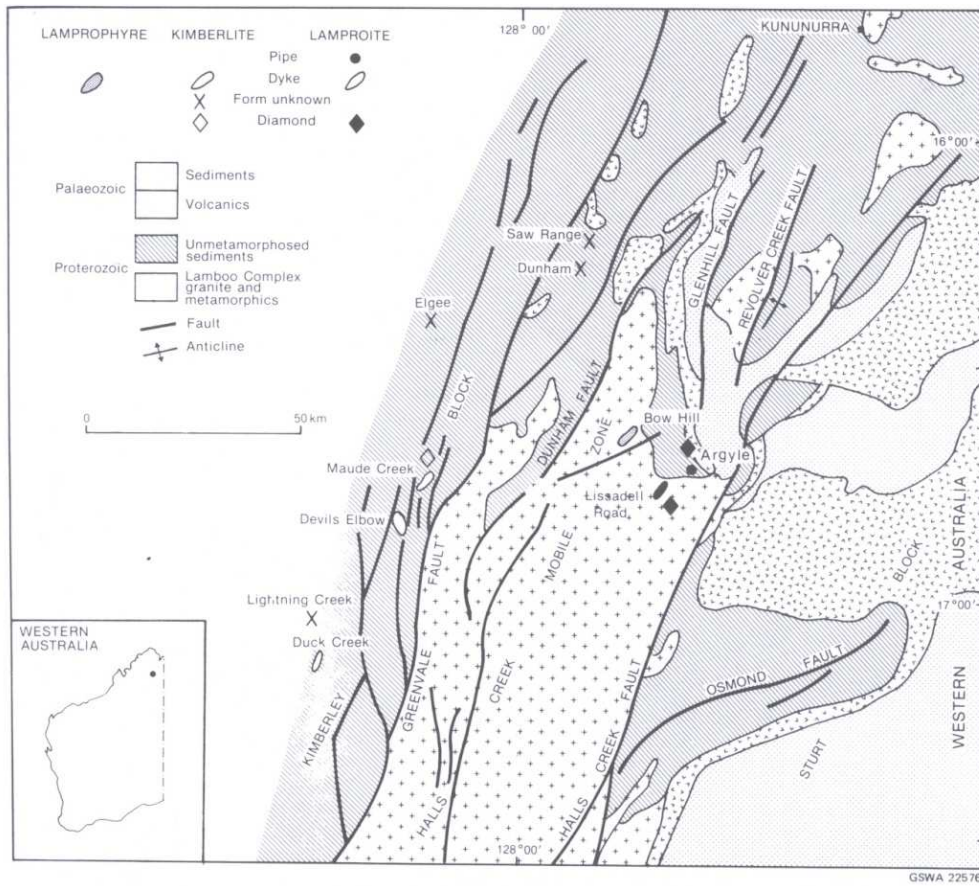


Figure 5-4: Structural controls on Diamond occurrence in the Kimberley region reproduced from Jaques et al. (1986).



**Figure 5-5: Location of kimberlites and lamproites in the East Kimberley province reproduced from Jaques et al., (1986) page 35.**

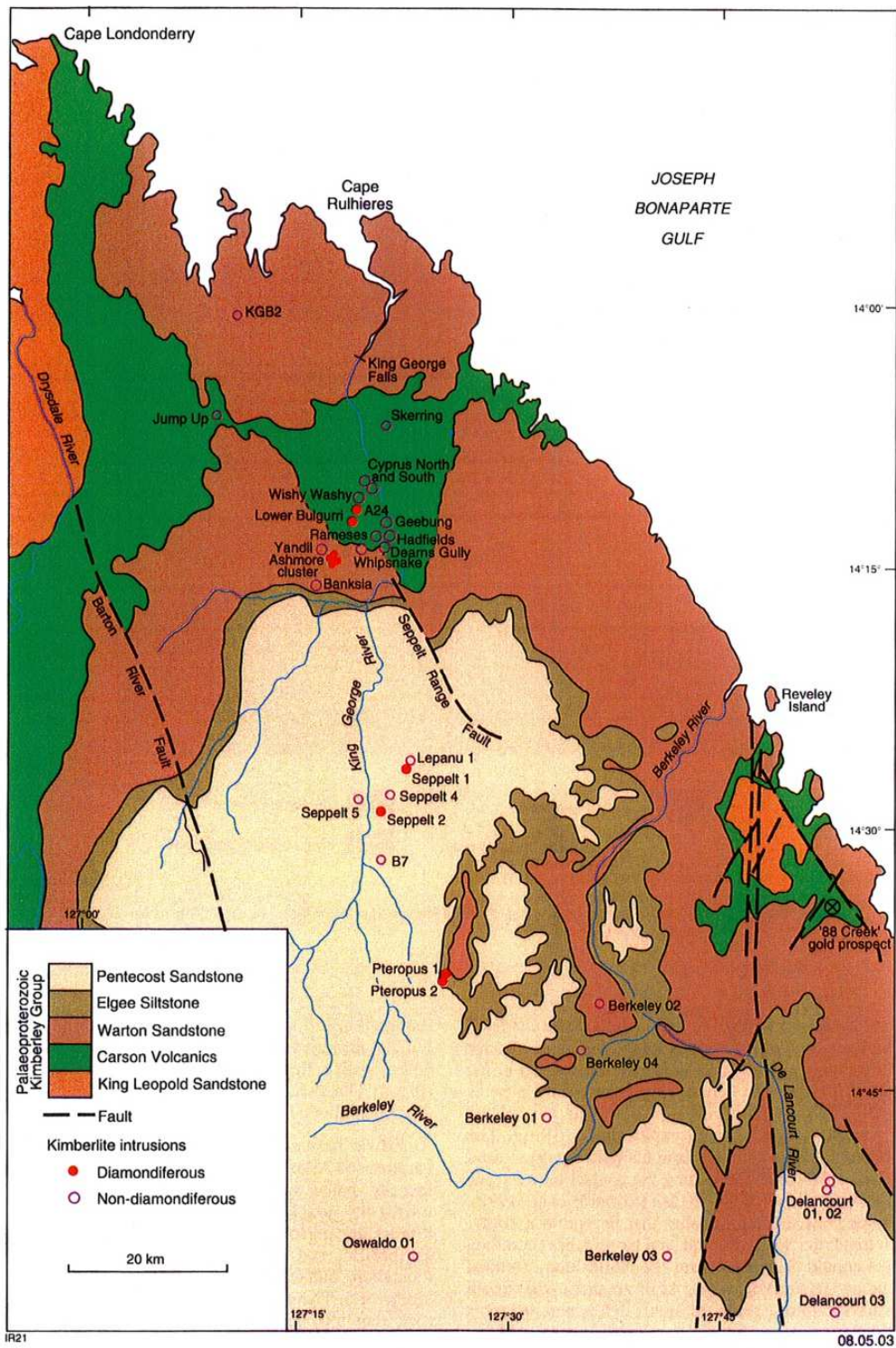


Figure 5-6: Location of kimberlites in the North Kimberley Province, showing locations of diamondiferous and non-diamondiferous kimberlite intrusions. Reproduced from Jaques (2002).

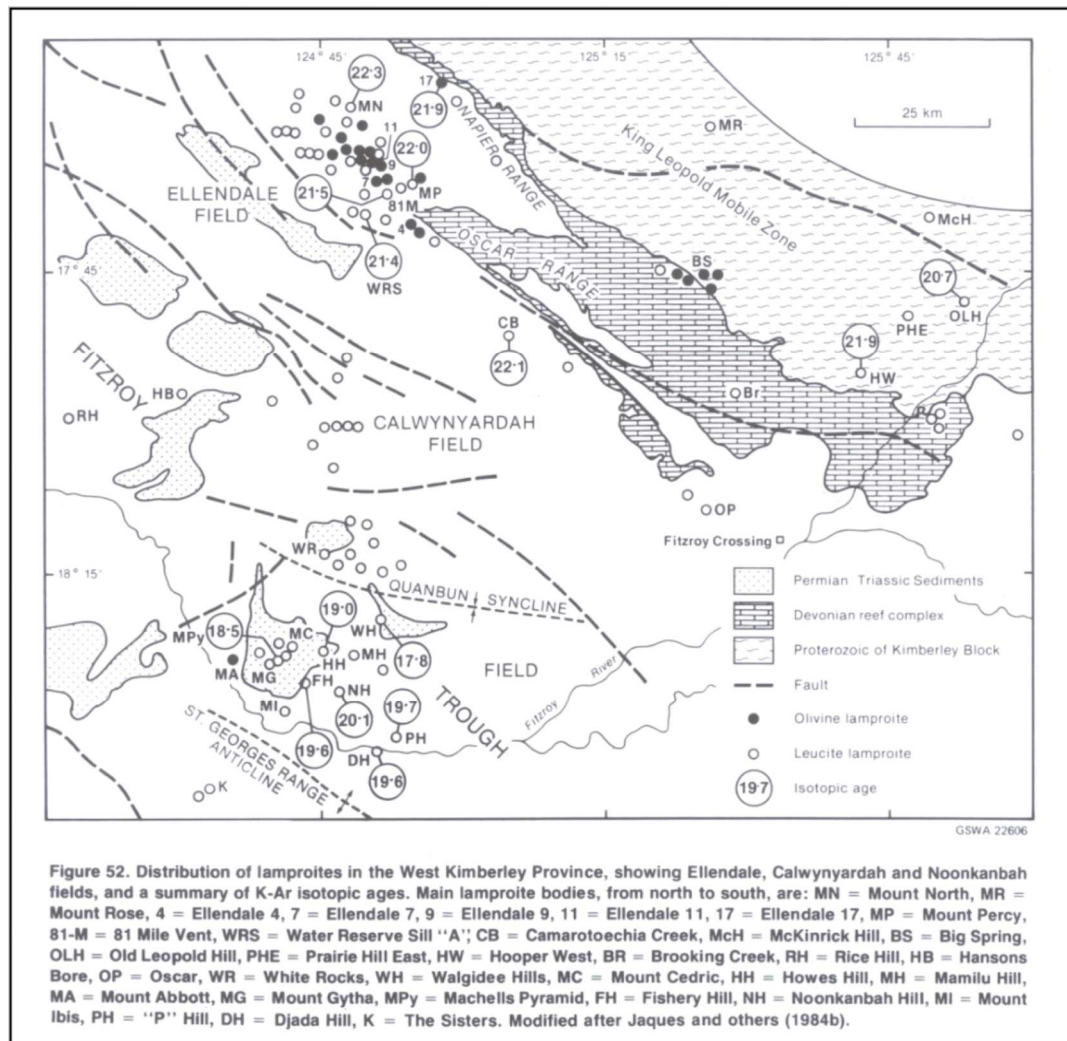


Figure 5-7: Location of lamproites in the West Kimberley province. Reproduced from Jaques et al. (1986) page 74.

## 5.2 SKIPPY seismic tomography studies

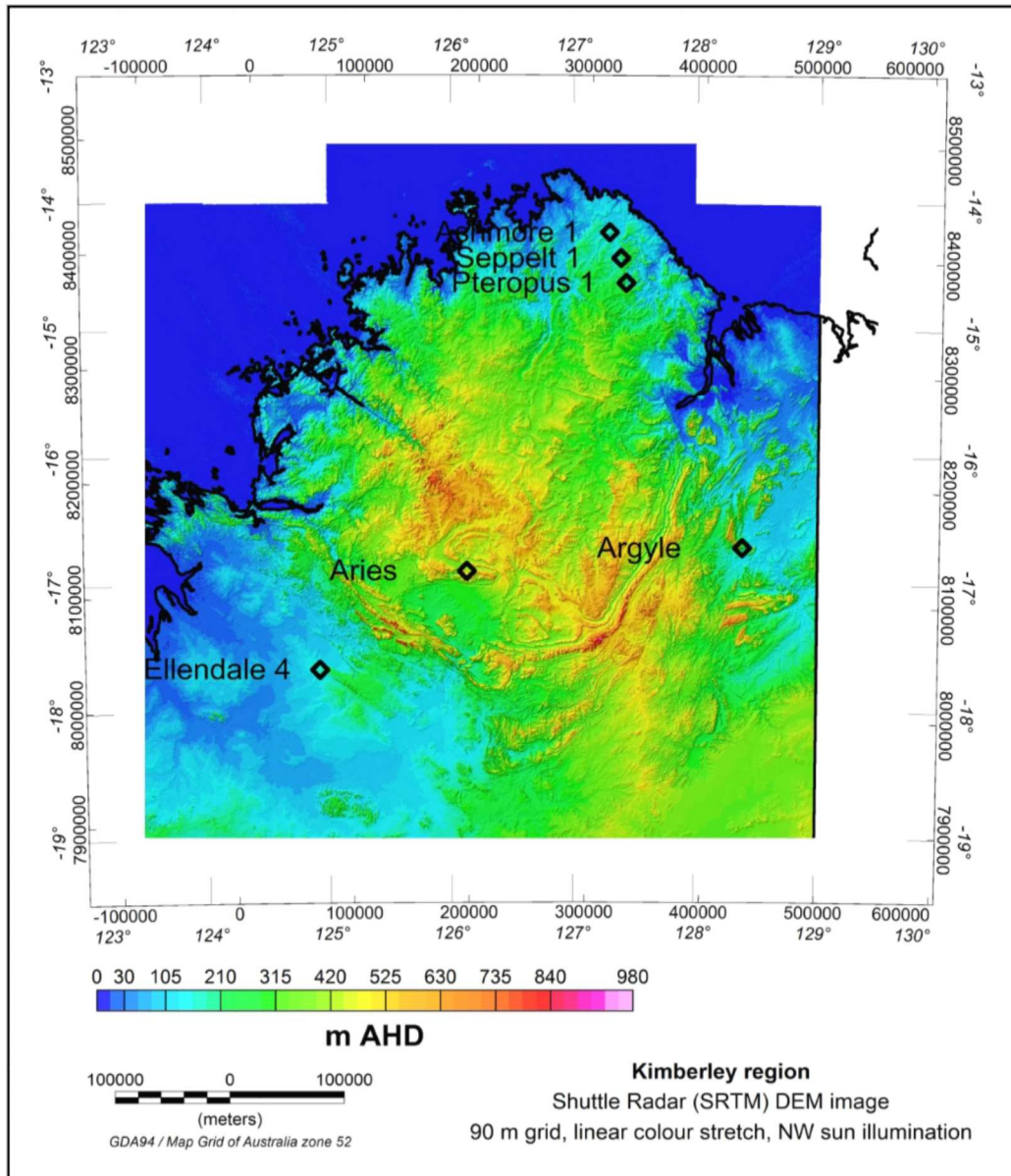
In the SKIPPY experiment from 1993 to 1996 (Van der Hilst et al., 1994) portable seismic stations were deployed across the whole continent at approximately 400 km spacing. Simons et al. (1999) present some results from Rayleigh wave studies using portable arrays of the SKIPPY project and from permanent stations from Geoscience Australia, IRIS and GEOSCOPE. These provided about 1600 source-receiver combinations and provide better coverage of the Archaean cratons of Western Australia than was previously available. Kennett (2003) summarised some results from this work. These studies show

very regional velocity distribution in the lithosphere down to about 400 km depth.

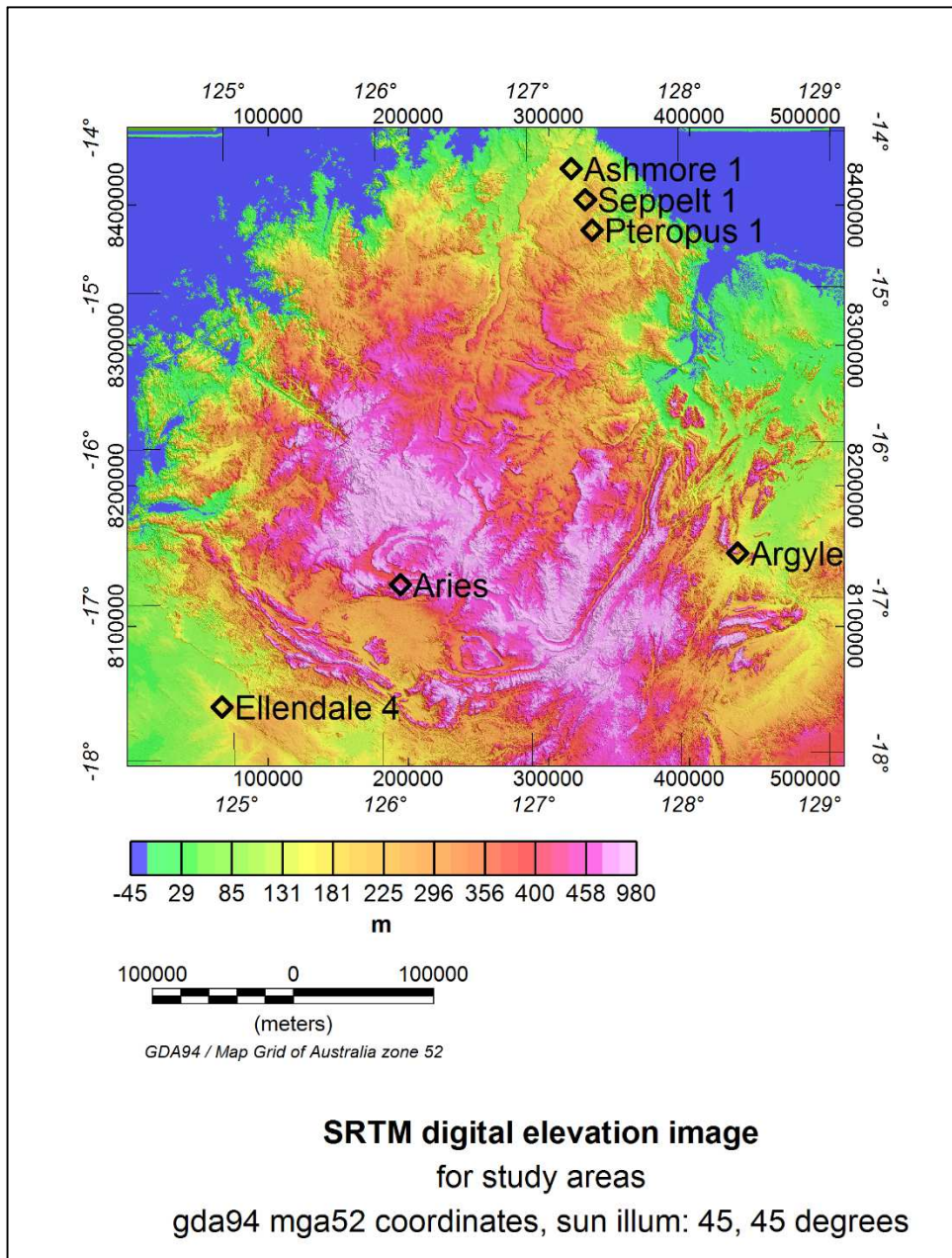
### **5.3 Digital elevation data**

Figure 5-8 shows a digital elevation image created from Shuttle Radar Topographic Mission (SRTM) data. These data are very useful for creating medium resolution digital elevation images. NASA conducted this mission on a Space Shuttle Endeavour flight in February 2000 and succeeded in one 10 day mission in mapping the Earth's surface from about 56 degrees south to 60 degrees north with a resolution of 1 second of arc – approximately 30 metres (Farr et al., 2011). This covered about 80 percent of the Earth's surface. SRTM used two synthetic aperture radar systems in the C band at 5.6 cm and the X band at 3.1 cm. The absolute accuracy of elevation data over Australia is stated by Farr et al. (2011) as 6.0 metres with a relative error of 4.7 metres. For the US, data are available with a horizontal resolution of 30 metres. For most other countries, data are available at 90 m resolution; although GA has by special arrangement acquired some data at 30 m resolution for selected parts of Australia. 90 metre data have been used to create the images shown as Figures 5-8, 5-9, 5-10 and 7-3. All of these images have been sun illuminated from the north-west.

Sun illumination has been used for many images in this thesis and helps to show more detail in the images. The illumination directions are selected to emphasis features at right angles to the illumination direction. The intensity of the image represents the degree of sun shading. The maximum intensity is shown when the local slope in the data is at right angles to the illumination direction. The colour is determined by the value of the variable being imaged e.g magnetic value or DEM value.



**Figure 5-8: Image showing locations of study pipes with regional digital elevation data for the Kimberley region using SRTM data. Sun illumination from NW with 45 degree elevation.**



**Figure 5-9: Digital elevation image for the Kimberley region using Shuttle Radar (SRTM) data with histogram equalisation colour stretch. Locations of study pipes are also shown on this image.**

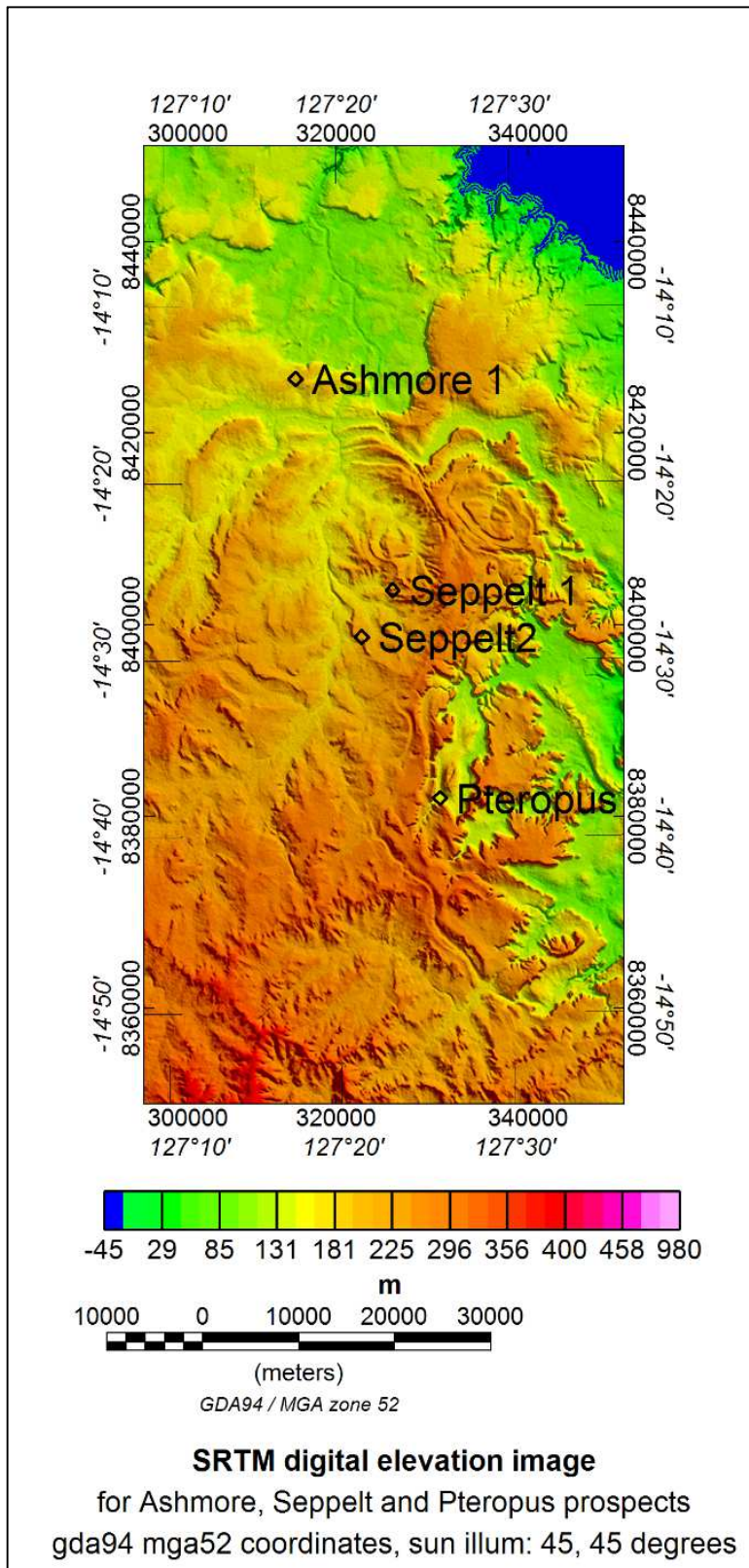


**Figure 5-10: Digital elevation image using Shuttle Radar (SRTM) data for the NE Kimberley region including the Ashmore, Seppelt and Pteropus prospects. Histogram equalisation colour stretch.**

#### **5.4 Regional aeromagnetic data**

Geoscience Australia released a 90 m gridded dataset in 2010. This resulted from a compilation of 400 m flight line spaced surveys. This grid has been used as the starting point for the regional aeromagnetic processing reported in this thesis. Figure 5-11 shows a total magnetic intensity (TMI) image for the whole of the Kimberley region. This uses a new grid produced in 2014 by the Geological Survey of WA.

Reduction to pole processing has been performed in the FFT domain using the Magmap facilities in Geosoft Oasis Montaj software and resulting images are shown as Figures 5-12 and 5-13. These include sun illumination from the north west and north east respectively. These directions have been used to highlight structural features which strike at right angles to these illumination directions.

International Geomagnetic Reference Field (IGRF) field parameters for the centre of the survey area have been used in the reduction to pole (RTP) computation as follows: For latitude of -16.0 degrees, longitude of 126.5 degrees, height of 100 metres AHD, and year 2010.5, IGRF was computed as  $F = 48789$  nT, declination = + 2.87 degrees, and inclination = - 45.63 degrees. These parameters were used in the RTP computation.

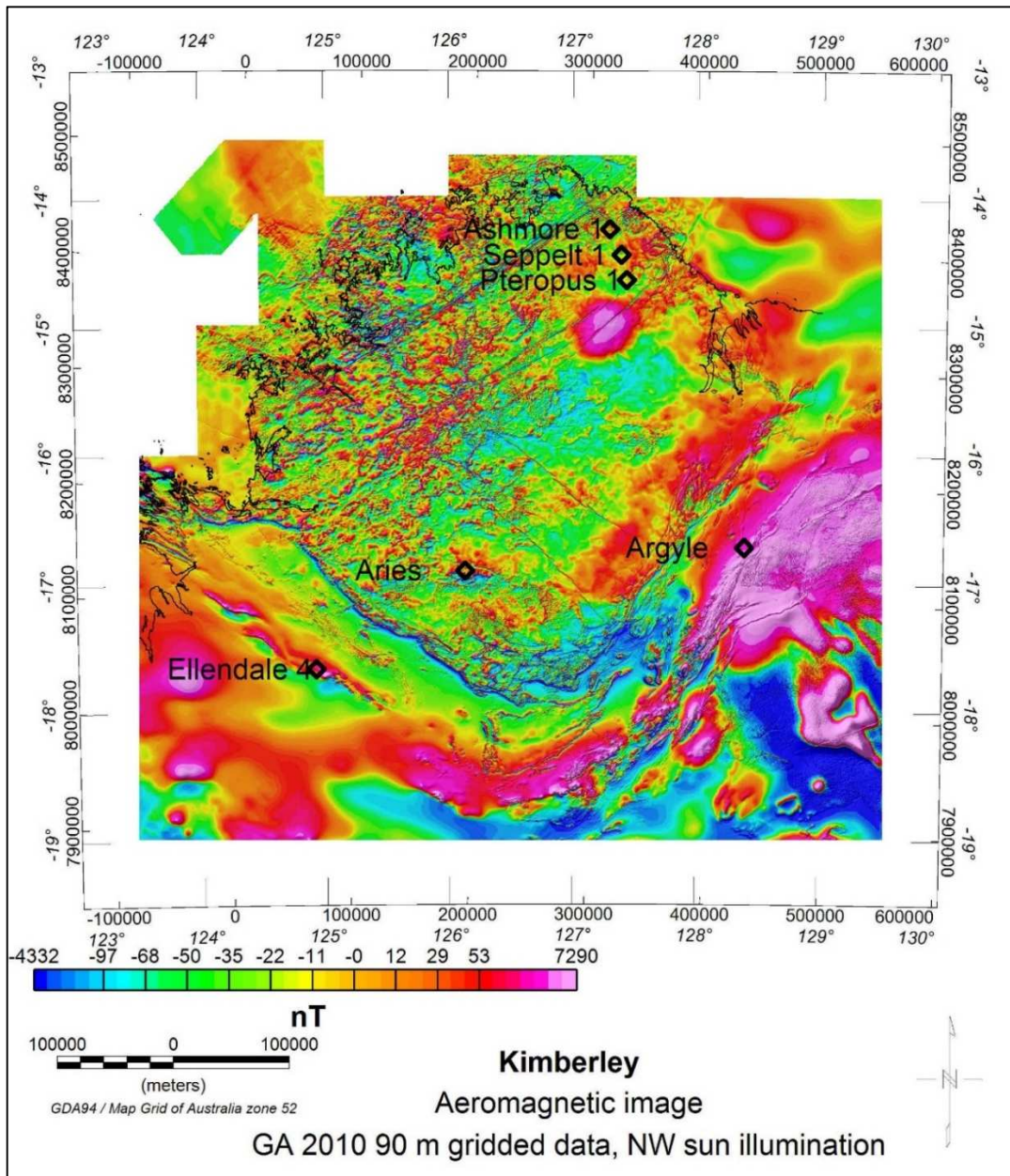


Figure 5-11: Total magnetic intensity (TMI) image for the Kimberley region using GSWA gridded data and NW sun illumination and elevation of 45 degrees.

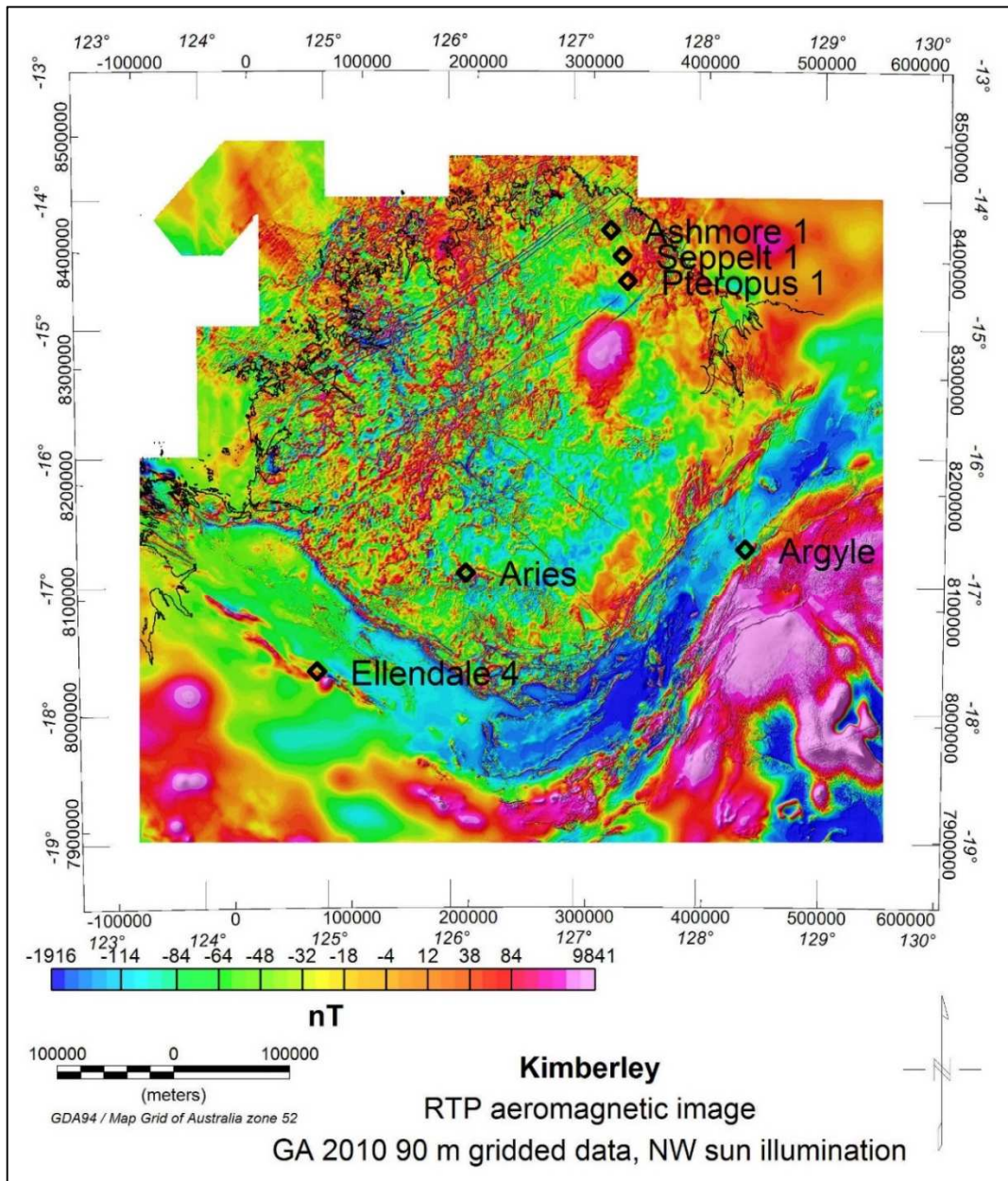
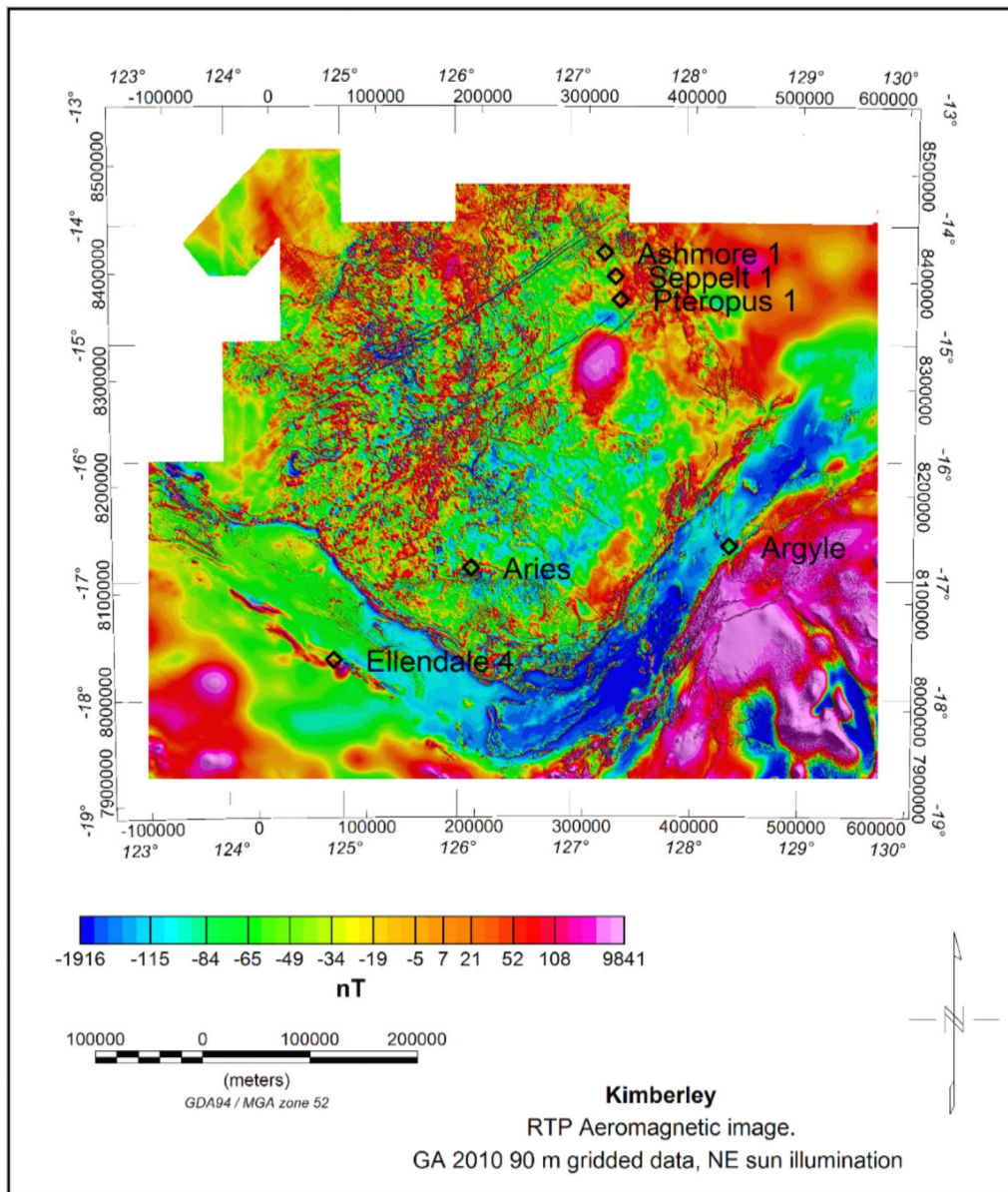


Figure 5-12 Aeromagnetic RTP image for the Kimberley region using GSWA gridded data and NW sun illumination with 45 degree elevation.



**Figure 5-13: Aeromagnetic RTP image for the Kimberley region using GSWA gridded data and NE sun illumination with 45 degree elevation.**

Gunn and Meixner (1998) published an interpretation of regional aeromagnetic and gravity data for the Kimberley region. Their summary interpretation map has been used in the construction of Figure 5-14. This has been georeferenced from their published map. The interpretation has been digitised by the author and many of the elements of their map have been included in the interpretation presented in this thesis. Small adjustments have been made to some of their

interpreted boundaries to better fit the now available RTP aeromagnetic and TMI data, and the Bouguer gravity and Isostatic Residual Gravity data. It should be noted that their 1998 interpretation used lower resolution aeromagnetic (400 metre grid) data than those used by this author (90 metre grid). The bodies interpreted from the aeromagnetic and gravity data have been numbered for convenience for discussion in the thesis and are included in some of the later maps.

This digitised interpretation has been used as the starting point for a new interpretation by the author. Additional faults have been added by digitising faults from georeferenced maps in the Argyle and Ellendale areas. Further bodies have been added particularly in the Aries and Ellendale areas. Faults have largely been mapped from the various aeromagnetic images.

Ten bodies have been mapped from a combination of the gravity and aeromagnetic data and are shown on Figures 5-15, 5-16, 5-19 and 5-21.

Body 1 is seen mainly in the gravity image Figure 5-19 and is attributed to a major dense intrusive. Some of this body coincides with outcropping mafic/ultramafic rocks (Gunn and Meixner, 1998). Argyle is located just to the north of this major gravity feature.

Body 2 is interpreted from the gravity data and is likely due to a dense intrusive. It is recognised as of higher surface elevation and shallower Moho depth

Bodies 3, 4 and 5 are interpreted from the gravity as non-magnetic granite intrusions (Gunn and Meixner, 1998)

Body 6 is a magnetic body which has been interpreted by Gunn and Meixner (1998) as a possible feeder source for the Hart dolerite

Body 7 is mainly seen in the magnetic data and is of low amplitude magnetic response. This has been attributed to granite (Gunn and Meixner, 1998). There is an area of outcropping granite shown in Figure 5-13, north east of Aries.

Body 8 is seen in the gravity image east of Seppelt 1 and is probably part of a larger dense body.

Body 9 is seen in the gravity results just west of Ellendale 4

Body 10 is seen in the gravity images east of Ellendale 4.

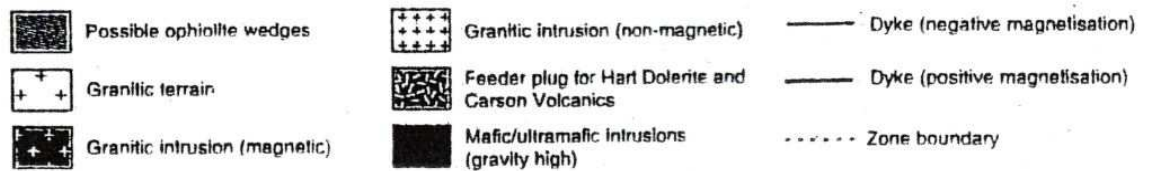
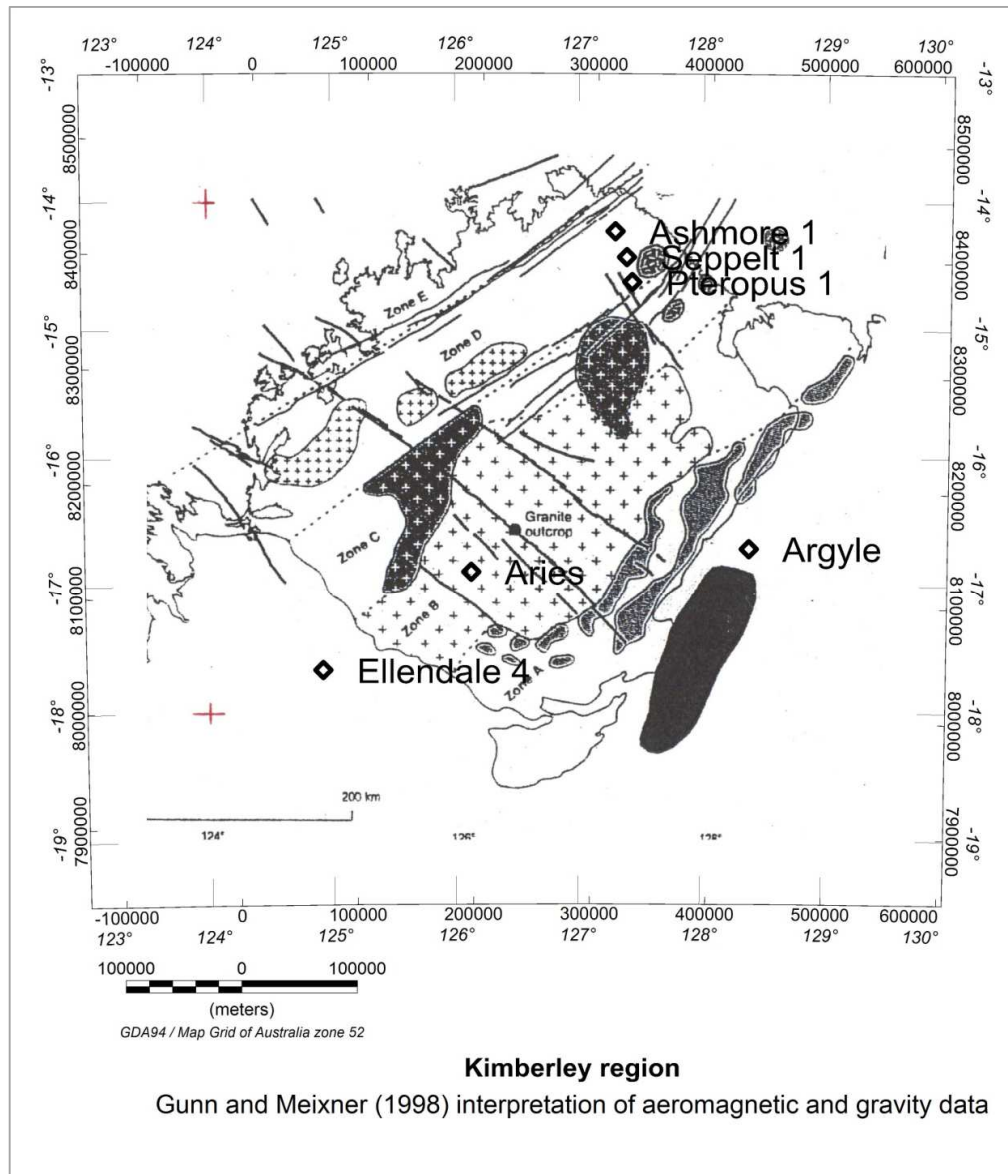


**Figure 5-14: Regional aeromagnetic and gravity interpretation by Gunn and Meixner (1998) with locations added for Argyle, Aries, Ashmore, Ellendale, Pteropus and Seppelt.**

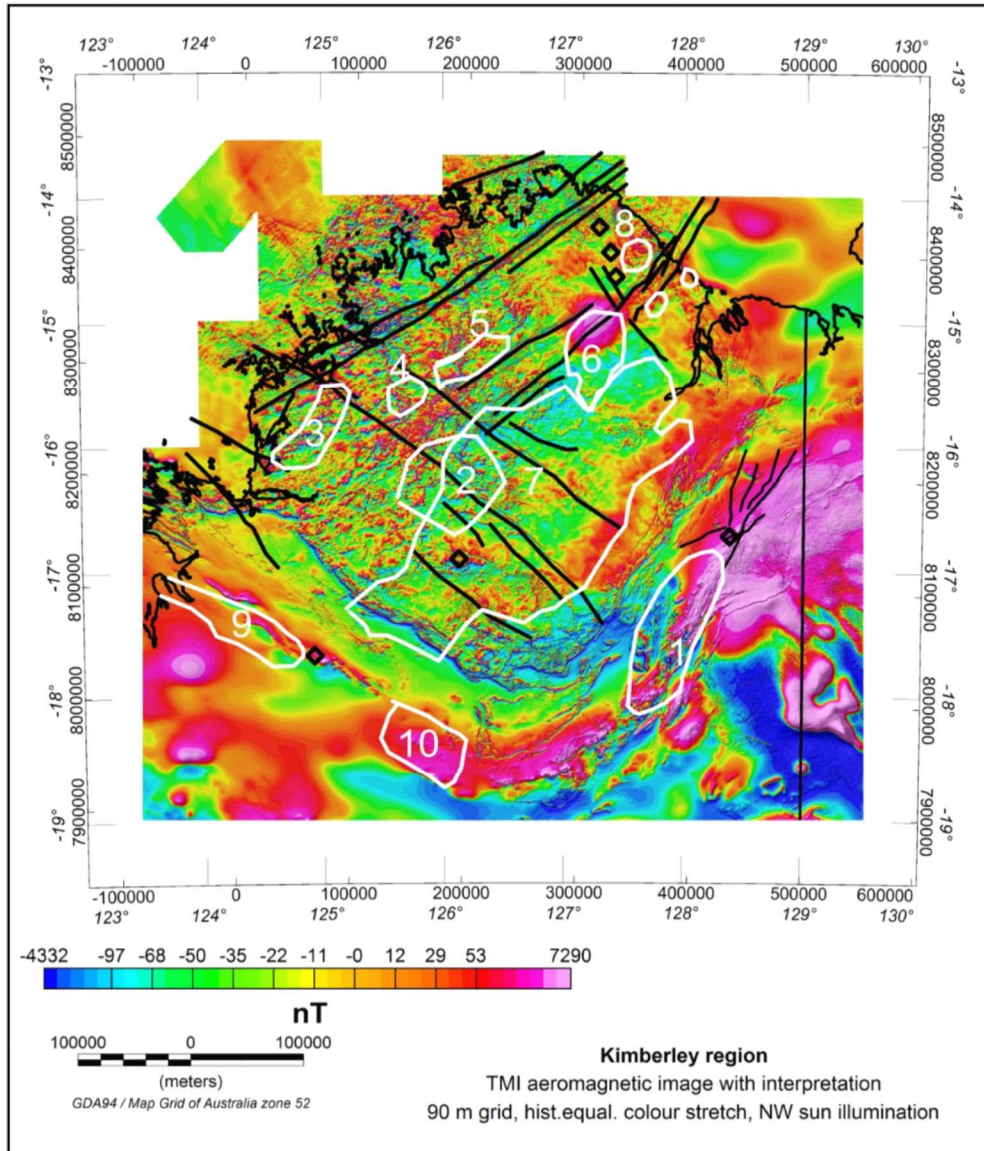


**Figure 5-15: Total magnetic intensity (TMI) image with regional aeromagnetic and gravity interpretation for the Kimberley region. The white polygons show the major units interpreted from this study. This is an extension of the interpretation of Gunn and Meixner (1998). Sun illumination from NW with 45 degree elevation.**

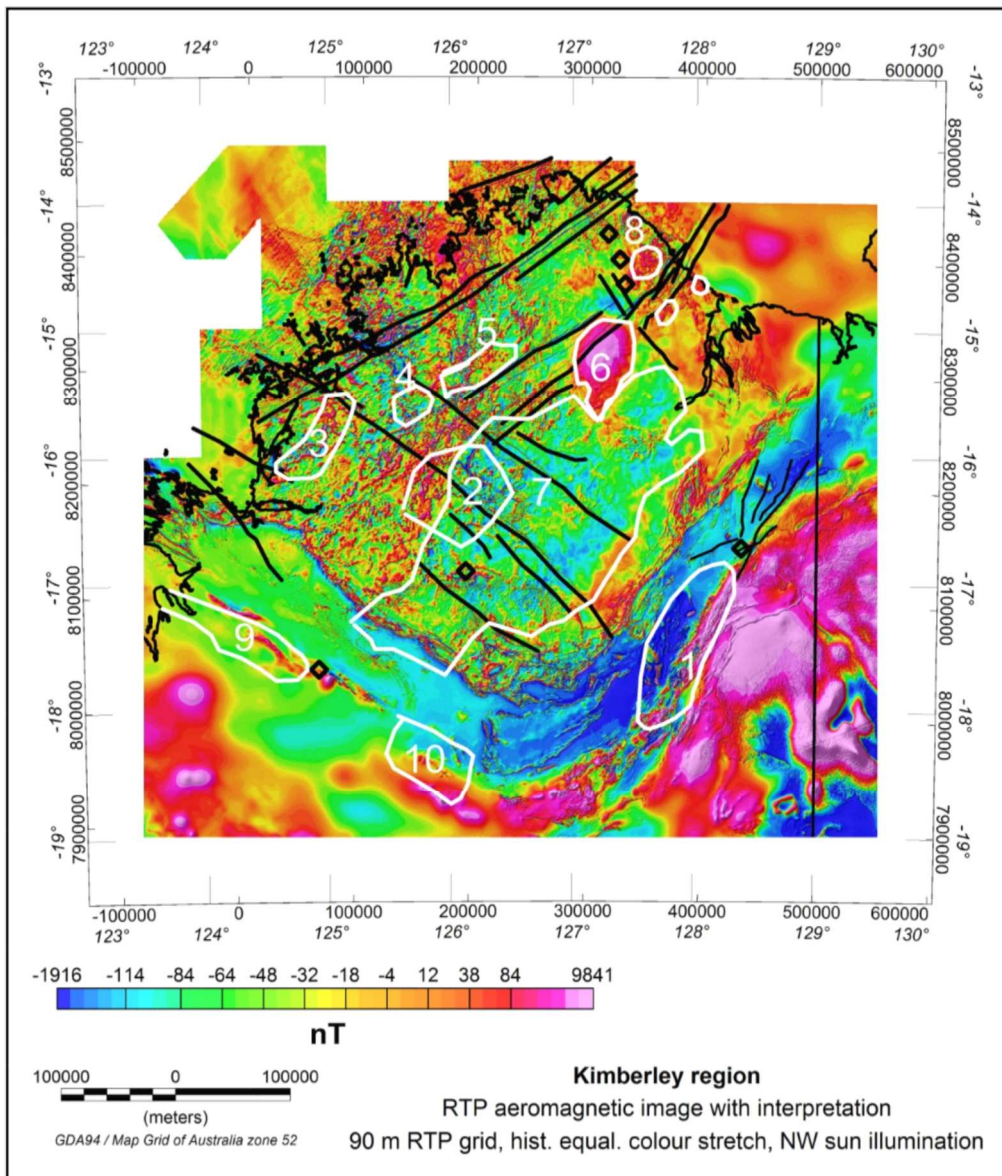


**Figure 5-16: RTP aeromagnetic image with regional aeromagnetic and gravity interpretation for the Kimberley region. The white polygons show the major units interpreted from this study. This is an extension of the interpretation of Gunn and Meixner (1998). Sun illumination from NW with 45 degree elevation.**

## 5.5 Regional gravity data

Data from Geoscience Australia's very extensive gravity database have been downloaded by the author as the starting point for processing and interpreting regional gravity data. Figure 5-17 shows a gridded version of the spherical cap Bouguer gravity data for a density of 2.67 g/cc. This figure uses sun illumination from the north west. This is optimum to highlight features at 90

degrees to this direction i.e north east strike. The author has also used north east and north illumination directions in some of the images used in this study. North east illumination highlights features with north west strike and north illumination treats both north west and north east striking features equally.

The GA gravity stations used are shown in Figure 5-18. For most of the Kimberley Block the station spacing is approximately 11 x 11 km. This is supplemented by long road traverses with station spacing of about 400 metres. Close to Ellendale 4, data spacing along traverses is about 800 metres. This is too wide to see gravity response from the Ellendale 4 lamproite pipe directly.

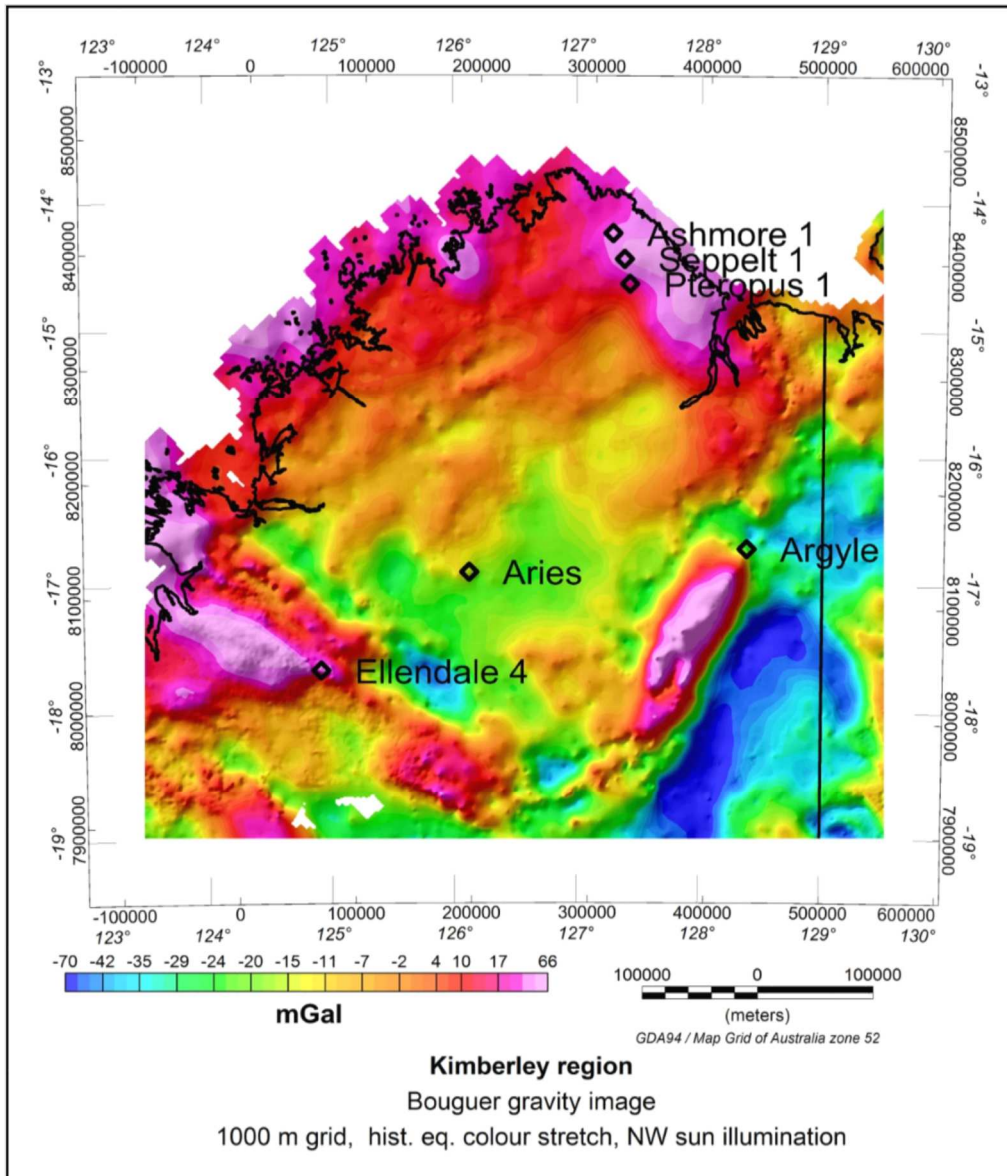


**Figure 5-17: Bouguer Anomaly image for Kimberley region using GA datasets. Density used is 2.67 g/cc. All of the studied pipes are located close to major gradients in the Bouguer gravity image. Sun illumination from NW with 45 degree elevation.**

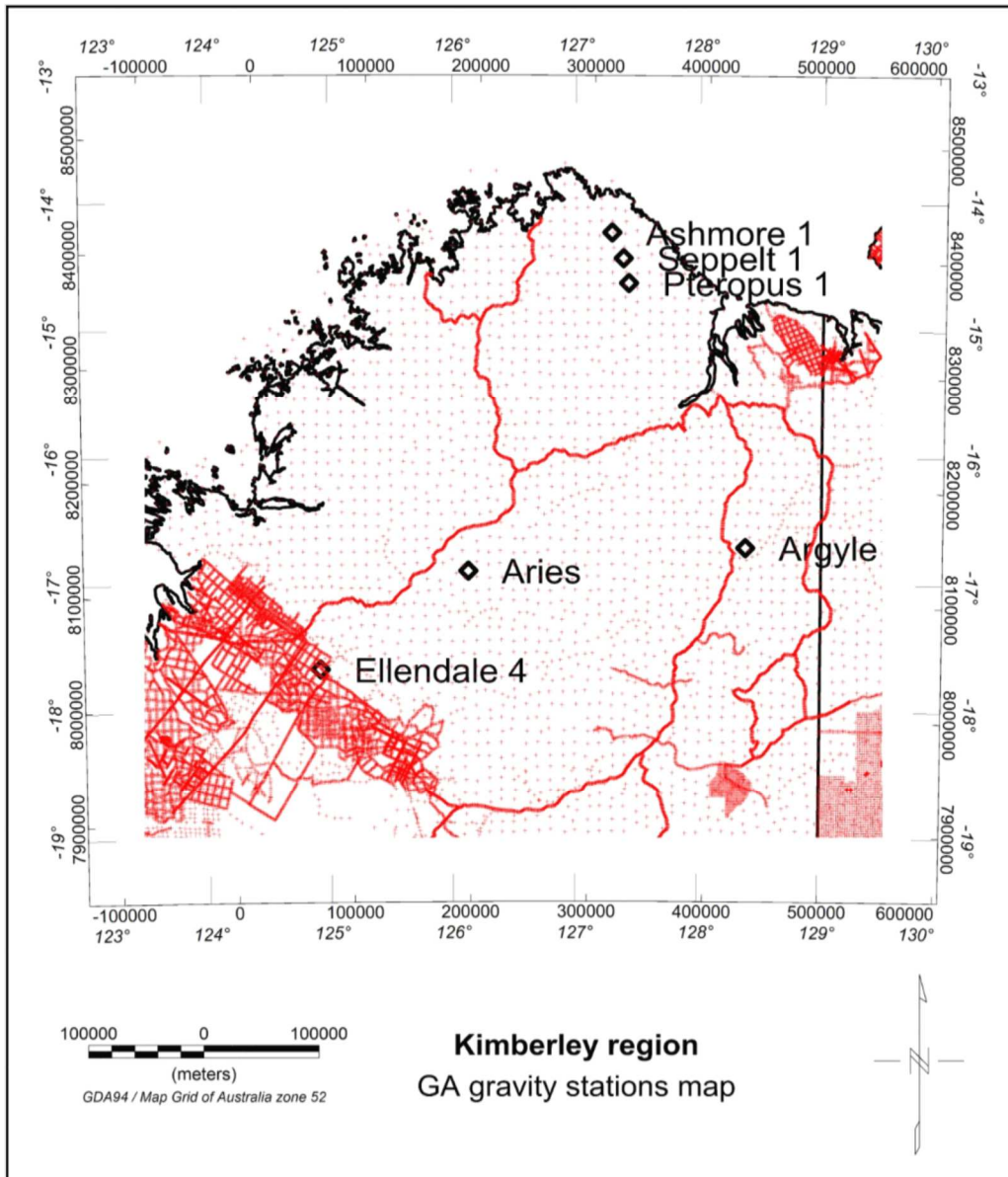


**Figure 5-18: GA gravity stations map for Kimberley region. This shows a regular 11 x 11 km coverage supplemented by road traverses with approx. 400 m station spacing and 800 m spaced traverses and stations close to Ellendale.**

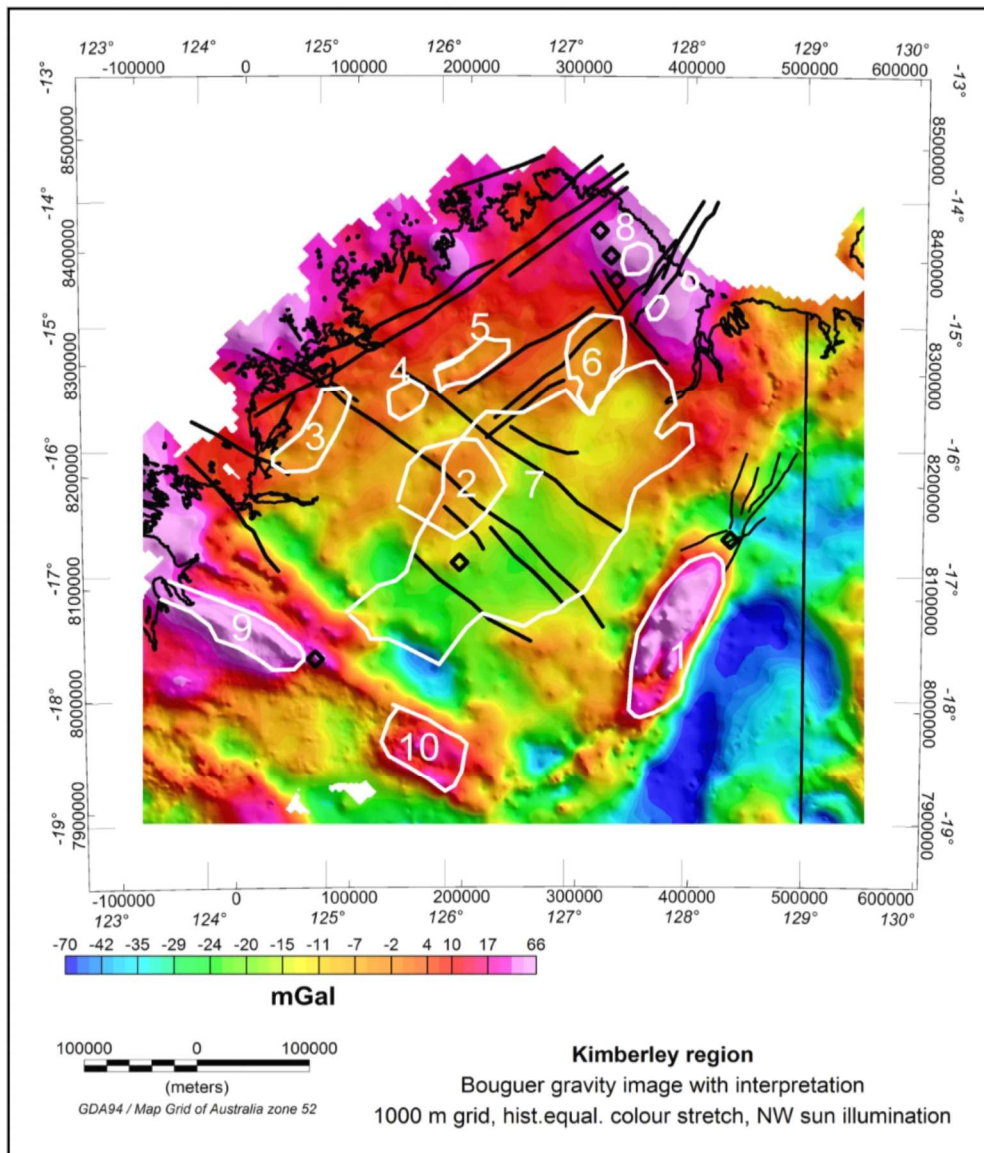


**Figure 5-19: Bouguer gravity image with regional interpretation** The white polygons show the major units interpreted from this study. This is an extension of the interpretation of Gunn and Meixner (1998). Sun illumination from NW with 45 degree elevation.

## 5.6 Regional airborne radiometric data

Airborne radiometric data are often acquired at the same time as aeromagnetic data from airborne geophysical surveys. Data are usually acquired every one second which corresponds to 50 – 65 metres on the ground. Gamma radioactivity is due to the various members of the Potassium 40, Uranium 238 and Thorium 232 decay series. The data are processed with corrections for

background, cosmic, height and channel interactions to produce data in percentage Potassium and ppm for Uranium and Thorium. Radioactivity is measured from the top 50 cm of the ground surface and is useful in geological and soil mapping. A convenient way to display the data is to create a colour composite RGB image for Potassium, Uranium and Thorium in that order. Sometimes total count data are included as the intensity part of the image. Figure 5-20 shows this image for the Kimberley region using 100 metre gridded data supplied by the NT Geological Survey (NTGS). This shows a wealth of detail and relates well to surface geology and soils. Figure 5-21 shows the same image but with the elements of the potential field interpretation superimposed.

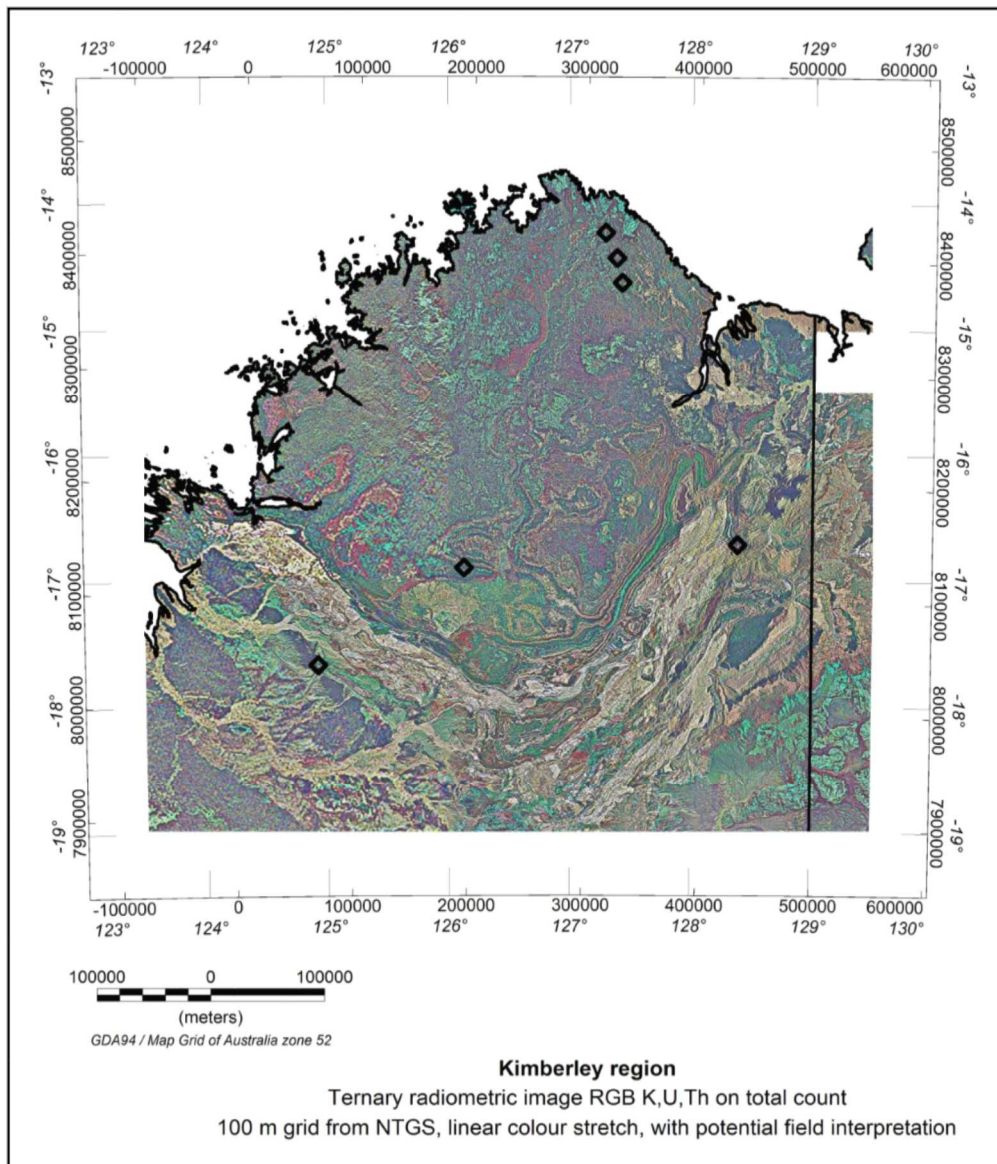


**Figure 5-20: Kimberley region ternary radiometric image RGB for K, U, Th on total count. 100 metre gridded data from NT Geological Survey. Locations of the study kimberlites and lamproites are shown with black symbols. The radiometric image is useful for assisting surface geological mapping.**

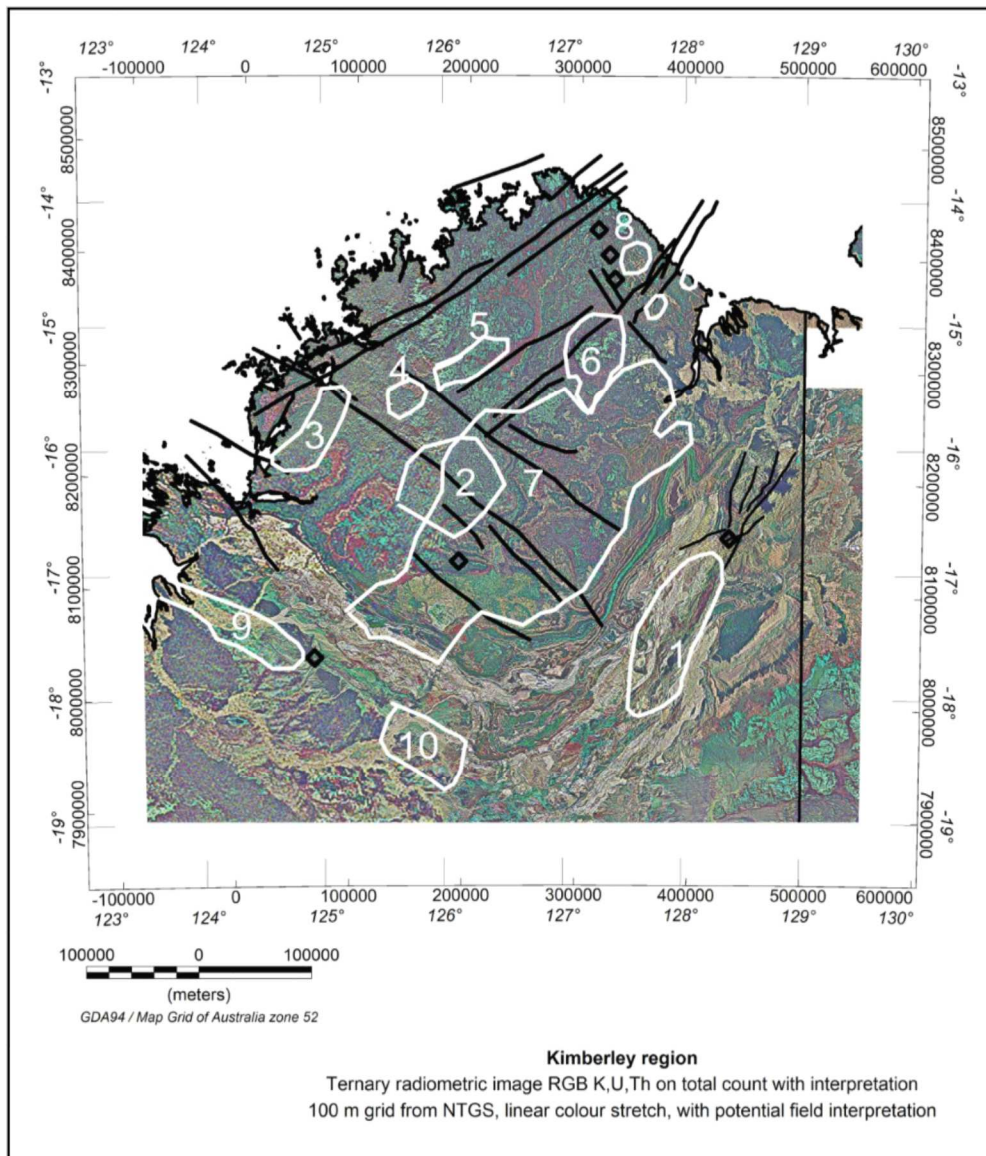


**Figure 5-21: Kimberley region. RGB radiometric image with regional aeromagnetic and gravity interpretation. The white polygons show the major units interpreted from this study. This is an extension of the interpretation of Gunn and Meixner (1998).**

## 5.7 Structures at cratonic scale

The location of kimberlites and lamproites are likely to be structurally controlled by faults or deep seated lines of crustal weakness, and it is important to locate cratonic scale structures as part of the exploration process. Seven topics have been investigated here:

1. Reconstructions of Rodinia between 1300 Ma and 750 Ma
2. Moho geometry
3. Isostatic Residual Gravity
4. Euler deconvolution mapping in 3D
5. Total horizontal gradient of upward continued reduced to pole aeromagnetic data
6. Multiscale edge detection using “worming” of aeromagnetic and gravity data
7. Texture analysis and detection of lineations

### **5.7.1 Reconstructions of Rodinia.**

Li et al (2008) have published a synthesis on the assembly, configuration and break-up of Rodinia. The reconstruction of Rodinia shows that the various continents were clustered around Laurentia in the centre. Extensive use has been made of polar wander curves from paleomagnetic studies and comparisons of the geology of possibly formerly adjacent continents.

Rodinia was assembled between 1300 Ma and 900 Ma and included virtually all the currently known continental blocks. Rodinia lasted a further 150 Ma before breaking up and going on to form Gondwanaland.

Figures 5-22 and 5-23 show postulated reconstructions of Rodinia at six intervals from 1100 Ma to 780 Ma. Further detail showing the progressive evolution at 5 Ma intervals, is shown in a powerpoint file assembled by Li et al (2008) and can be viewed as a continuous movie at: <http://www.sciencedirect.com/science/article/pii/S0301926807001635>

Figures 5-22 and 5-23 show that Australia has moved over very large distances during the life of Rodinia and has at times been close to areas of active rifting.

The pipes at Aries, Ashmore, Seppelt and Pteropus have ages of emplacement between 820 Ma and 800 Ma. This time period corresponds to major rifting and movement of Rodinia which may have been significant to the emplacement of these Kimberlite bodies. Major mantle plumes have been interpreted at about

825 Ma, 800 Ma and 780 Ma. (Li et al, 2007). These ages are very close to the measured Pb-U ages for Aries (820 +/- 20 Ma) and the emplacements at Ashmore, Seppelt and Pteropus which have all been dated at about 800 Ma. The reconstruction for 825 Ma shows Australia at about 60 degrees north and located above a mantle plume (labelled as a superplume in Figure 5-23). The 825 Ma superplume event was followed by continental rifting. NW Australia is shown on the outside of the aggregated land masses and NW Australia is shown to be adjacent to open sea.

Schissel and Smail (2001) have summarised work on earth structure, ore deposits and mantle plumes. The association of kimberlite emplacement with mantle plumes is controversial but is a very active research area and is one of the favoured mechanisms relating to kimberlite emplacement.

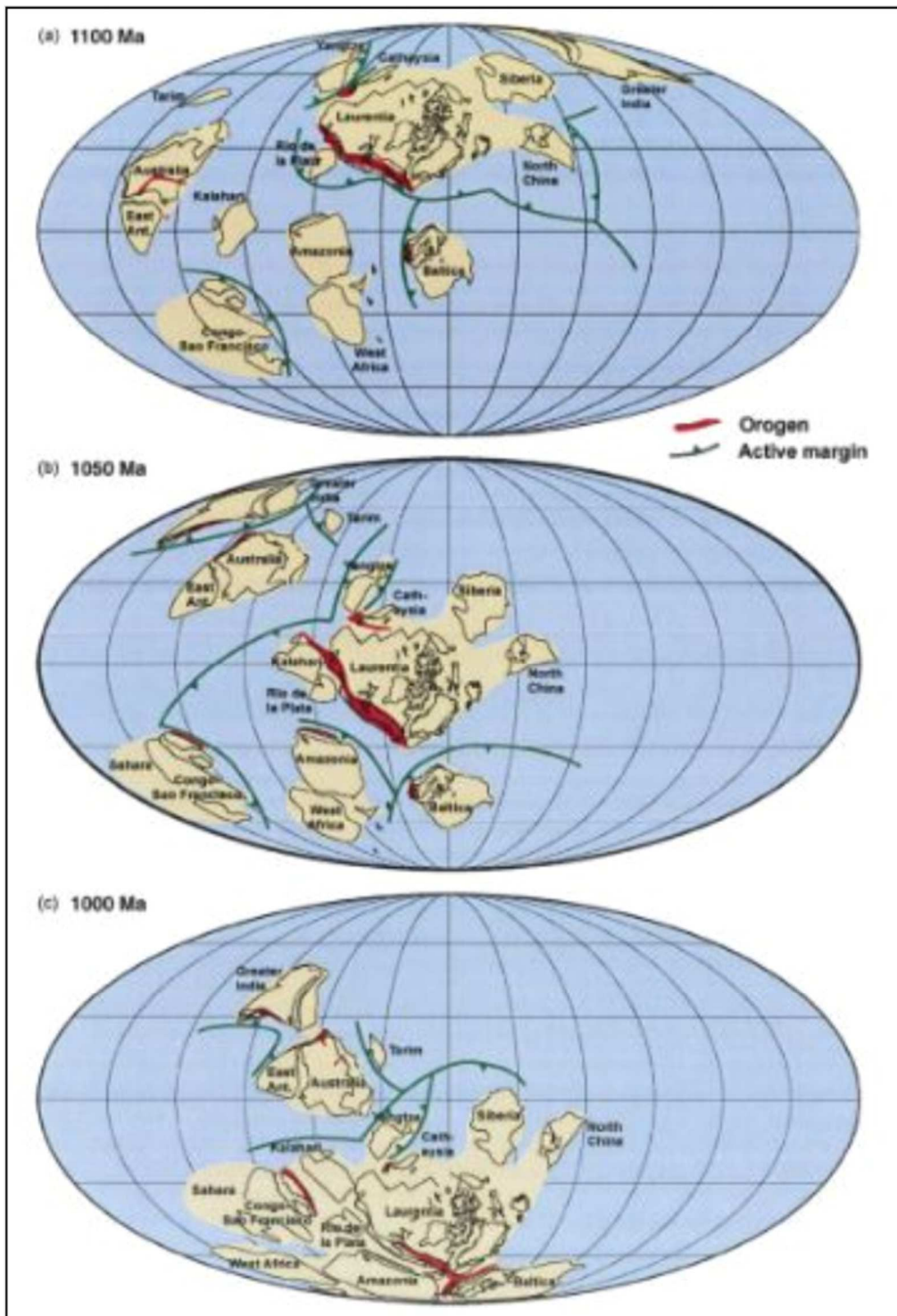


Figure 5-22: Reconstructions of Rodinia from 1100 Ma to 1000 Ma, after Li et al (2008)

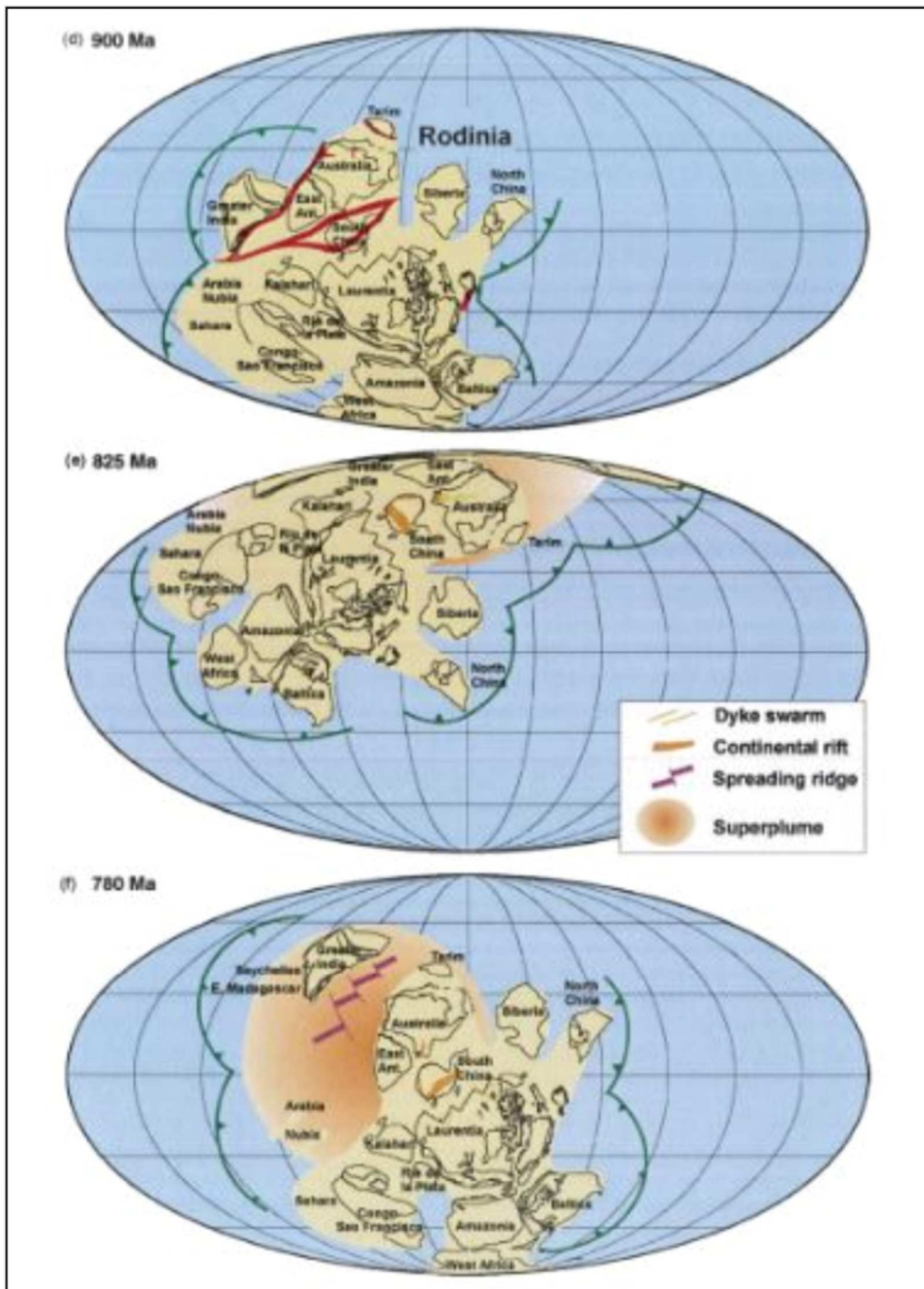
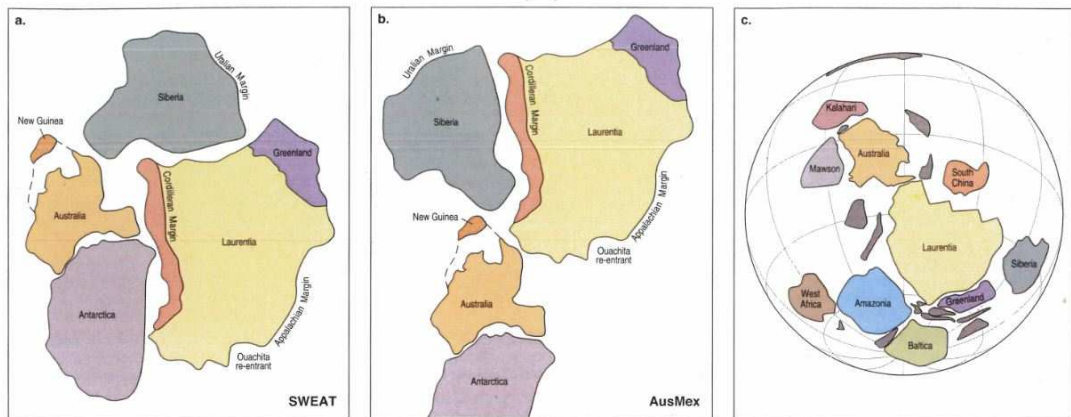


Figure 5-23: Reconstructions of Rodinia from 900 Ma to 750 Ma, after Li et al (2008)

There are many other reconstructions of Rodinia in the literature and some variations are shown in Figure 5-24.



**Figure 5-24: Alternative reconstructions of Rodinia, Blewett (2012)**

- a. SWEAT: South West US and East Antarctica. Hoffman (1991)
- b. AusMex: Australia – Mexico. (Wingate et al (2002)
- c. Modified AusMex. Pisarevski et al, (2003)

### 5.7.2 Mohorovicic discontinuity geometry

Aitken (2010) presented results of a Mohorovicic discontinuity (Moho) geometry gravity inversion experiment named MoGGIE which produced a new model for the Australian Moho. The Moho is a close equivalent to the crust-mantle boundary. His model consisted of six layers:

ocean, sedimentary basins, upper crust, lower crust, eclogitised crust and mantle.

The model covers 4695 x 3825 km with 15 x 15 km vertical prisms extending down to 99 km. Aitken computed the initial Moho surface by Delaunay triangulation using 230 estimates of crustal thickness from seismic reflection and refraction data (Collins, 1991). Three-dimensional gravity inversion used VPmg software (Fullagar et al, 2008). This uses density optimisation and geometry optimisation independently.

The MoGGIE experiment used inversion of free-air gravity data and honoured seismic constraints, where available. Aitken (2010) has produced a text file for the Moho depth over the whole continent at 15 x 15 km intervals. This includes:

depth to Moho, depth to top of upper crust, depth to top of lower crust and depth to top of eclogite layer.

Data for the Kimberley and surrounding region have been extracted for these surfaces by the author and also converted to MGA 52 coordinates.

Depth to Moho is shown in Figure 5-25 which includes Moho depth contours with 1 km intervals and locations of the six diamond deposits of Argyle, Aries, Ashmore 1, Ellendale 4, Pteropus 1 and Seppelt 1. Figure 5-26 shows the magnitude of the slope (in degrees) of the Moho surface. This shows slopes in the range 0 to 30 degrees. Figure 5-27 shows a 3D image of the top of the Moho surface together with a surface digital elevation image using Shuttle Radar Topographic Mission data and the locations of six selected diamond occurrences.

From Figures 5-25, 5-26 and 5-27, it can be seen that the diamond occurrences are located close to increases in slope of the Moho surface. Typical maximum gradients close to these occurrences are in the range 0.2 to 0.4 vertical km per horizontal km. This represents local slopes in the range 12 to 24 degrees. These areas of locally steeper gradients are offset, within about 15 km, from the diamond occurrences. Slopes at the occurrences are tabulated below together with Moho depths. It is interpreted by the author that areas of marked change in slope of the Moho surface are areas favourable for kimberlite and lamproite intrusions.

Depths and slopes of the Moho surface have been computed from the Moho depth and slope grids (15 x 15 km) as follows:

Argyle: 43.1 km, slope 3.0 degrees

Aries: 40.0 km, slope 1.8 degrees

Ashmore 1: 34.7 km, slope 3.9 degrees

Ellendale 4: 33.7 km, slope 4.5 degrees

Pteropus 1: 35.1 km, slope 7.9 degrees

Seppelt 1: 34.8 km, slope 6.0 degrees

Symonds et al (1994) estimated a crustal thickness for the Kimberley Block, of 30 – 35 km comprising three layers;

- Upper layer 10 km thick with seismic velocity of 5.8 km/s
- Basement layer up to 13 km thick with velocity of 6.2 km/s
- Lower crustal layer 12 km thick with velocities 6.8 – 7.4 km/s

These total depths of 30 - 35 km from Symonds et al (1994) are similar to those computed by Aitken (2010) but much more data were available for the Aitken compilation.

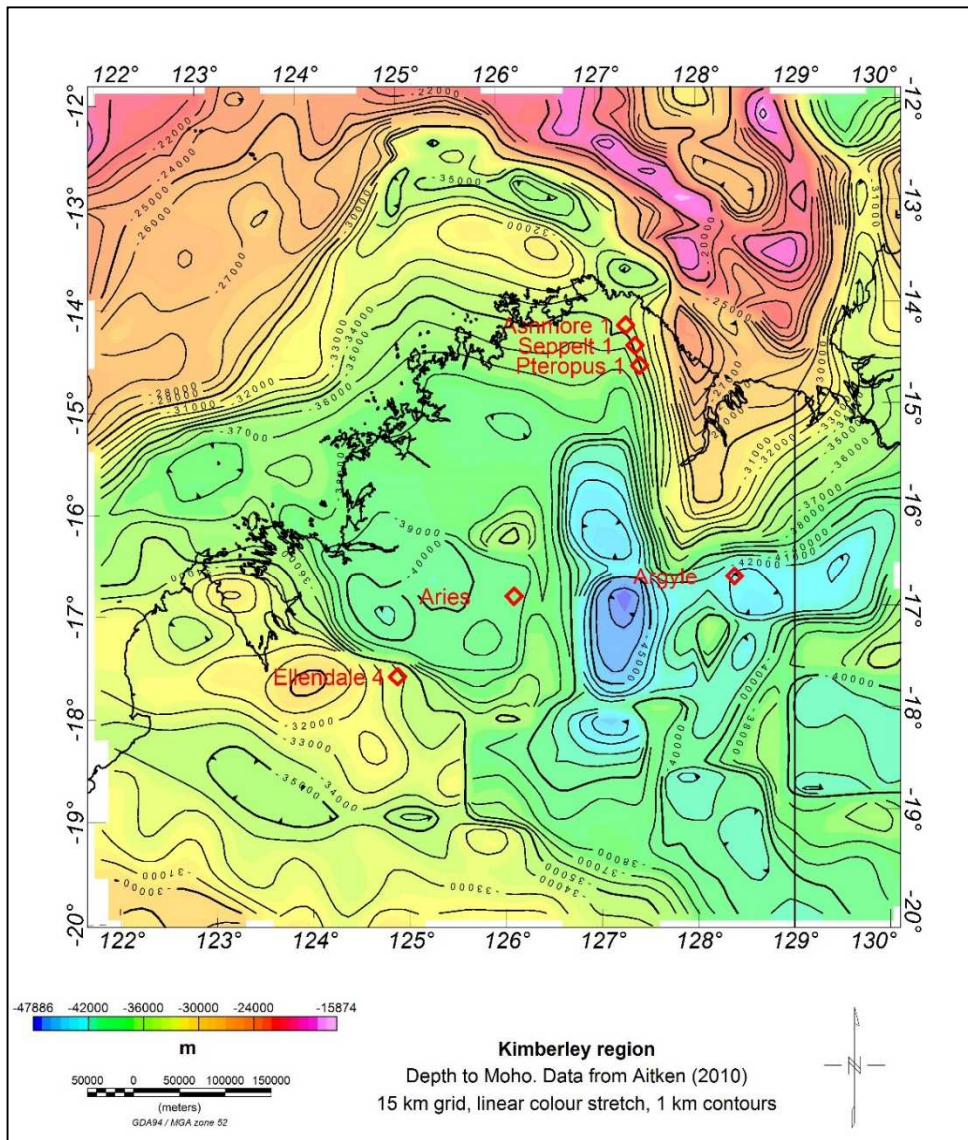


**Figure 5-25: Depth to Moho for the Kimberley Block and surrounding region. Computed from data supplied by Aitken (2010). All the study pipes are located close to marked changes in slope of the Moho surface.**

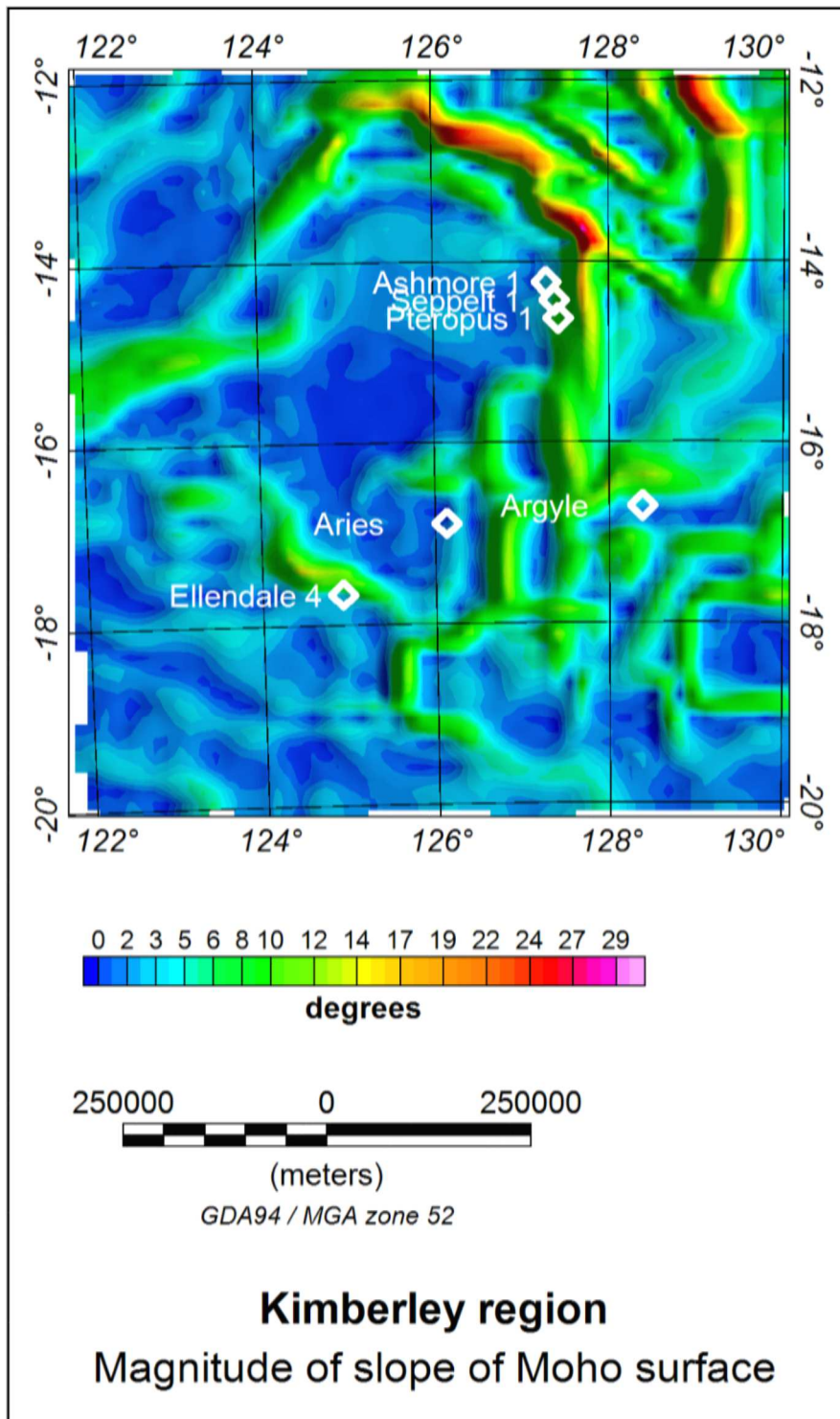


**Figure 5-26: Magnitude of slope (in degrees) of Moho surface. All the study pipes are located close to marked changes in slope of the Moho surface. Image has been sun illuminated from the east with 45 degree elevation.**

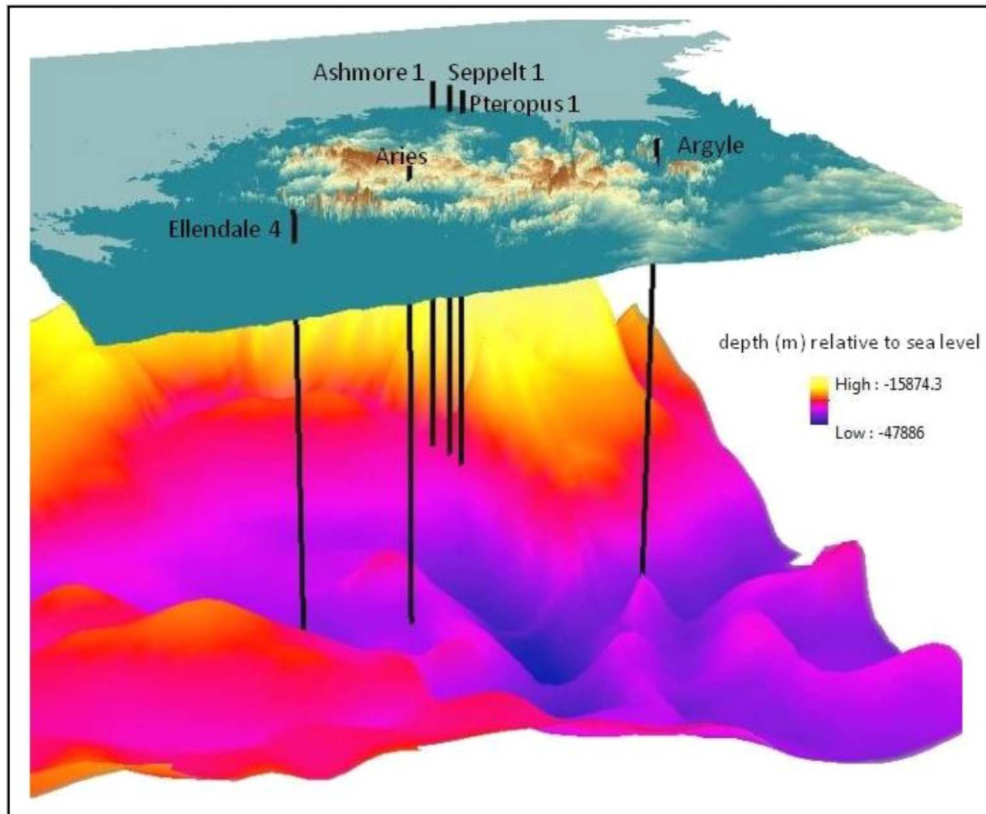


**Figure 5-27: 3D view of Moho surface. Top surface is digital elevation data from Shuttle Radar Topographic Mission (SRTM) data. The six vertical black lines shows the Argyle, Aries, Ashmore, Ellendale 4, Pteropus and Seppelt pipes projected vertically down from known positions at surface. Moho depth scale is in metres relative to sea level. All the study pipes are located close to marked changes in slope of the Moho surface.**

### **5.7.3 Isostatic Residual Gravity**

Lockwood (2004) computed an Isostatic Residual Gravity grid for Western Australia. Part of this grid that covers the Kimberley region of WA has been extracted, in this study, and converted from latitude and longitude geographic coordinates to GDA 94 MGA zone 52 coordinates. A vertical gradient image has also been computed for the Kimberley region. Two images are included here as Figures 5-28 and 5-29. The Isostatic Residual Gravity computation used a modified Airey method, and allows for variations in depth to the mantle from onshore topography. Offshore, the computation also compensates for sea water depth. Both images have been sun illuminated from the north and histogram equalisation has been used in the colour display. The locations of diamond

deposits Argyle, Aries, Ashmore, Ellendale 4, Seppelt 1 and Pteropus 1 have also been included. Figure 5-28 shows that all six of these deposits referred are located on the flanks of major Isostatic Residual Gravity high features.

The vertical gradient of the Isostatic Residual Gravity provides further more detailed resolution of gravity anomalies and it is seen that Aries is also located on a small closure in the gradient image. This image is helpful in identifying further prospective structural areas for diamond search.

The amplitude of the Analytic Signal, sometimes referred to as the total gradient, has also been calculated for the Isostatic Residual Gravity and this image is shown as Figure 5-32. The amplitude of the analytic signal is calculated using this equation:

$$\text{Amplitude of Analytic Signal} = \{ (dI/dx)^2 + (dI/dy)^2 + (dI/dz)^2 \}^{0.5} \quad \text{. eqn 5.1}$$

where I is Isostatic Residual Gravity and the derivative terms are the gradients of this variable in the east, north and vertical directions. It can be seen that the Analytic Signal provides good definition of the gradients present in the Isostatic Residual Gravity data. The above equation 5.1 is adapted from Roest et al (1992) who developed it for magnetic interpretation.

#### **5.7.4 Euler deconvolution**

Euler deconvolution has been widely used in aeromagnetic and gravity interpretation because it requires no prior knowledge of density or magnetization contrasts and no particular interpretation model (LaFehr and Nabighian, 2012). The method has been documented by Thompson (1982), Reid et al (1990) and Reid (1997). The technique has been widely studied and many papers written to further develop the method.

The method is based on the Euler equation:

$$(x - x_0) \frac{\partial T}{\partial x} + (y - y_0) \frac{\partial T}{\partial y} + (z - z_0) \frac{\partial T}{\partial z} = N(B - T) \dots\dots\text{eqn 5.2}$$

where  $(x_0, y_0, z_0)$  is the position of a source whose total magnetic field intensity  $T$  is detected at  $(x, y, z)$ ,  $B$  is background value of  $T$ , and  $N$  is structural index which is related to the rate of falloff of anomalies with distance from the source. This in turn is related to the geometry of the source.

Using Geosoft Oasis Montaj software the method is applied by:

1. Calculating the three partial derivatives of  $T$  with respect to  $x$ ,  $y$  and  $z$ .
2. Set up a window with  $n \times n$  grid points, where  $3 < n < 20$
3. Select a suitable value  $N$  and search for solutions to the Euler equation.
4. For a window width of  $n$  there are  $n \times n$  equations from which to solve for the four unknowns  $x_0$ ,  $y_0$ ,  $z_0$ , and  $B$ . This is done using a least squares technique and provides a measure of the uncertainty of the depth solutions  $z_0$ .
5. Move across to the next grid point and repeat steps 1, 2, 3
6. All the solutions are saved in a database for further analysis.
7. Solutions can be plotted out as a map or depths gridded and displayed as an image.

For this project Euler deconvolution was run on the Isostatic Residual Gravity data using Geosoft Oasis Montaj software. The Euler equation holds approximately for gravity and the structural index  $N$  applicable is one less than the value  $N$  for magnetics. This is problematical for fault solutions with gravity as this requires  $N$  values of about zero. Some implementations of Euler deconvolution treat  $N$  as an unknown and solve for  $N$  values as well as the position, depth and background solutions. In the Geosoft Located Euler deconvolution method, peak positions are determined using Analytic Signal computation after step 1 and this limits the number of potential solutions.

For this project the purpose here was to identify linear fault solutions with reasonably long strike length. The Located Euler method was used with

structural index of 0.05 which is appropriate for long linear features such as faults. A window width of 20 x 20 grid points was used for the Euler computations and a cut-off of 5 percent accuracy applied to the results. The Euler method uses a least squares approach and because there are more equations than unknowns the method computes the standard deviation of the computed depth solution as a percentage of the depth. In this work 5 percent was found to be an appropriate figure to use. Solutions were retained and plotted for solutions with up to 5 percent standard deviation relative to their depth.

Figure 5-33 shows Euler locations superimposed on the Analytic Signal of the Isostatic Residual Gravity image. Figure 5.34 shows an image of the depths computed as a grid from the Euler estimates. The grid mesh used was 1 x 1 km. Depths are seen down to about 7500 metres below ground level.

#### **5.7.5 Multiscale edge detection applied to Isostatic Residual Gravity**

Multiscale edge detection is based on finding local maxima points in the total horizontal gradients of gridded gravity and magnetic data. The assumption is made that these positions correspond to the edges of geological source bodies (Fitzgerald and Milligan, 2013). Milligan et al. (2003) showed that where these displayed lateral continuity they could be mapped as strings. This is repeated at different levels of continuation of the gridded gravity or magnetic datasets. The assumption here is that the lower levels of continuation correspond to shallower sources whilst the higher levels correspond to deeper sources (Milligan et al, 2003a).

By mapping the positions of horizontal maxima using multilevel data we can display results in three dimensions where the z dimension comes from the height of each continuation level. The magnitudes of the total horizontal gradient maxima are computed and preserved as intensity or amplitude data.

Earlier descriptions and more of the mathematics involved in this technique, which is also called “worming”, are found in the papers of Hornby et al., (1999), Boschetti et al., (2000), Holden et al., 2000 and Boschetti et al.(2001).

Multiscale edge detection was run on the Isostatic Residual Gravity data using the routine available in the Intrepid Geophysics package. Further description of this technique and application is documented in Fitzgerald and Milligan (2013).

The Isostatic Residual Gravity grid used here has a cell size of 1130 x 1130 m. Continuation to 12 levels was computed with a multiplier of 1.4 times applied between levels. The levels used were:

1582 m, 2215 m, 3101 m, 4341 m, 6077 m, 8508 m, 11901 m, 16675 m, 23245 m, 32683 m, 45756 m, 64058 m.

Results of this computation are shown as Figures 5-35 and 5-36. The latter figure uses the Isostatic Residual Gravity as a shaded backdrop to the image to show the worms relative to the data from which they have been computed.

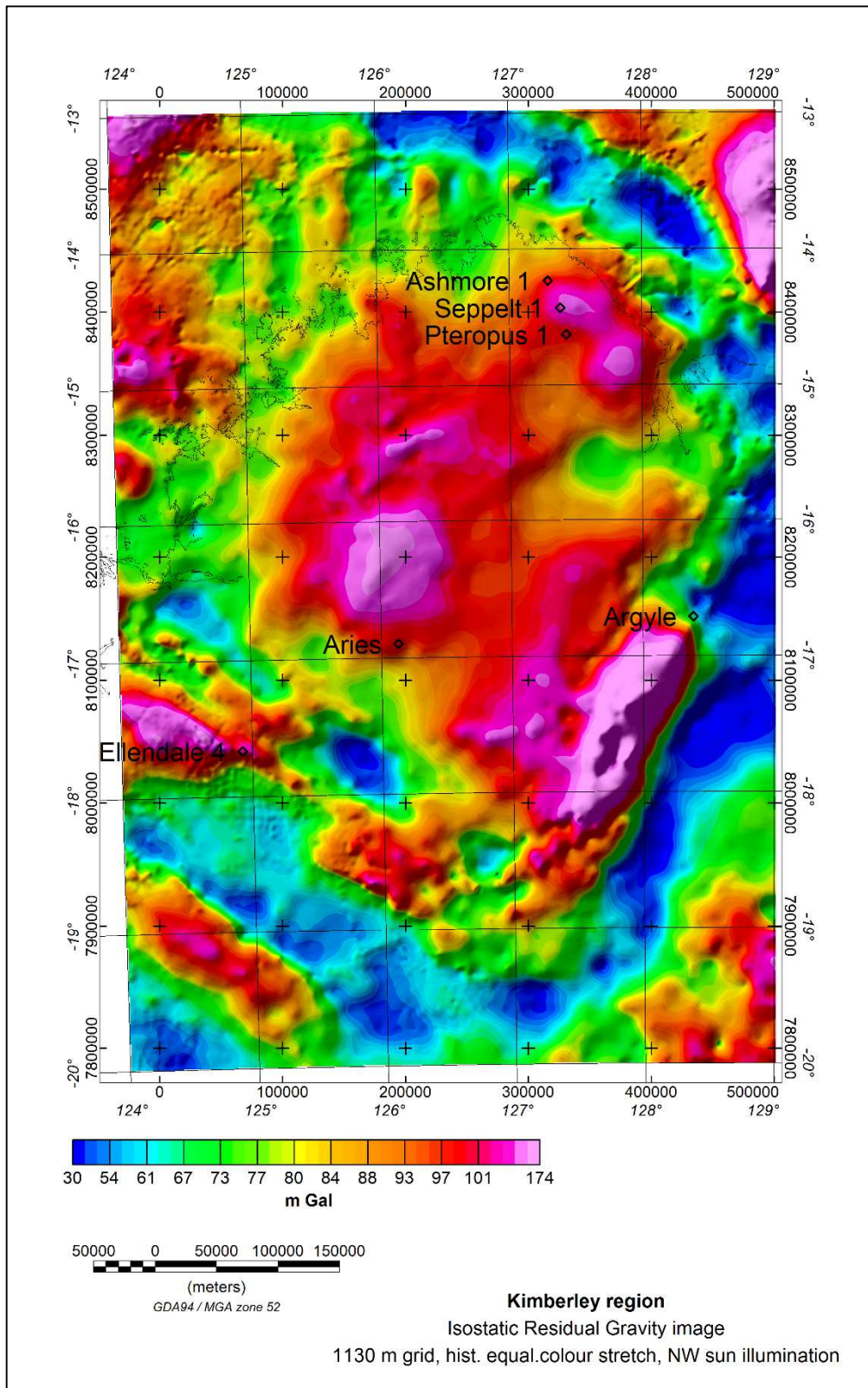


**Figure 5-28: Isostatic Residual Gravity image for the Kimberley region. The black diamond symbols show location of the study pipes. Sun illumination from the NW with 45 degree elevation.**

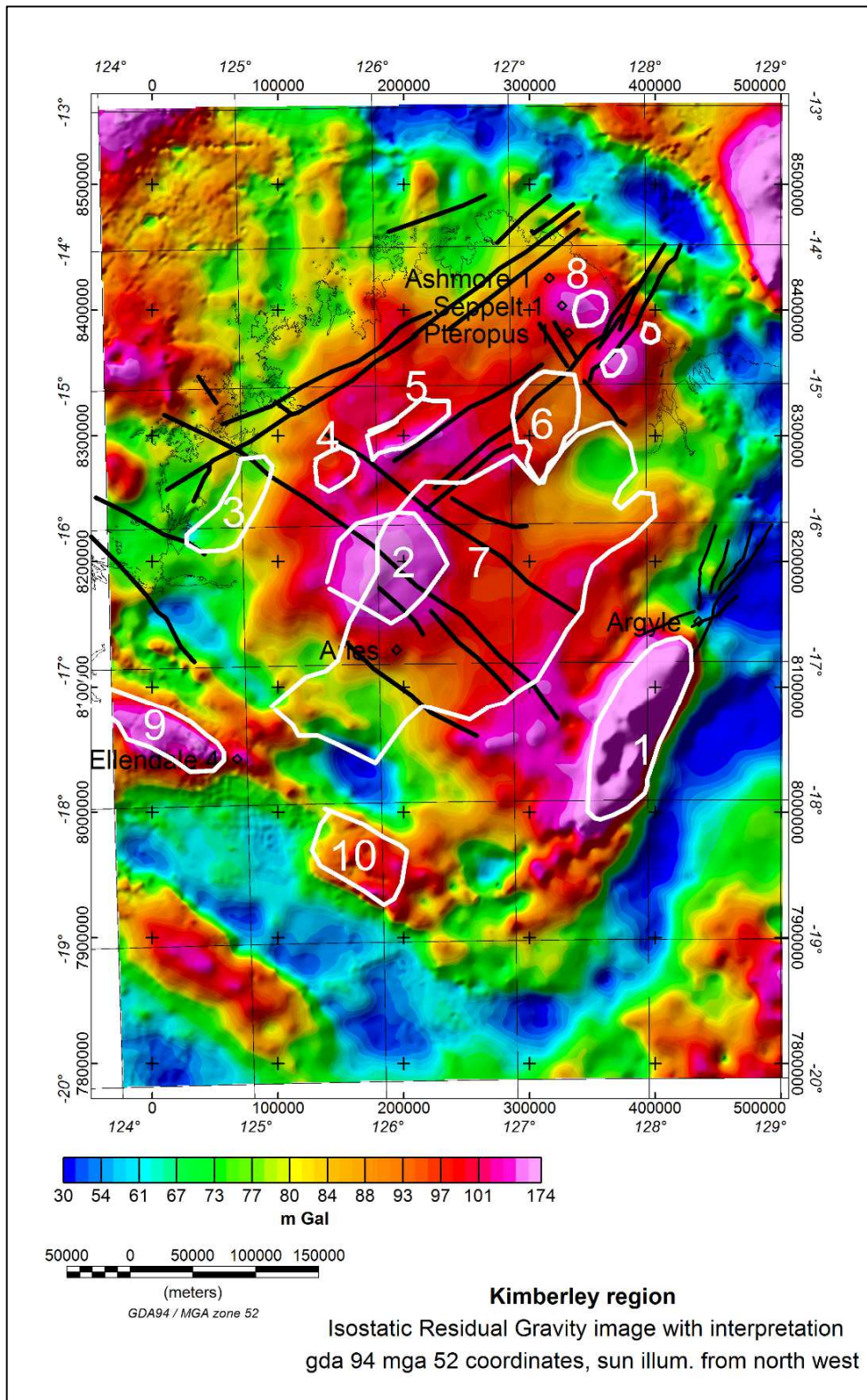


**Figure 5-29: Isostatic Residual Gravity with interpretation.** The white polygons show the major units interpreted from this study. This is an extension of the interpretation of Gunn and Meixner (1998). Sun illumination from NW with 45 degree elevation.

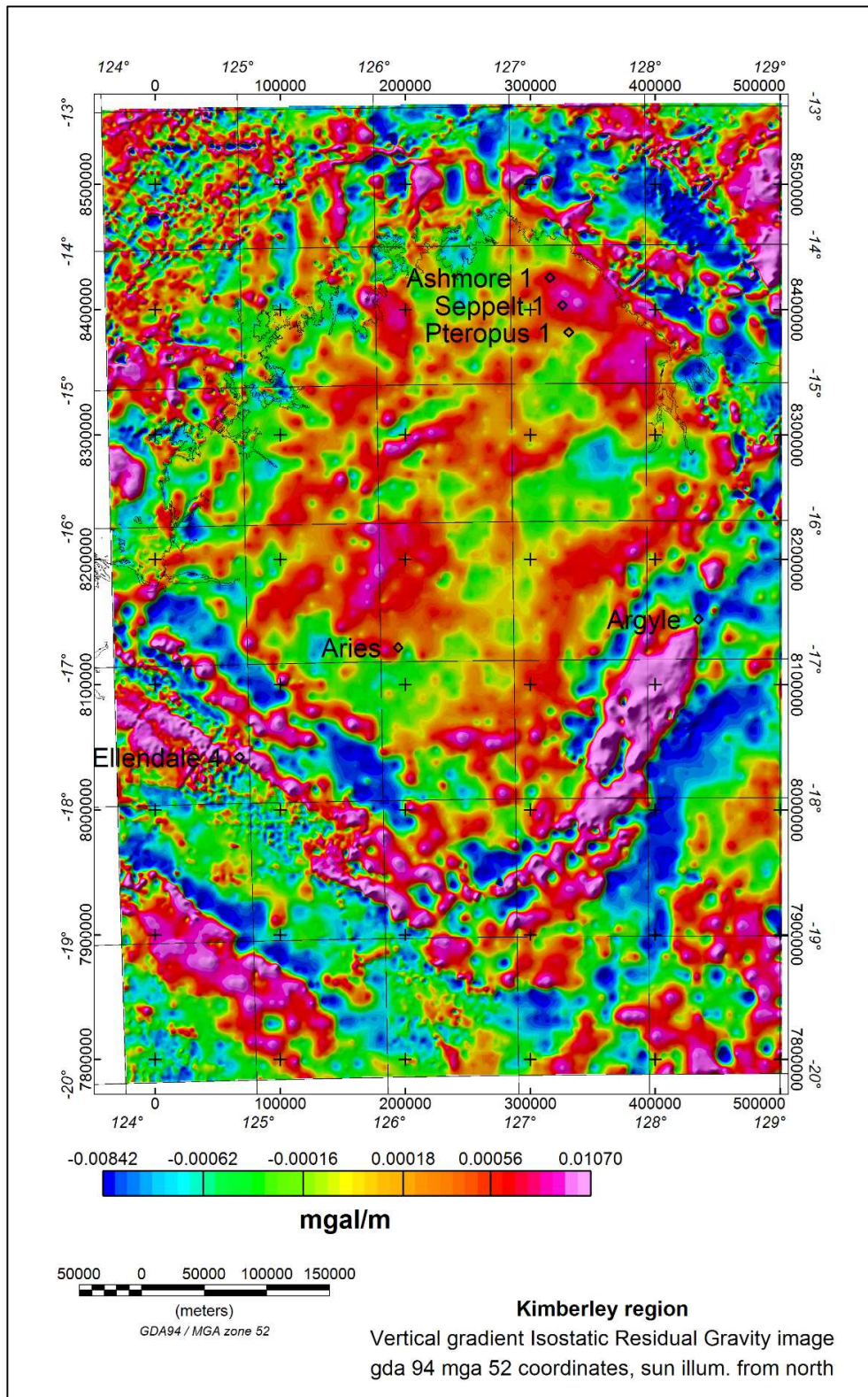


**Figure 5-30: Vertical gradient of Isostatic Residual Gravity image for the Kimberley Region. The study pipes are located close to significant horizontal changes in the vertical gradient of the Isostatic Residual Gravity. Sun illumination from the north with 45 degree elevation.**

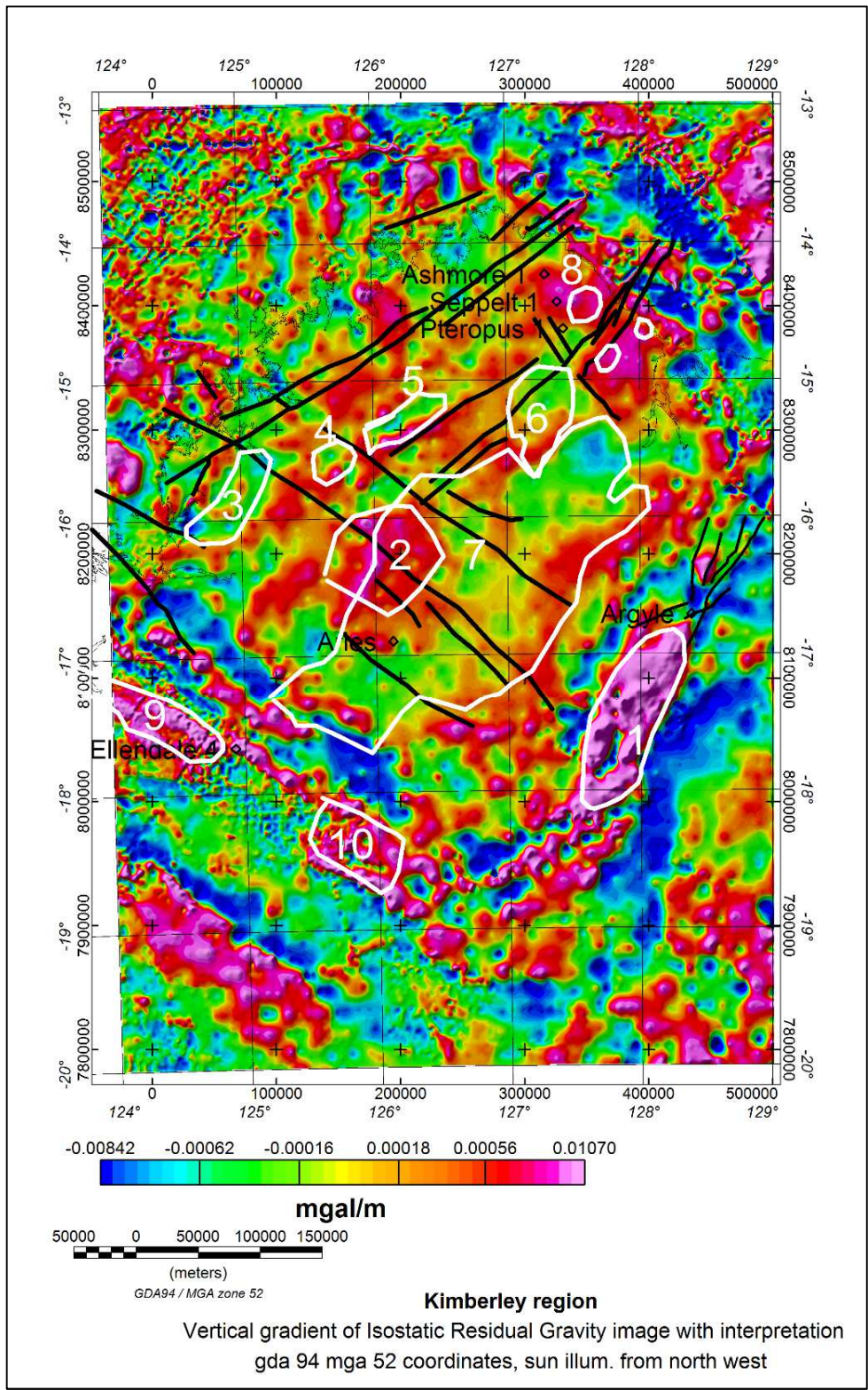


**Figure 5-31: Vertical gradient of Isostatic Residual Gravity image with interpretation.** The white polygons show the major units interpreted from this study. This is an extension of the interpretation of Gunn and Meixner (1998). Sun illumination from NW with 45 degree elevation.

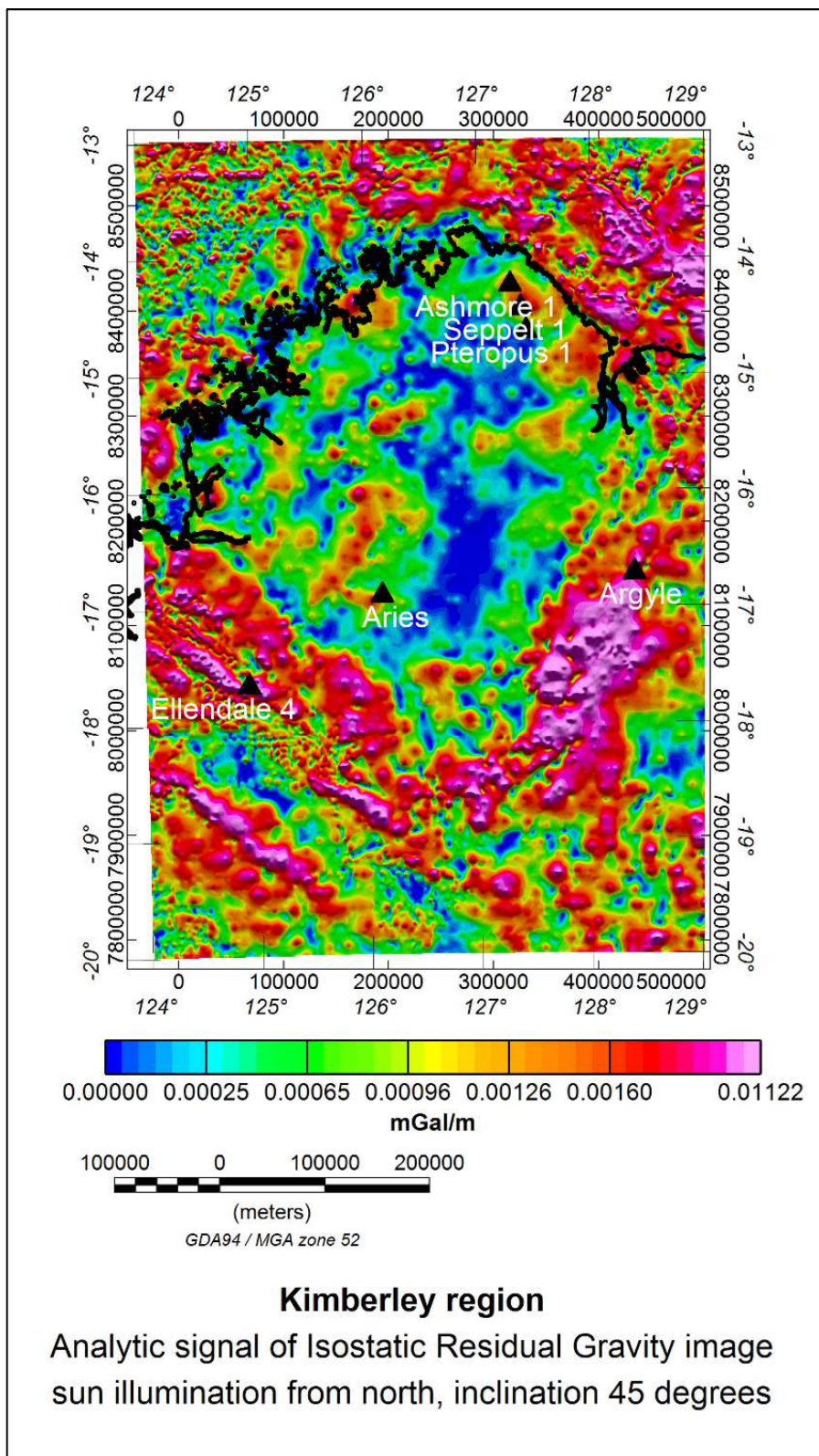


**Figure 5-32: Analytic Signal of Isostatic Residual Gravity image for Kimberley Region. Sun illumination from north with 45 degree elevation.**

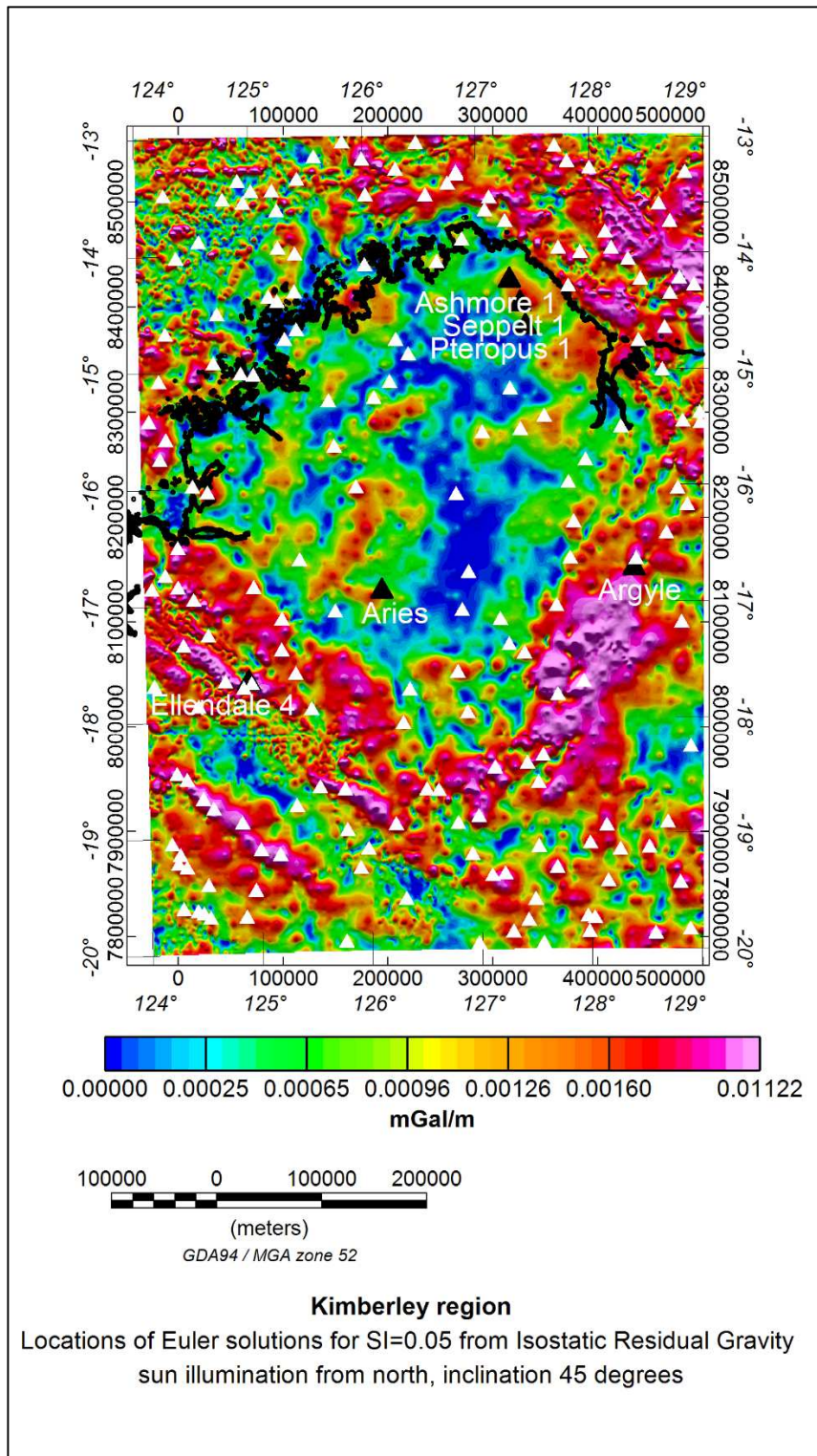


**Figure 5-33: Euler solution locations for structural index of 0.05, shown as white triangles, on analytic signal image computed from Isostatic Residual Gravity data. Sun illumination from north with 45 degree elevation.**

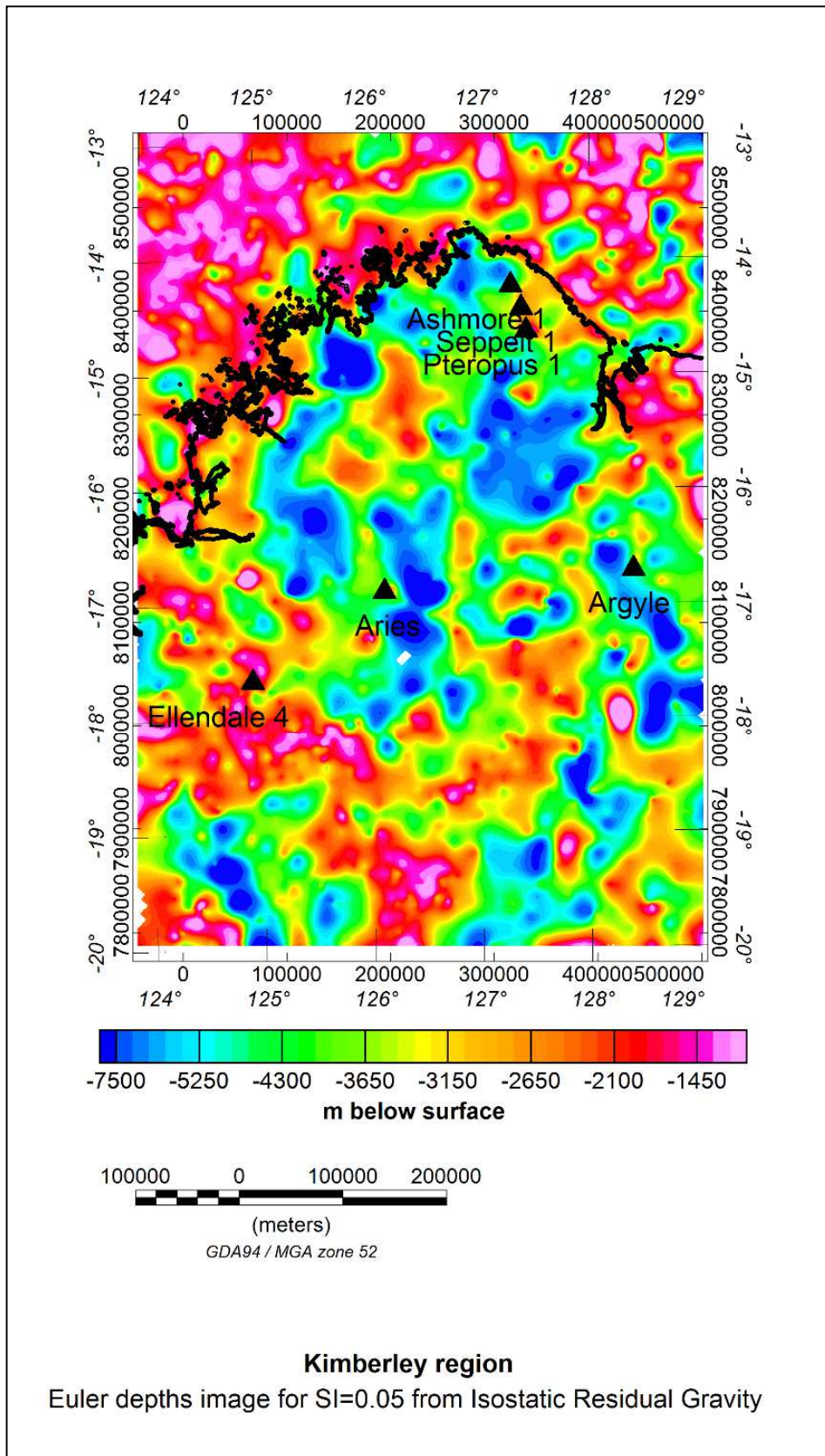
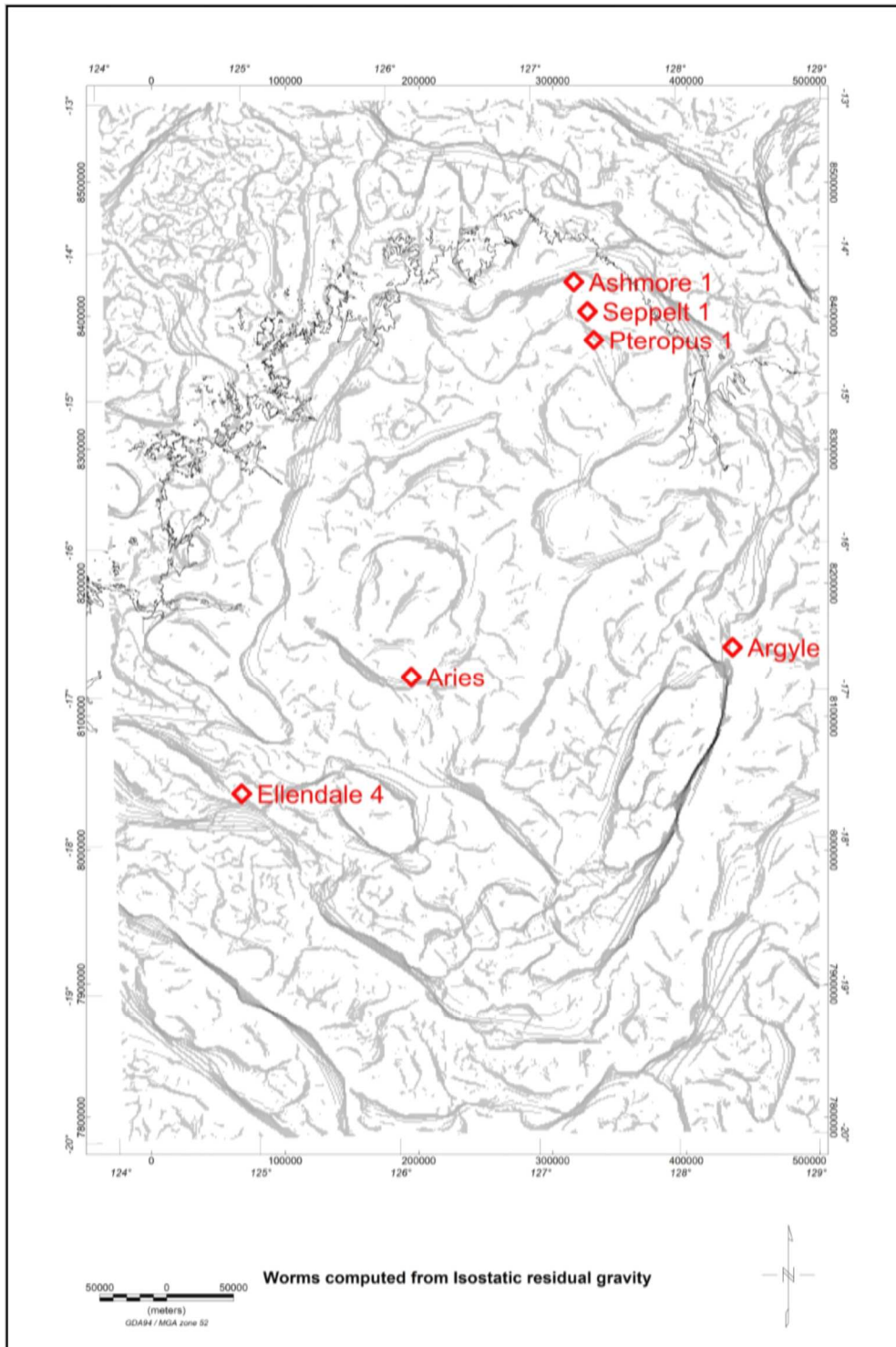
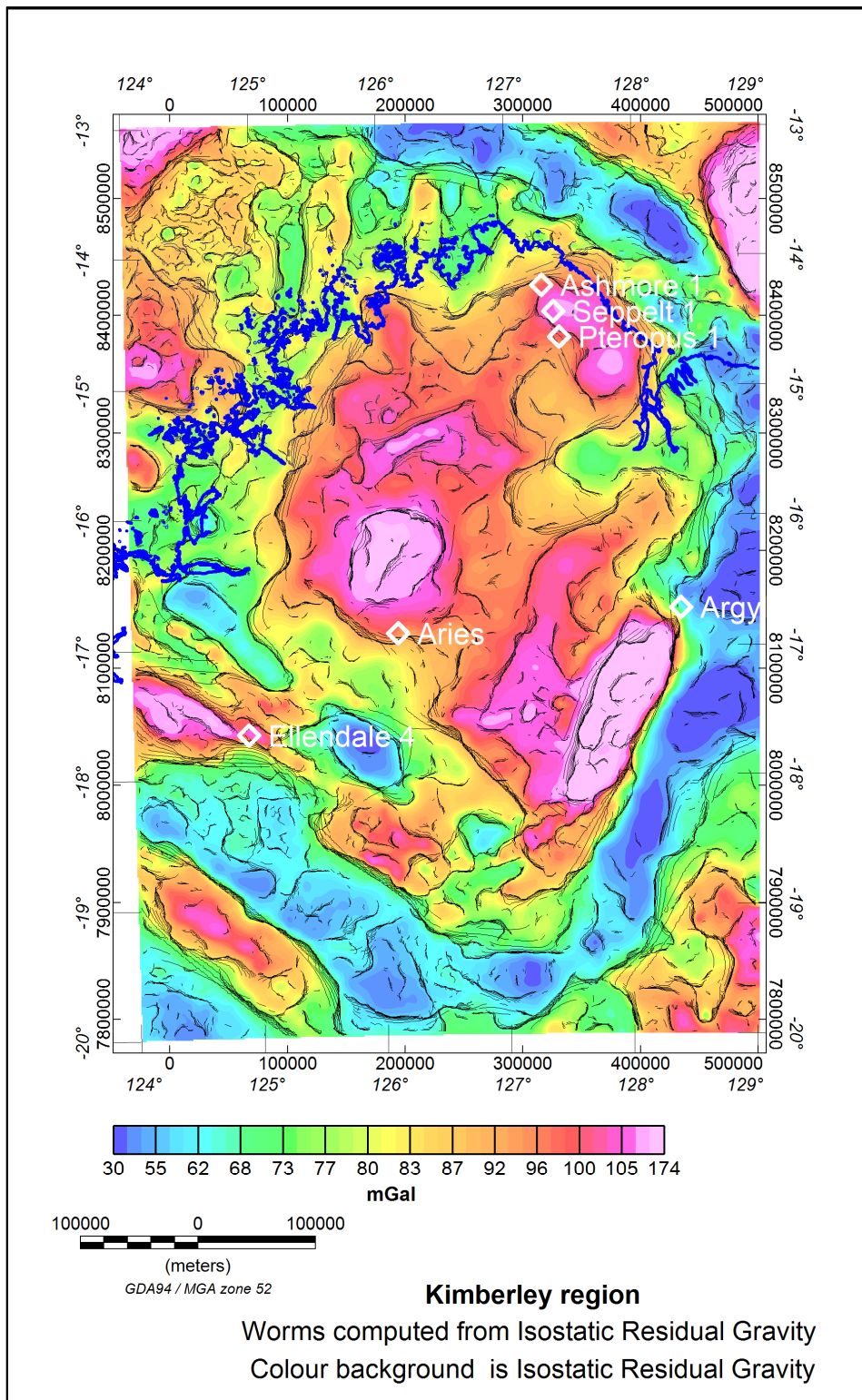


Figure 5-34: Euler depths image for structural index of 0.05 computed from Isostatic Residual Gravity.



**Figure 5-35: Worms computed from Isostatic Residual Gravity.** The study pipes are all located along structures highlighted by the worming processing.



**Figure 5-36: Worms computed from Isostatic Residual Gravity and shown superimposed on an image of the Isostatic Residual Gravity.**

### 5.7.6 Total horizontal gradient computation on upward continued reduced to pole aeromagnetic data

To look for deep structures, it is appropriate to upward continue aeromagnetic data to minimise effects of near surface magnetic sources. Figure 5-37 shows horizontal gradient images computed from reduced to the pole (RTP) GA aeromagnetic data with a grid spacing of 272 metres. These are not based on the latest 90 m RTP grid. The 272 m grid has been upward continued by 1600 metres. The total horizontal gradient has been computed for this upward continued dataset using this equation:

$$\text{total horizontal gradient} = \{ (dT/dx)^2 + (dT/dy)^2 \}^{0.5} \quad \dots \text{eqn 5.3}$$

where T is the upward continued reduced to pole aeromagnetic data, x is east direction and y is north direction. The approach followed here is similar to Jaques and Milligan (2004). This is similar to calculating the analytic signal, but without including the vertical gradient. From this study, the image using the total horizontal gradient appears sharper than the image that results from the analytic signal. The resultant grid has been sun illuminated from the north and shown as a greyscale image with normal distribution to form Figure 5-37. Kimberlite and lamproite intrusions are shown as red symbols on this figure. There are many linear features striking approximately SW-NE, and these are probably mainly dykes and faults. There are other trend directions also apparent in these images, e.g. approx. NW – SE. Figure 5-19 shows that some of the kimberlite intrusions in the northern Kimberley close to Ashmore, Seppelt and Pteropus are close to these interpreted dykes, and this is interpreted as a major structural direction.

Upward continuation of the reduced to pole aeromagnetic data to 5000 m reduces still more the nearer surface features and emphasises deeper structures.

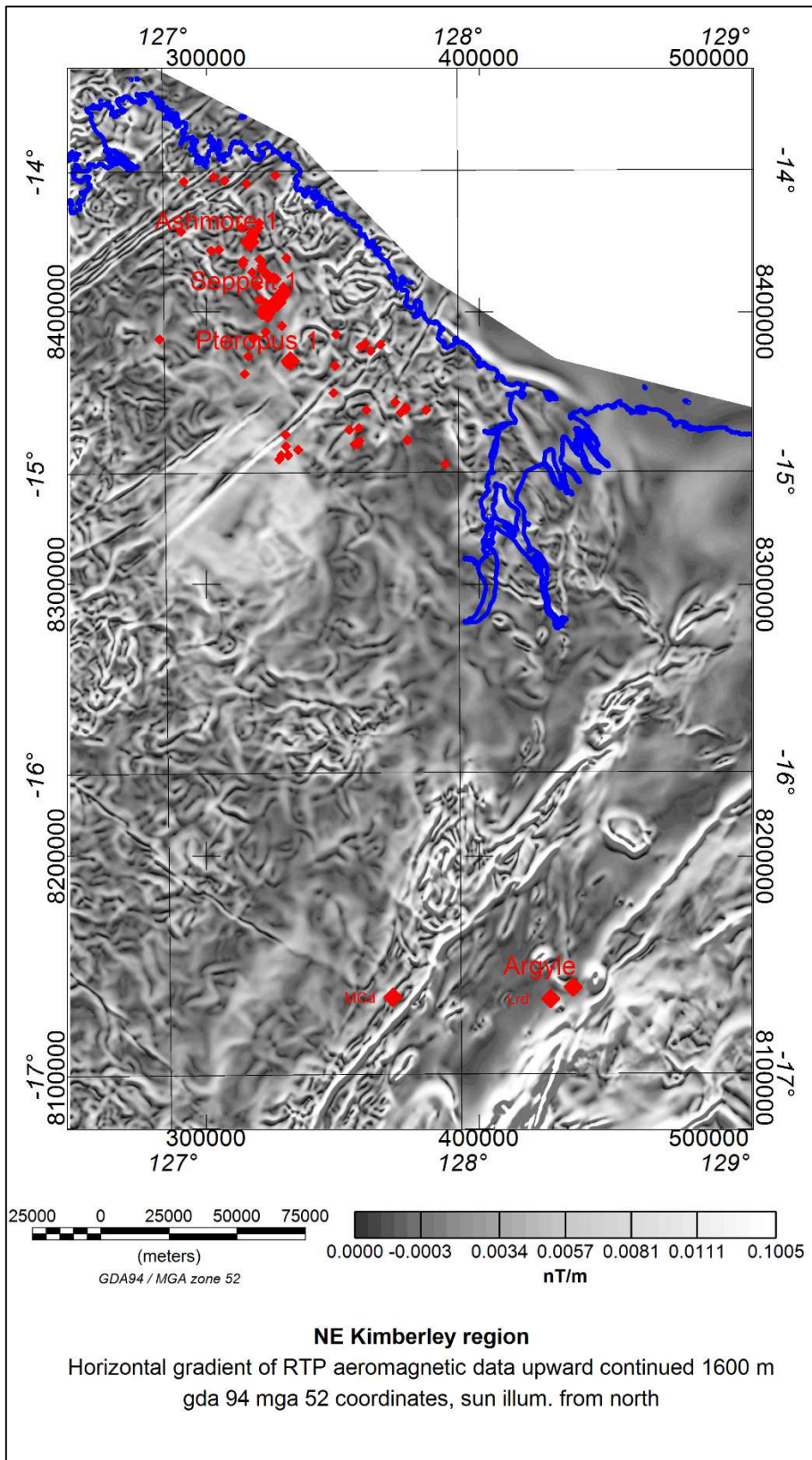


**Figure 5-37: NE Kimberley total horizontal gradient of RTP aeromagnetic data upward continued by 1600 m. Red symbols show locations of kimberlite and lamproite intrusions. Sun illumination from north with 45 degree elevation.**

### **5.7.7 Multiscale edge detection using aeromagnetic data**

The background to multiscale edge detection is provided in section 5.7.5 of this thesis where the technique is applied to Isostatic Residual Gravity data.

In this section of the thesis, multiscale edge detection has used pseudogravity computed from GA aeromagnetic data upward continued to fifteen elevations of: 272, 470, 677, 975, 1404, 2021, 2910, 4191, 6035, 8690, 12513, 18019, 25948, 37365 and 53805 metres above ground level. This was done using software developed by CSIRO which produces Fractal Graphics format files of x, y, z and amplitude. These have been loaded into a combined Geosoft Oasis Montaj database and 3D gridded to create a 2 x 2 x 2 km voxel dataset. This is shown as a 3D view in Figure 5-38. The colour here represents the amplitude of the worm data. Height in this view is the height to which the data have been upward continued. Level plans have been computed through the voxel dataset at elevations of 5 km, 10 km, 15 km and 20 km, and are shown as Figures 5-39, 5-40, 5-41 and 5-42. These plans also include the locations of Argyle, Aries, Ashmore 1, Ellendale 4, Seppelt 1 and Pteropus 1.

Argyle and Ellendale 4 are seen to be located on major structures seen in the magnetic data. The other four pipes are located close to minor structures.

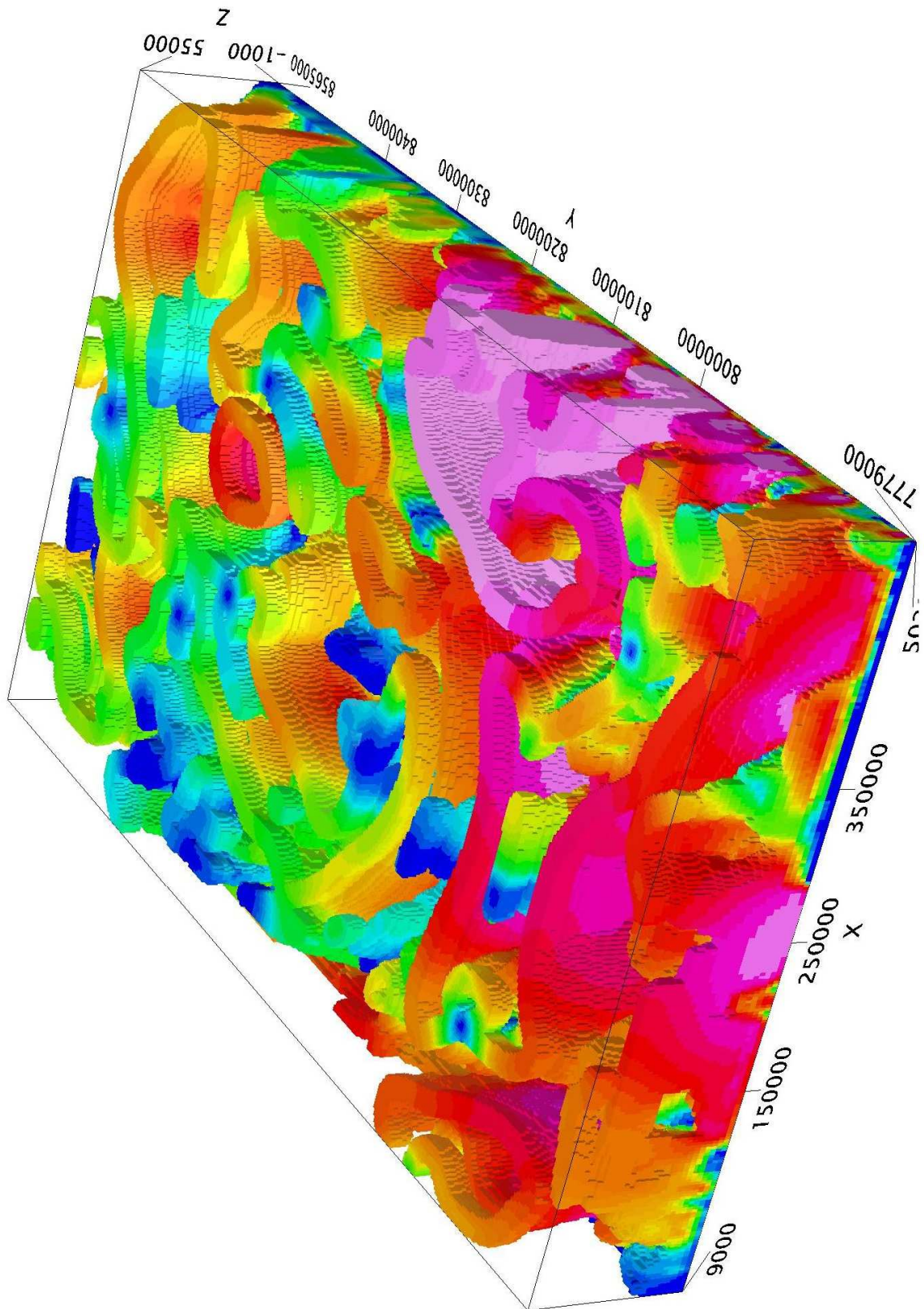


Figure 5-38: Magnetic worms as 3D voxel (2 x 2 x 2 km) image, view to the NW. View from right hand side of page.

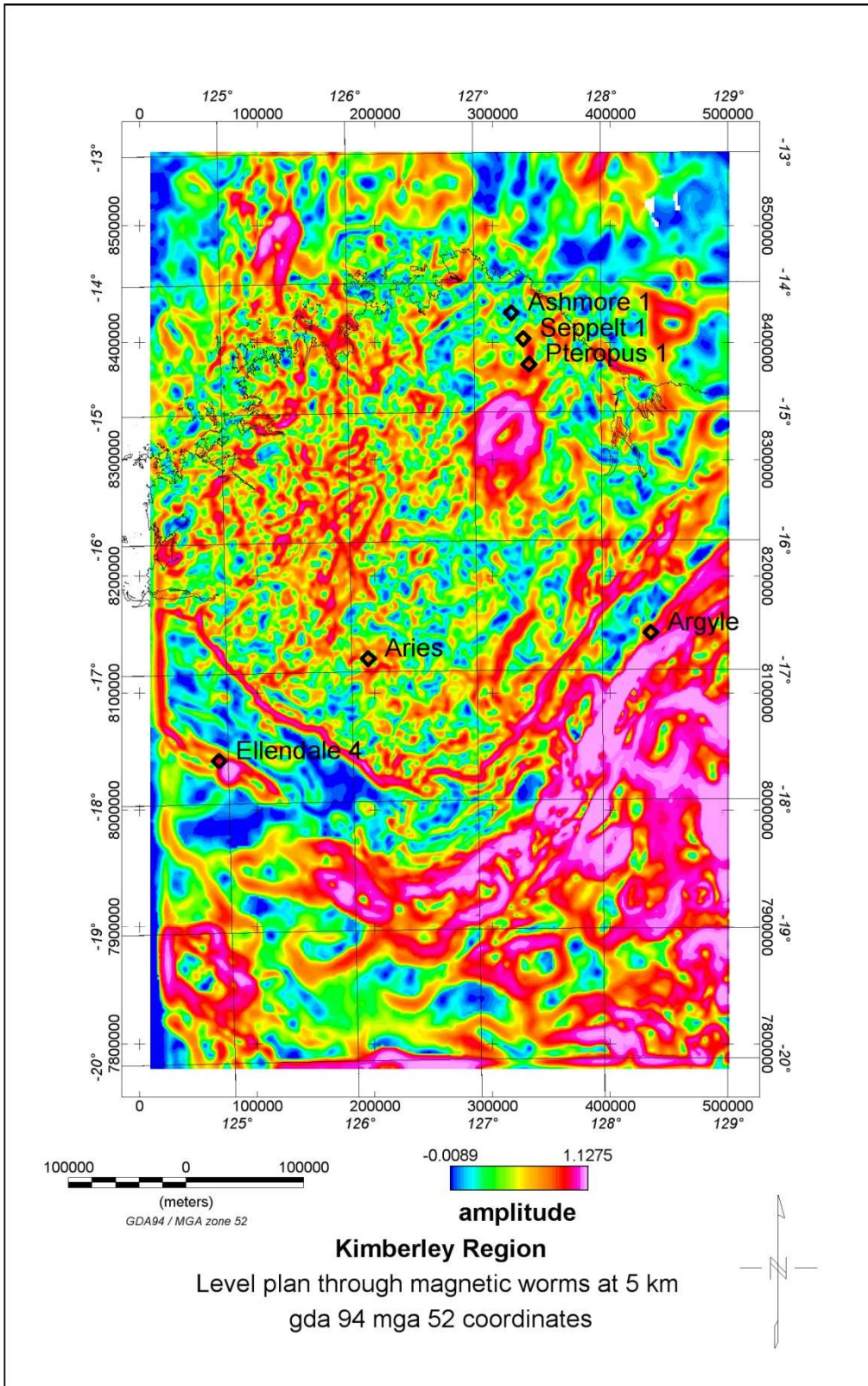


Figure 5-39: Level plan through magnetic worms at 5 km elevation.

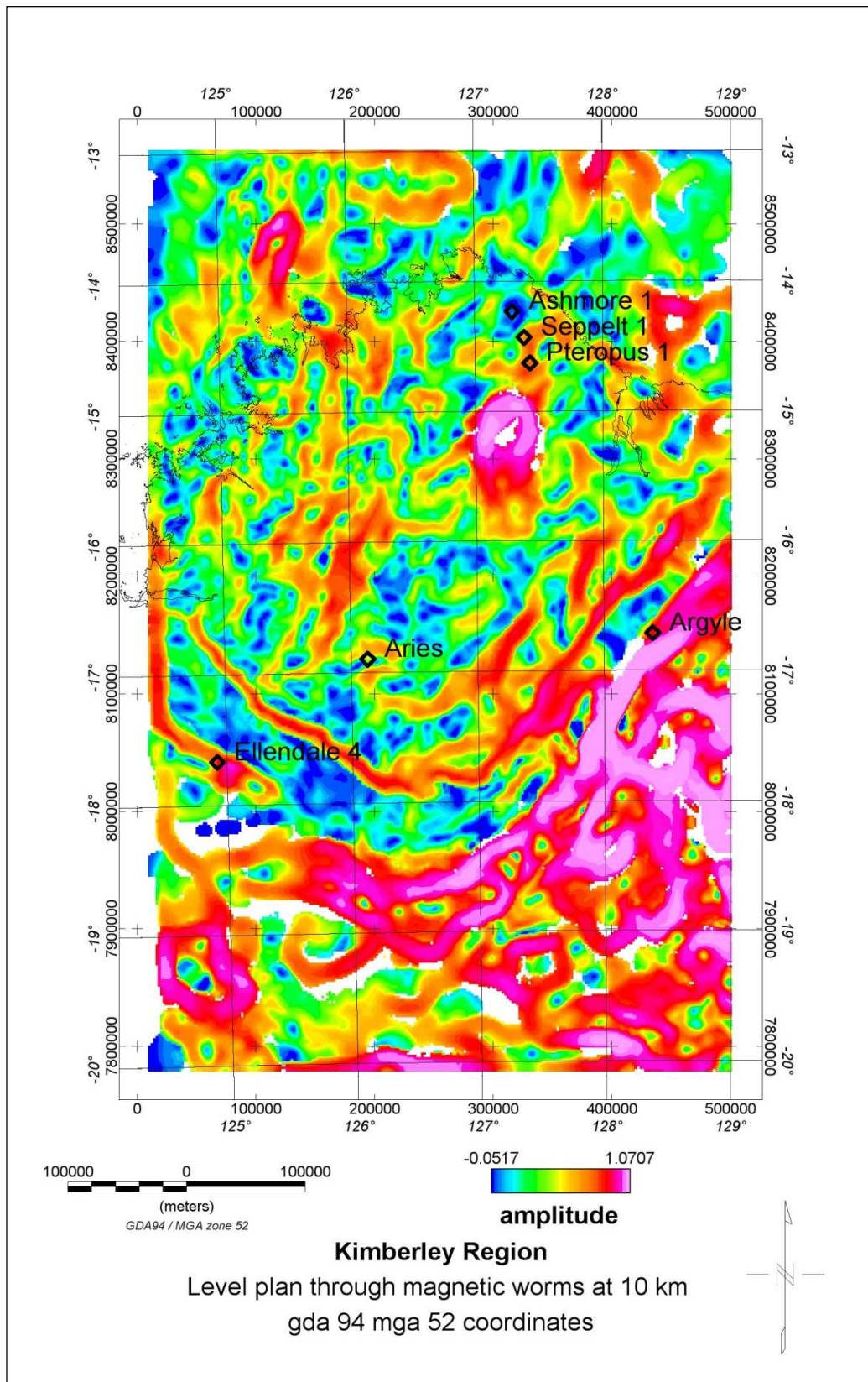
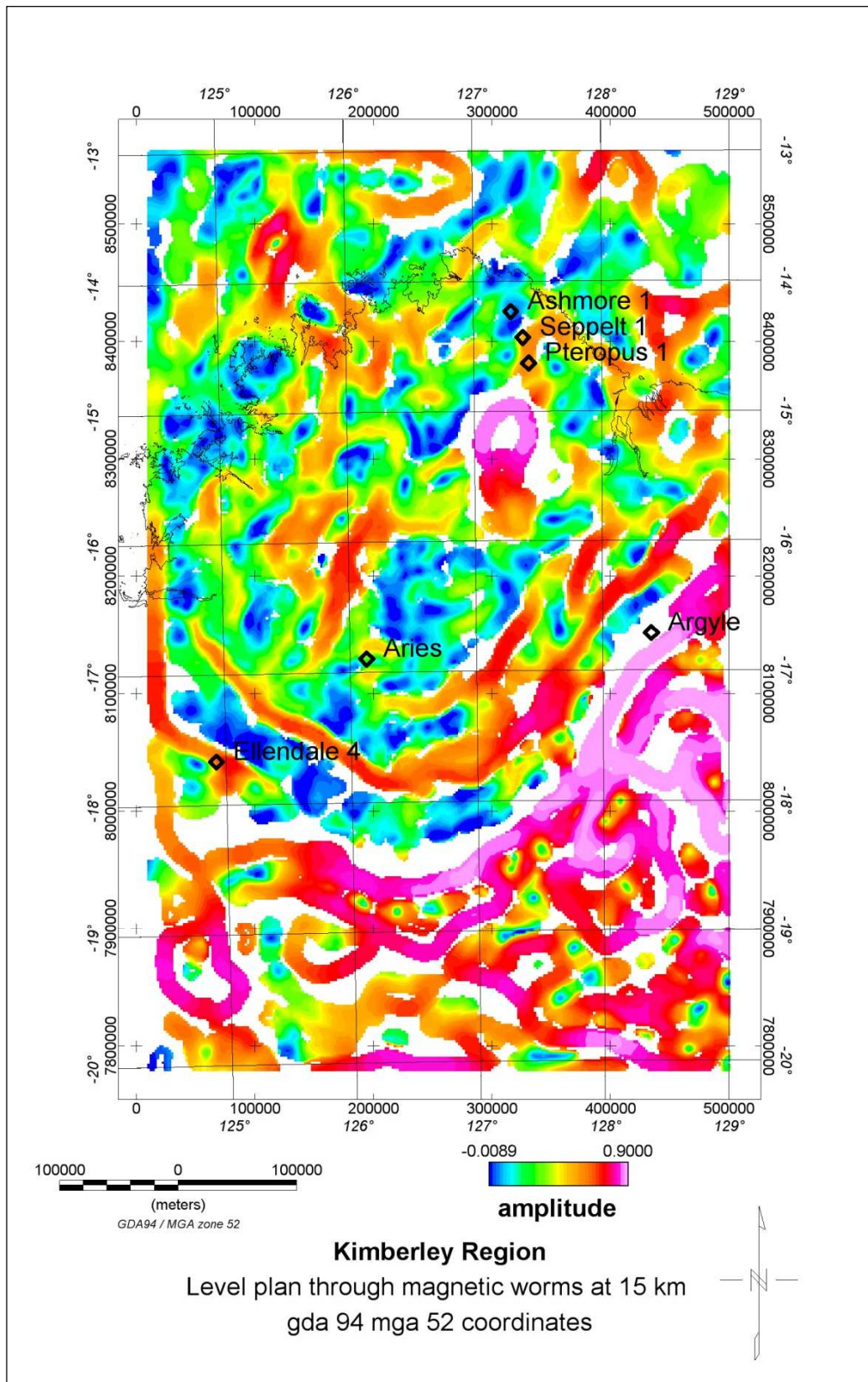


Figure 5-40: Level plan through magnetic worms at 10 km elevation.



**Figure 5-41: Level plan through magnetic worms at 15 km elevation.**

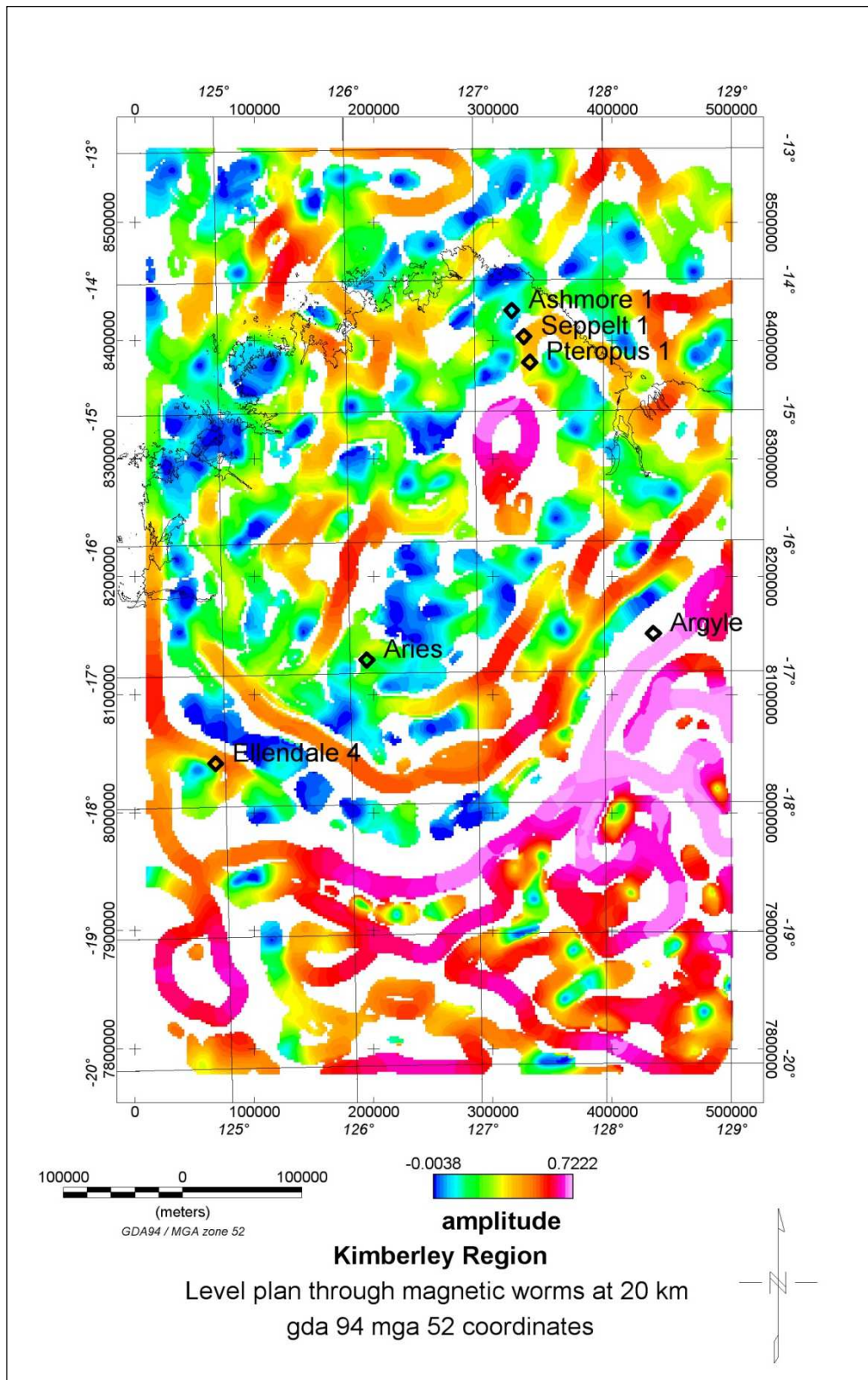


Figure 5-42: Level plan through magnetic worms at 20 km elevation.

### **5.7.8 Texture analysis and trend detection from aeromagnetic data**

Texture analysis and trend identification routines have been coded by the Centre of Exploration and Targeting (CET) at University of Western Australia (UWA). These are available as an add-on module to the Geosoft Oasis Montaj software package.

This has been used on some of the North Kimberley geophysical datasets. Figure 5-43 shows Reduction to Pole (RTP) aeromagnetic data for an area in the North Kimberley region. This has been computed from a 91 m grid from Geoscience Australia .Data were acquired in 2010 using 400 m flight line spacing and 100 m flying height. Lineations have been extracted from the RTP dataset with the following workflow:

- Computation of phase symmetry using an algorithm of Kovesi (1997)
- Amplitude thresholding, based on amplitude and width
- Skeletonisation and vectorisation
- Plotting out the vector elements

The output from this process is shown in Figure 5-44. This figure also shows Ashmore 1, Seppelt 1 and Pteropus 1 pipes in red. Figure 5-45 shows a zoomed in version of part of Figure 5-44 with other kimberlites discovered since 1990, added in blue. It can be seen that many of these kimberlites align with some of the lineations. Some of the approximately NE trending lineations continue offshore in the Bonaparte Gulf area. These are interpreted as major fractures.

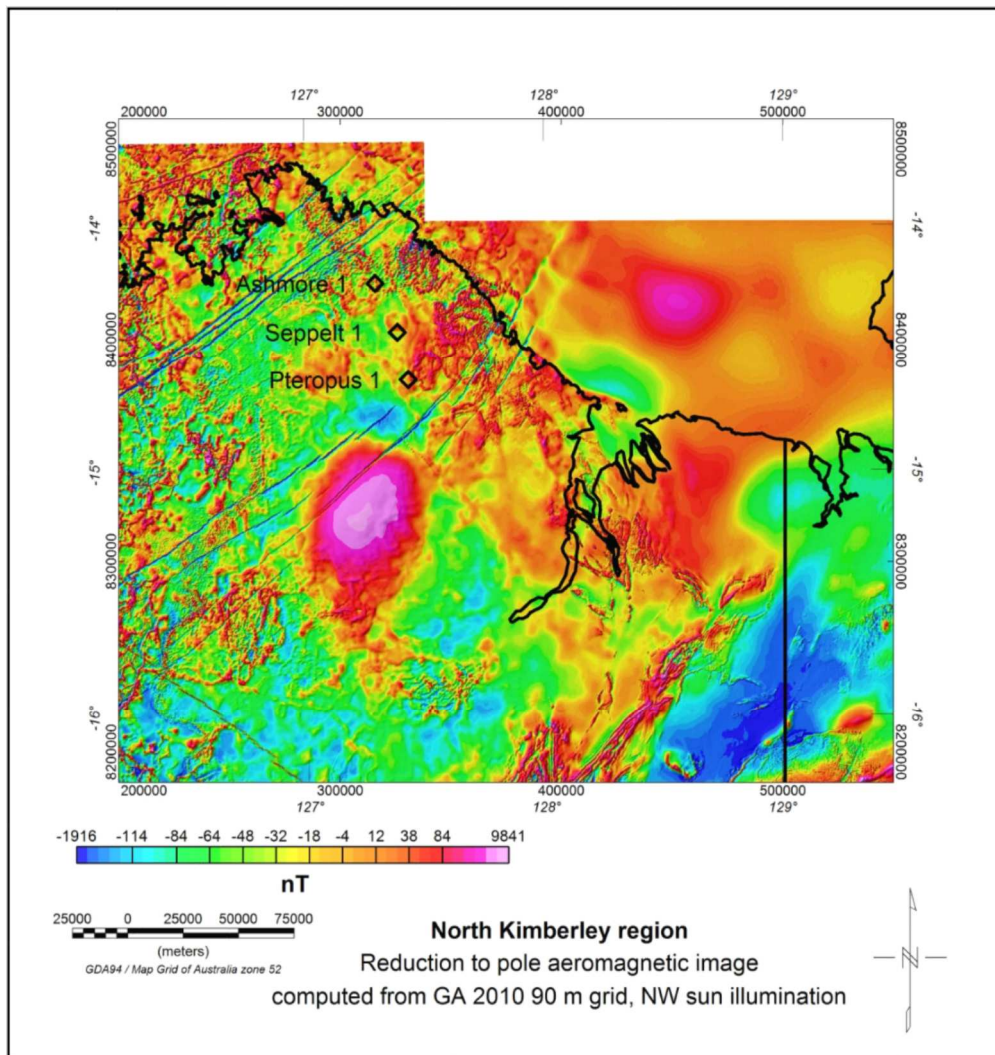


**Figure 5-43: RTP aeromagnetic image of North Kimberley region. Locations of pipes at Ashmore, Seppelt 1 and Pteropus 1 are also shown. Sun illumination from NW with 45 degree elevation.**

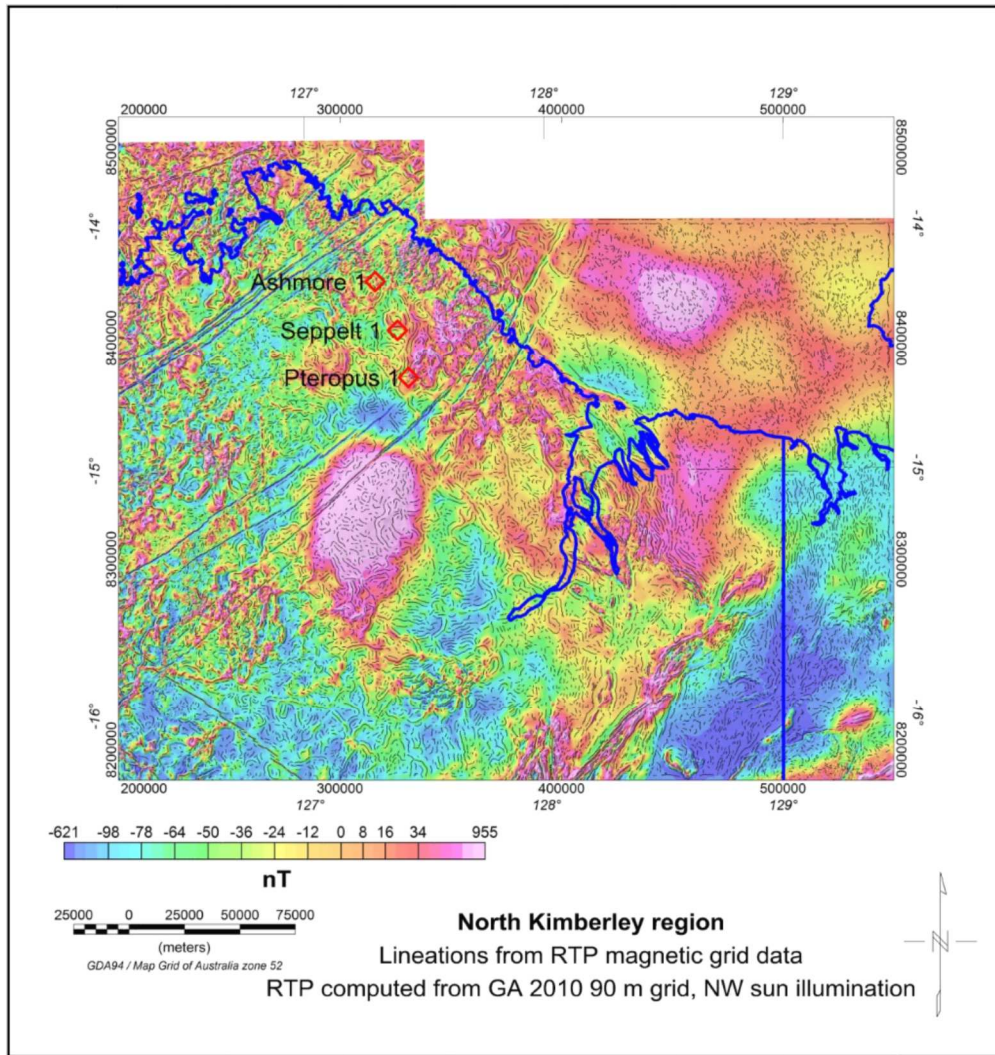


**Figure 5-44: Lineations computed from RTP aeromagnetic grid for North Kimberley region. Locations of pipes at Ashmore, Seppelt 1 and Pteropus 1 are also shown. Sun illumination from NW with 45 degree elevation.**

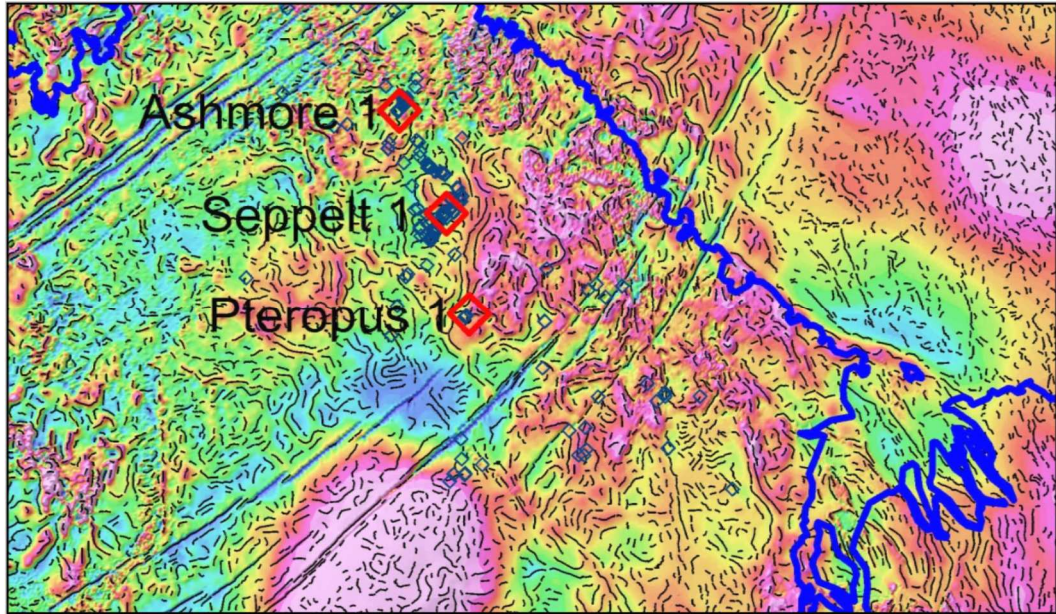


Figure 5-45: Zoomed in version of part of Figure 5-43 with post 1990 kimberlite discoveries added and shown by blue diamonds.

### 5.7.9 Discussion of regional datasets for cratonic studies

The six different topics reported in this section are all complementary.

Use of the new crustal model reported by Aitken, 2010 has shown that the example diamond occurrences / deposits all occur within 15 km of local gradient maxima in the slope of the Moho surface and with Moho depths varying from about 34 to 43 km.

The use of the Isostatic Residual Gravity allows for variation in depth to Moho and provides definition of local target areas for further exploration. The known diamond occurrences are generally located close to the boundaries of the main anomalies in the Isostatic Residual Gravity. Further exploration is recommended in these boundary locations where they coincide with major structures.

Euler deconvolution and analytic signal computation of both gravity and aeromagnetic data are useful in highlighting local structures and target areas for exploration.

Horizontal gradients of upward continued and reduced to pole aeromagnetic data are useful in clarifying major structures and potential exploration targets.

The use of multiscale edge detection ('worming') with gravity and aeromagnetic data is useful as it provides a way of visualising results from different depths and helps to show which are the major structures which persist with depth. Two different software packages have been used for worming in this thesis. Both packages compute amplitudes as well as x,y,z coordinates. The Isostatic Residual Gravity worms show structures close to each of the six diamond occurrences which have been used as type areas in this work.

Figure 5-46 illustrates the use of Isostatic Residual Gravity together with the Moho slope data to help define priority areas for future exploration. All six of the studied pipes occur close to the margins of well-defined gravity highs as shown by the Isostatic Residual Gravity 100 mGal contour lines shown in white. The pipes are also located on structures highlighted by the gravity worms shown in red. All these pipes are located within 15 km of local maxima in the Moho slope. Future exploration can look for more areas that meet these criteria. Other datasets (e.g using aeromagnetic data) may help to provide further structural control to further refine target areas. Although I have created a working hypothesis indicating a relationship between the location of diamondiferous pipes, gradients in the Moho surface and Isostatic Residual Gravity, clearly this is based on limited data and further confirmation by drilling and geophysics is required to test these ideas.

It is noted that exploration to date in the Kimberley region is limited and concentrated close to areas where pipes have already been found. However it is widely known that pipes occur in clusters and this reinforces the idea to further explore close to known pipes. More pipes have been found close to Ashmore and also close to Ellendale 4. The work presented in this thesis provides an approach that can be extended to include other datasets and test other exploration strategies. A magnetotelluric survey has been carried out in this region in 2012 (Spratt et al, 2014) with soundings at 155 locations and these results should be included in developing exploration strategies. More

drilling and more gravity surveys and modelling are also recommended in exploration for diamonds in the Kimberley region.

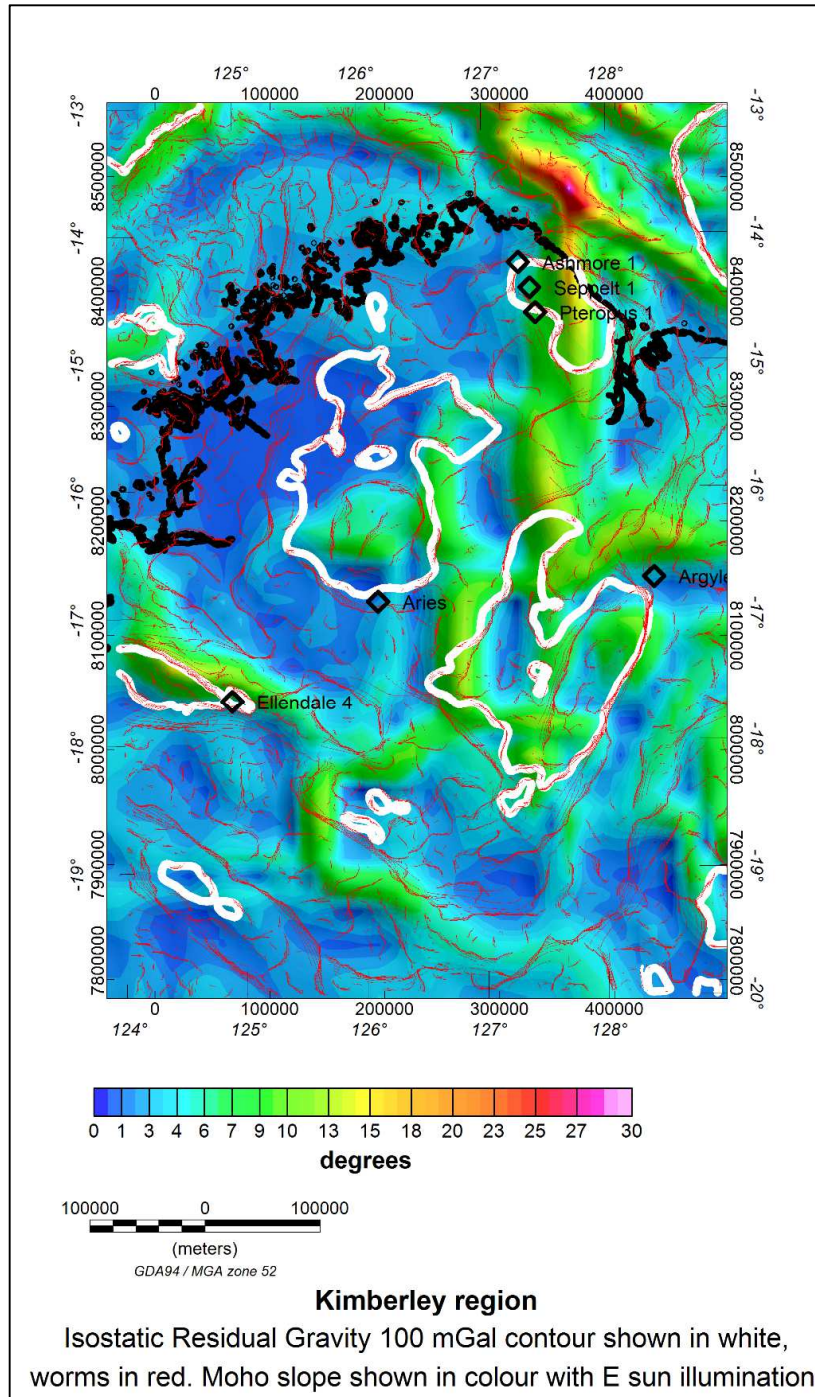


**Figure 5-46 Isostatic Residual Gravity worms and 100 mGal contour. This is combined with Moho slope sun illuminated colour image. Sun illumination is from the east with 45 degree elevation. Note that the six study pipes are all located close to the margins of major gravity highs and also close to gravity worm locations.**

## **6 EXPLORATION AT ASHMORE**

### **6.1 Geology**

Local geology for this area is provided in the regional geological mapping of the Drysdale 1:250 000 map sheet by Gellatly and Sofoulis (1969). The part that includes Ashmore is shown in Figure 6-1. The Ashmore pipes are located in Proterozoic Warton Sandstone. In the north east part of this local area there are extensive areas of Carson Volcanics. These are below the Warton Sandstone in the Kimberley Group.

### **6.2 Previous exploration**

Four diamondiferous kimberlite pipes each with a surface area of 0.5 ha were discovered between 1995 and 1997 at Ashmore in the Beta Creek area of the North Kimberley Kimberlite Province, Western Australia. Initially, two pipes were found by drilling beneath localised soil concentrations of indicator-minerals. Figure 6-2 shows a cross section through the Ashmore 1 pipe. At depth, the pipes contain approximately 800 Ma magmatic cores surrounded by breccias with both country-rock and kimberlite fragments. However, to a depth of 45 m, the kimberlitic material is extensively weathered to clay and unconformably overlain by up to 20 m of slightly silicified, silty sandstone possibly of Cretaceous age. Reddicliffe et al (2003) provides further detail on the geology and mineralogy of the Ashmore cluster of pipes and also for Seppelt 1 and 2 pipes.

Since their discovery, the Ashmore pipes have provided sites for detailed magnetic, electromagnetic and gravity orientation studies that have resulted in the discovery of two additional pipes within the Ashmore group of pipes. This work was done as the first part of Curtin University research in this area in 1997. Figure 6-3 shows some diamonds from the Ashmore area.

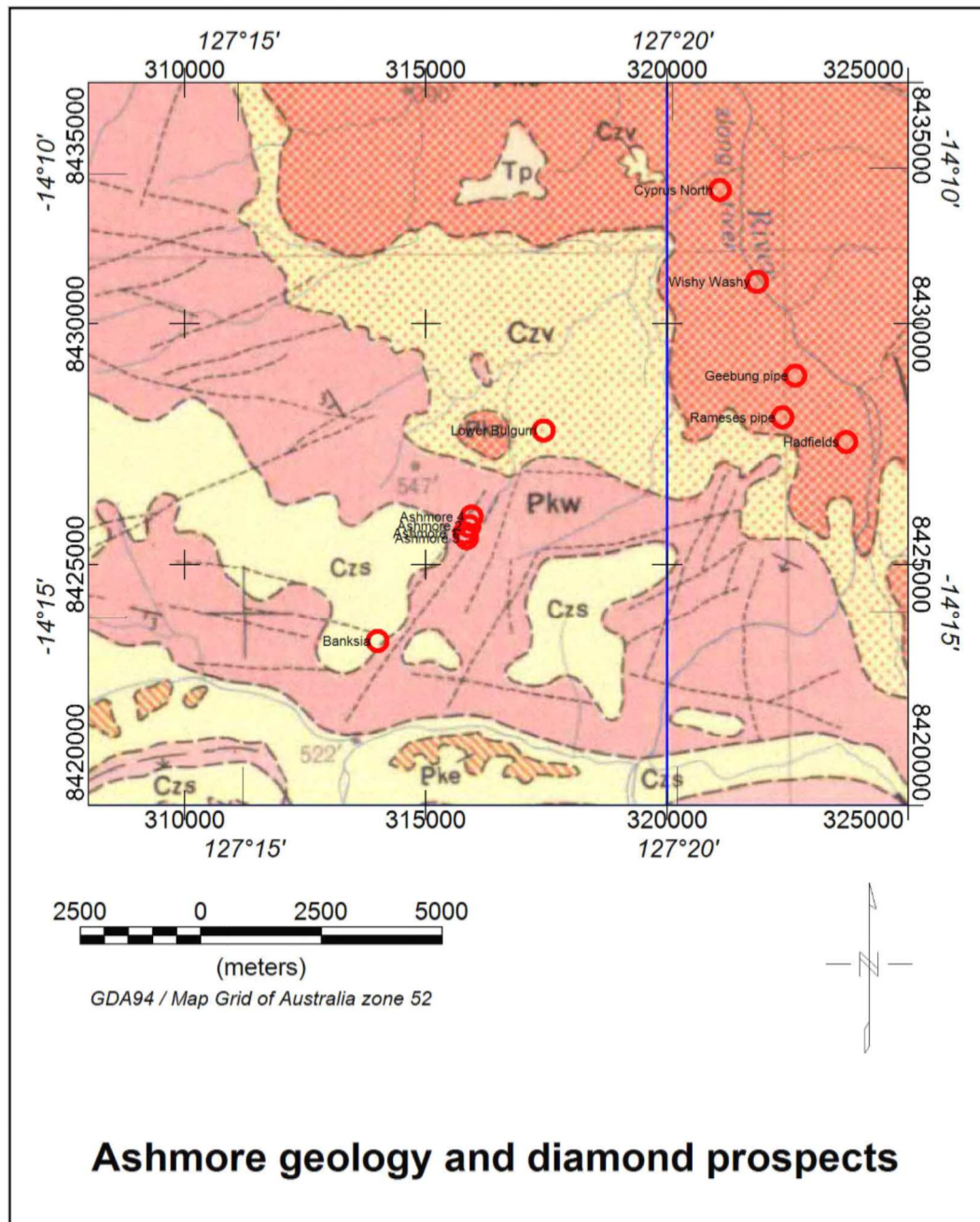


**Figure 6-1: Ashmore regional geology reproduced from mapping of the Drysdale 1:250,000 scale map sheet by Gellatly and Sofoulis (1969). Czv is Cainozoic volcanic derived soil, Czs are soil and colluvium, PkC (in orange) are Carson Volcanics, Pke is Elgee Siltstone, Pkw is Warton Sandstone and Tp is ferruginous laterite. Locations of various pipes in the vicinity of Ashmore are also included as red symbols.**

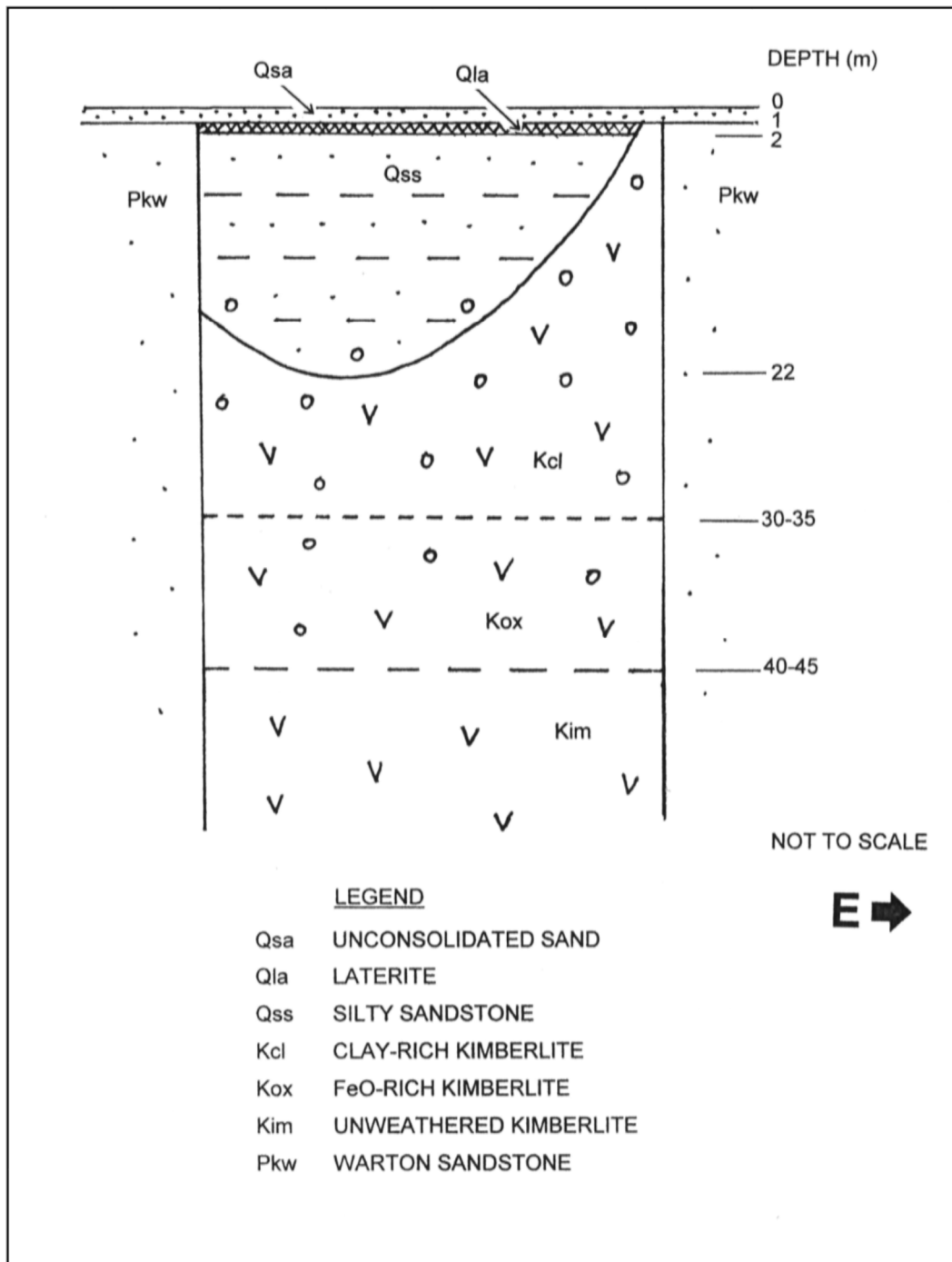


Figure 6-2: Cross section through Ashmore 1, reproduced from Ramsay (1997)



**Figure 6-3: Selected diamonds above 0.5 ct from Ashmore (Striker Resources Annual Report Year 1999).**

### **6.3 Ground elevation data at Ashmore**

Topographic surveying was done for the Ashmore gravity 1997 and 1998 surveys using a total station. This was done by a surveyor on contract to Striker Resources. Figure 6-3 shows the ground elevation image acquired for these surveys. This image shows 0.5 metre contours with a linear colour stretch. The centres of Ashmore pipes 1 to 4 are also shown on this map. These are the centres as determined from the 1997 and 1998 gravity surveys. Figure 6-3 shows that the Ashmore pipes 1, 2 and 3 are located close to, but just down slope from, an east-west trending topographic high. Ashmore 4 is located well down slope and to the north of this ridge.

### **6.4 Low level aeromagnetic survey at Ashmore**

Aeromagnetic data were acquired by Geotrex (1996) as part of a low level DIGHEM helicopter EM and magnetic survey. The survey was flown in August 1996 with 100 m line spacing and flight line direction 29-209 degrees. Magnetic data were acquired with a Cesium Vapour magnetometer flown at 40

metres above ground level. EM data were acquired at 30 metres above ground level.

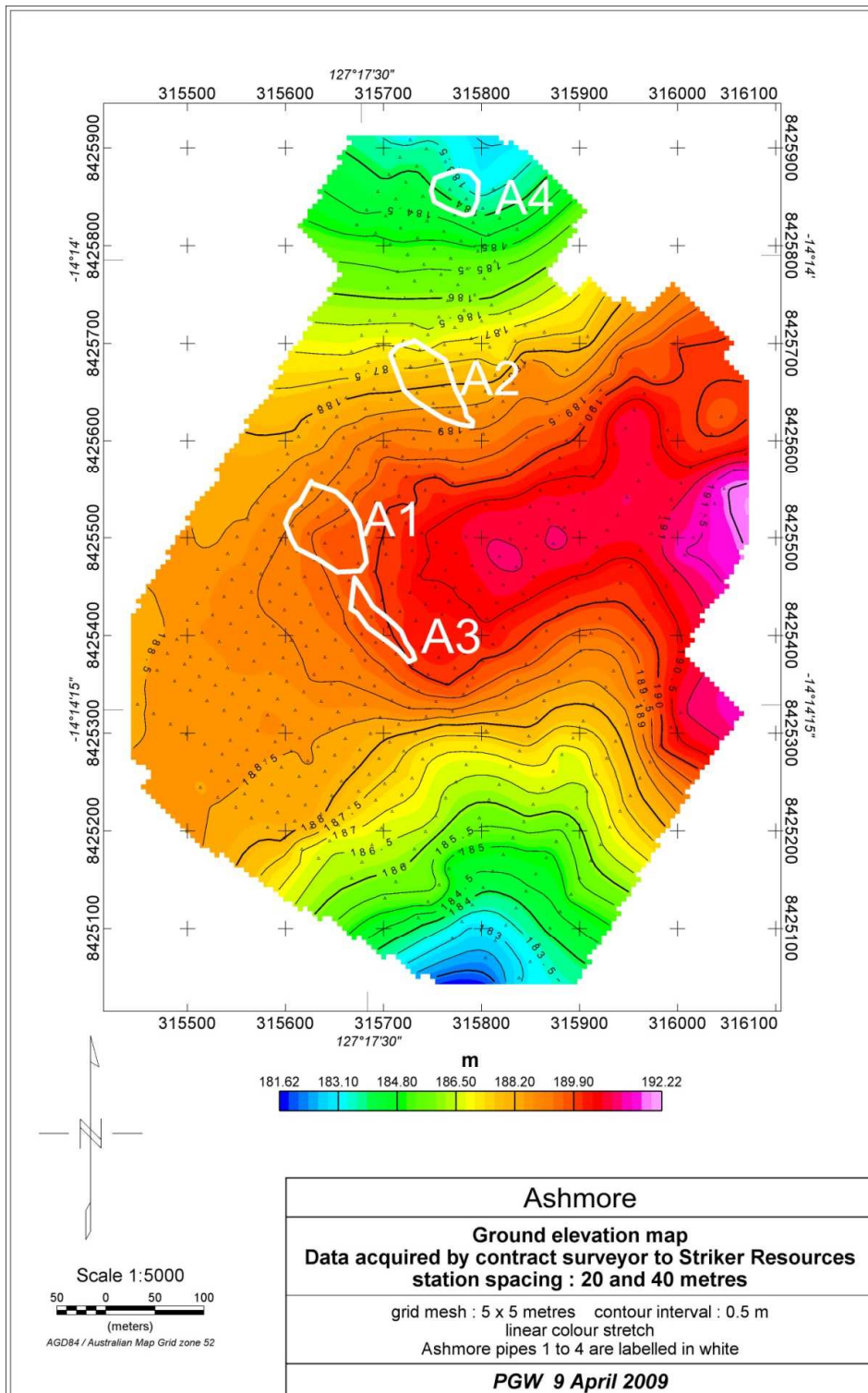


**Figure 6-4: Ashmore ground elevation data acquired by total station surveying for 1997 and 1998 gravity surveys. Pipe outlines and labels are shown in white. The Ashmore pipes are just downslope from a small topographic high.**

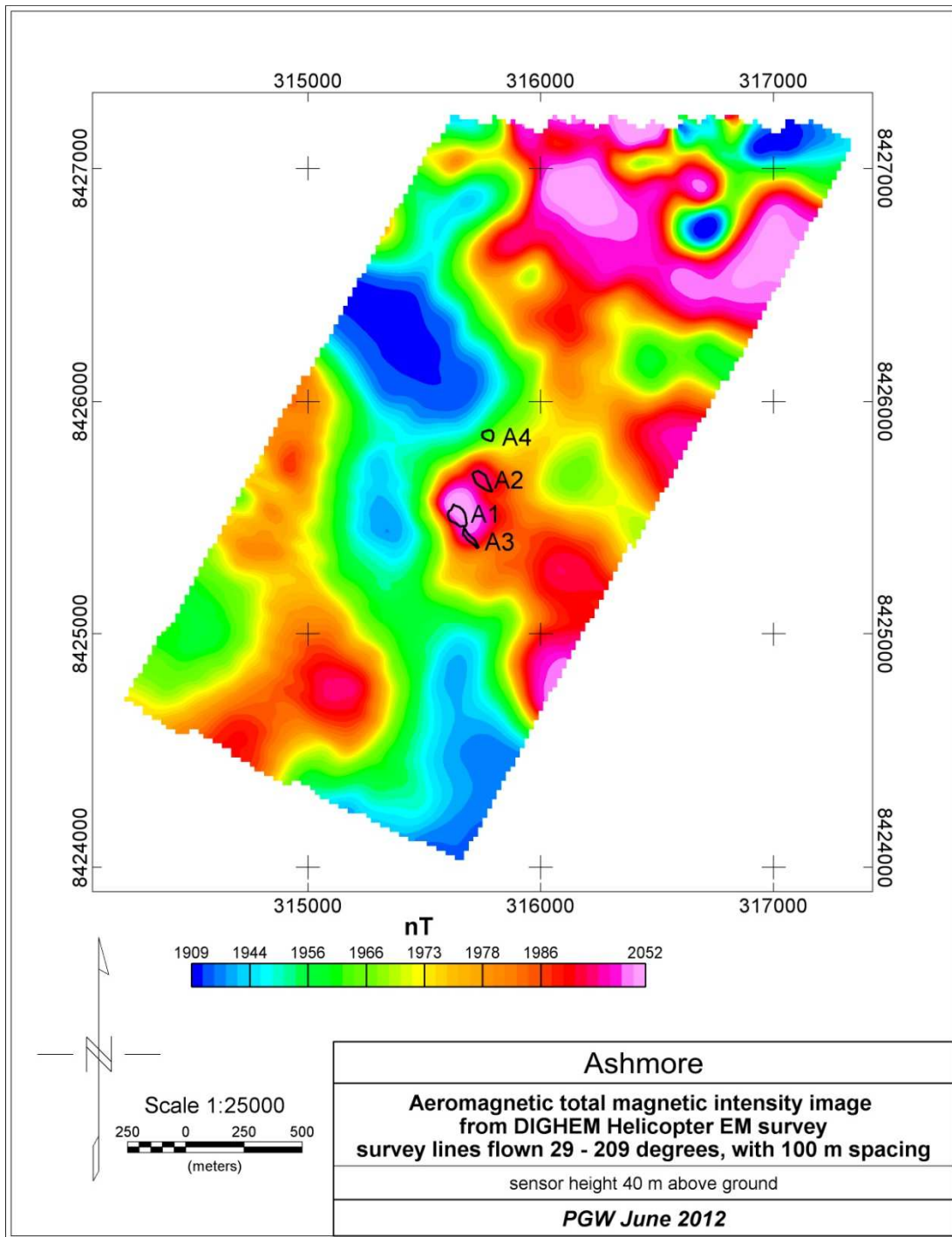


**Figure 6-5: Total magnetic intensity image of Ashmore area from DIGHEM helicopter electromagnetic and magnetic survey. Ashmore pipes 1 to 4 are shown labelled in black on the image. The pipes 1, 2 and 3 are associated with a positive magnetic anomaly. Ashmore 4 does not appear to have a magnetic signature.**

Figure 6-5 shows that the Ashmore area is shown as a magnetic high which reflects the magmatic kimberlite material. In the northern part of the image, the magnetic response is due to the very extensive Carpentarian age Carson Volcanics. Where these are present it is difficult to recognise magnetic signatures due to kimberlites. At Ashmore, the host rock is Warton Sandstone which is essentially non-magnetic and therefore makes it easy to recognise magnetic signatures of kimberlites.

### 6.5 Heliborne DIGHEM frequency domain electromagnetic surveys

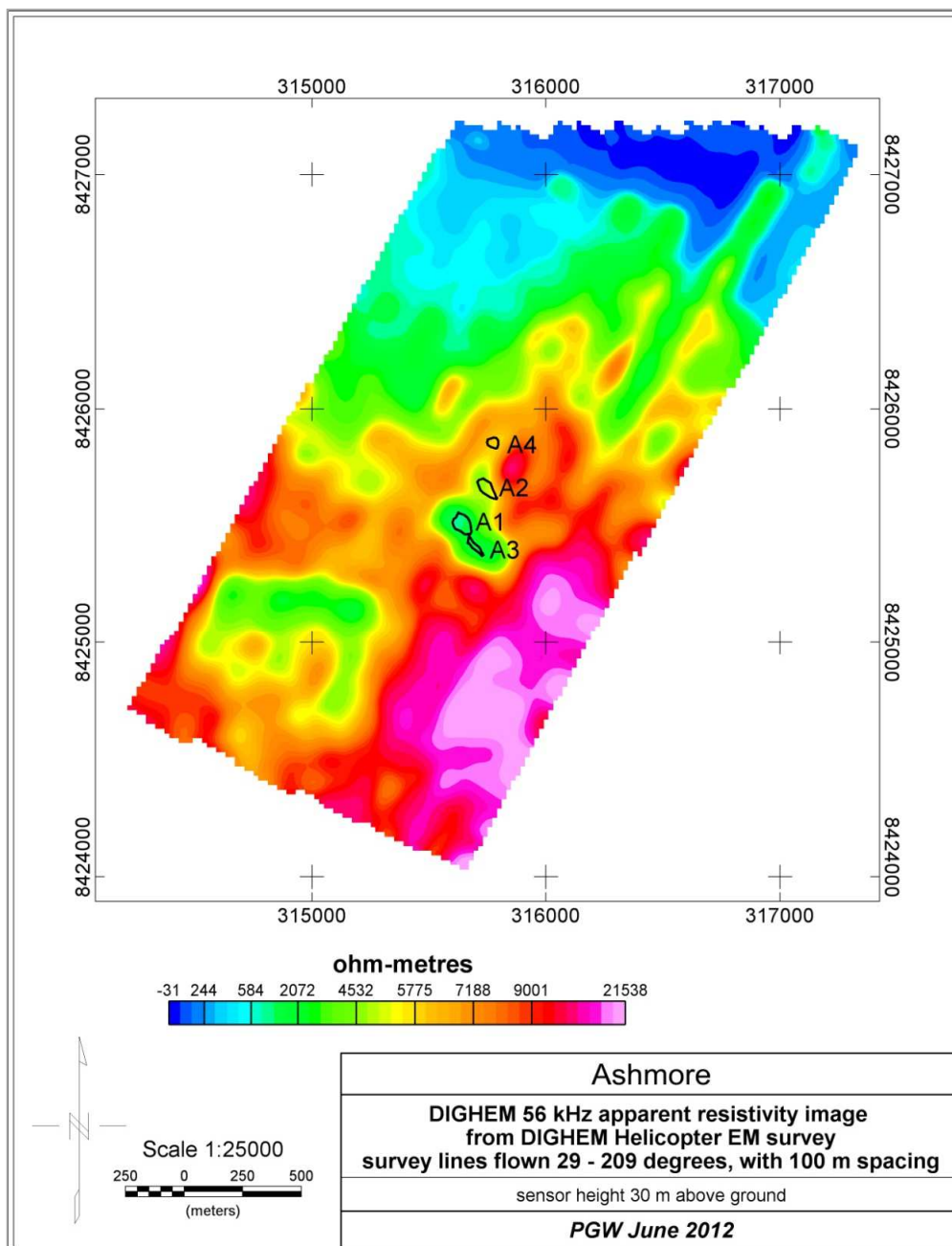
DIGHEM surveys were flown over Ashmore and Lower Bulgurri in 1995 and 1996, (Geoterrex, 1996), using 100 metre line spacing and helicopter height of 60 metres above ground. EM bird height was 30 metres above ground. The DIGHEM coil specifications are shown in Table 6-1.

**Table 6-1: Coils and frequencies used in the DIGHEM surveys.**

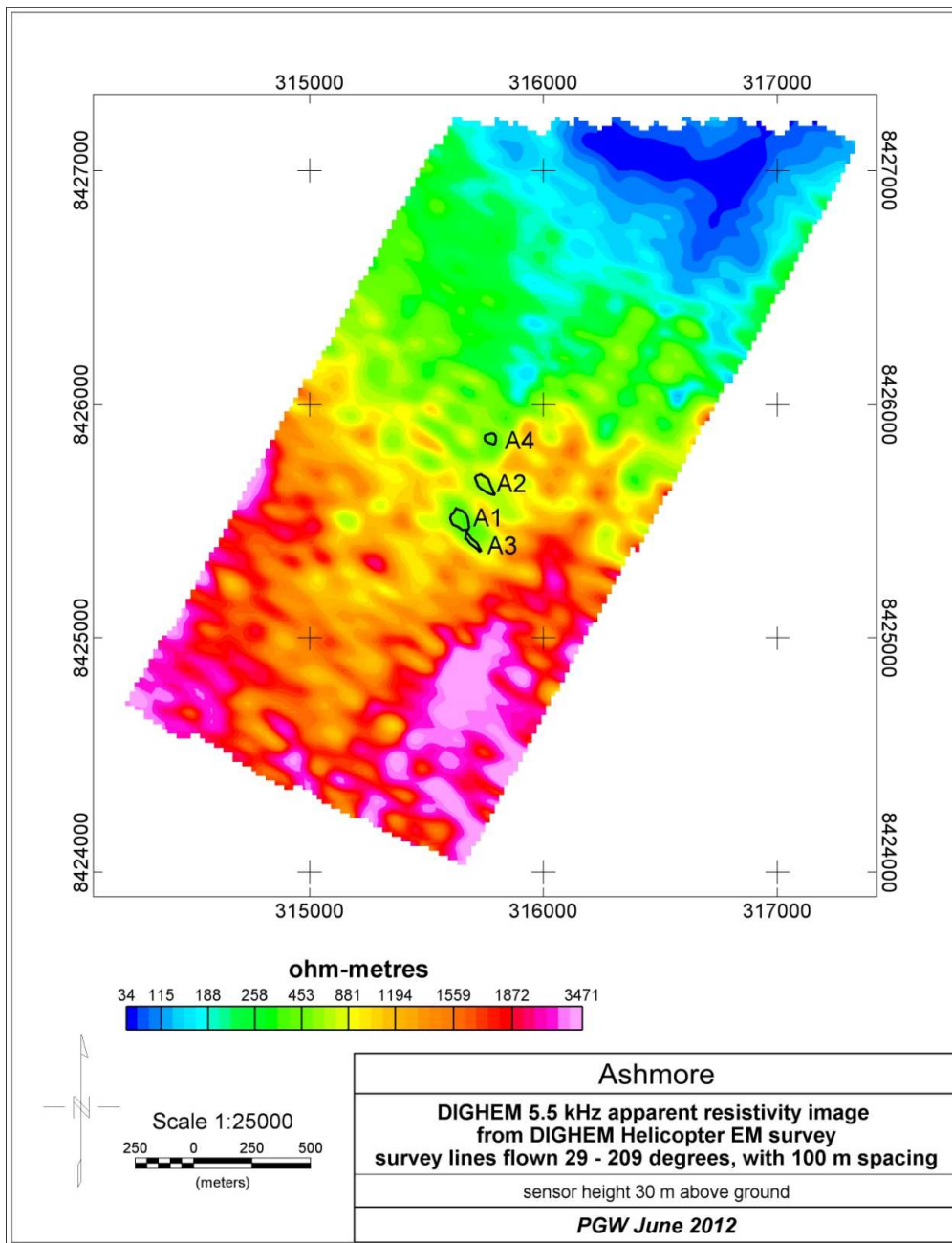
Coil	Coil Frequency (Hz)		Coil Separation (m)	Coil orientation	Sensitivity (ppm)
	Nominal	Actual			
1	400	387	8.1	Coplanar	0.06
2	900	890	8.1	Coaxial	0.06
3	5500	5621	8.1	Coaxial	0.10
4	7200	7272	8.1	Coplanar	0.10
5	56000	55640	6.3	Coplanar	0.30

Figure 6-5 shows the apparent resistivity image from the 56 kHz horizontal coplanar coils. This is the highest frequency used during this survey and gives the shallowest penetration. With 2000 ohm-metre sandstone this gives a skin depth of 95 metres. Figure 6-5 shows that the area of the pipes is characterised by lower resistivity than the surrounding host rocks – mainly Warton

Sandstone. This lower resistivity or higher conductivity is attributed to clays that have developed over the top of the pipes during weathering. Figure 6-6 shows the apparent resistivity image from the 5.5 KHz data and this has a skin depth of about 300 metres for a resistivity of 2000 ohm-metres. Skin depth in metres is approximately  $504 \times (\text{resistivity/frequency})^{0.5}$  (Parasnis, 1997, page 232) where resistivity is in ohm-metres and frequency is in hertz.



**Figure 6-6: Dighem 56 KHz Apparent resistivity image for Ashmore and surrounding area. Ashmore pipes 1 to 4 are shown labelled in black text on the image as A1 to A4. The pipes are located in relatively more conductive ground than surrounding areas but are not sufficiently distinctive to be detectable from their conductivity signature. 56 KHz is the highest frequency used on this survey and emphasises near surface conductivity.**



**Figure 6-7: Dighem 5.5 KHz Apparent resistivity image for Ashmore and surrounding area. Ashmore pipes 1 to 4 are shown labelled in black on the image.**

## 6.6 Ground gravity at Ashmore

Gravity data were acquired in 1997 and 1998 by the author and students Sumner and McChesney using a Scintrex CG3 digital gravity meter. Survey lines were spaced at 40 metres, but some were later infilled with a line spacing of 20 metres. Station spacing was 20 metres. The gravity meters were calibrated at Kununurra Airport at a Geoscience Australia absolute gravity station. This enabled establishment of sites at Geebung airstrip, and also at the Striker Resources Beta Creek camp where we had well established absolute values. Other gravity station bases were also established for the Ashmore and Seppelt areas. This enabled all the new gravity data to be tied into the Geoscience Australia database and meant that each new gravity dataset could easily be added to previous survey data. This was continued with later contract surveys done by Haines Surveys to the author's specifications.

Absolute gravity bases are shown in Table 6-2.

**Table 6-2: Established absolute values for the Striker Resources gravity bases.**

<b>Location</b>	<b>AMG52 Easting</b>	<b>AMG52 Northing</b>	<b>Absolute Gravity (mGals)</b>
Kununurra Airport	469180	8254730	978392.316
Geebung airstrip	322011.8	8428846.5	978338.886
Beta Creek camp	315904.0	8421467.0	978340.416

The first gravity work by Curtin University for Striker Resources was done in July 1997 at Ashmore and within the first week it was shown that Ashmore pipes 1 and 2 were detectable by gravity. Use of gravity surveying led to the rapid identification of new drill targets at Ashmore 3 and 4 (Figure 6-7). These targets were subsequently confirmed by drilling.

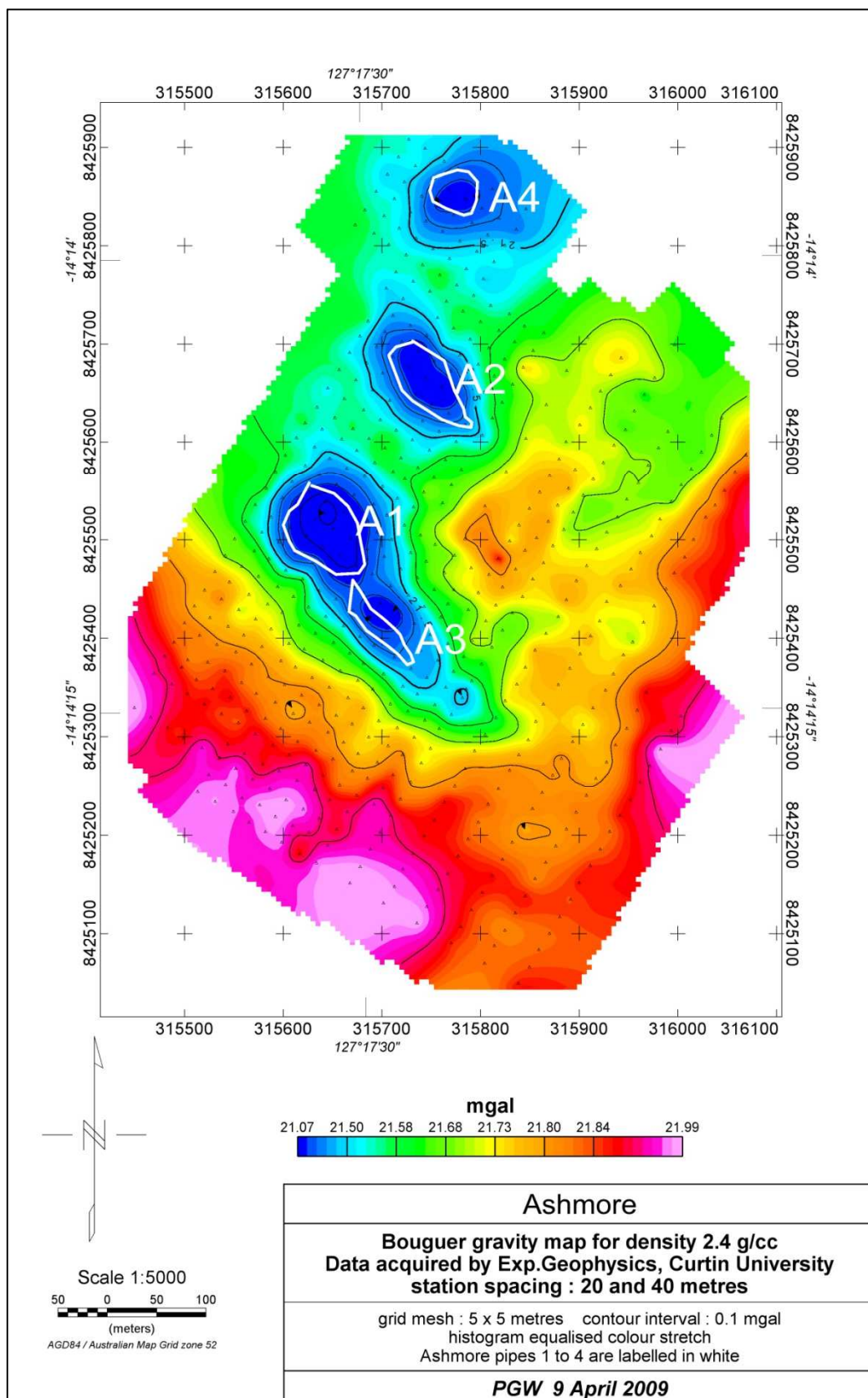


**Figure 6-8: Ashmore Bouguer gravity map for density 2.4 g/cc. All four pipes are well defined by the gravity results which show gravity lows over all these pipes.**

## **6.7 Ground magnetic survey at Ashmore**

Ground magnetic data were acquired at Ashmore in 1997 by Curtin University staff and students. Survey lines were spaced 20 m apart and magnetic readings were acquired every 1 m along survey lines. A Geometrics G856 proton precession magnetometer was used to acquire the data with the sensor 2 metres above the ground. Survey lines followed the local grid, which was oriented 31 degrees east of magnetic north. Data were converted to AMG grid coordinates following detailed topographic surveying using a total station. A second G856 magnetometer was used as a magnetic base station. Data from this magnetometer were subtracted from the mobile G856 data to remove diurnal variations.

Diurnally corrected magnetic data were gridded with grid mesh spacing of 5 x 5 metres and are displayed in Figure 6-8. This shows considerable surface noise and to minimise this, the gridded data were upward continued by 10 metres. This was followed by reduction to pole and used to create Figure 6-9. This also includes 0.1 mGal Bouguer gravity contours which outline the pipe positions well. It can be seen that pipes A1 and A3 have a corresponding magnetic response. The eastern part of pipe A2 is magnetic and pipe A4 is very weakly magnetic.

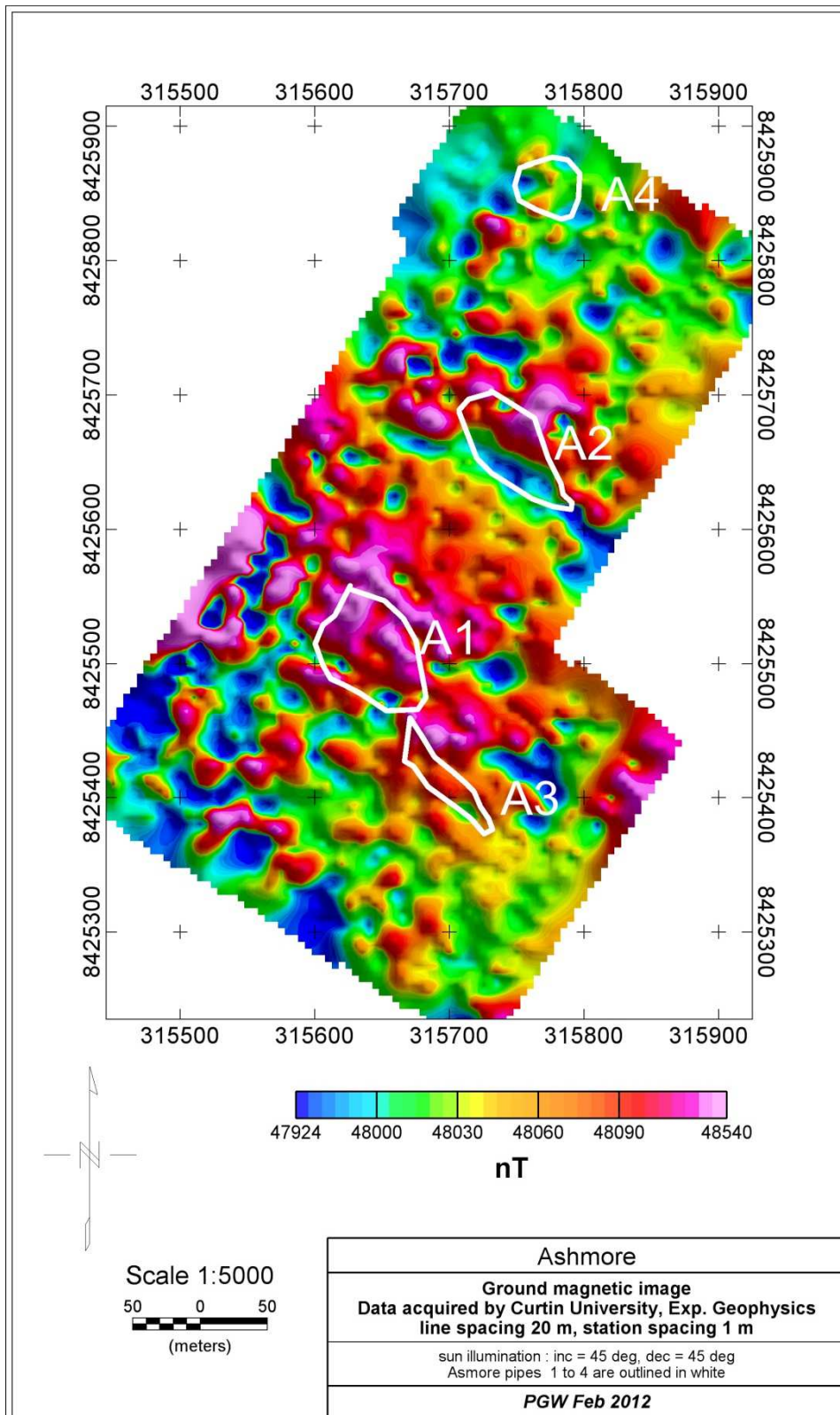
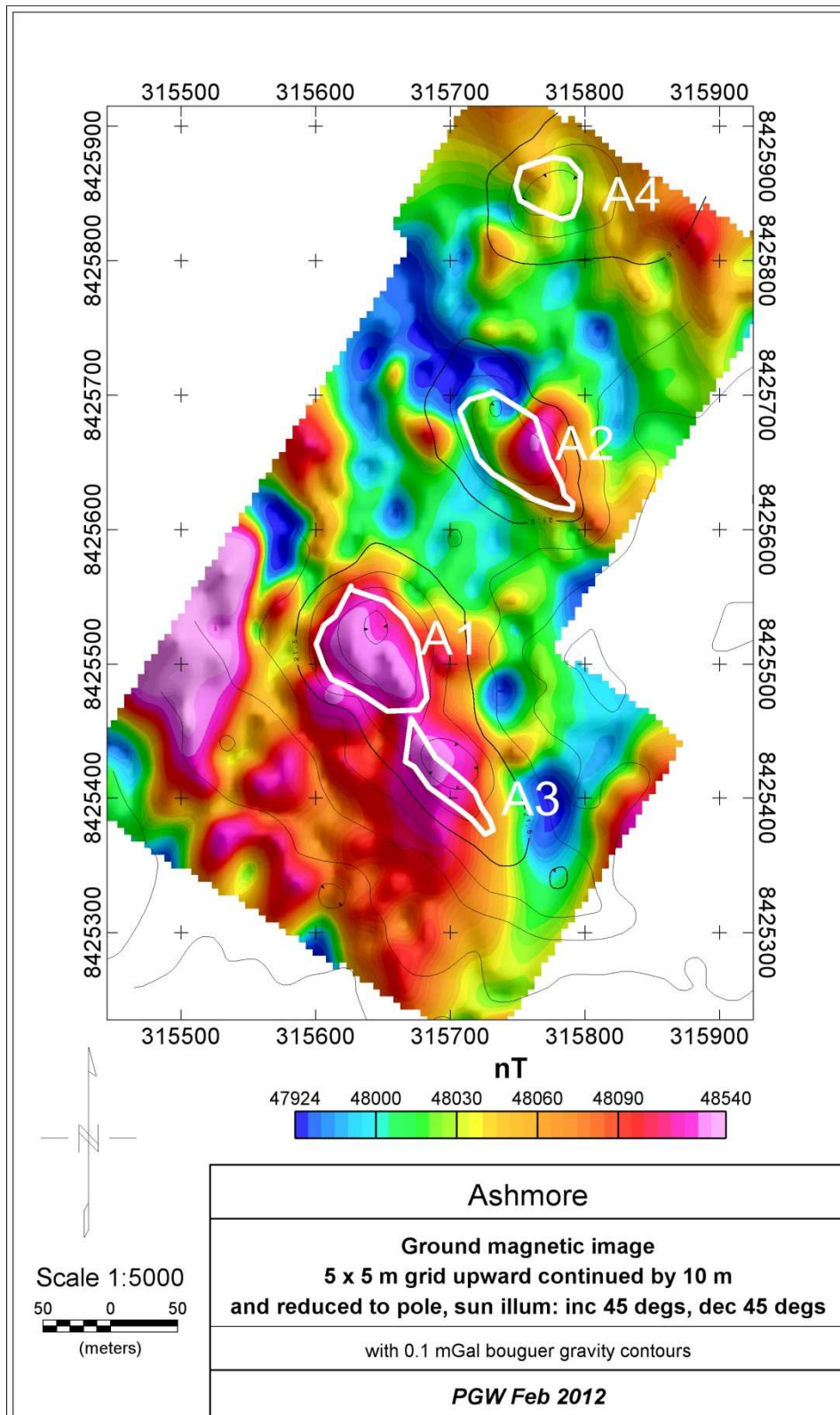


Figure 6-9: Ashmore ground total magnetic intensity map. The Ashmore pipes 1, 2 and 3 are all magnetic but due to surface magnetic sources are not as clearly seen without reduction to pole and upward continuation. The results following those two additional processing steps are shown in Figure 6-10. Sun illumination from NE with 45 degree elevation.



**Figure 6-10: Ashmore ground magnetic data upward continued by 10 m and reduced to pole. Pipe outlines are shown in white. Contours are of Bouguer gravity. Pipes A1, A2 and A3 are well seen in the ground magnetic data of this image. The Ashmore 4 does not appear to be magnetic. Reduction to pole and upward continuation have clarified the magnetic response over Ashmore 1, 2 and 3 pipes.**

## **6.8 Ground electromagnetic survey at Ashmore**

Frequency domain ground electromagnetic data were acquired at Ashmore using Geonics EM 34 equipment. This used a frequency of 1600 hertz and coil spacing of 20 metres. Lines and stations were spaced at 20 metres. Two modes were used; horizontal coplanar coils and vertical coplanar coils. Results from the more commonly used, vertical coplanar data are shown as Figure 6-11. This shows very clear conductivity highs over each of the pipes A1, A2, A3 and A4. These highs are attributed to conductive clay that develops during weathering of the kimberlite pipes. The surrounding sandstone has very low conductivity, hence there is good conductivity contrast between the weathered cap over the pipe and the country rock.

Using two different coil orientations provides different results which can be used to establish geometric properties of the conductors.

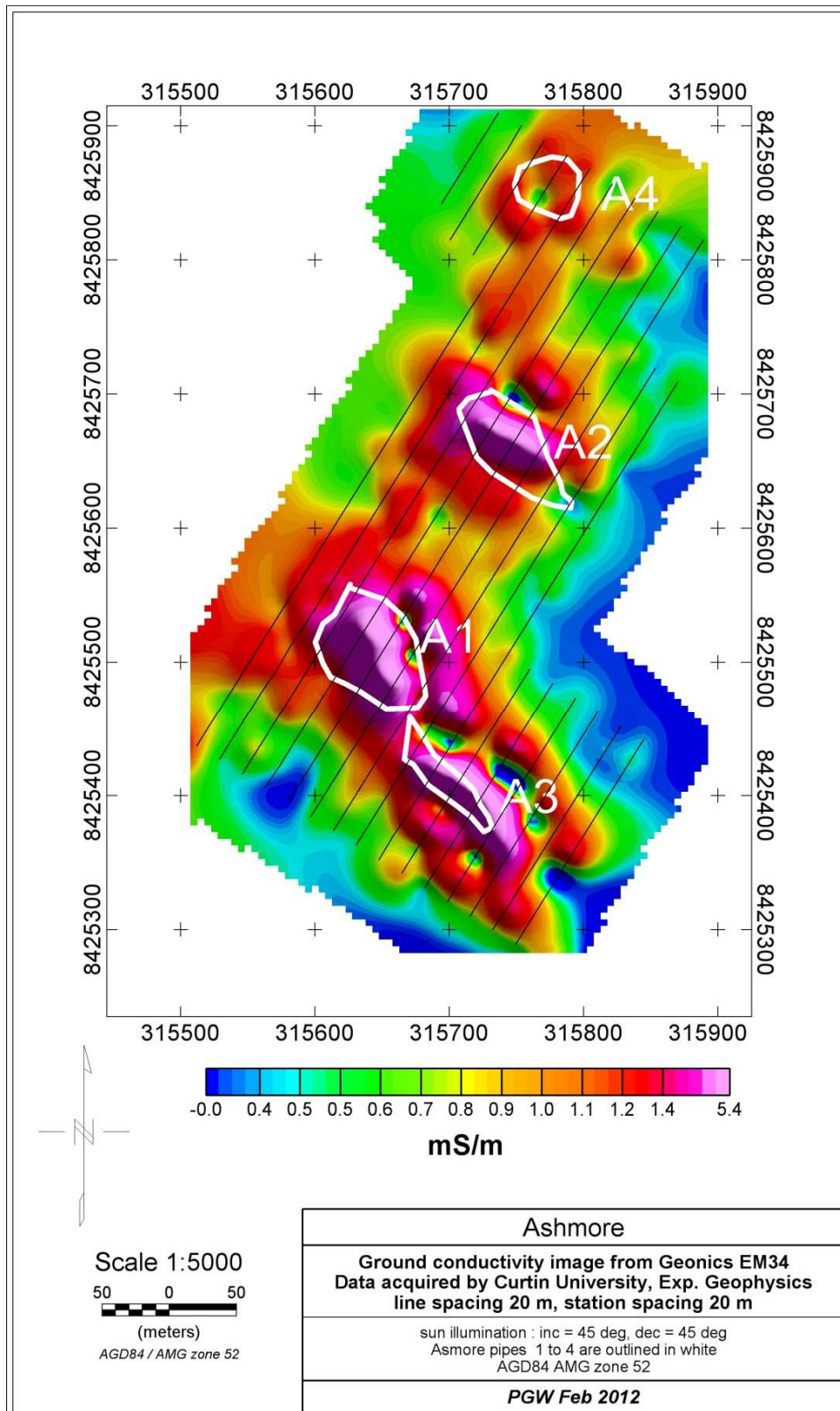


**Figure 6-11: Ashmore ground conductivity map from Geonics EM34 1600 Hz frequency domain survey. Ashmore pipes 1 to 4 are shown labelled in white. Note that pipes A1, A2, and A3 are well defined by the conductivity results. A4 area is less conductive but more conductive than its surrounding area.**

## **6.9 Discussion on integrated datasets**

The Ashmore pipes are characterised geophysically by magnetic, electromagnetic and gravity anomalies that contrast with the surrounding Proterozoic sandstone. Although the magnetic anomaly is a response from the magmatic kimberlite, the electromagnetic and gravity anomalies are products of the weathering, erosion and depositional backfill of the pipes. The pipes are much better defined from their ground gravity and conductivity responses due mainly to the weathered clays that have developed over the pipes. The clays have low density (less than 2 g/cc) compared with the surrounding sandstone and provides sufficient density contrast for the gravity method to work well. The line and stations spacing for the gravity were 40 metres, with some infilling to 20 metres which proved effective. The ground conductivity measurements also used 20 metre line and station spacing.

The gravity work led to the discovery of further pipes which were subsequently proved by drilling to be kimberlitic. The aeromagnetic data from the DIGHEM survey showed a magnetic target over the Ashmore area, coincident with conductivity highs. The ground magnetic data (Figure 6-8) showed considerable surface noise. This was considerably reduced by upward continuation by 10 metres. The gravity and EM measurements were the most useful in defining pipe locations at Ashmore.

## **7 EXPLORATION OVER SEPELT PROSPECTS**

### **7.1 Geology**

Local geology for the Seppelt areas is shown in Figure 7-1. This is from the regional 1:250 000 scale mapping of the Drysdale and Londonderry mapsheets, by Gellatly and Sofoulis (1969). The geological data are available digitally on a CD-ROM available from GSWA. The area of the Seppelt prospects show extensive areas of Proterozoic Pentecost Sandstone middle unit (Pkpm symbol on map). This unit forms part of the Kimberley Group, and crops out in a succession of escarpments and dip slopes. (Gellatly and Sofoulis, 1969). The middle unit of the Pentecost Sandstone is up to 350 metres thick and comprises a thin basal bed of grey glauconitic quartz sandstone overlain by white quartz sandstone. Cross-beds are common in the Pentecost Sandstone and indicate currents from the north and north-west. Faults are rare, but show two principal trend directions: 040 and 330 degrees.

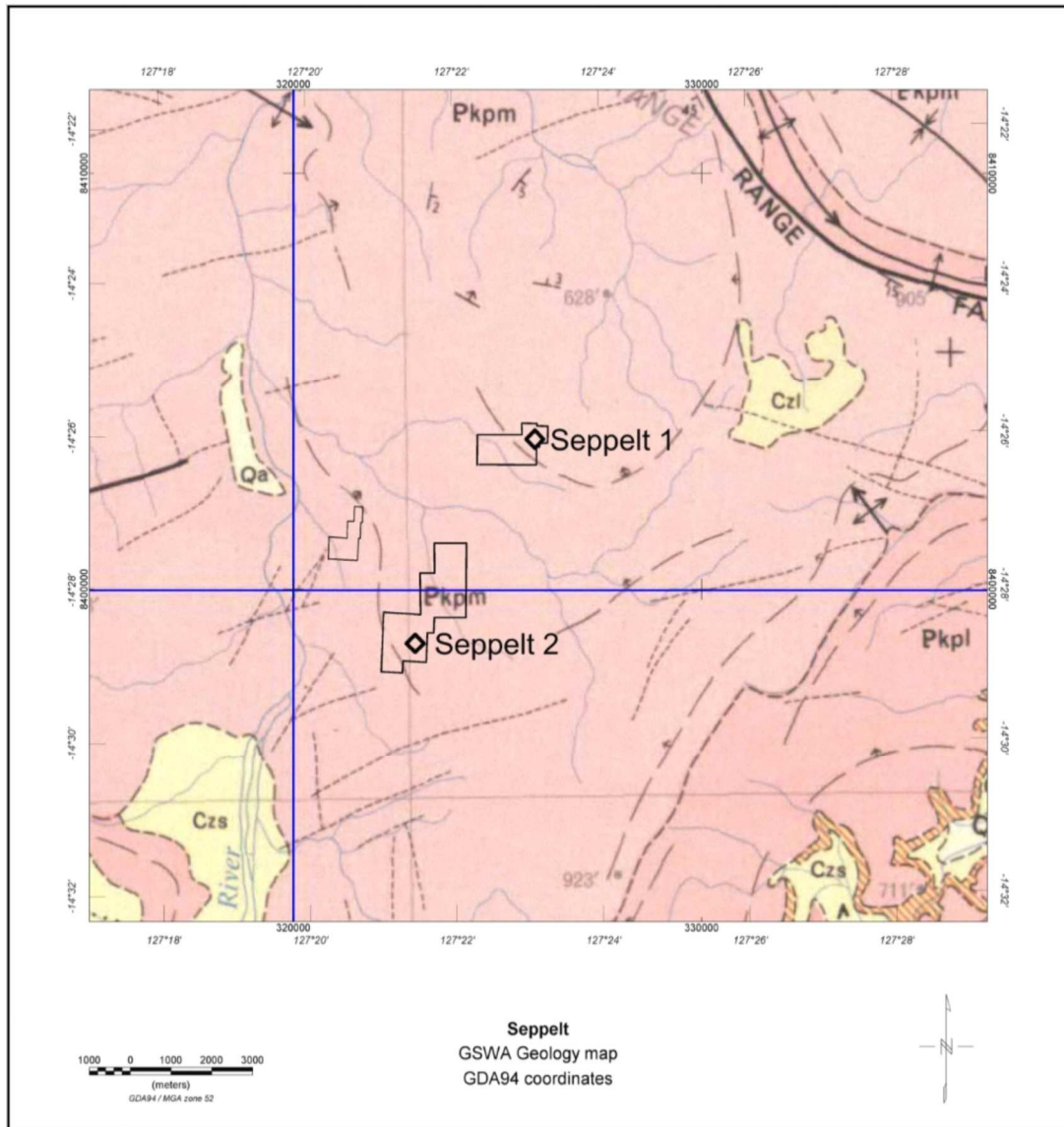


**Figure 7-1: Surface geology of the Seppelt areas reproduced from GSWA 1:250 000 Drysdale map sheet by Gellatly and Sofoulis (1969). Pkpm is Pentecost Sandstone (middle unit), Pkpl is Pentecost Sandstone (lower unit), Czs is Cainozoic sand, Czl is Cainozoic laterite and Qa is Quaternary alluvium. Black polygons show the locations of ground geophysical survey areas Seppelt 1 and Seppelt 2.**

## 7.2 Previous exploration

The Seppelt Project area comprises a number of related kimberlite dykes, blows and pipes constrained within a narrow corridor over a strike length of some 6 km. The main prospects are Seppelt 1 and Seppelt 2, but as shown in Figure 7-2, there are other nearby prospects including Seppelt 3, Seppelt 4, Seppelt 5 and Seppelt 6.

### *Seppelt 1*

Stockdale Prospecting in joint venture with BHP Minerals, carried out extensive exploration within the Forrest River area in the years 1990 – 1994 (Sumpton and Smith, 1997). The Seppelt 1 kimberlite was discovered during this period and resulted from sampling heavy mineral stream sampling which yielded large numbers of kimberlitic spinels and diamonds in drainage samples. The initial discovery was followed by low level (60 m) close spaced (100 m) aeromagnetic survey which showed a distinctive circular anomaly against a quiet magnetic background. This was subsequently drilled and proved to be a kimberlite pipe with two lobes intruding Pentecost Sandstone. The top 30 m of the kimberlite pipe has been extremely weathered to kaolinite, below which is found hypabyssal kimberlite. Measured magnetic susceptibilities showed the pipe to be strongly magnetic with values up to 0.04 SI units. However, there is a strong reversely magnetised remanent component which reduces the amplitude of the observed magnetic anomaly over Seppelt 1. Gravity surveying showed a residual gravity low of about 0.5 mGal, which was attributed to weathering of the upper part of the pipe. EM methods were also used here with a DIGHEM helicopter survey and a ground EM Geonics EM 34 frequency domain survey. Both showed responses attributed to the weathered top of the pipe. Striker Resources in a statement to the ASX in January 2002 advised that the inferred resource at Seppelt 1 was 1.7 m tonnes of kimberlite which with an inferred grade of 40 carat per tonnes yielded a resource of approximately 700,000 carats of diamonds. This was calculated down to 140 metres in the north lobe and 110 metres in the south lobe. The mineralisation was open at depth so there was good prospect of further reserves being added with further drilling and investigation.

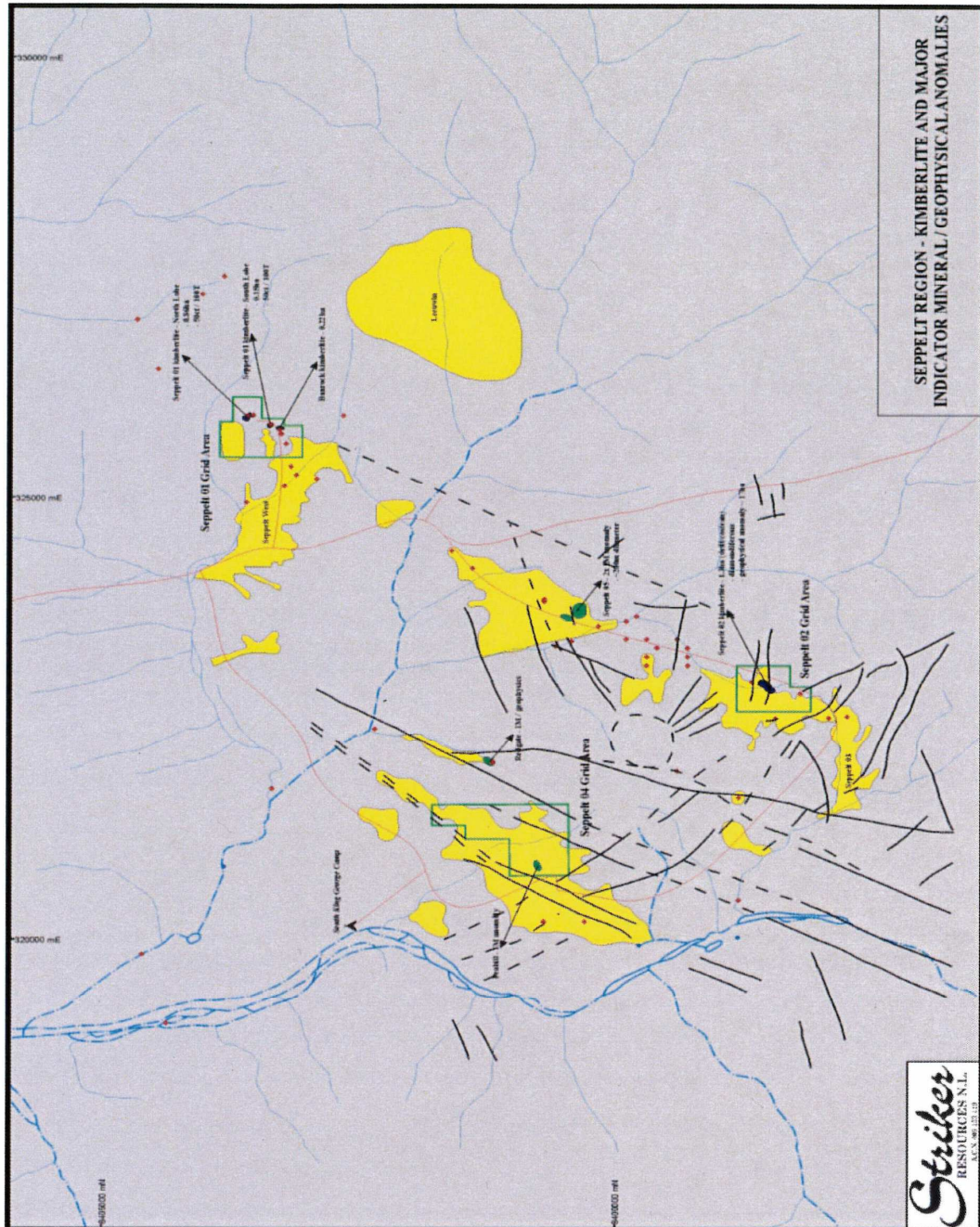


Figure 7-2: Seppelt location map showing the main prospects, reproduced from announcement by Striker Resources to the ASX on 2002

### Seppelt 2

Seppelt 2 is a kimberlite pipe comprised of both weathered kimberlite and infill gravels. The gravels have a variable grade and persist to a depth of 36 m.

Beneath the gravels is weathered kimberlite with a grade of 211 cpht. The Seppelt 2 pipe has an inferred resource of 200,000 t to 200 m depth (North Australian Diamonds Limited, formerly Striker Resources, website, May 2006).

Later exploration at Seppelt focused on the discovery of kimberlites within the already identified Seppelt structural corridor as well as the immediately surrounding area. Exploration to date has identified a number of areas where both indicator minerals and commercially sized diamond occurrences remain unresolved. These include the Coolabah, Collison, and Collison North areas.

### **7.3 Digital elevation data for Seppelt prospects**

Shuttle Radar (SRTM) data have been used to create the regional digital elevation image shown here as Figure 7-3. From the SRTM image it can be seen that both Seppelt 1 and Seppelt 2 are located on the western side of hills which may well be fault controlled with approximately NW-SE trending faults. Detailed elevation data for Seppelt 1 and Seppelt 2, from the gravity survey are shown in Figures 7-4 and 7-5. Seppelt 1 is located on the southern side of an east west ridge. Seppelt 2 is located at the upper end of a shallow sloping low relief drainage area.

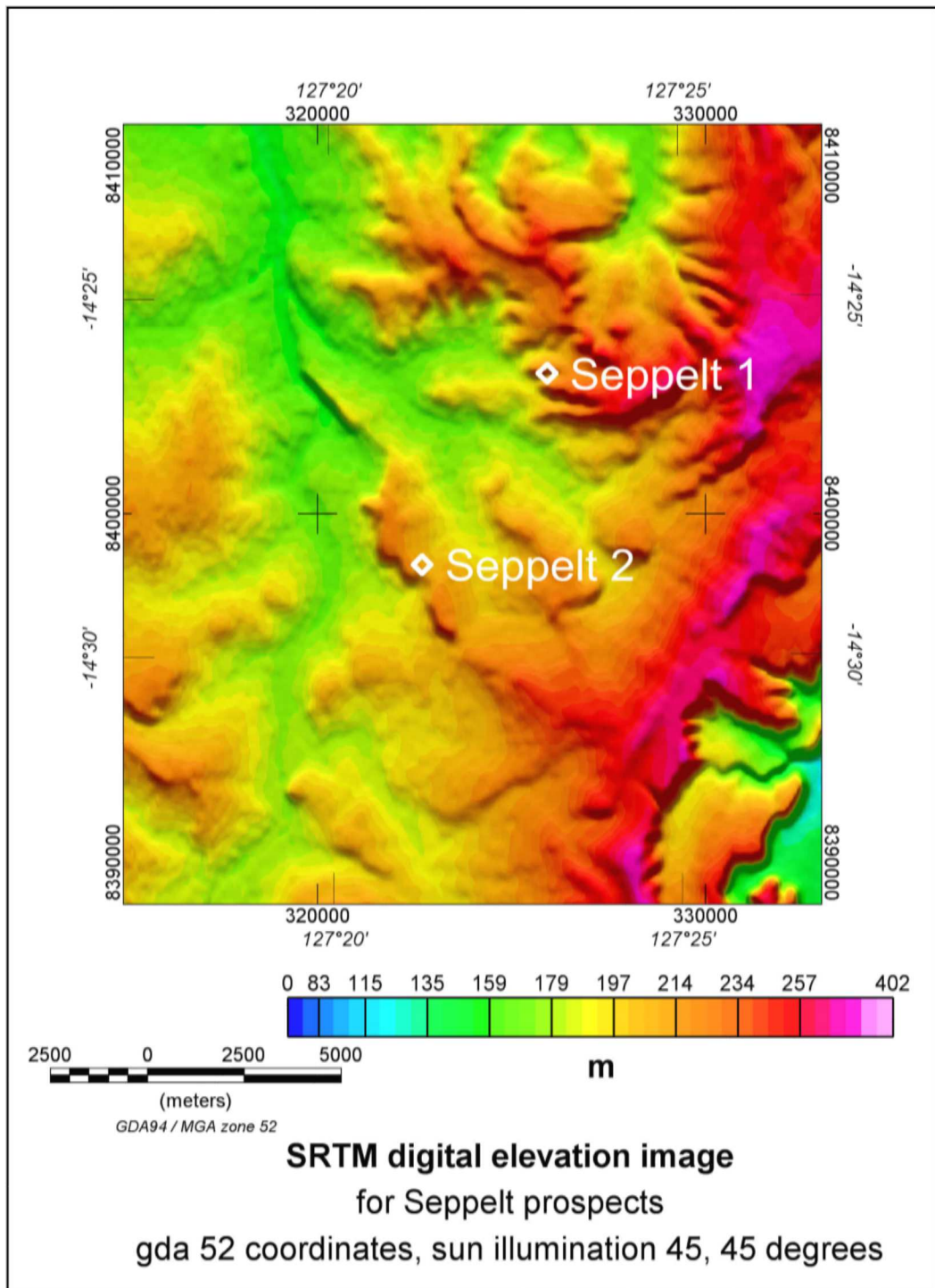
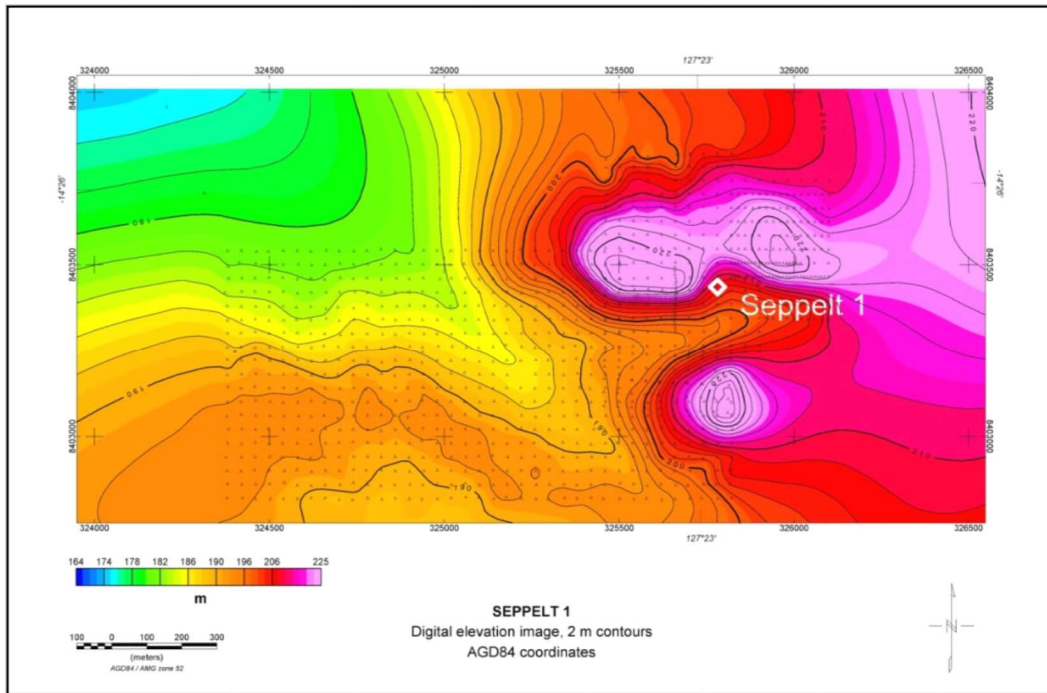
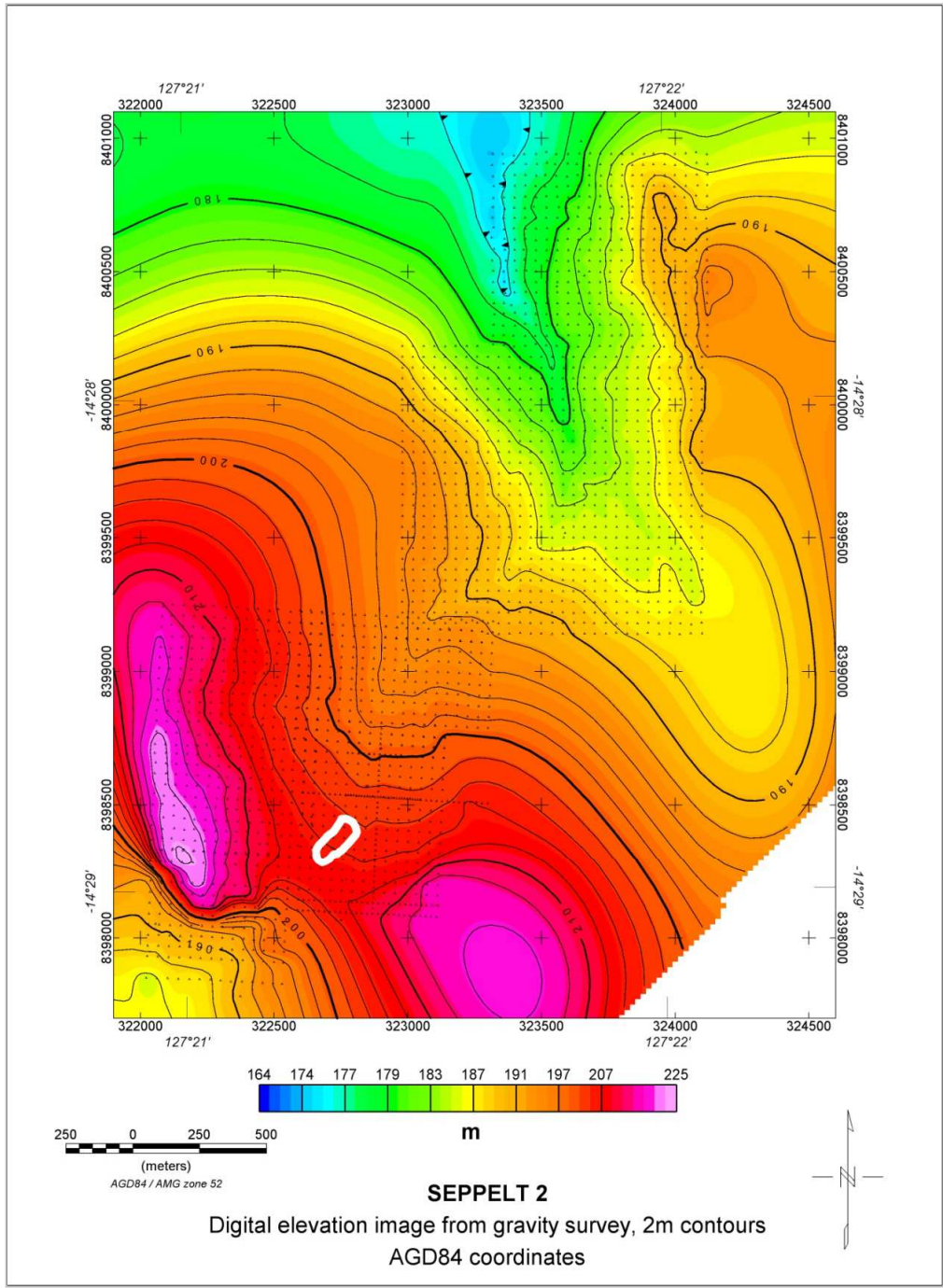


Figure 7-3: Seppelt area SRTM digital elevation image. Seppelt 1 and 2 appear to be close to NNW striking faults.



**Figure 7-4: Seppelt 1 detailed digital elevation image from gravity survey height data. Seppelt 1 is located close to and down slope from an east west topographic ridge.**



**Figure 7-5: Seppelt 2 digital elevation image from gravity survey height data. Seppelt 2 is located in a shallow gradient area between higher ground to the south east and north west.**

#### 7.4 Helicopter electromagnetic survey of Seppelt areas

A helicopter electromagnetic survey was flown over the Seppelt areas in September 2000 for Striker resources. The survey was flown by Geoinstruments using the Hummingbird bird mounted frequency domain system. EM bird system parameters are listed in Table 7-1. The system also included a Geometrics G822 magnetometer mounted in the bird. Bird height was approximately 30 metres above ground level. Survey lines were flown north-south with a spacing of 100 metres. Some additional 100 m spaced east-west lines were added over the Seppelt 1 area.

**Table 7-1: Coils and frequencies used in the Hummingbird survey.**

Coil	Coil Frequency (Hz)		Coil Separation (m)	Coil orientation	Resolution (ppm)
	Nominal	Actual			
1	880	880	6.3	Coplanar	0.5
2	980	980	6.3	Coaxial	0.5
3	6600	6606	6.3	Coplanar	0.5
4	7000	7001	6.3	Coaxial	0.5
5	34000	34133	6.3	Coplanar	0.5

In addition to the electromagnetic and magnetic data, digital terrain data were also computed from this survey. A digital terrain image for the Seppelt areas is shown in Figure 7-6. This has been computed using a linear colour stretch. Apparent resistivity data were computed from the in phase and quadrature data for each of the five frequencies measured. Apparent resistivity for the highest frequency: 34133 Hz is shown in Figure 7-7. With a skin depth of approximately 3 metres, this frequency shows surface apparent resistivity. For clay weathering over the pipes we expect to see low resistivity features and this

is indeed seen for Seppelt 1 and Seppelt 2. Seppelt 4 and 6 prospects also show low resistivity. Pipe outlines are also included for Seppelt 1 and Seppelt 2.

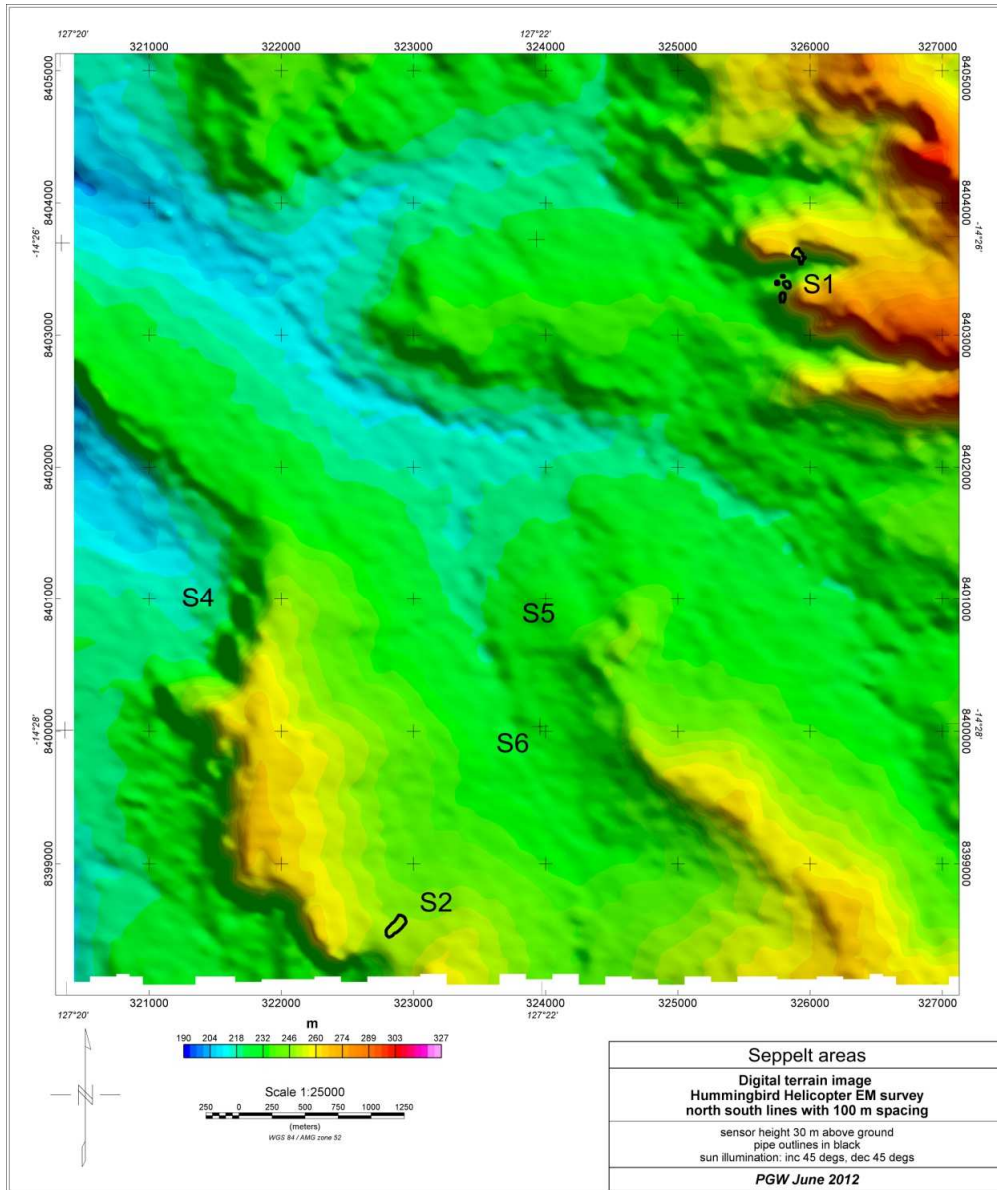


**Figure 7-6: Seppelt areas digital terrain image from Hummingbird HEM survey. A regional structure trending about 315 degrees is seen in the topography of the Seppelt 1 area. Topographic control is not evident for the other Seppelt prospects. Topographic control is better seen in the SRTM image which is shown as Figure 7-3. Sun illumination from NE with 45 degree elevation.**

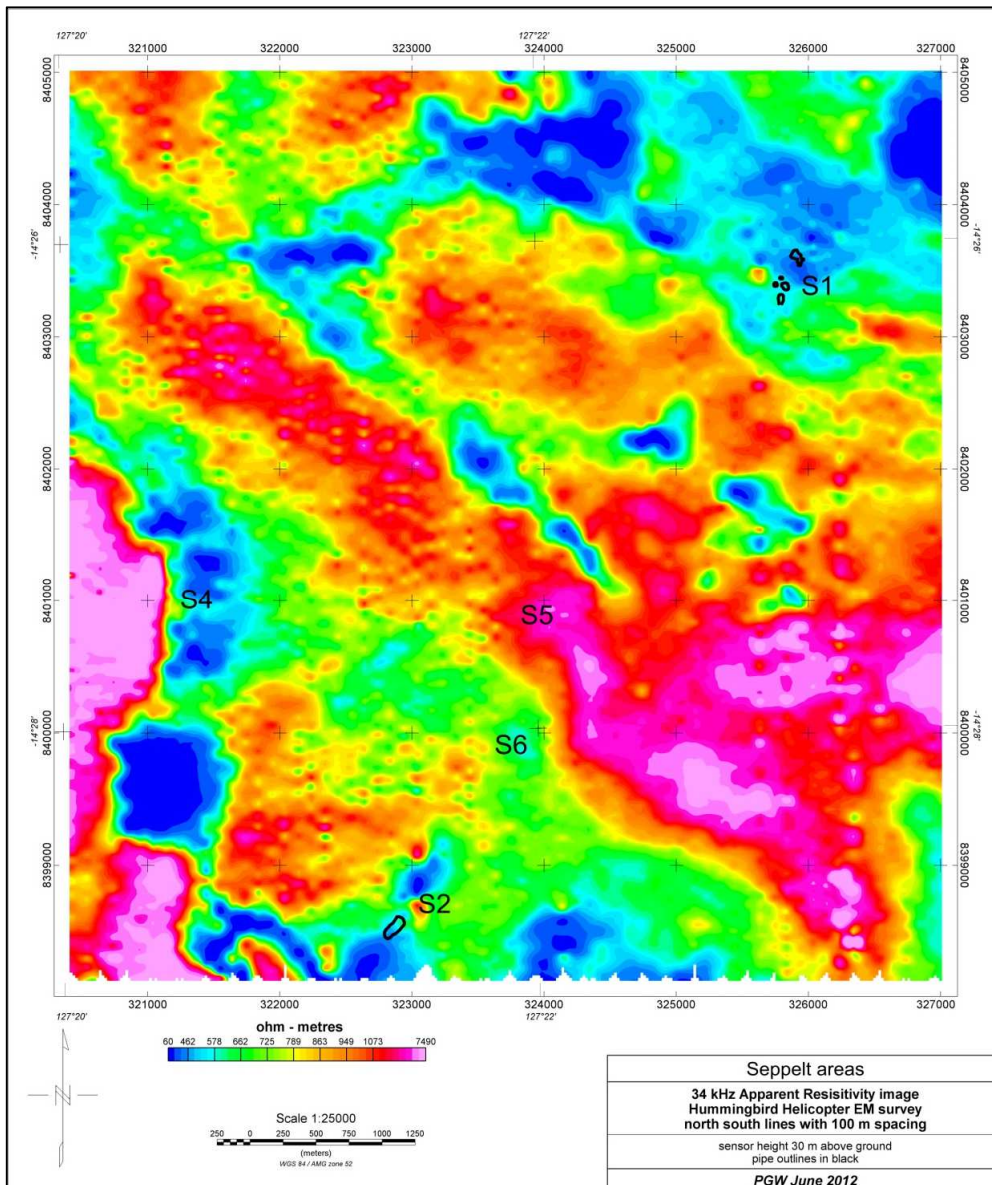


**Figure 7-7: Seppelt areas 34 kHz apparent resistivity image. Pipe outlines for Seppelt 1 and 2 are shown in black. Seppelt 1, 2, 4 and 6 are located in ground of lower resistivity than surrounding areas. Seppelt 5 is in ground of higher resistivity.**

## **7.5 Aeromagnetic surveys**

Aeromagnetic data over Seppelt 1 shows a clear positive dipolar anomaly over both lobes of Seppelt 1. This is illustrated by Figure 7-8, which was computed using gridded aeromagnetic data from Stockdale Prospecting (now De Beers). The north lobe has an aeromagnetic anomaly of about 12 nT and the south lobe about 2 nT. Flying height is not specified, but is likely to be about 60 metres above ground. Drillcore measurements on samples from Seppelt 1 showed strong reversed magnetisation. Magnetic susceptibility on core samples showed a value of 0.04 SI units (Sumpton and Smith, 1997). This is strongly magnetic compared with many other kimberlites. Figure 7-9 shows a regional aeromagnetic image for the Seppelt and Pteropus areas. The aeromagnetic anomalies are of low amplitude and are only seen because the local host rocks are weakly magnetic. These two pipes were only detected in the magnetic data by flying low level and closely spaced aeromagnetic surveys.

## **7.6 Ground magnetic surveys at Seppelt 1 and Seppelt 2**

A ground magnetic survey at Seppelt 1 was conducted in 1999 by Curtin staff and students, with east west lines spaced 40 m apart. Readings were made with a Geometrics G856 proton magnetometer, with 2 m station spacing. A second G856 magnetometer was used as a base station to record the diurnal variation during the survey. These data were subtracted from the data obtained with the mobile magnetometer. Figure 7-10 shows an image after upward continuation by 10 m and reduction to pole. The reduction to pole operation used an inclination of -44 degrees and a declination of +3.1 degrees. These were selected using the geographic coordinates for these areas and the International Geomagnetic Reference Field (IGRF) routine in Geosoft Oasis Montaj software. The known pipes at Seppelt 1 are shown with white outlines in Figure 7-10.

The main pipe at Seppelt 1 is the most northerly pipe shown in Figure 7-10. There are further pipes to the south west of the main Seppelt 1 pipe. Three of the pipes at Seppelt 1 are seen to be magnetic.

A similar survey was conducted at Seppelt 2 and results for this survey are shown as Figures 7-11. Seppelt 2 does not appear to be magnetic, but is located just north of a magnetic feature.

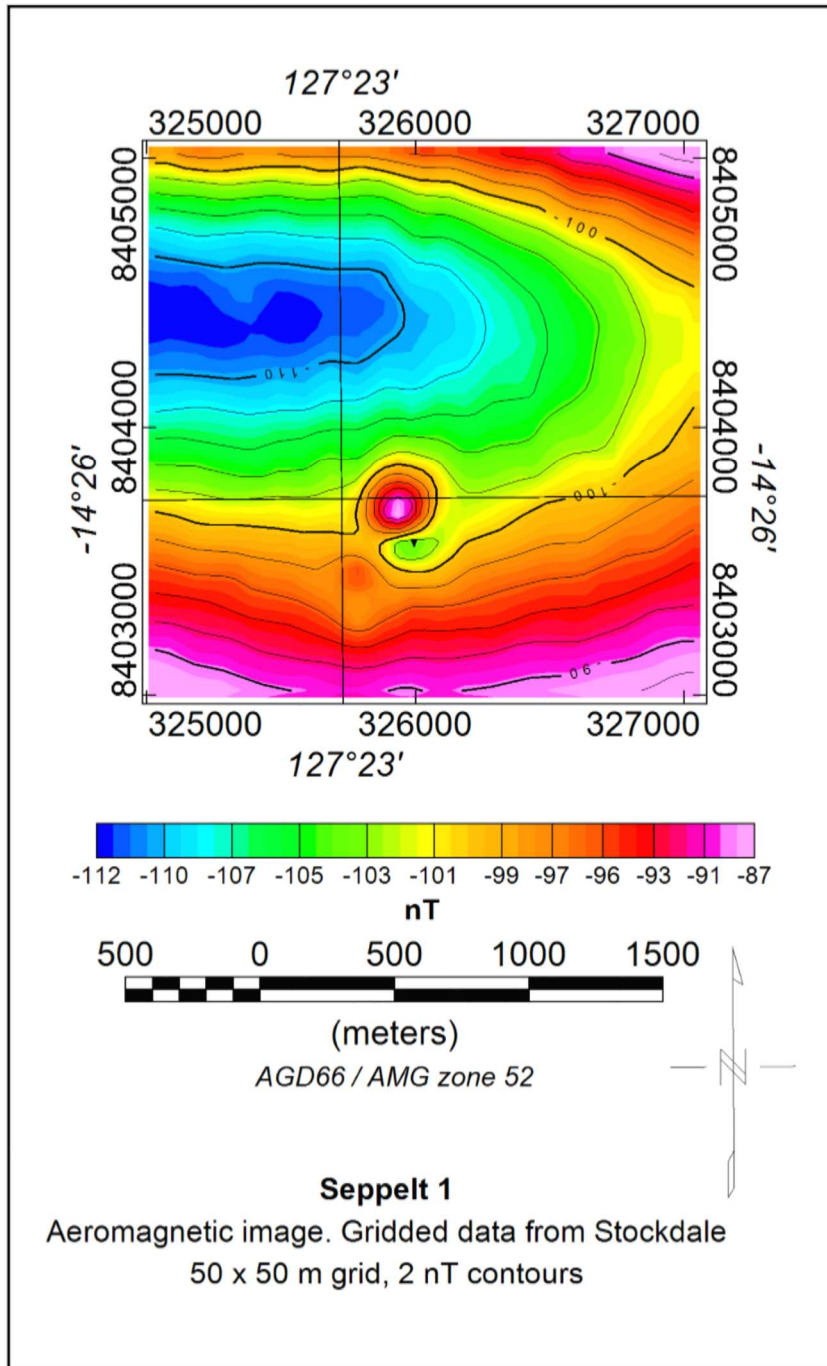
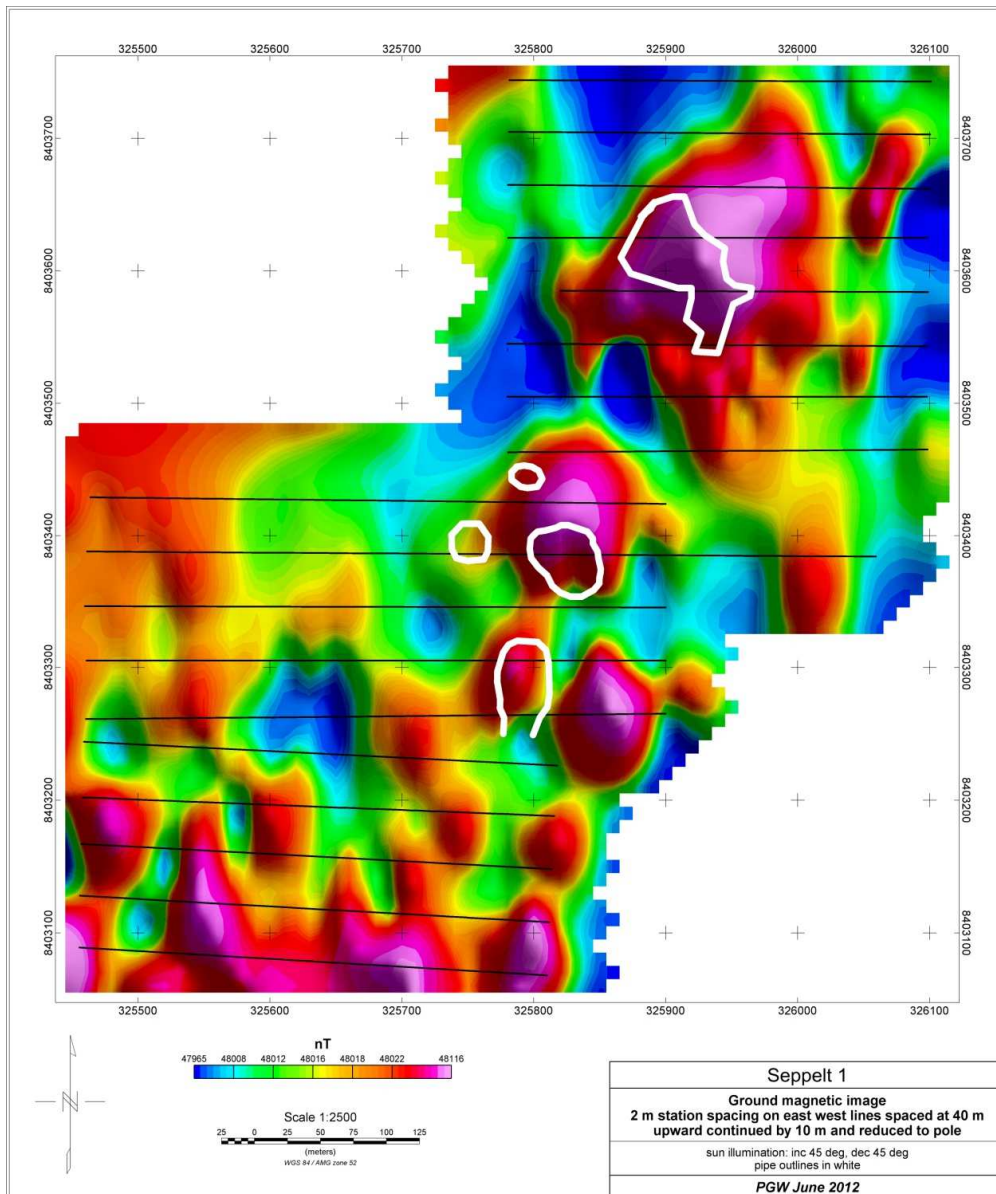
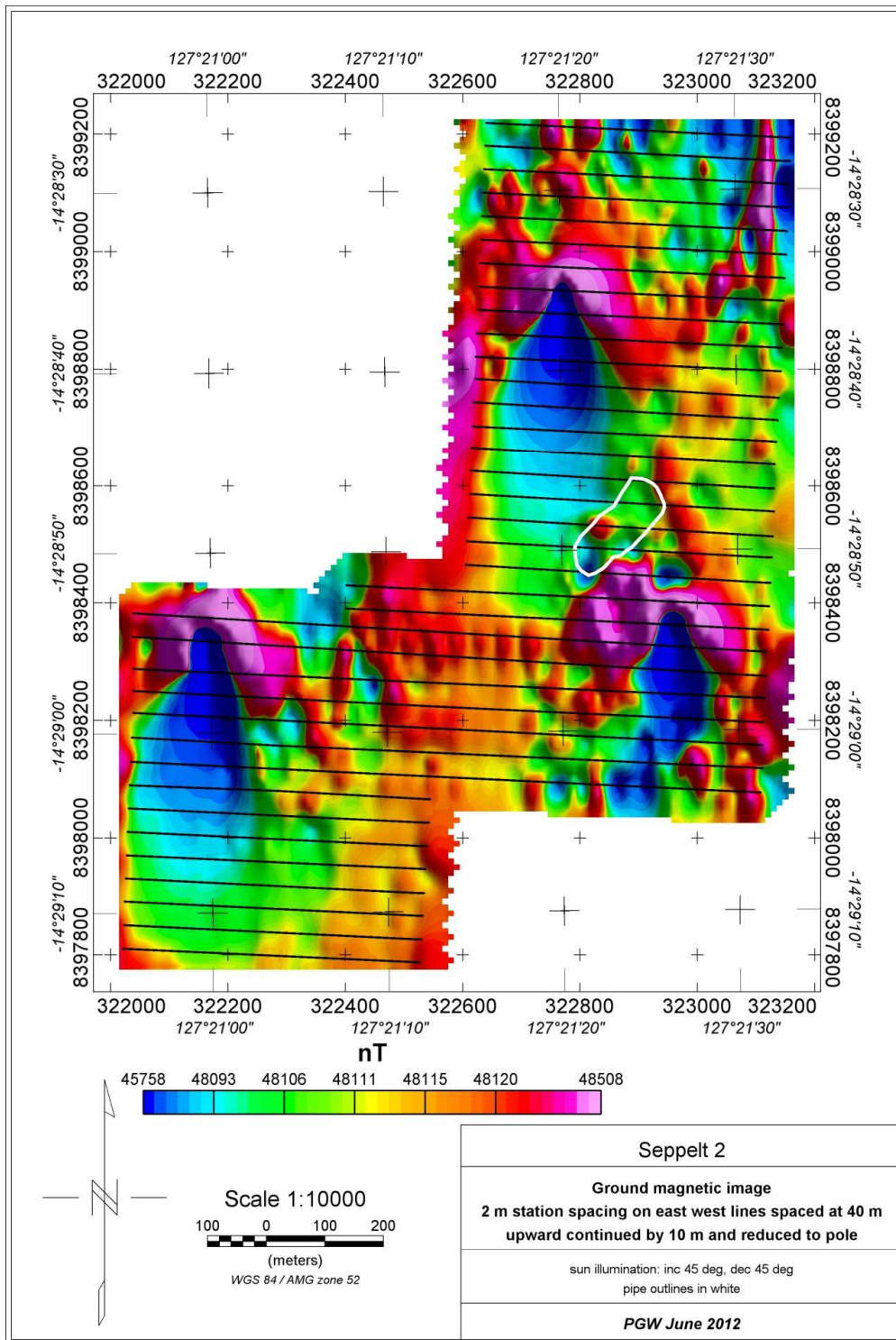


Figure 7-8: Detailed total magnetic intensity aeromagnetic image over Seppelt 1 using gridded data from Stockdale Prospecting. Seppelt 1 has an associated aeromagnetic anomaly of about 14 nT.





**Figure 7-10: Seppelt 1 ground magnetic image. Data have been upward continued by 10 m and reduced to pole. Kimberlitic areas are shown outlined in white. Seppelt 1 has associated ground magnetic anomalies as seen in this image. Sun illumination from NE with 45 degree elevation.**



**Figure 7-11: Seppelt 2 ground magnetic image. Data upward continued by 10 m and reduced to pole. Seppelt 2 location is shown outlined in white. Seppelt 2 does not appear to be magnetic but is close to magnetic features. Sun illumination from NE with 45 degree elevation.**

## **7.7 Ground gravity at Seppelt 1, 2, 4, 5, and 6**

Ground gravity surveys were carried out in the Seppelt areas in 1998, 1999 and 2000. These were done with 40 m x 40 m station spacing and used Scintrex CG3 and CG5 gravity meters. The initial surveys were done by Curtin University and later surveys by Haines Surveys. For the Curtin University surveys, detailed topographic surveying was done by conventional surveying using a total station. This surveying work was done by a surveyor contracted to Striker Resources. The Haines surveys were done using real time kinematic GPS and these provided x, y and z data to a repeatability of about 3 cm. Some linking stations were done outside the defined Seppelt prospects as shown as triangles in Figures 7-12. and 7-13.

Local base stations were used to monitor gravity meter drift corrections and as with all the other gravity done by Curtin University, and by contractor Haines Surveys, these base stations were tied back to the network of base stations established in Striker Resources North Kimberley tenements. These in turn were tied into a Geoscience Australia absolute base station at Kununurra airport.

The combined Bouguer gravity results from the various Seppelt areas / prospects are shown in Figure 7-12. This shows a steady gradient increasing to the north east, where there is a major gravity high. A third order polynomial surface was computed for the entire Seppelt grid and this was subtracted to produce a third order residual surface (Figure 7-13), which shows more clearly the local gravity features. Bouguer gravity and residual Bouguer gravity images for Seppelt are shown as Figures 7-14 and 7-15. Bouguer gravity and residual Bouguer gravity for Seppelt 2 are shown as Figures 7-16 and 7-17, respectively. Seppelt 1 and 2 have small negative residual anomalies as does Seppelt 4.

The Seppelt 2 prospect is located in a shallow depression on the northern side of elevated ground as shown in Figure 7-5. The gravity results here are subtle even after subtraction of a third order regional surface. The residual results show that there is a major structure striking approximately NE (see Figure 7-

13) and as seen in Figure 7-2, this is one of a number of faults with this direction that encompass the Seppelt prospects.

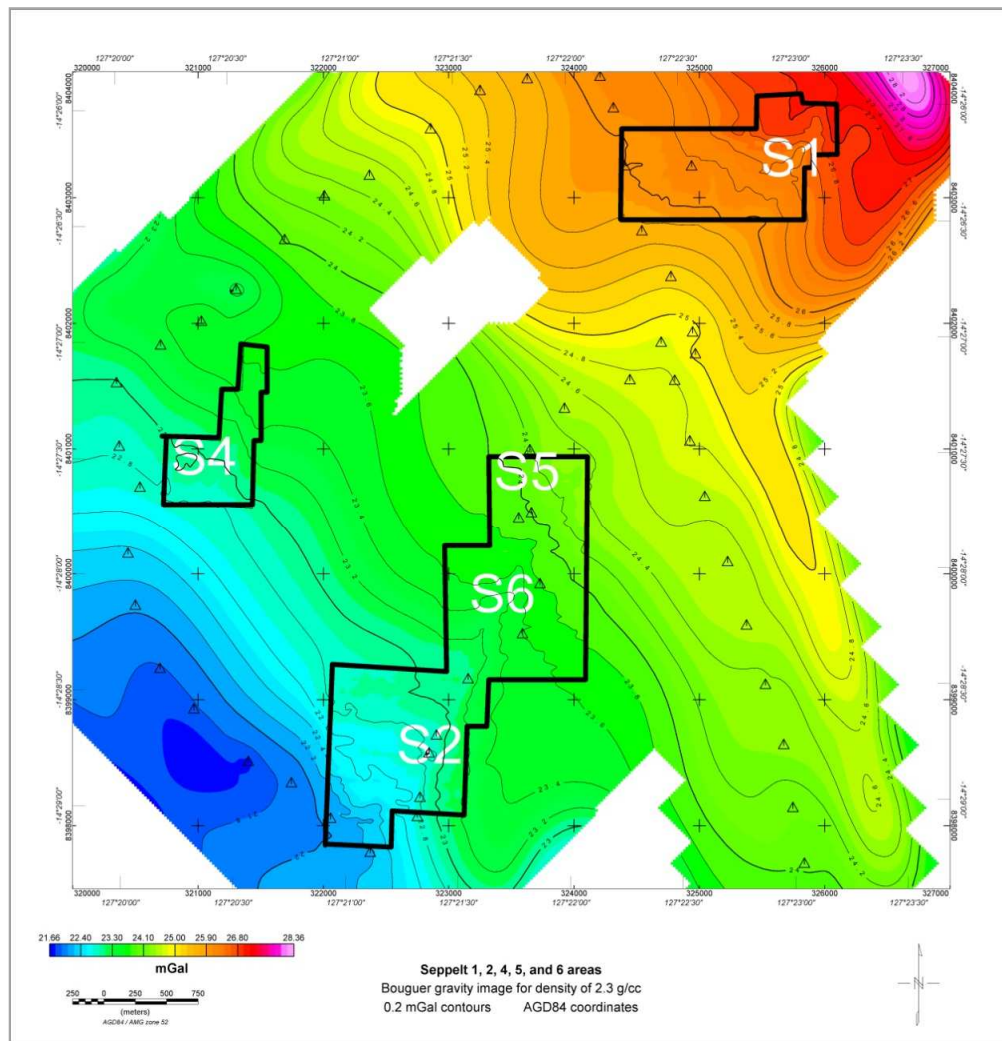


**Figure 7-12: Seppelt areas 1, 2, 4, 5 and 6. Bouguer gravity image with 0.2 mGal contours. Regional residual separation is required to clearly show the gravity over pipes in this area. The result of this separation is shown as Figure 7-13.**

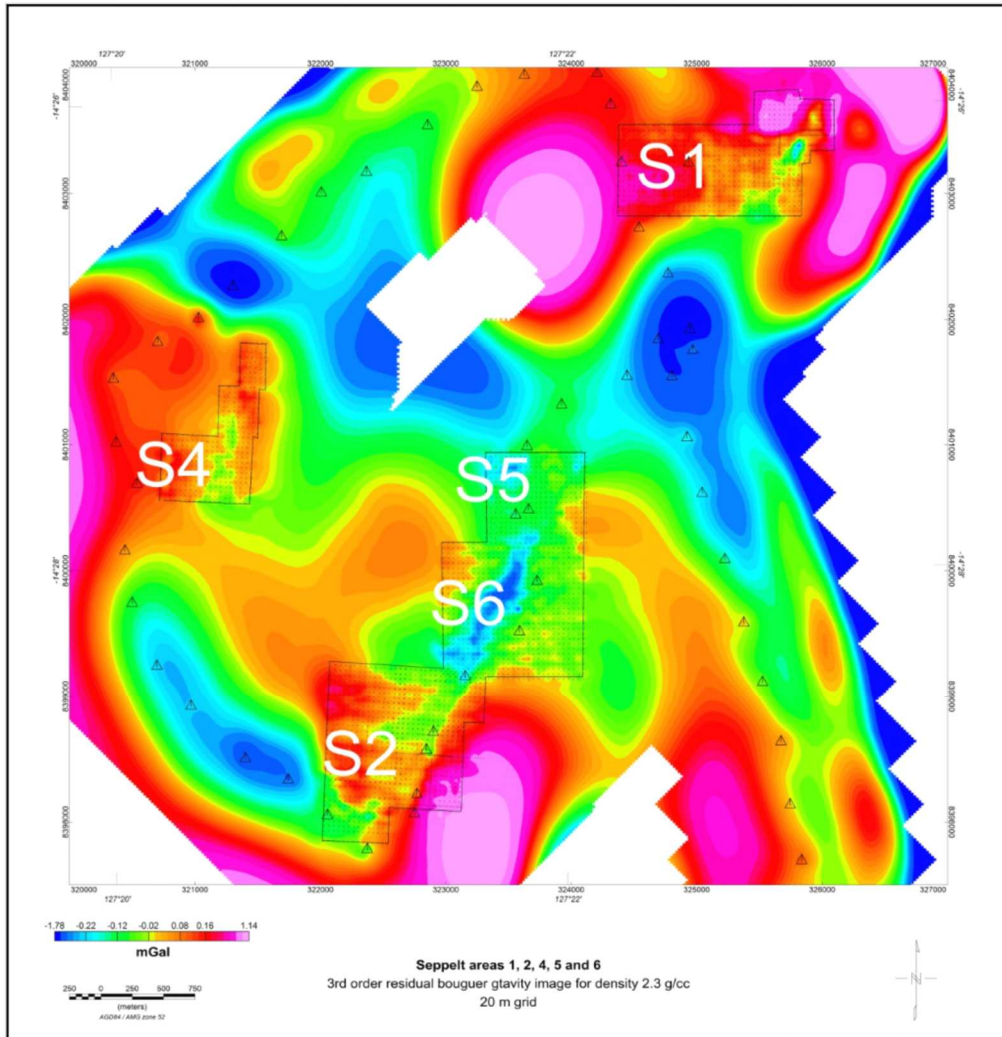


**Figure 7-13: Seppelt areas 3rd order residual Bouguer gravity image. Note the important north east trending structure that links through from Seppelt 2 to Seppelt 1.**

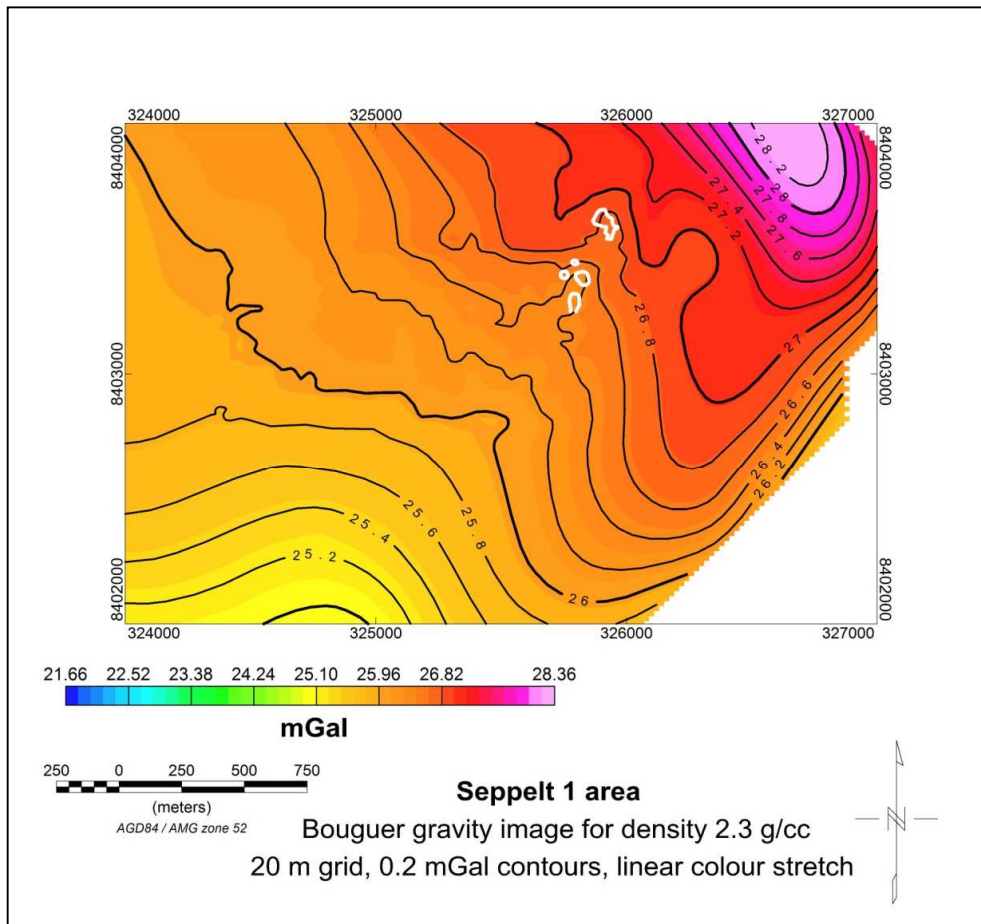


**Figure 7-14: Seppelt 1 Bouguer gravity for density 2.3 g/cc. Pipe locations are outlined in white. Regional residual separation is required to better define the location of Seppelt 1. The result of this separation is shown as Figure 7-15.**

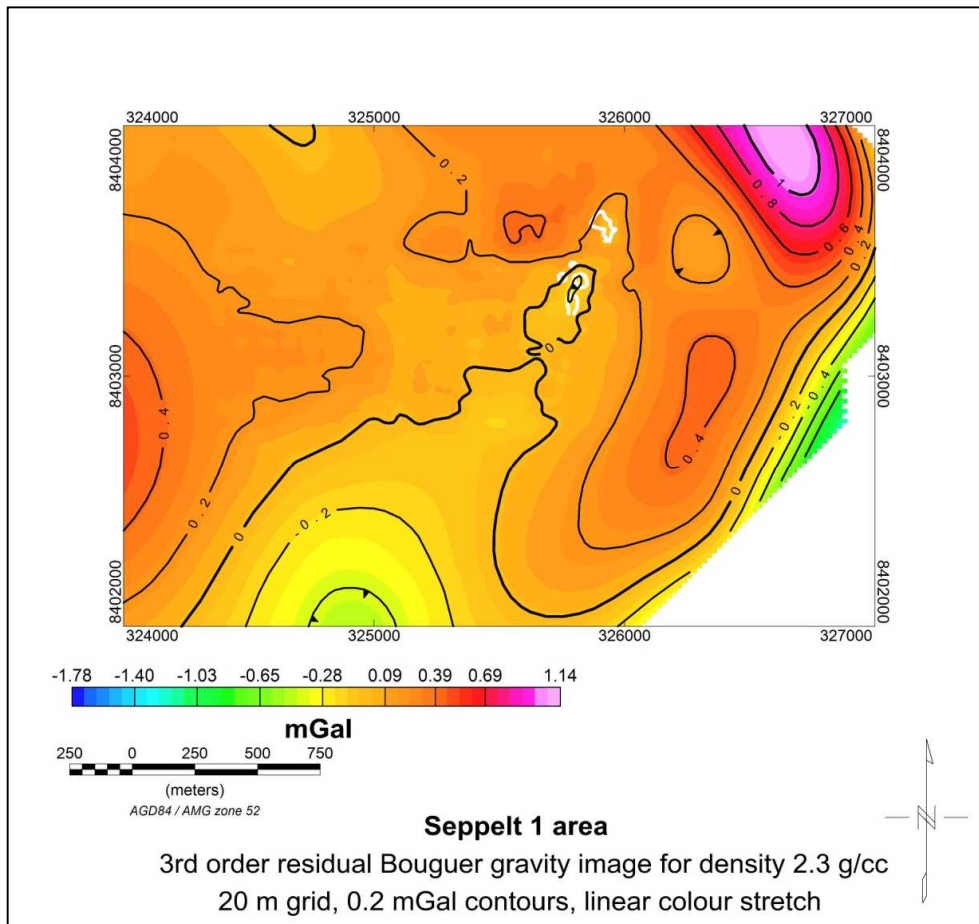


**Figure 7-15: Seppelt 1 3rd order residual Bouguer gravity image for density 2.3 g/cc. Seppelt 1 has a small residual negative gravity anomaly associated with weathering over this pipe. Pipe outlines shown in white.**

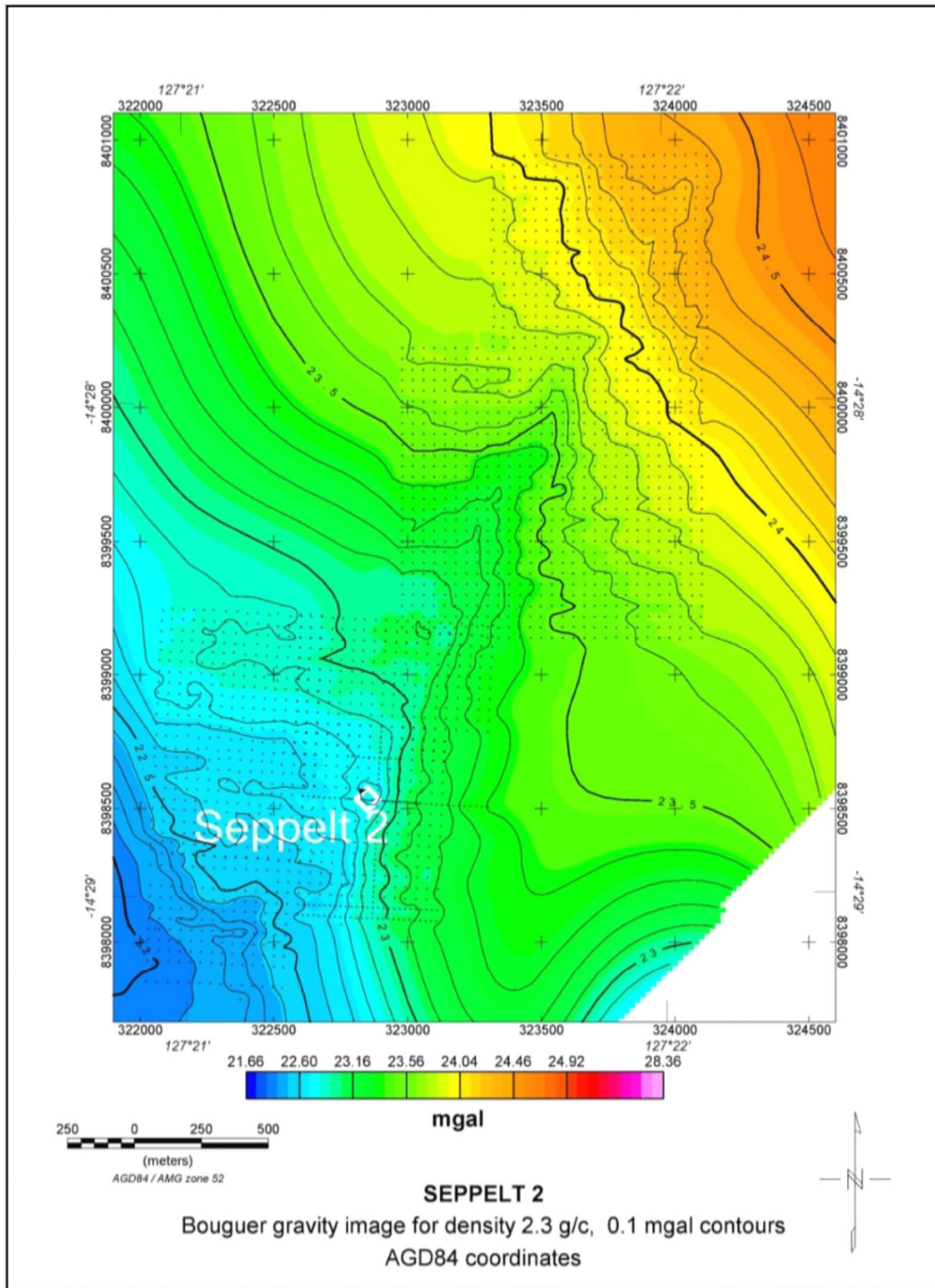
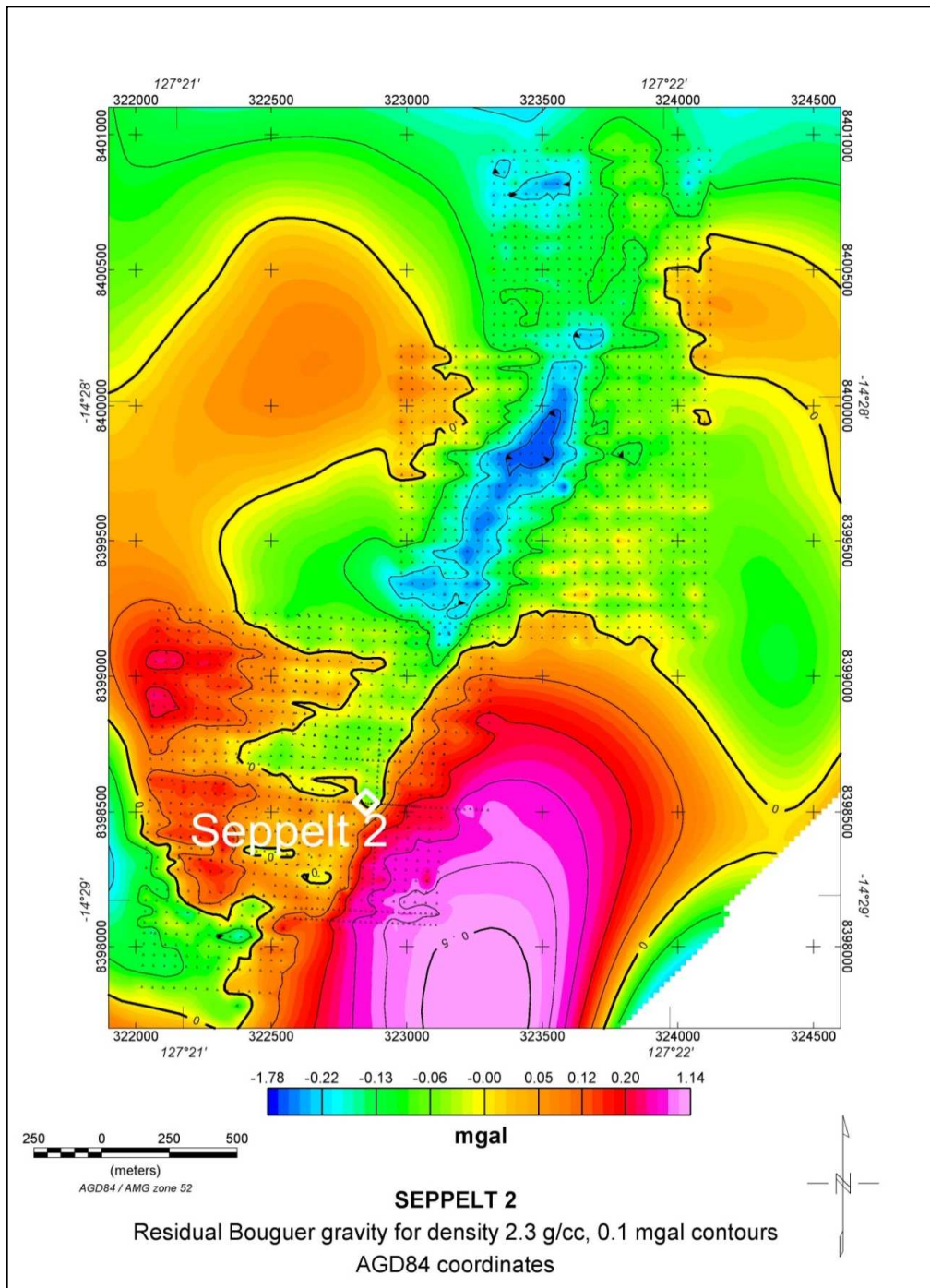


Figure 7-16: Seppelt 2 Bouguer gravity image for density 2.3 g/cc. Seppelt 2 is not obvious in this image.



**Figure 7-17: Seppelt 2 3rd order residual Bouguer gravity for density 2.3 g/cc. Seppelt 2 is located in a small residual gravity low along a major structure trending about 040 degrees.**

## **7.8 Ground electromagnetic surveys at Seppelt 1 and 2**

Ground electromagnetic surveys were carried out using Geonics EM 34 frequency domain equipment operating at 1600 Hz and with 20 metre transmitter-receiver coil separation. Two modes were used at Seppelt 1: Horizontal coplanar coils were positioned with the coils laid on the ground, and vertical coplanar coils with the plane of each coil vertical and aligned along the line direction. Vertical coplanar mode only was used at Seppelt 2. Line spacing at Seppelt 1 was 40 metres. Line spacing at Seppelt 2 was 80 metres. The conventional way to use the Geonics EM34 instrument is with the coils in vertical coplanar mode. Using both horizontal and vertical coplanar modes produces somewhat different results as is seen in Figure 7-18 and Figure 7-19. This can be used to infer information about conductive source geometry. With the correct spacing of the coils (established as a null position from real component data) the instrument provides a read out of apparent conductivity in milli-siemens per metre.

The ground conductivity data have been gridded with a grid spacing of 10 metres for Seppelt 1 and 20 metres for Seppelt 2, in Oasis Montaj. Images are shown in Figures 7-18, 7-19, and 7-20. The ground electromagnetic results have shown that there are significant conductivity anomalies associated with weathering over Seppelt 1 and nearby prospects such as Montana, which is located just west of Seppelt 1. The northern side of Seppelt 2 shows higher conductivity, but is part of a more extensive conductive area whose origin is not known.

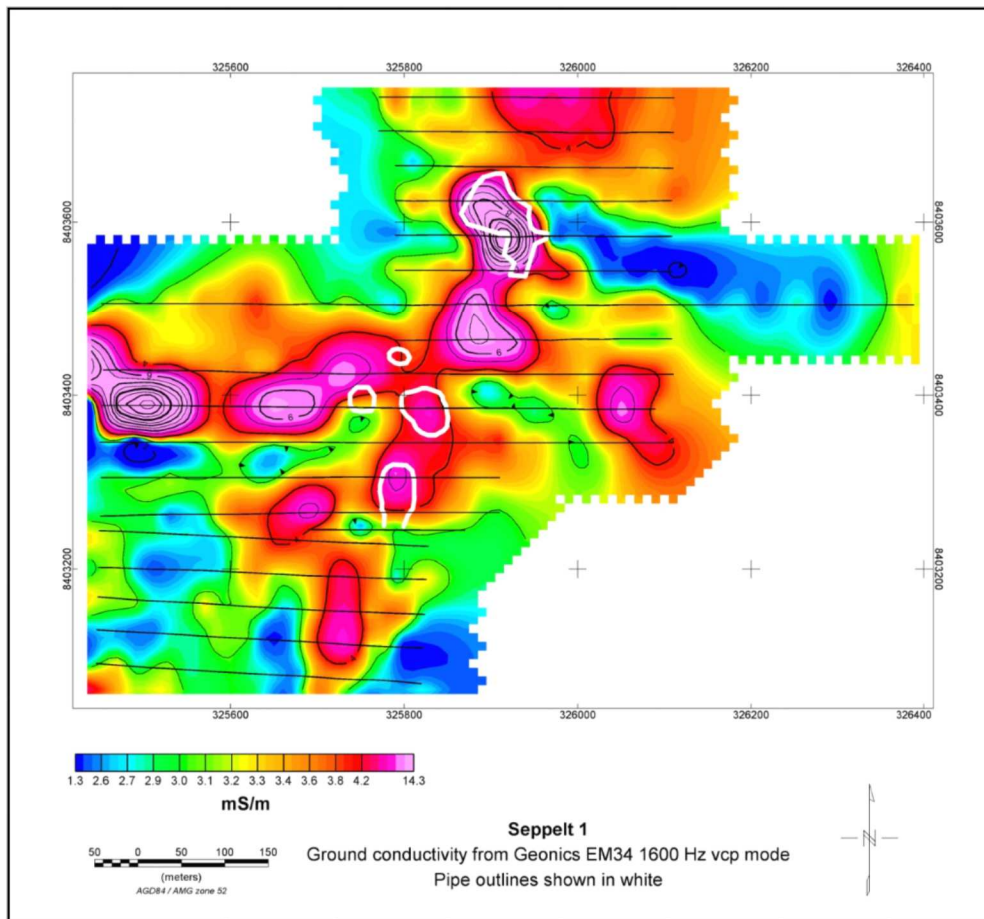


**Figure 7-18: Seppelt 1 ground conductivity image from Geonics EM 34 survey using vertical coplanar (VCP) coils at 1600 Hz with 40 m line spacing and 20 m station spacing. Pipes outlines are shown in white. Ground conductivity contour interval 1 mS/m. The pipes have clear conductivity responses due to conductive weathering caps. More potential pipes are evident in this image.**

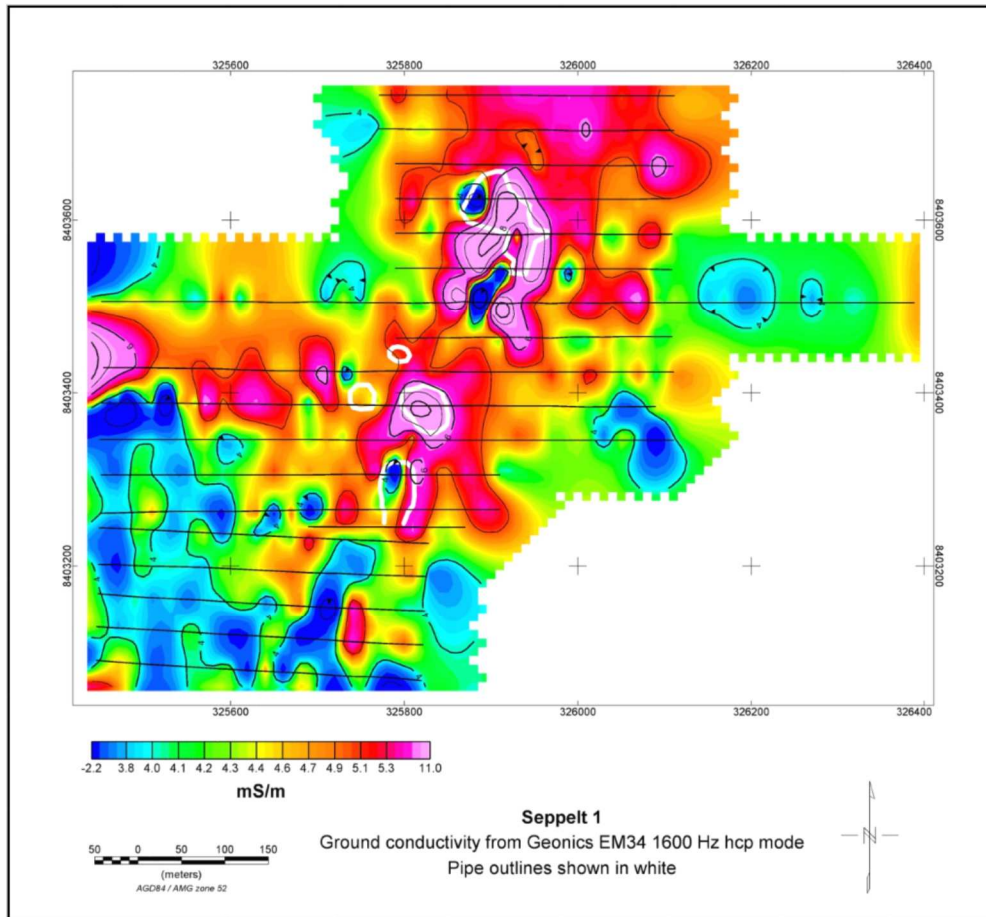


**Figure 7-19: Seppelt 1 ground conductivity map from Geonics EM 34 survey using horizontal coplanar (HCP) coils at 1600 Hz with 40 m line spacing and 20 m station spacing. Pipe outlines are shown in white. Ground conductivity contour interval is 1 mS/m. This image contrasts with Figure 7-18. The difference is due to the different orientation of the coils.**

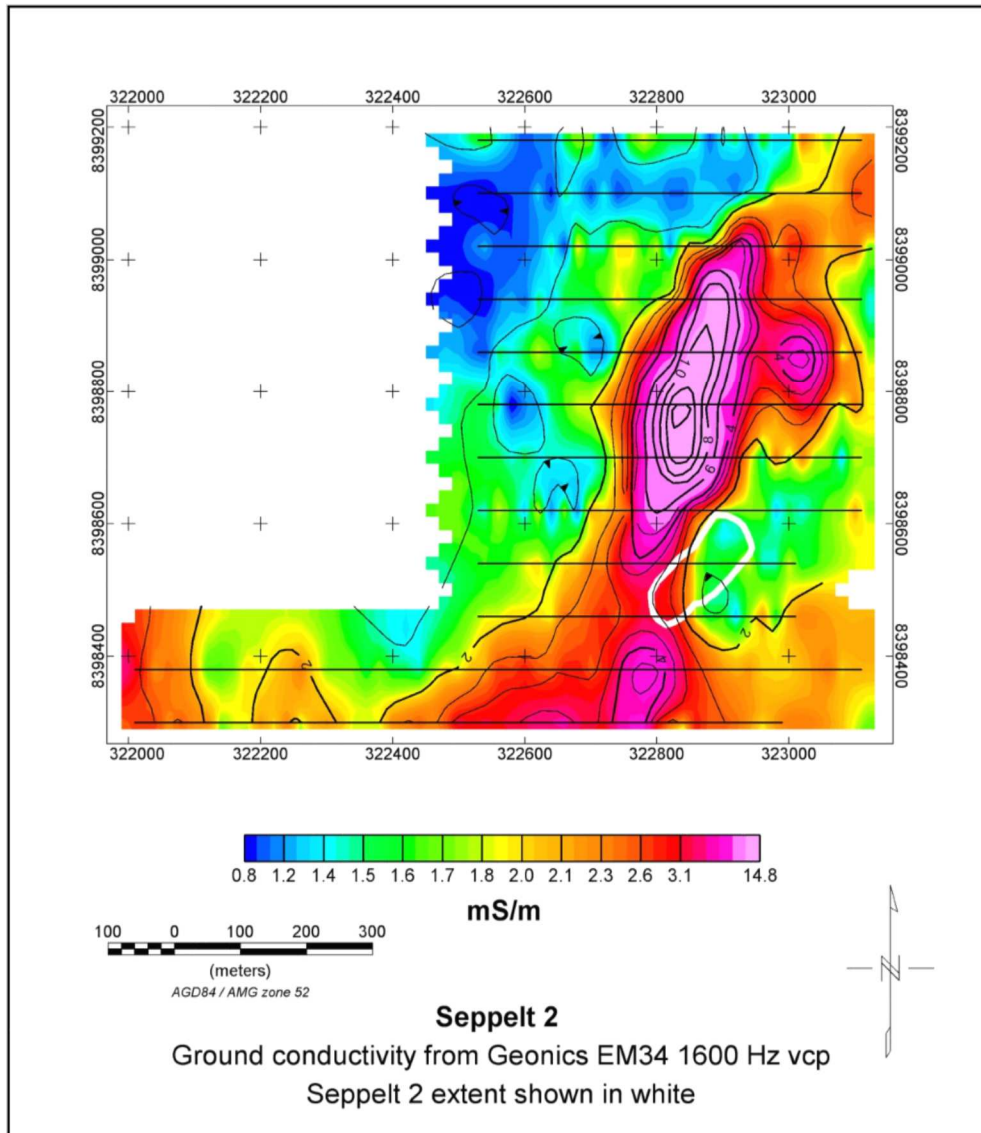


**Figure 7-20: Seppelt 2 ground conductivity map from Geonics EM 34 survey using vertical coplanar coils at 1600 Hz, with line spacing of 80 m and station spacing of 20 m. Pipe outline is shown in white. South western end of pipe is seen in ground of elevated conductivity but there is higher conductivity to the north of the pipe which appears not to be related to Seppelt 2. Ground conductivity contour interval is 0.5 mS/m.**

## **7.9 Discussion on integrated datasets for Seppelt areas**

The Seppelt 1 and 2 pipes are characterised geophysically by magnetic, electromagnetic and gravity anomalies that contrast with the surrounding Proterozoic sandstone. Although the magnetic anomalies are likely to be response from the magmatic kimberlite, the electromagnetic and gravity anomalies are products of the weathering, erosion and depositional backfill over the pipes. Seppelt 1 is on elevated ground, as shown in Figure 7-4, whilst Seppelt 2 is lower in the landscape and in a local drainage drainage feature (Figure 7-5). Figure 7-3 shows that both prospects are located at the intersection of topographic features, which are interpreted as being due to underlying intersecting NW-SE and SW-NE faults.

Aeromagnetic data over Seppelt 1 show a clear dipolar anomaly with amplitude of 12 nT. This feature is seen on the southern side of a more extensive deep seated magnetic feature. Ground magnetic data over Seppelt 1 are useful, especially after upward continuing the data by 10 metres and reducing the data to the pole. Seppelt 2 is not seen in either the aeromagnetic data or the ground magnetic data.

100 metre spaced Hummingbird helicopter electromagnetic data over the Seppelt areas showed a number of low resistivity areas which may indicate potential clay areas over kimberlite pipes. This is seen close to Seppelt 1 and 2, but also over Seppelt 4 and between Seppelt 1 and Seppelt 5.

The ground conductivity response of Seppelt 1, using the EM 34 data, is shown in Figures 7-18 and 7-19. These show each lobe of the prospect is separate and that there are other prospects west of Seppelt 2: e.g. Montana prospect. The conductivity response of Seppelt 2 (Figure 7-20) is not distinctive and there is a more conductive area immediately north of where Seppelt 2 has been defined. The source of this anomaly is not known, but warrants further work.

Ground gravity survey was more successful at Seppelt 1 than Seppelt 2, where the anomaly was of very low amplitude even after subtracting a third order regional trend surface to compute a residual image. Gravity has shown a long,

linear gravity gradient which extends from south of Seppelt 1 in a NE direction towards Seppelt 2. This is recognised as an important structural direction in the Seppelt group of prospects.

## **8 EXPLORATION AT PTEROPUS**

### **8.1 Geology**

Local geology for the Pteropus area is shown in Figure 8-1. This is from the regional 1:250 000 scale mapping of the Drysdale and Londonderry map sheets by Gellatly and Sofoulis (1969). This area comprises extensive outcrops of Proterozoic Elgee Sandstone, Warton sandstone and Pentecost Sandstone. Further detail is provided in Jaques et al. (1986) from which Figure 8-2 has been reproduced. This is based on work by Muggeridge et al. (1978) and Shaw et al. (1985). The two Pteropus pipes are located close to the Pteropus Creek, near the base of steep cliffs on the southern and western sides as shown in Figure 8-3. The pipes have been dated at 805 +/- 10 Ma, (Pidgeon et al. 1989).

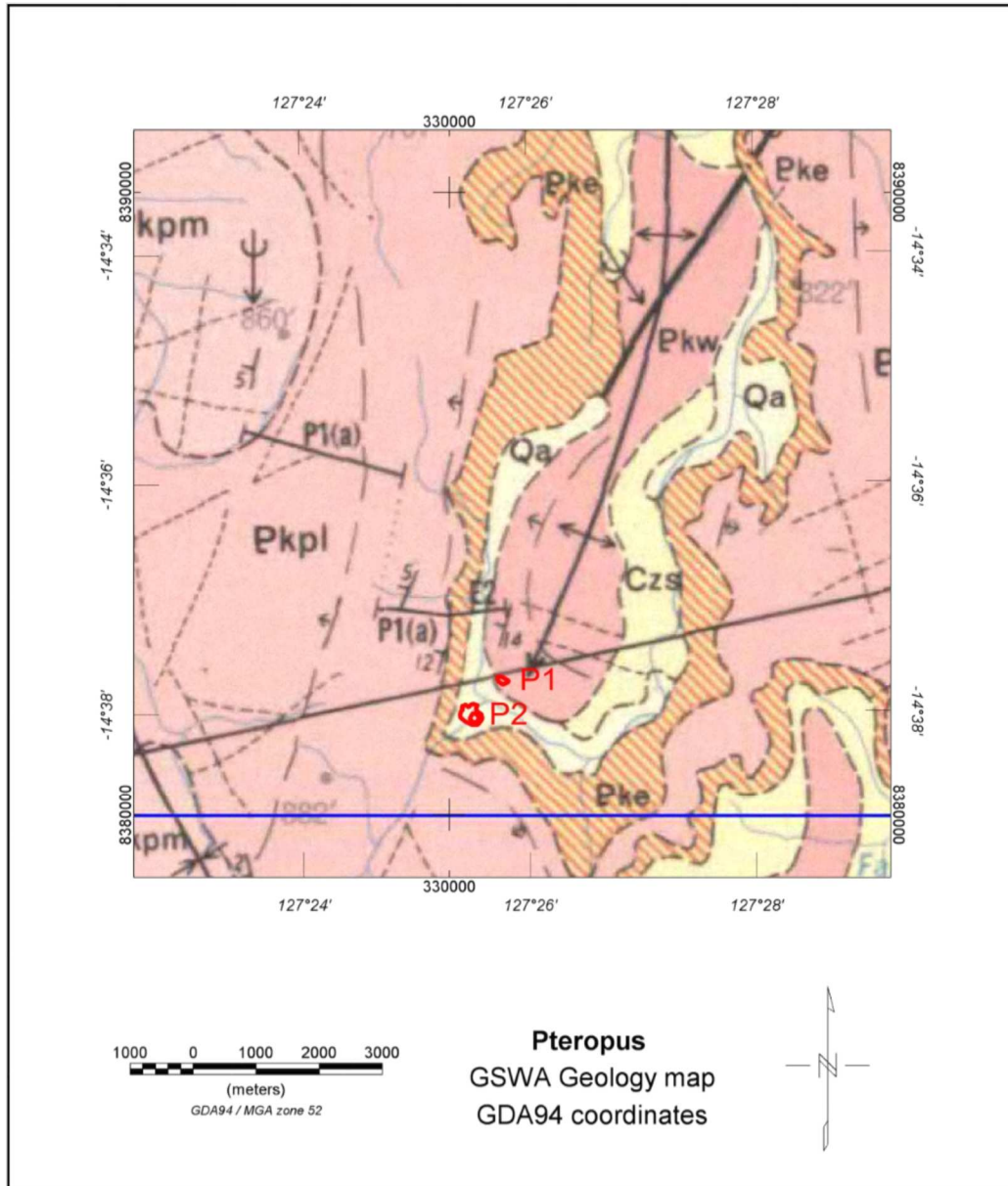


**Figure 8-1: Geology of Pteropus area from GSWA 1:250 000 Drysdale map sheet mapped by Gellatly and Sofoulis (1969). Pke is Elgee Sandstone, Pkw is Warton Sandstone, Pkpm is Pentecost Sandstone (middle unit), Pkpl is Pentecost Sandstone (lower unit), and Qa is Quaternary alluvium. Pteropus 1 and 2 pipes are outlined and labelled in red.**

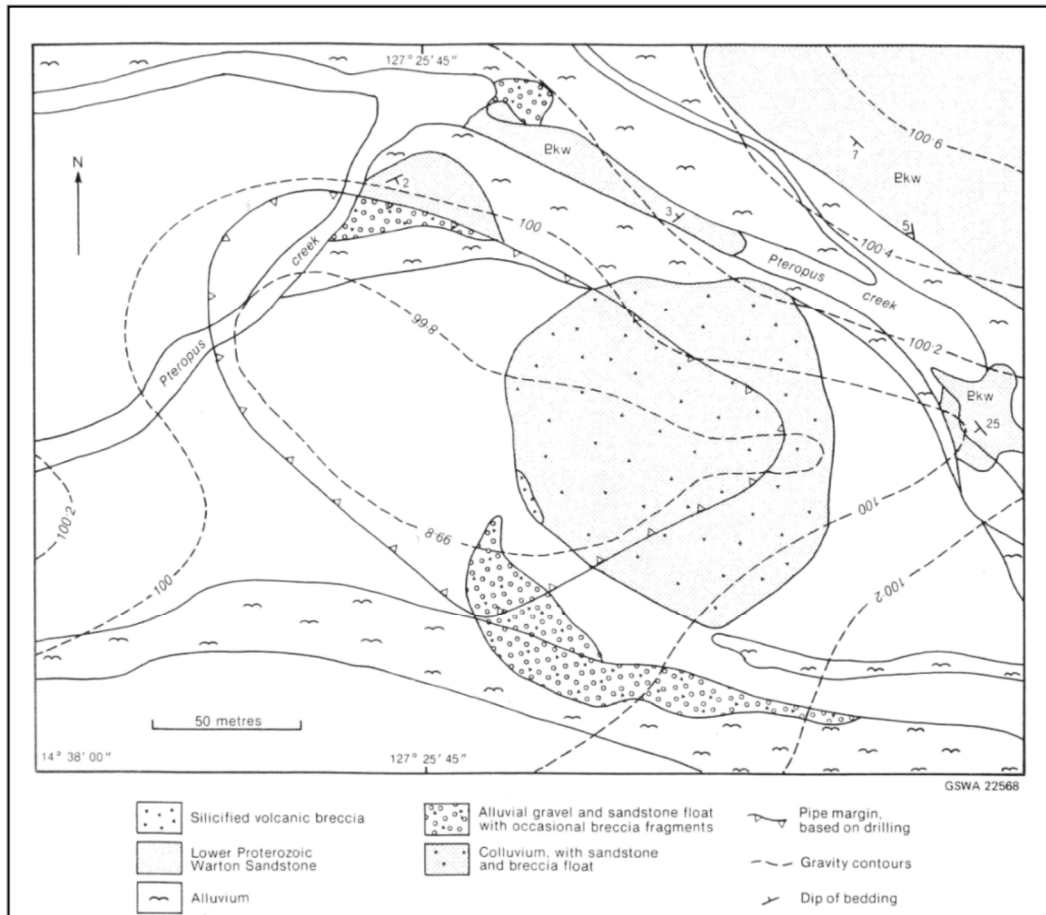


**Figure 8-2: Surface geology and ground gravity contours, with 0.2 mGal intervals at Pteropus 1 breccia pipe. Reproduced from Jaques et al. (1986) page 29. A gravity low of about – 0.6 mGal is seen over the pipe.**

## 8.2 Previous exploration

The Pteropus 1 pipe was discovered in early 1976 (Jaques et al., 1986) by tracing detrital ilmenite, zircon and diamond to their source. Surface geology and ground gravity contours are shown in Figure 8-2. This 2 ha pipe intrudes Warton Sandstone and is exposed in a river valley at the south-western end of the core of an anticline. Gravity was used to outline this pipe, with an area of about 90 x 160 metres and a gravity low of about -0.6 mGal. This pipe was also recognised in aeromagnetic data as a small dipolar anomaly (Sumpton and Smith, 1997). The pipe was subsequently confirmed by drilling to be kimberlitic. Note that Pteropus was not visited as part of the fieldwork completed by the author.

The Pteropus 2 pipe was discovered in 1992 about 500 m southwest of Pteropus 1 by drilling a magnetic anomaly associated with detrital indicator minerals (McMonnies, 1993, Smith and McClenaghan, 1994). Pteropus 2 comprises hypabyssal kimberlite that grades from pure kimberlite into kimberlitic breccia and then into country rock. Unlike Seppelt 1, it has not undergone extreme weathering (Sumpton and Smith, 1997). This pipe covers an area of approximately 10 ha.

### **8.3 Elevation data**

Pteropus 1 and 2 pipes are located on low ground at the base of steep cliffs to the west and south of the pipes. The digital elevation data from Falcon gravity gradiometry survey are shown in Figure 8-3. The Falcon system includes a high resolution scanning laser system which scans out to each side of the aircraft to a vertical angle of about 45 degrees. In addition to use for terrain corrections in the gravity processing, the local digital elevation data are a very useful product in their own right and are valuable in following up the locations of the gravity results.

### **8.4 Airborne gravity gradiometry using the Falcon system**

The Falcon airborne gravity gradiometry system was developed by BHP Billiton starting with a gradiometer system developed by Lockheed Martin for use in submarines. The original work by Lockheed Martin became de-classified and was the starting point for airborne geophysical development by BHP Billiton and also Bell Geospace. The Falcon system contains accelerometers on spinning discs and measures gravity gradients. These are used to compute the various gravity components and their gradients. The system is commonly flown in a Cessna Caravan aircraft and is also now available for use in helicopters. The fixed wing version also usually includes a cesium vapour magnetometer. Typical flying height is 80 metres above ground level.

A Falcon airborne gravity gradiometer survey was flown in December 2000 over a 45 square kilometre area in the Pteropus area by BHP Minerals Pty. for and with Striker Resources. The survey was flown with north south lines

spaced at 100 m. This area was challenging, as the Pteropus 1 and 2 kimberlite pipes are surrounded by steep cliffs to the west and south. Additionally, the survey was flown in hot turbulent conditions which would have increased instrumental noise levels. However, the survey was successful in detecting both Pteropus 1 and Pteropus 2 and highlighted at least two further targets which were followed up by Striker Resources in the 2001 field season ; but did not discover further pipes or mineralisation. Results from the Falcon survey are shown in Figures 8-3 to Figure 8-7. Figure 8-3 shows the local digital elevation data and the outlines of the two pipes. Figure 8-4 shows the calculated Bouguer gravity and shows that the two pipes are located in gravity lows of approximately 0.3 mGal. However these lows are considerably more extensive than the areas currently known as the pipe locations. It is possible that the pipes are larger than currently mapped or the gravity lows may also be due to other sources.

Figure 8.5 shows the gravity gradient  $G_{zz}$  image for the same area. This shows more closures than the Bouguer gravity image but is not as useful.

Total magnetic intensity and first vertical gradient aeromagnetic results from the Falcon survey are shown in Figures 8-6 and 8-7, and show very low amplitude features in the areas of Pteropus 1 and Pteropus 2. However it should be noted that the magnetometer was about 80 metres above ground level and the most diagnostic magnetic results over kimberlite pipes are usually acquired at much lower levels – typically 40 metres.

A Hummingbird helicopter electromagnetic survey was conducted over the Pteropus area in 2000. This survey was flown with north south survey lines spaced at 100 metres and flown with EM and magnetic sensors in the bird flown at about 30 metres above ground level. The highest frequency 34 kHz apparent resistivity results are shown, together with DEM contours, in Figure 8-8. This shows low surface resistivities (high conductivities) over the low ground in which the Pteropus pipes are located, but it is not possible to definitely attribute this response to weathered material over the pipes. The description in Jaques et al. (1986) does not mention any clay weathering being present.

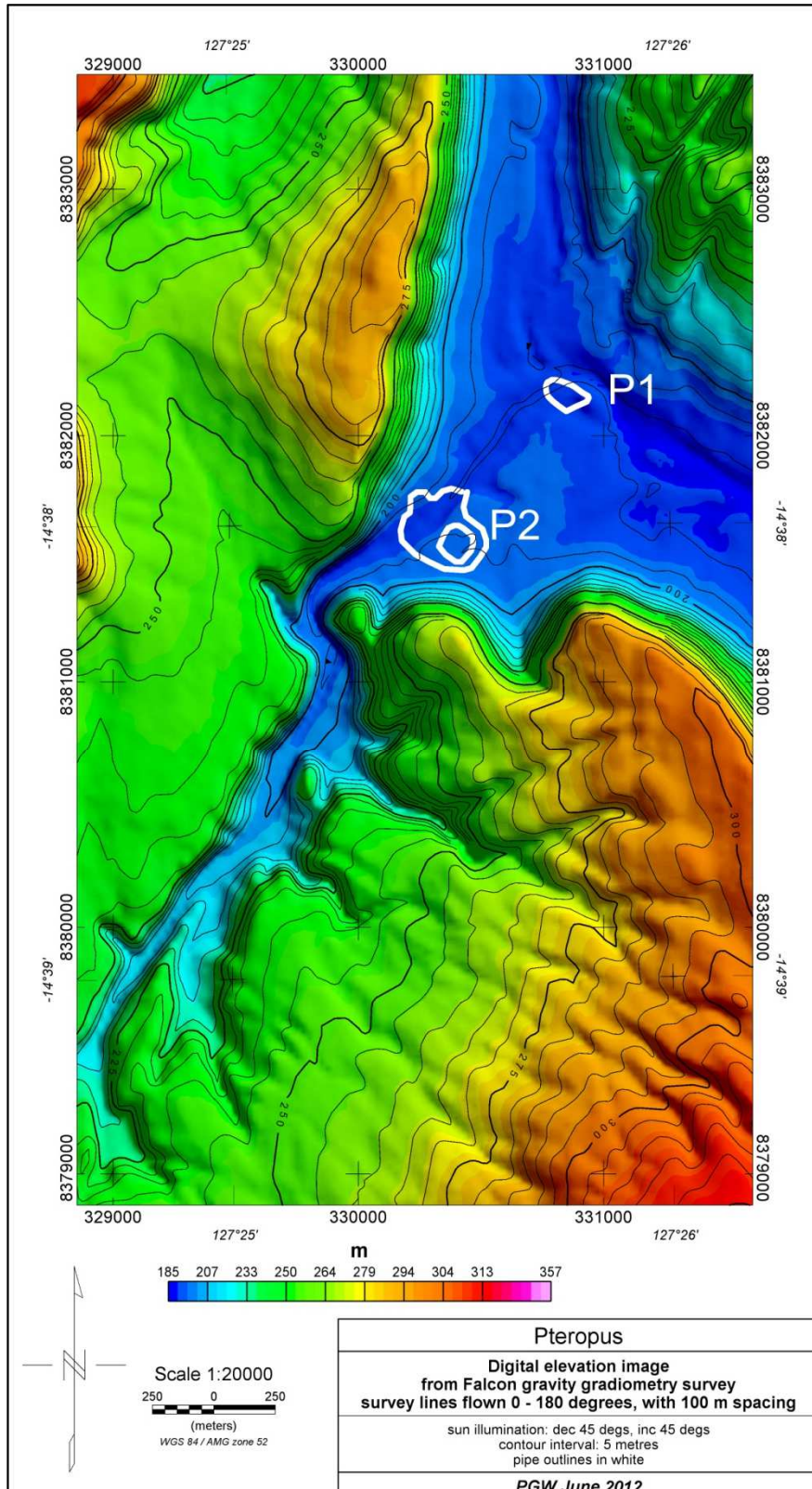


**Figure 8-3: Pteropus digital elevation image from Falcon gravity gradiometry survey. This shows the pipes are located in low lying ground close to the base of steep cliffs. Sun illumination from NE with 45 degree elevation.**

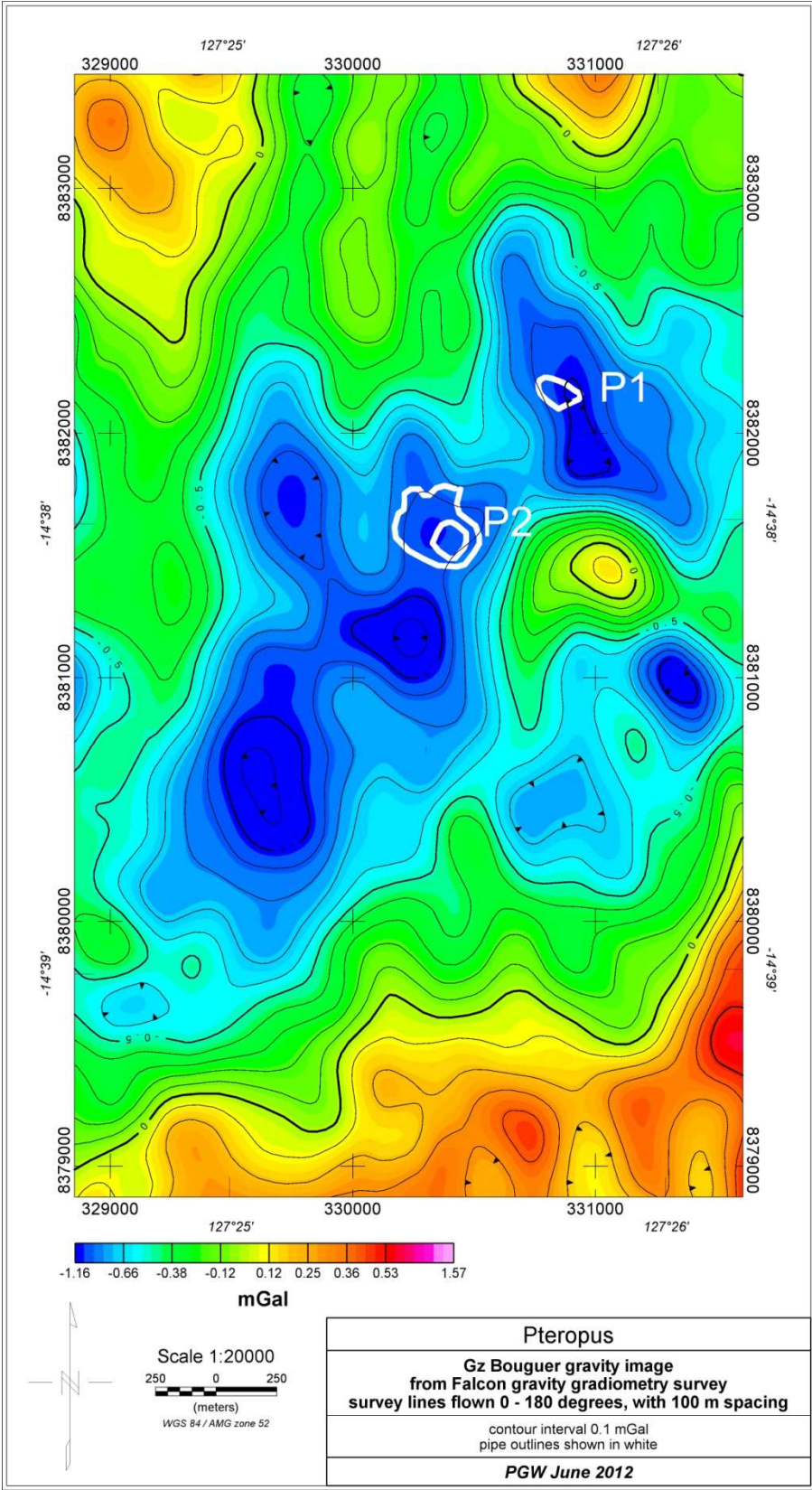


**Figure 8-4: Pteropus calculated Bouguer gravity (Gz) image from Falcon survey. The pipes are located in areas of gravity lows but the lows are more extensive than the known pipes.**

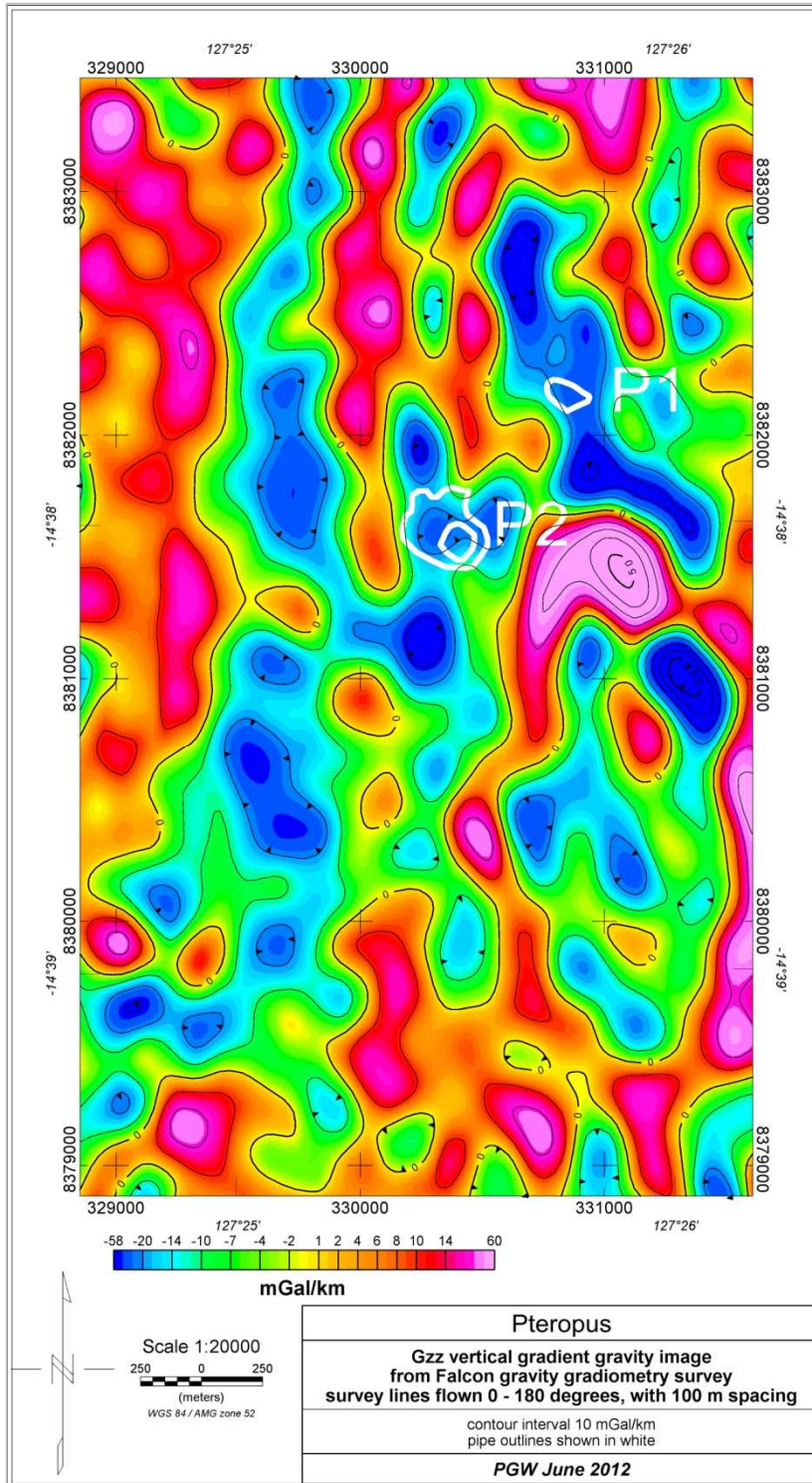


**Figure 8-5: Pteropus calculated Bouguer gravity gradient (Gzz) image from Falcon survey. The pipes are located in areas of gravity gradient lows but the lows are more extensive than the known pipes.**

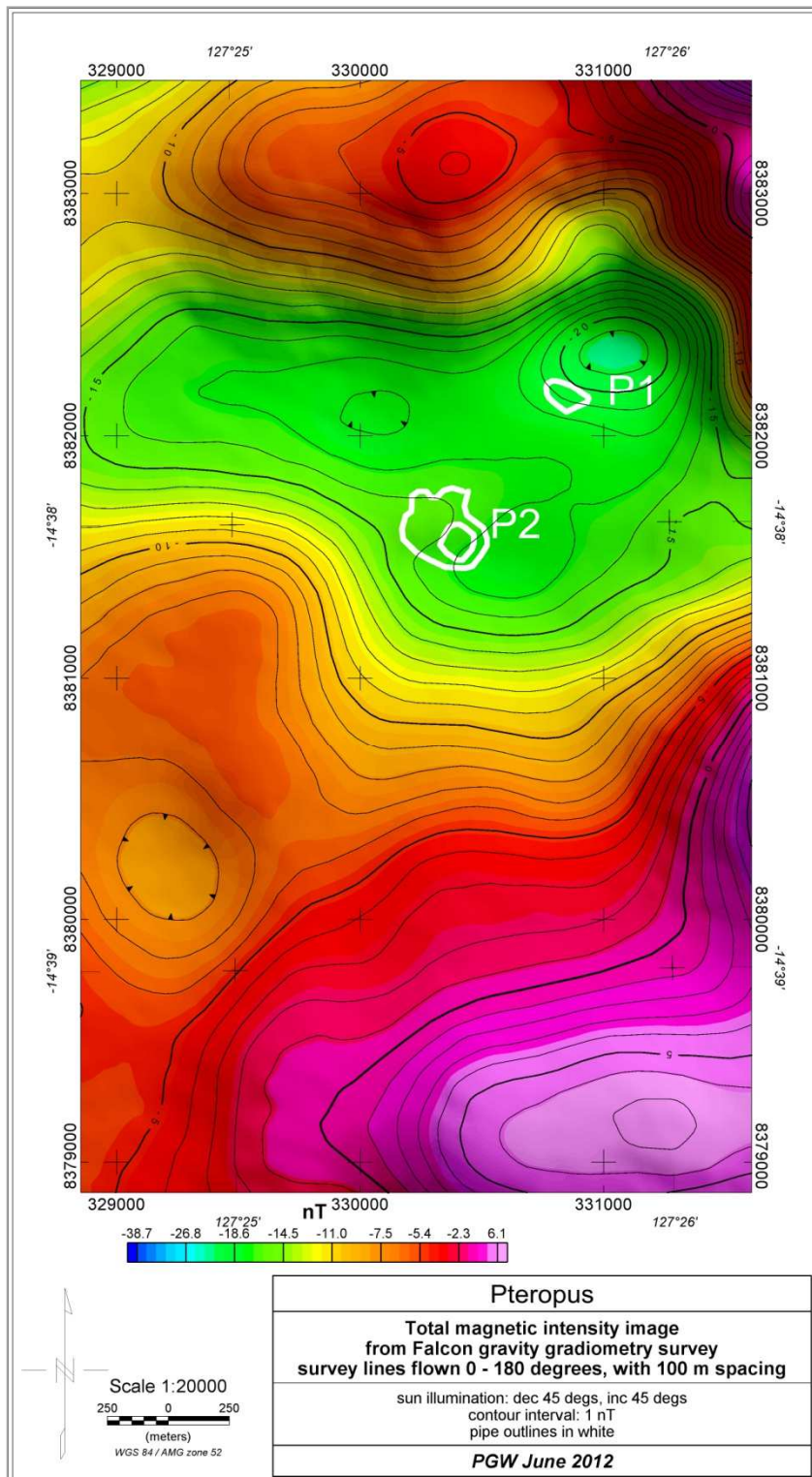


**Figure 8-6: Pteropus aeromagnetic image from Falcon survey. Pteropus 2 is seen to have a small aeromagnetic anomaly associated with the pipe but Pteropus 1 is not seen directly in the aeromagnetic data. The low to the north east of Pteropus 1 is related to the high to the north of Pteropus 1. Sun illumination from NE with 45 degree elevation.**

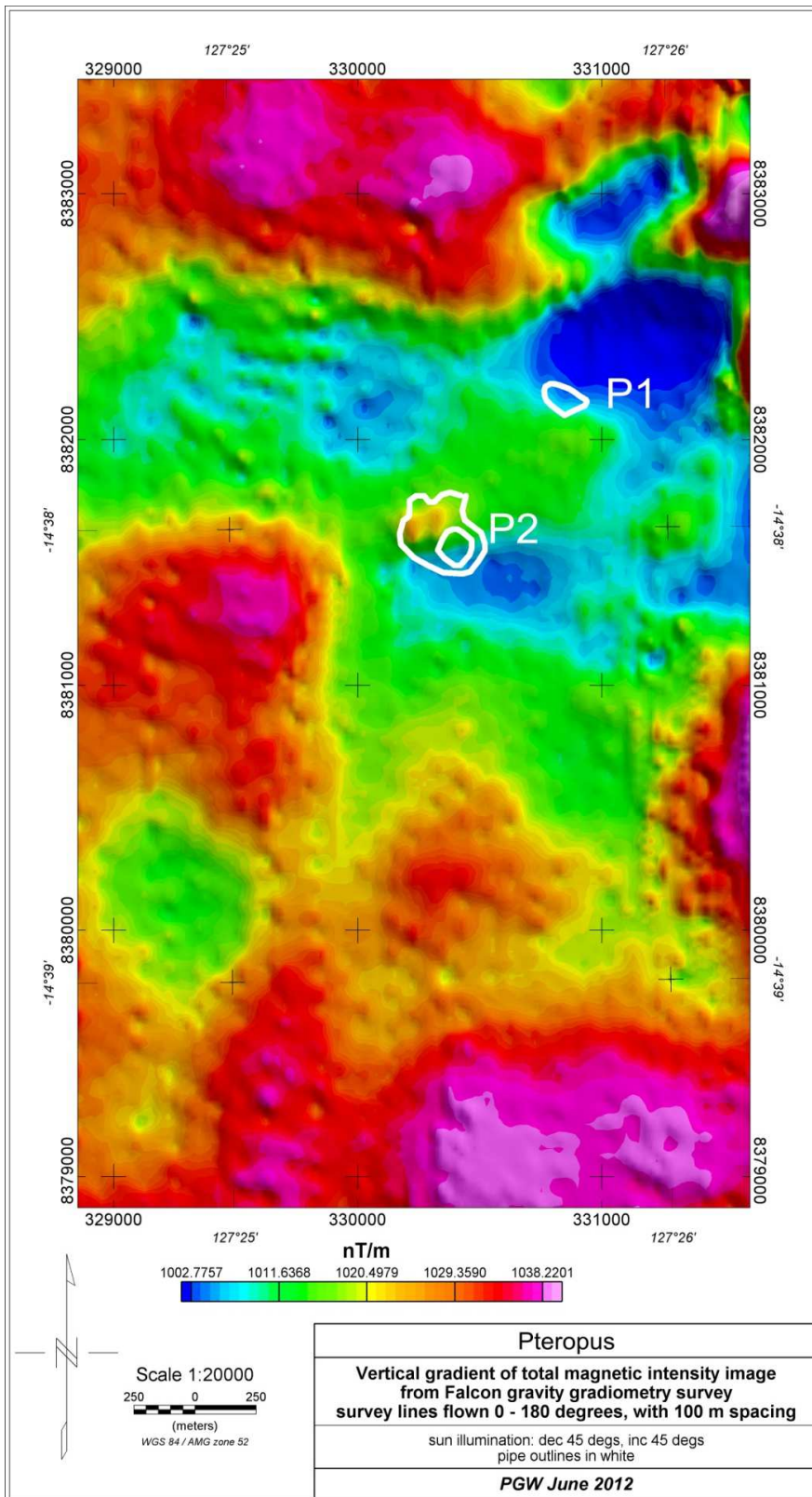


**Figure 8-7: Pteropus calculated first vertical gradient aeromagnetic image from Falcon survey. Pteropus 2 has a small gradient feature at the north western end but Pteropus 1 is not seen in this image. Sun illumination from NE with 45 degree elevation.**

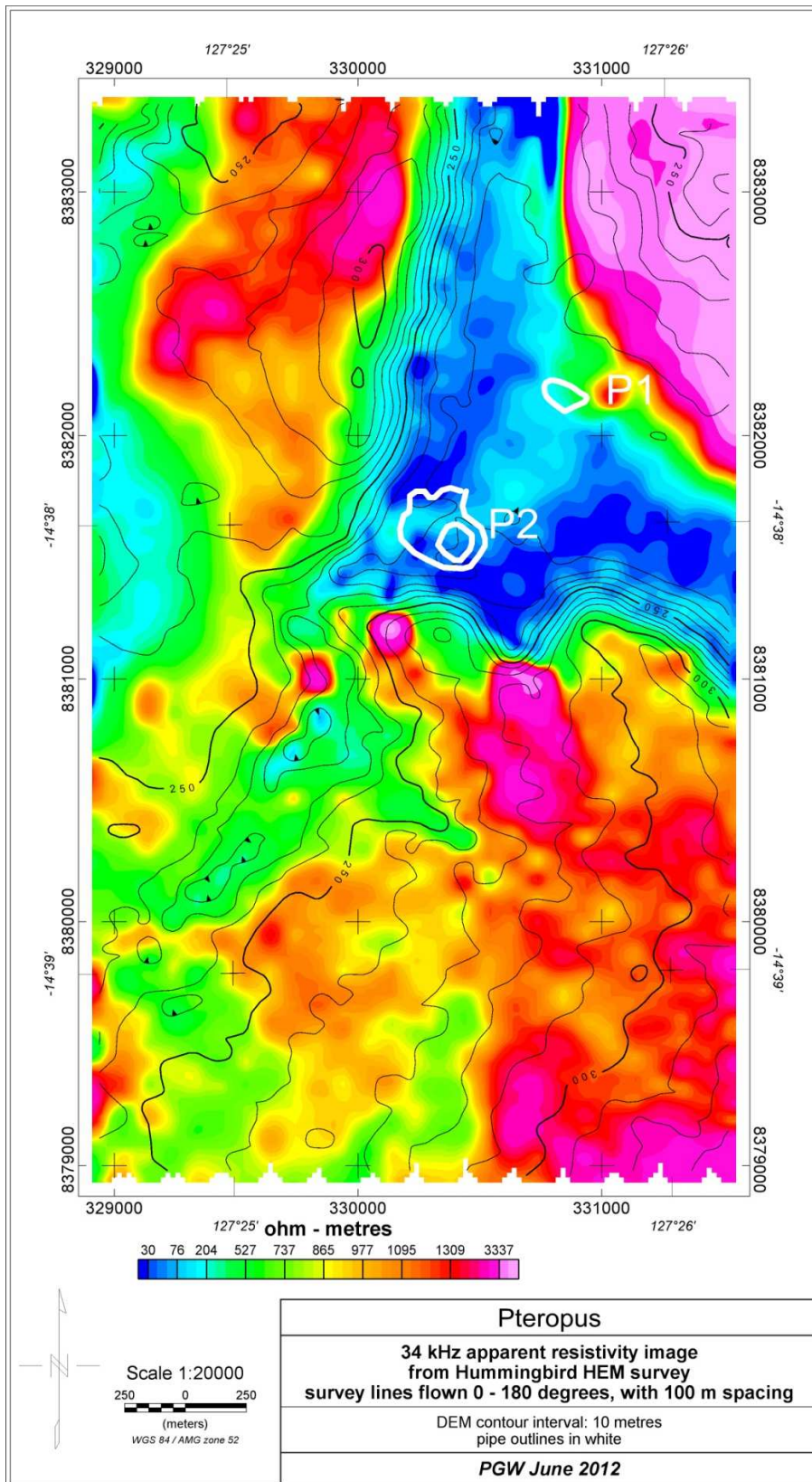


**Figure 8-8: Pteropus 34 kHz apparent resistivity from Hummingbird HEM survey with terrain contours overlain. The pipes are located in areas of low resistivity but these are more extensive than the pipes.**

## **8.5 Discussion on integrated datasets at Pteropus**

Ground gravity was used to help define the extents of both Pteropus 1 and 2. This showed residual Bouguer gravity anomalies of  $-0.6$  mGal over Pteropus 1 and  $-1.6$  mGal over Pteropus 2 (Sumpton and Smith, 1997). Falcon gravity gradiometry appears to have been successful over both pipes, but the results were hard to differentiate from other nearby, more extensive negative anomalies seen in the image (Figures 8-4). The laser scanned elevation data are very useful by-products from the Falcon gravity gradiometry survey and provided good detail in this area. A number of potential targets from the Falcon survey were followed up, but failed to locate further pipes. They are attributed to variations in the regolith thickness and density.

Both Pteropus 1 and 2 have weak aeromagnetic signatures – see Figures 8-6 and 8-7 and would not have been detected from these data.

The Hummingbird helicopter EM results showed high conductivity features over both pipes, but did not differentiate the pipes from the surrounding areas.

## 9 EXPLORATION AT ARIES

### 9.1 Geology

Local geology for the Aries area is shown in Figure 9-1. This is from the south west part of the GSWA regional 1:250 000 scale mapping of the Mount Elizabeth map sheet. The Aries kimberlite has four lobes: South, Central, North and North extension (Ramsay et al, 1994) The kimberlite intrudes King Leopold Sandstone and Carson Volcanics in the central Kimberley Basin (Downes et al, 2007).

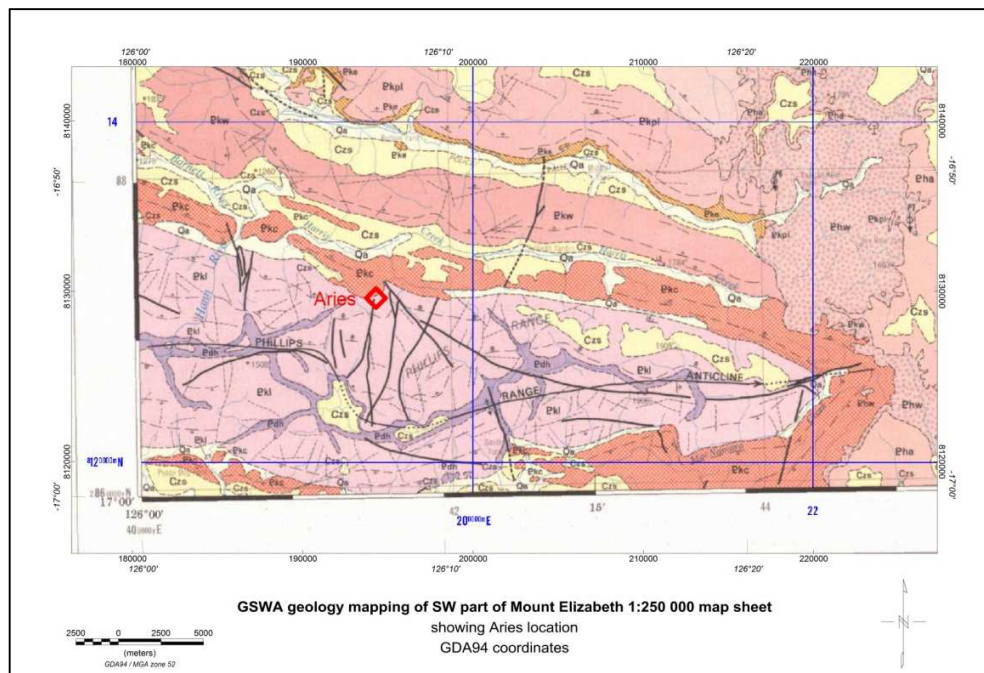


**Figure 9-1: Geology of the SW part of the Mount Elizabeth 1:250 000 map sheet showing location of the Aries kimberlite. Pdh is Hart Dolerite. Pkc is Carson Volcanics, Pkl is King Leopold Sandstone. Pkw is Warton Sandstone. Reproduced from GSWA geological mapping of Mount Elizabeth mapsheet.**

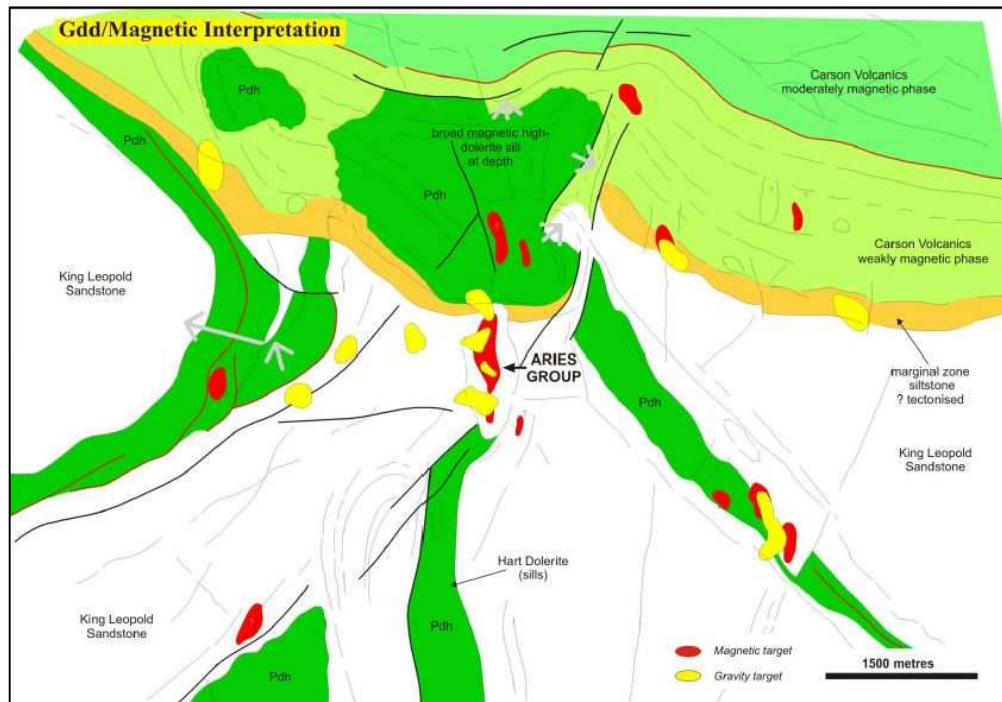


**Figure 9-2: Aries interpreted geology from aeromagnetic and airborne gravity datasets. After Isles and Moody (2004a).**

## 9.2 Previous exploration

The Aries, 20 ha kimberlite pipe, was discovered in 1985 in the Phillips Range in the central Kimberley by a Triad-Freeport joint venture using traditional drainage sampling methods. Its discovery and age determination (about 820 Ma) are described by Towie et al. (1991). The surface expression of the kimberlite pipe comprises three depressions of up to 20 m depth which are clearly visible on aerial photography. This is similar to some kimberlite pipes in South Africa where depressions in surface topography provide leads to aid in discovery.

### 9.3 Elevation data

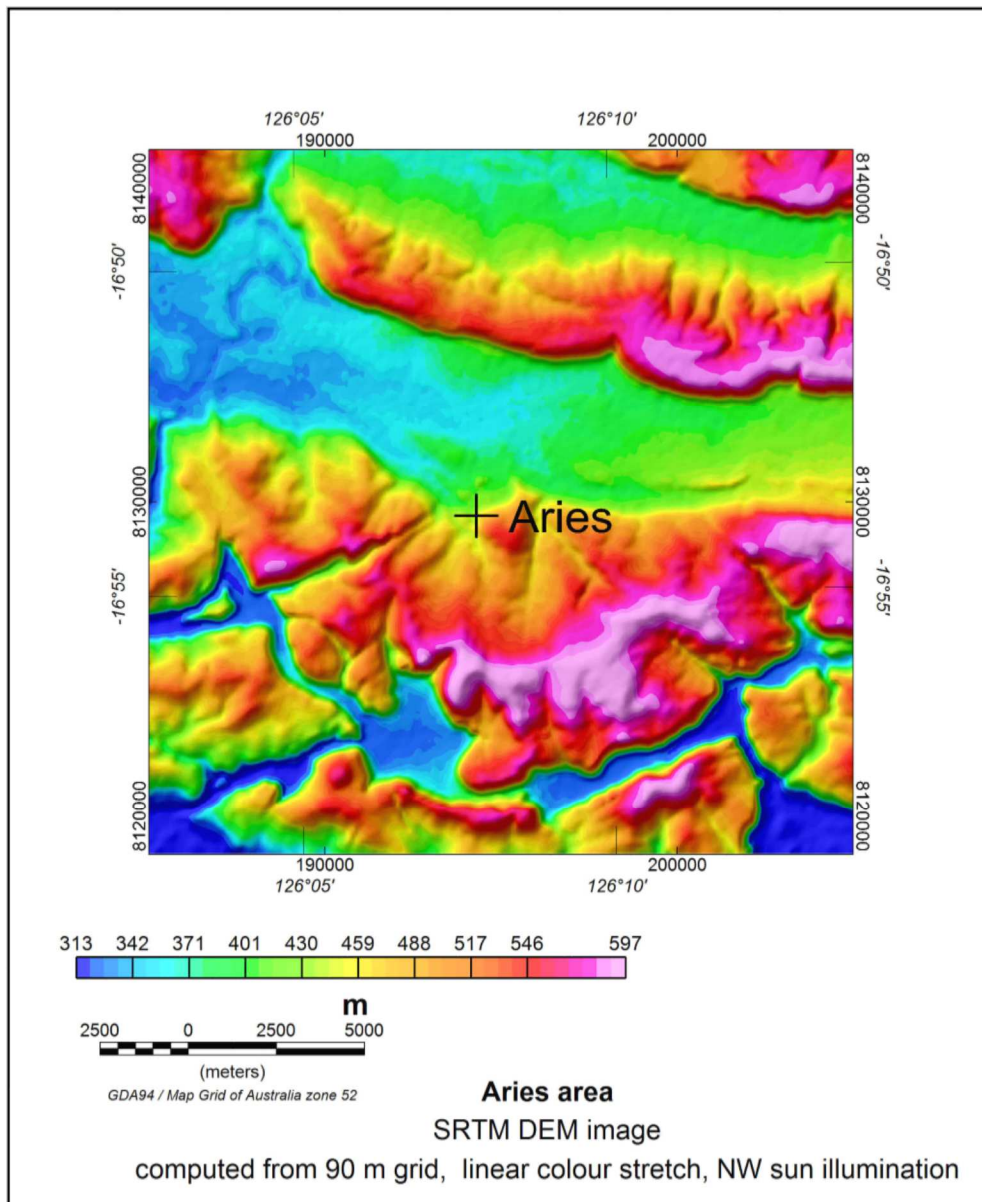


**Figure 9-3: Shuttle Radar Topographic Mission (SRTM) digital elevation model (DEM) image for Aries area. The Aries pipe is located just north of high ground in the southern part of the image. Sun illumination from NW with 45 degree elevation.**

## 9.4 Aeromagnetic data

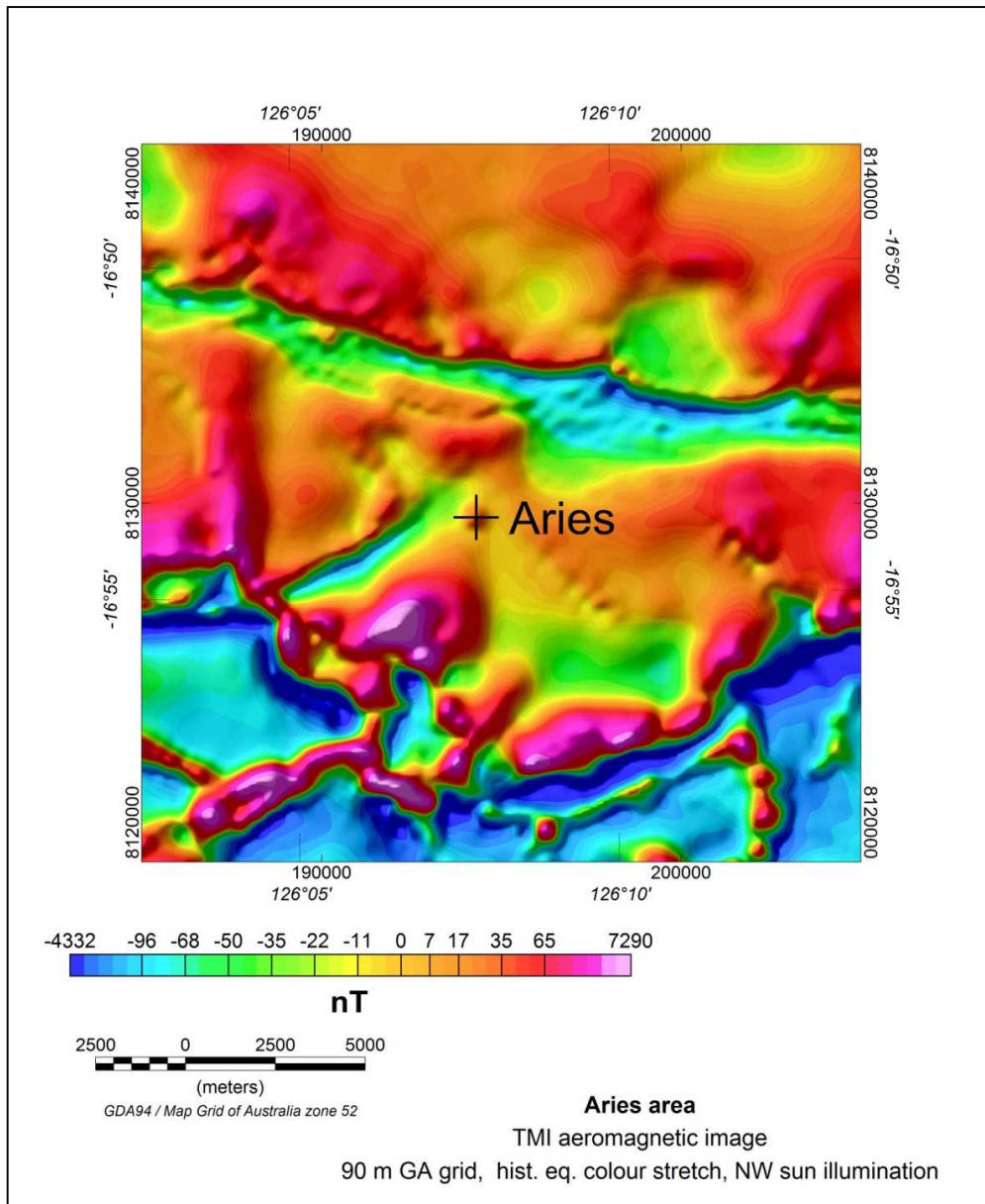


**Figure 9-4: Aries area total magnetic intensity image. The Aries pipe has a small positive magnetic anomaly associated with the pipe. Sun illumination from NW with 45 degree elevation.**

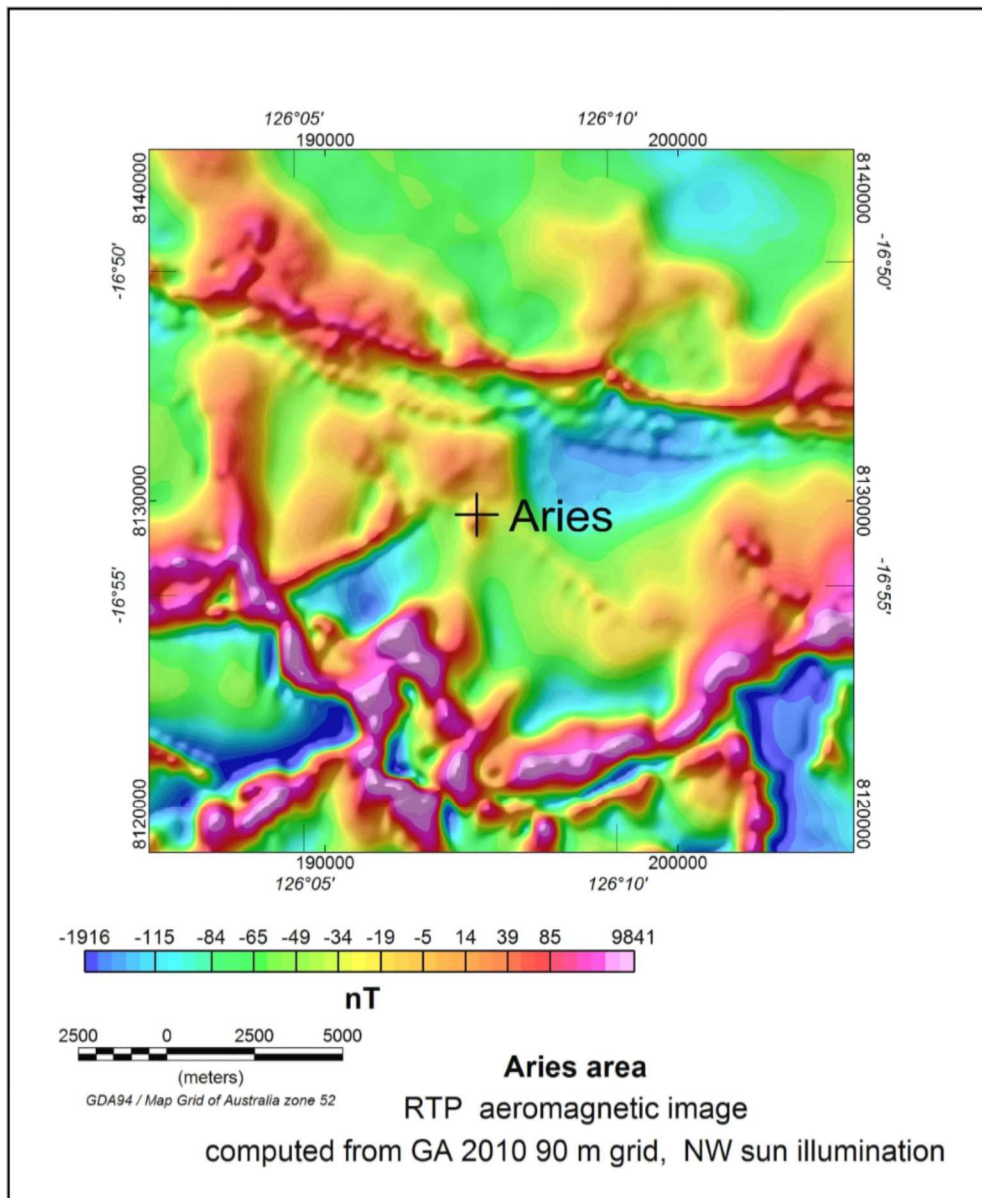


**Figure 9-5: Aries area reduction to pole (RTP) aeromagnetic image. The Aries pipe has a small positive magnetic anomaly associated with the pipe. Sun illumination from NW with 45 degree elevation.**

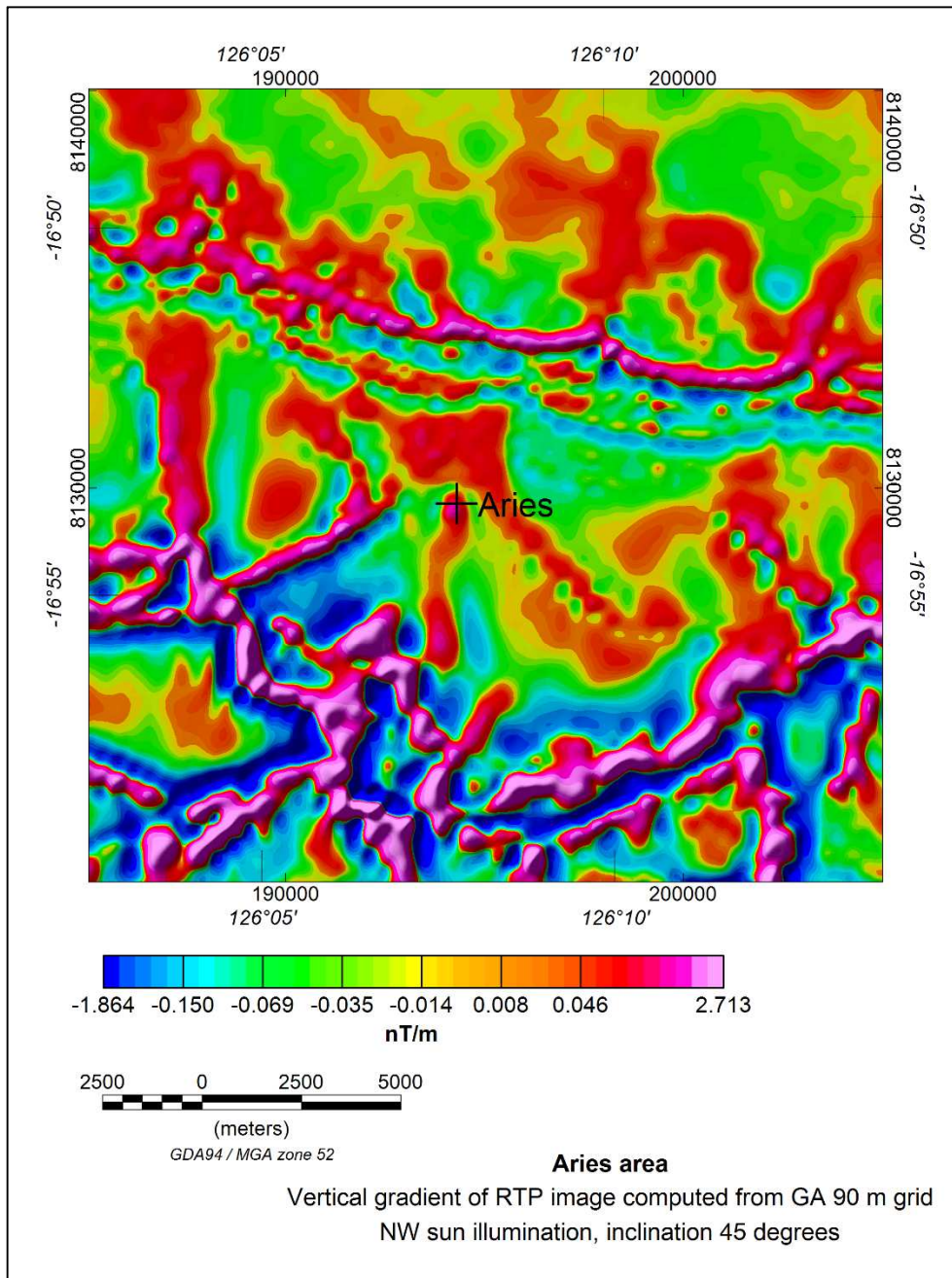


**Figure 9-6: Aries area vertical gradient of RTP image. Sun illumination from NW with 45 degree elevation.**

## 9.5 Gravity data

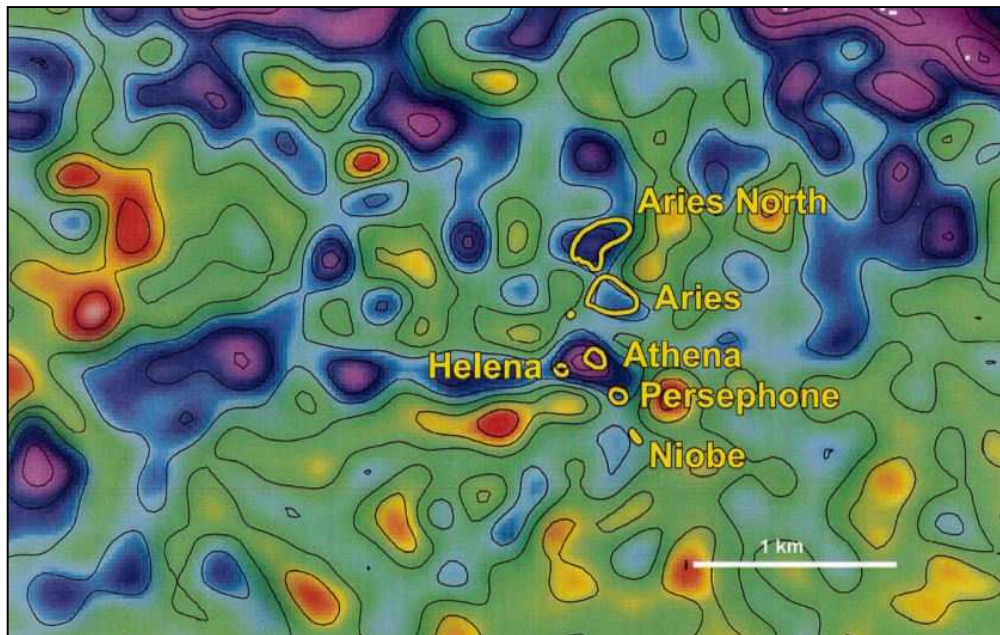


Figure 9-7: Aries area vertical gravity gradient ( $G_{zz}$ ) image from Falcon airborne gravity gradiometry. Contour interval 10 eotvos. Map reproduced from Isles and Moody (2004b). The various pipes are associated with lows on the vertical gradient of the gravity.

## 9.6 Discussion on integrated datasets at Aries

Aries has a surface expression coincident with some shallow (20 m) depressions. The location is just north of east west trending higher ground. The aeromagnetic images computed from GA 400 m spaced survey data shows Aries with a positive aeromagnetic response in both the total magnetic intensity and reduced to pole images and a local high in the vertical gradient of the reduced to pole aeromagnetic data. It is also seen in the Falcon gravity gradiometry image with a series of vertical gradient lows. There are other similar gravity gradient lows nearby and these are worth further investigation.

## 10 EXPLORATION AT ELLENDALE

### 10.1 Geology

Regional geology for the Ellendale area is documented by Jaques et al (1986).

The Ellendale lamproite pipes occur in flat-lying Permian sandstones and Devonian to Carboniferous shales and limestones on the Lennard Shelf, within the King Leopold Mobile Zone. Ellendale 4 is close to the Oscar Fault which strikes NW-SE. See Figure 10-9.

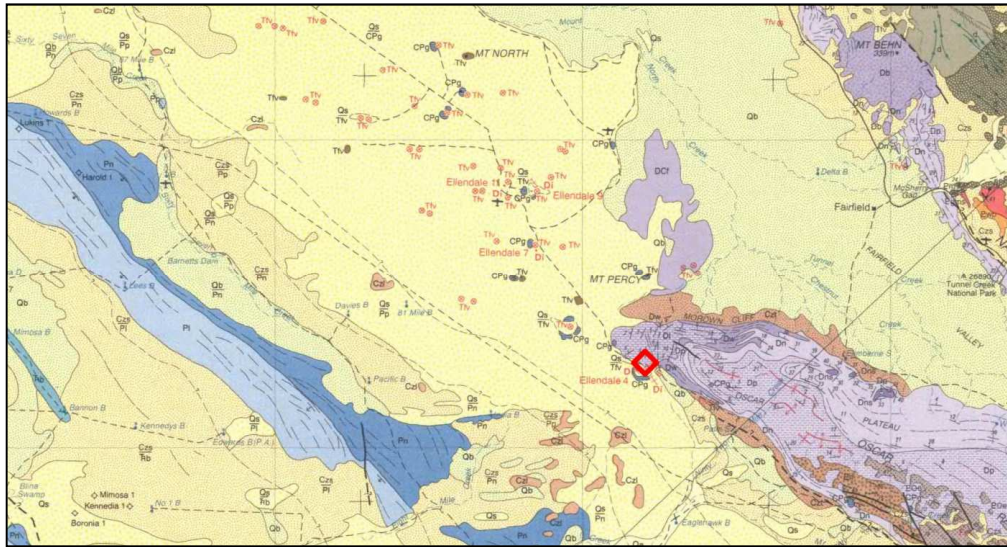


**Figure 10-1: Ellendale geology from GSWA cdrom of 1:250 000 geology sheets. Legend is shown in Figure 10-2.**

Ellendale pipes have been dated at 20 – 22 Ma (Wellman 1972), These dates have been confirmed by later authors.



**Figure 10-2: Legend for West Kimberley geology map shown in Figure 10.1. After Hassan (2004)**

## **10.2 Previous exploration and mining**

The Ellendale lamproite province was discovered in 1976 during routine geochemical drainage sampling. (Atkinson et al, 1984). This led to the discovery of the Ellendale 4 pipe and others followed rapidly afterwards during detailed aeromagnetic survey. Follow up work included ground electromagnetic (Turam, Sirotem and VLF) surveys. INPUT and later DIGHEM airborne electromagnetic surveys were also used effectively (Jenke and Cowan, 1994). Aeromagnetic responses were generally less than 10 nT and the anomaly shapes often indicated that remanent magnetisation is present in some of the pipes (Jenke and Cowan, 1994). With a low magnetic background it was easy to see the magnetic responses due to the pipes.

Kimberley Diamond Company acquired the Ellendale mine from Gem Diamonds Ltd in early 2013. Gem Diamonds had been mining there since 2007. Production comes from Ellendale 4, 7, 9 and 11 pipes (Register of Australian Mining, 2013).

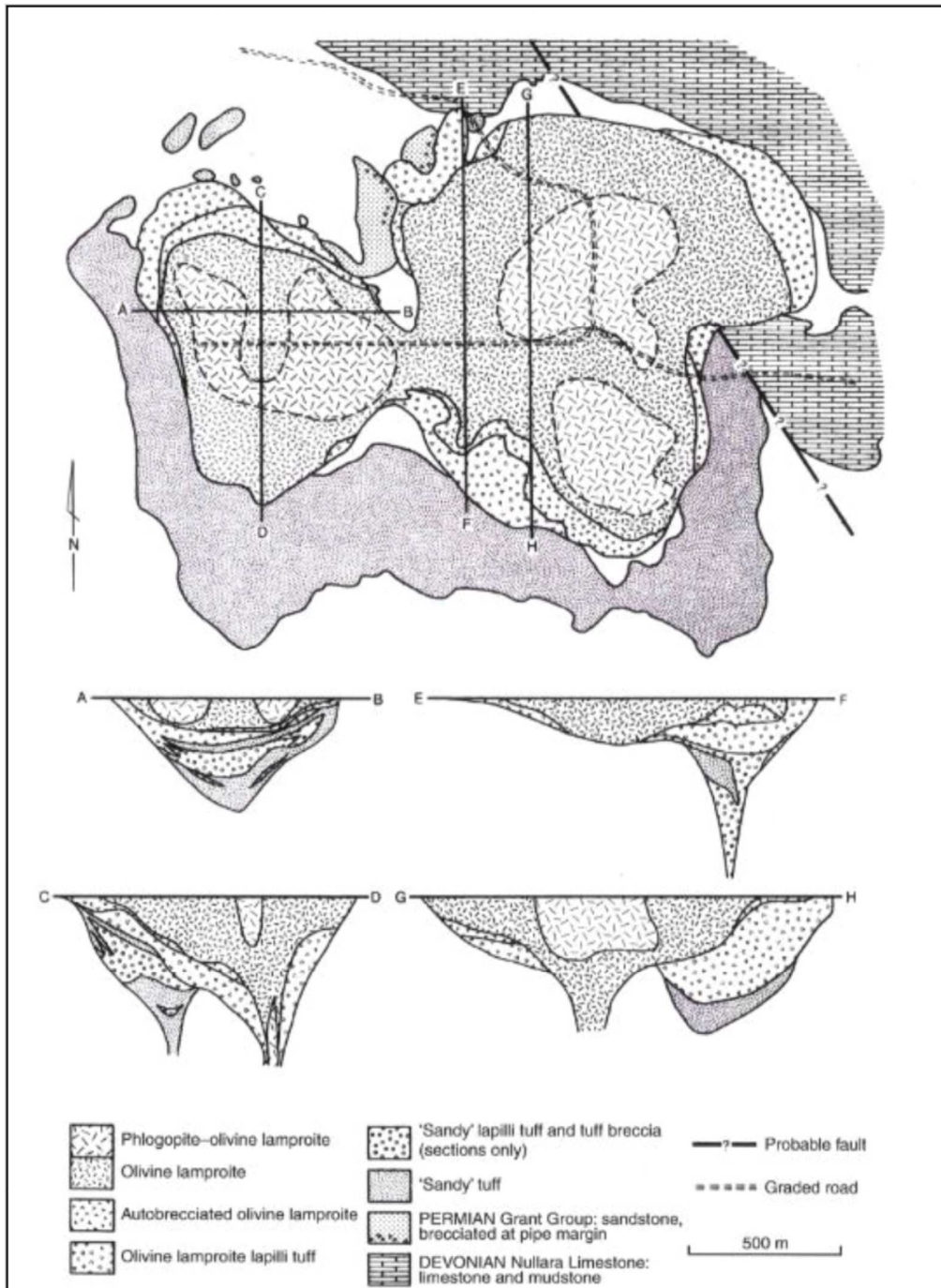
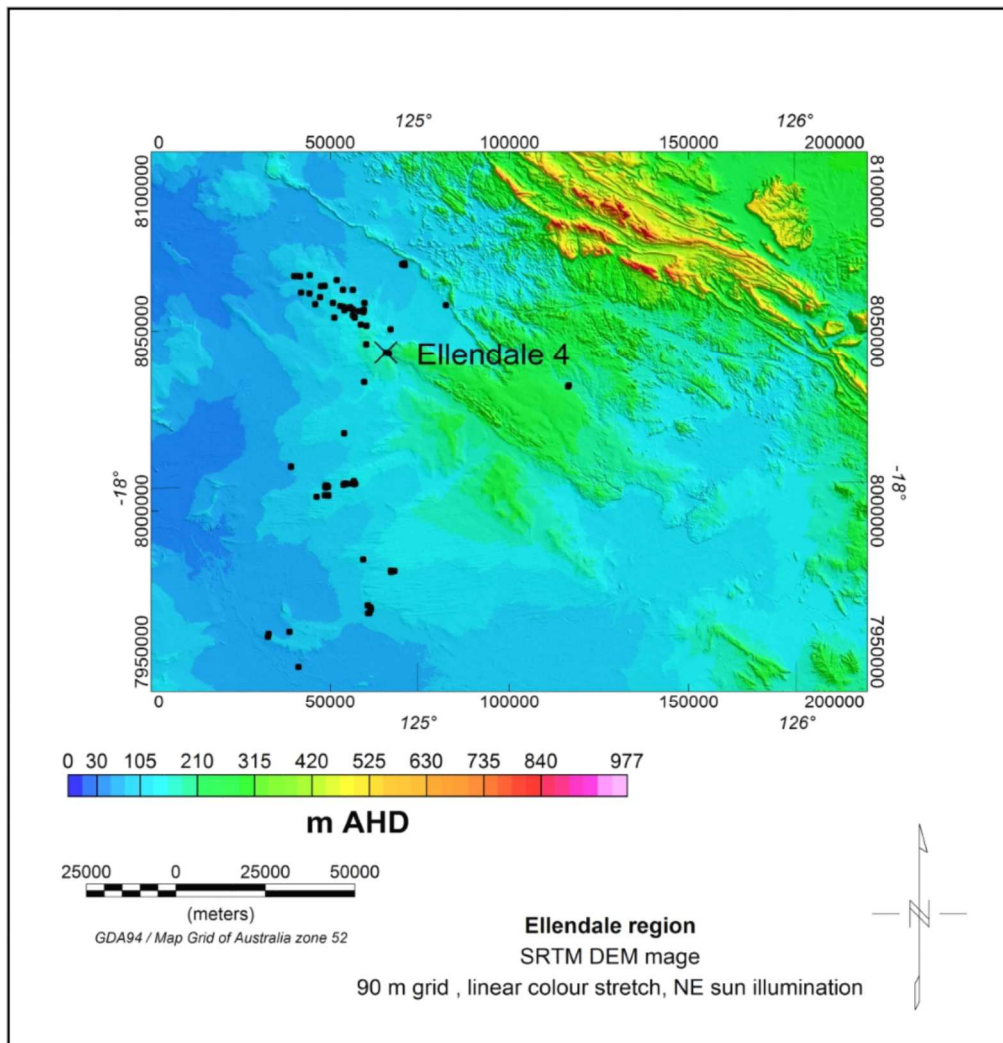


Figure 10-3: Geological map of Ellendale 4 with four cross sections. After Jaques et al (1986), page 103

### 10.3 Elevation data



**Figure 10-4: Ellendale SRTM DEM image. Black dots indicate locations of lamproite intrusions. Ellendale 4 is indicated with a black cross. Ellendale 4 is aligned with a NW trend in the DEM image. Sun illumination from NE with 45 degree elevation.**

## 10.4 Aeromagnetic data

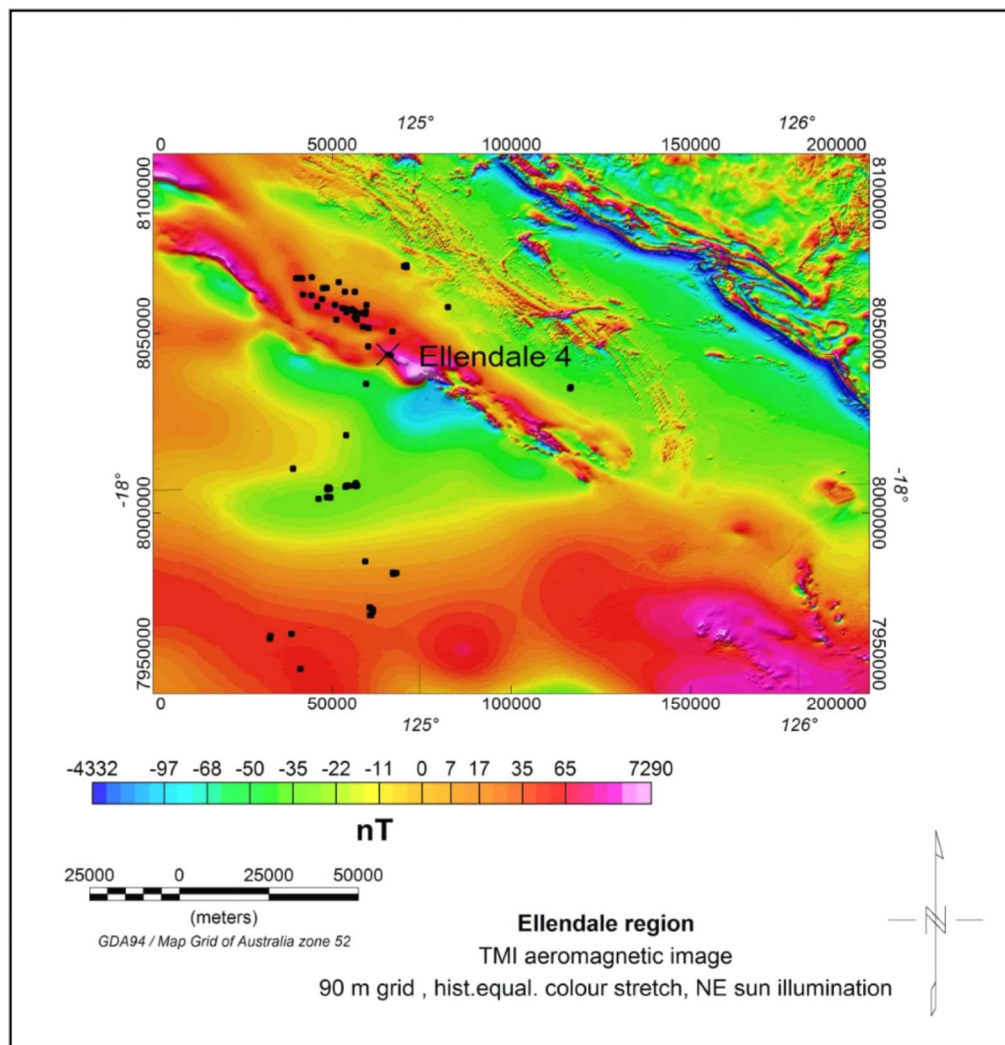


**Figure 10-5: Ellendale region. TMI aeromagnetic image. Black dots indicate locations of lamproite intrusions. Ellendale 4 location is indicated with a black cross. Sun illumination from NE with 45 degree elevation.**

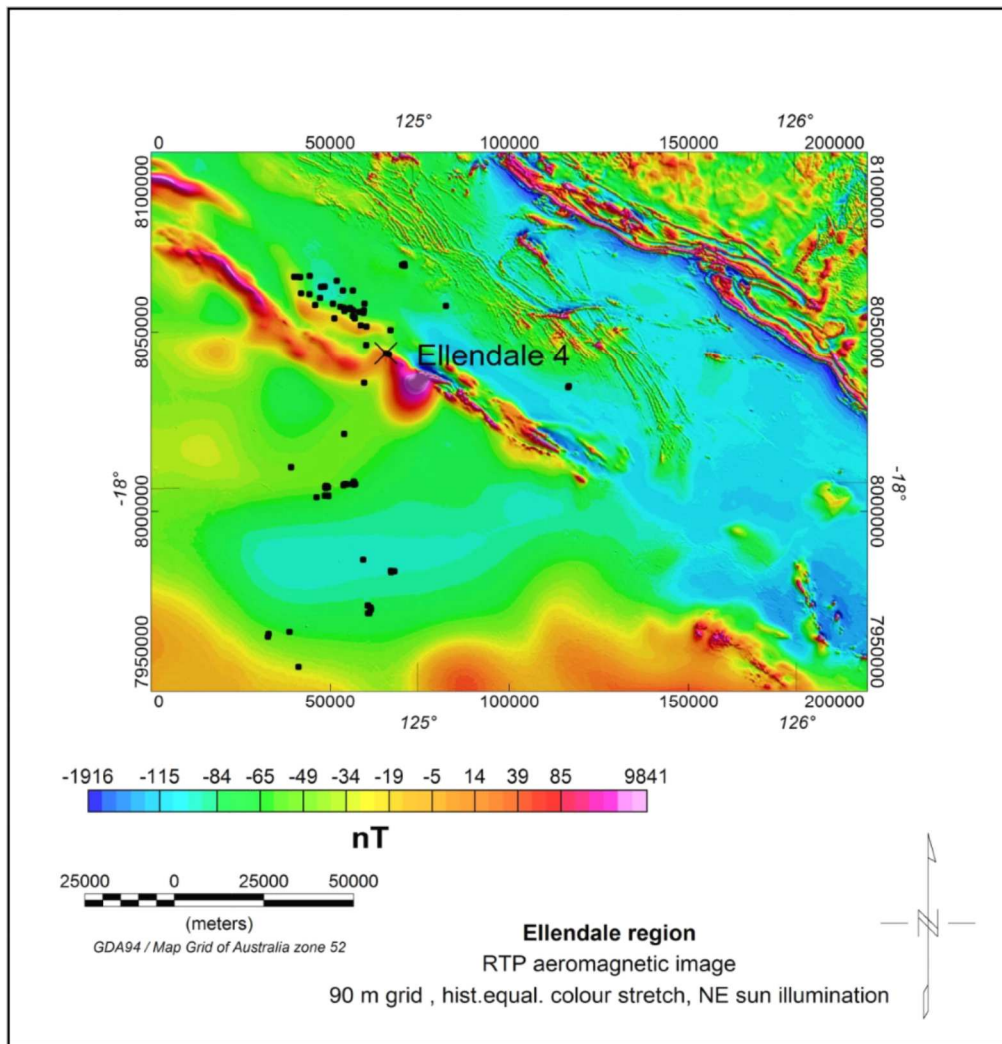


**Figure 10-6: Ellendale region. RTP aeromagnetic image. Black dots indicate locations of lamproite intrusions. Ellendale 4 is indicated with a black cross. Sun illumination from NE with 45 degree elevation.**

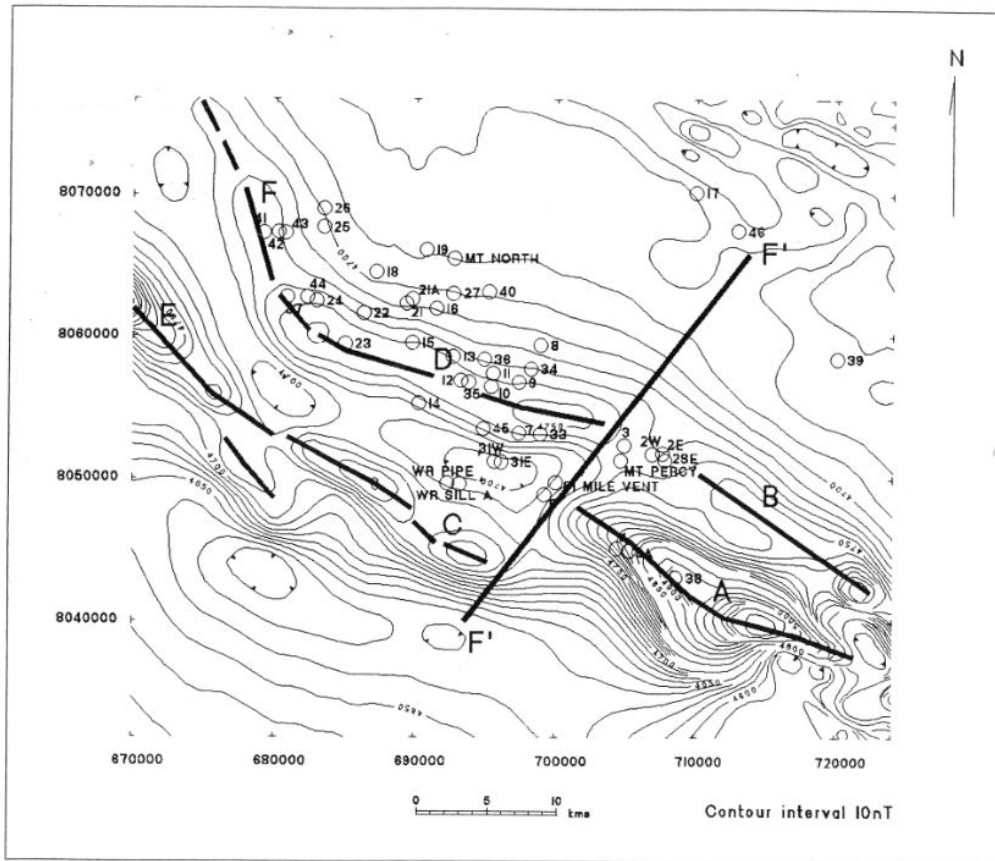
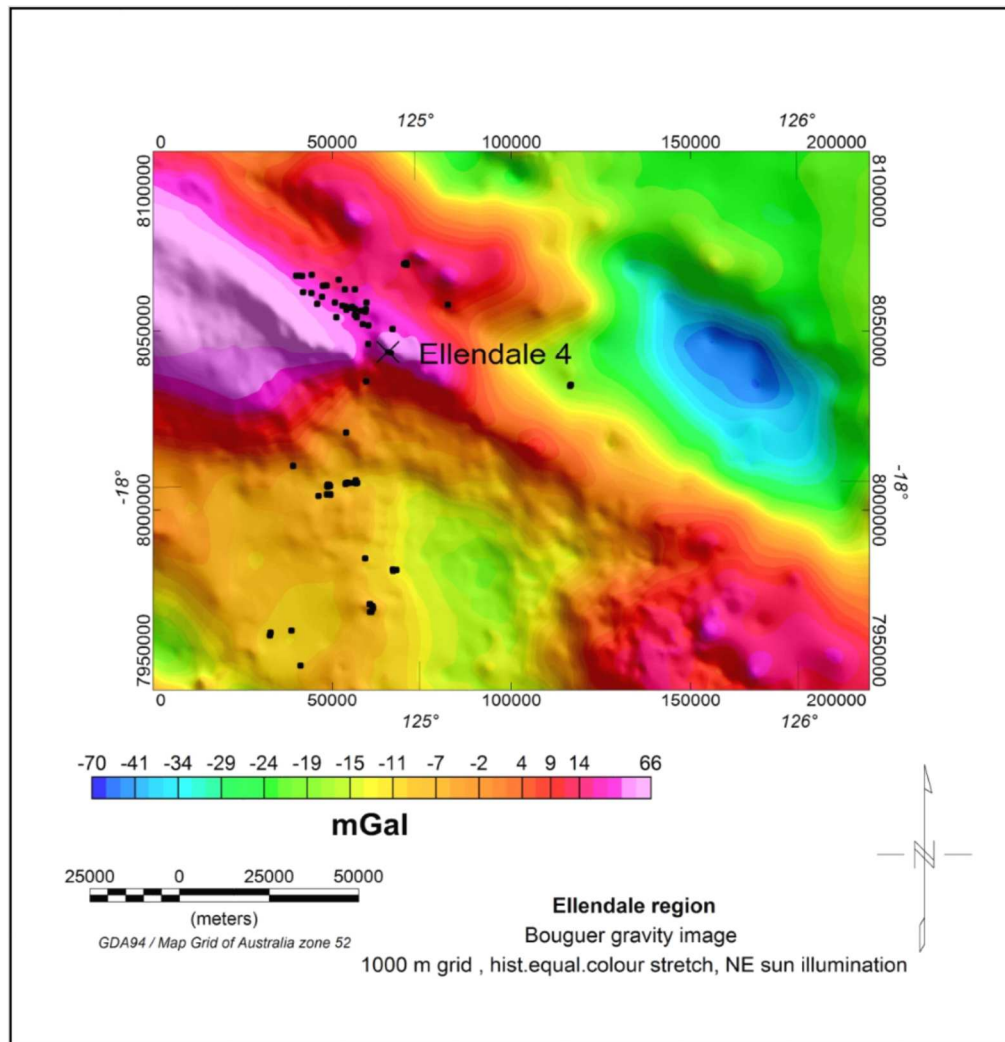


Figure 10-7: Ellendale aeromagnetic contours with 10 nT intervals. Thick black lines indicate interpreted faults. Lamproite pipes are shown numbered. After Jenke and Cowan (1994)

## 10.5 Gravity data

Regional Geoscience Australia gravity data are shown in Figure 10-8. Ellendale 4 and other nearby pipes are located close to the eastern end of a major gravity feature.



**Figure 10-8: Ellendale regional Bouguer gravity image using GA data. Black dots indicate locations of lamproite intrusions. Ellendale 4 location is marked with a black cross. Ellendale 4 is located on a prominent gravity high feature. Sun illumination from NE with 45 degree elevation.**

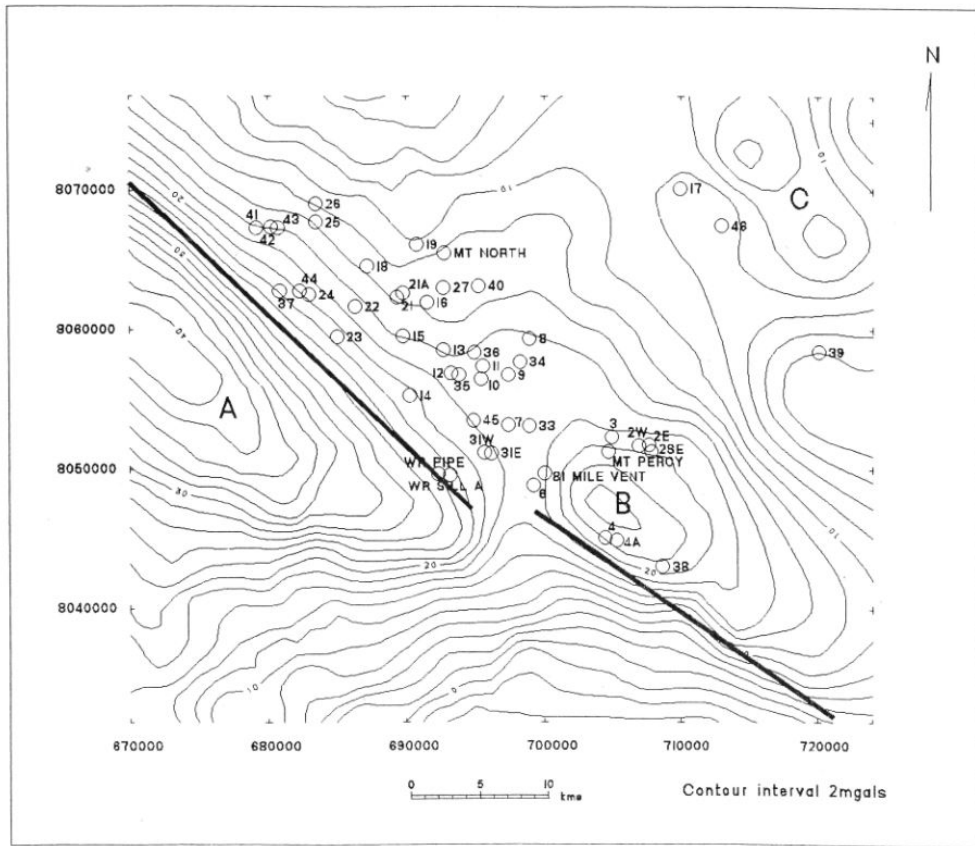
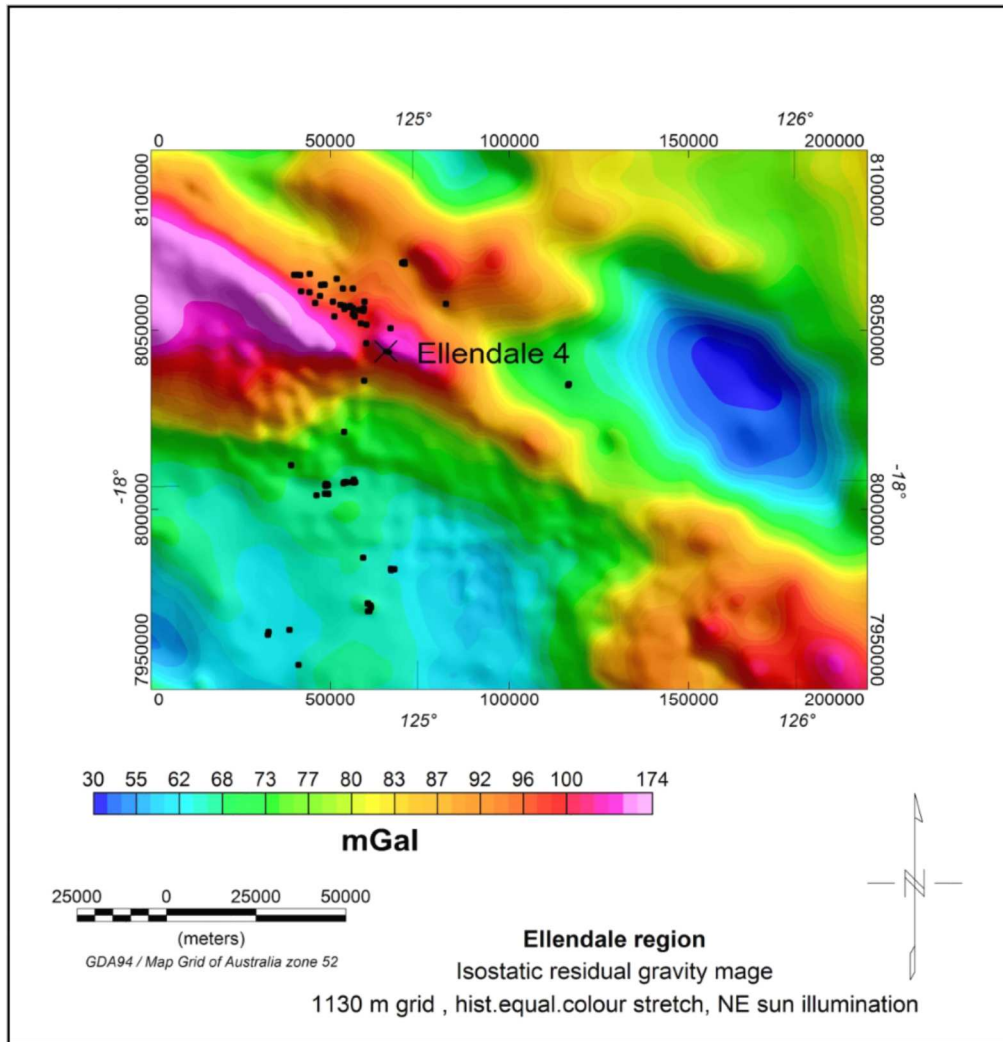
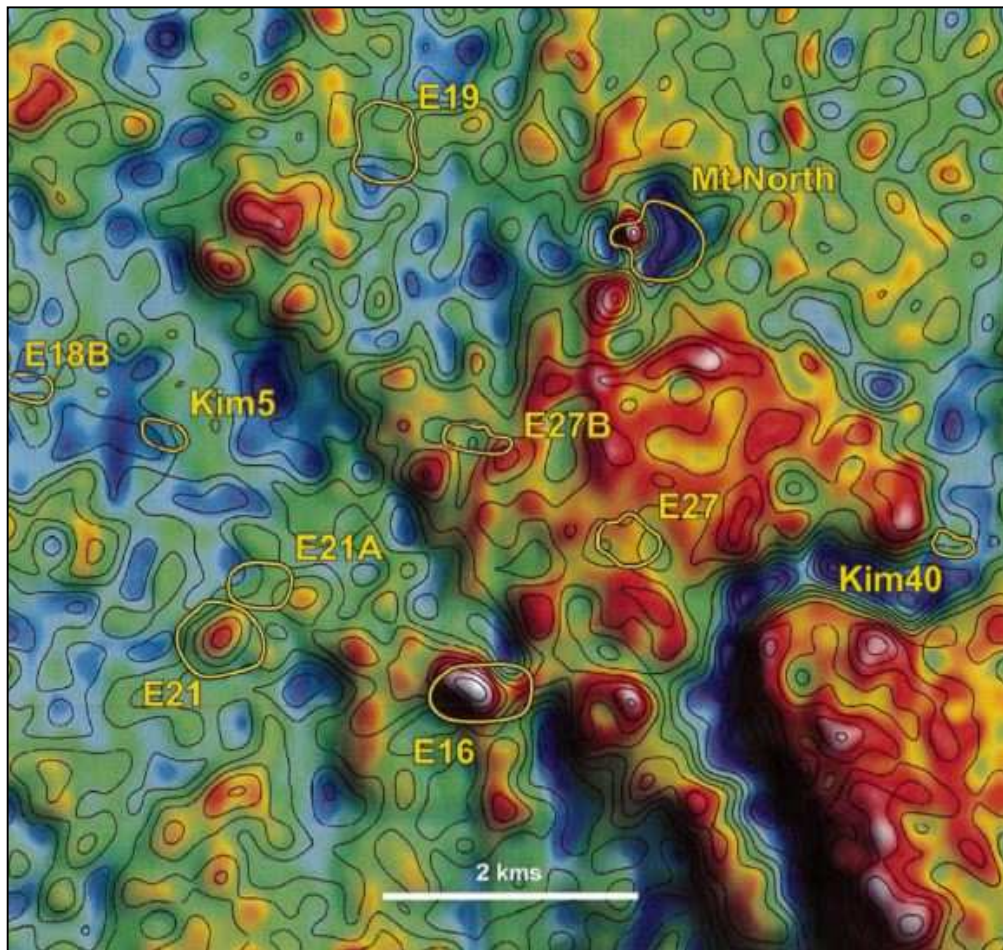


Figure 10-9: Ellendale ground gravity contours with 2 mGal contour intervals. Thick black lines indicate faults. Numbers refer to pipe numbers. After Jenke and Cowan (1994).



**Figure 10-10: Ellendale region. Isostatic Residual Gravity image. Black dots indicate locations of lamproite intrusions. Ellendale 4 location is marked with a black cross. Ellendale 4 is located on a prominent gravity high feature. Sun illumination from NE with 45 degree elevation.**

Falcon fixed-wing gravity gradiometry was used at Ellendale (Isles and Moody, 2004) and produced useful results. Gravity vertical gradient ( $G_{zz}$ ) results are shown in Figure 10-11. This showed both positive and negative anomalies over pipes.



**Figure 10-11: Ellendale. Falcon gravity gradiometry ( $G_{zz}$ ) image with known pipes. 5 eotvos contour interval. After Isles and Moody (2004b). Ellendale pipes here are coincident with positive and negative  $G_{zz}$  features.**

## **10.6 Discussion on integrated datasets at Ellendale**

Aeromagnetic data were very useful in detecting lamproite pipes in the Ellendale area. This was assisted by having very low magnetic backgrounds. Airborne gravity gradiometry using the Falcon system was trialled at Ellendale but produced many possible targets with varying gravity gradient signatures (see Figure 10-11) and it would require considerable work to prioritise which anomalies should be followed up for further investigation. Similar work at Pteropus, reported earlier in this thesis, produced many potential targets but many were shown to be due to variations in regolith properties.

## 11 DISCUSSION

Airborne and ground geophysical methods have been used effectively in the exploration for diamonds in the Kimberley region of Western Australia and have led to significant discoveries. Unfortunately, apart from Argyle, few of these have been economic to date. Diamonds have been mined at Ellendale.

The ages of pipe emplacement at Aries, Ashmore, Pteropus and Seppelt are all in the range 800 – 820 Ma. Mantle plume activity was present at about 780, 800 and 825 Ma and may well have been significant for diamond pipe intrusion. Rodinia reconstructions show that significant continental movement and rifting were present at these times. Argyle was emplaced at about 1178 Ma (Pidgeon et al, 1989) and less detail is available in the Rodinia reconstructions at this time. Ellendale pipes are very recent at about 20 to 22 Ma. Pipe emplacement in the Kimberley regions fit with the worldwide age distribution of pipes (Figure 2-3).

Table 11-1 provides a summary of airborne and ground geophysical results for the Ashmore, Seppelt and Pteropus study areas. Aries and Seppelt 4 are included here for comparison.

Statistical analysis of the results shown in table 11-1 shows:

1. All ten of the pipes studied are in locations within 15 km of significant changes in slope in the Moho surface. These are interpreted as due to deep structures. The slope data are shown in Figure 5-26.
2. Digital elevation data (SRTM) shows that structural control is evident in 4 out of 10 of the pipes.
3. Aeromagnetic data shows the cluster of pipes at Ashmore collectively but not individually. Seppelt 1, Aries and Ellendale 4 are all seen as individual pipes. i.e 3 of 10 are seen as individual pipes.

**Table 11-1: Summary results for individual study areas**

	<b>Ashmore 1 - 4</b>	<b>Seppelt 1 and 2</b>	<b>Pteropus 1 and 2</b>	<b>Aries</b>	<b>Ellendale 4</b>
<b>Depth to Moho</b>	34.7 km, within 15 km of local maximum in Moho surface gradient	35.0 km, within 15 km of local maximum in Moho surface gradient	35.0 km, within 15 km of local maximum in Moho surface gradient	40.0 km, within 15 km of local maximum in Moho surface gradient	33.7 km, within 15 km of local maximum in Moho surface gradient
<b>Structural control seen in topography</b>	not defined	Yes – see topo in figure 7-3	yes – see figure 7.3	close to local topo structure	no
<b>Aeromagnetic response</b>	yes – detects Ashmore 1 to 3 as a group, but not individually. Ashmore 4 not detected	Seppelt 1 about 12 nT in 60 m high aeromagnetic survey  Seppelt 2 not detected	not detected	detected  low amplitude	less than 10 nT
<b>Ground magnetic response</b>	yes – detects individual Ashmore 1, 2, 3 pipes but not Ashmore 4	Seppelt: can detect individual kimberlite bodies  Seppelt 2 not detected	not detected	Info not available	low amplitude
<b>Airborne EM response</b>	conductive area but individual pipes not defined	conductive areas but pipe not defined	conductive areas but pipes not defined		detected by Input EM
<b>Ground EM34 response</b>	Yes - each pipe well defined	Seppelt 1 pipes well defined See figures 7-18 and 7-19.  Seppelt 2 not detected	not detected	not surveyed	not surveyed

	Ashmore 1 - 4	Seppelt 1 and 2	Pteropus 1 and 2	Aries	Ellendale 4
<b>Ground gravity response</b>	yes - each pipe well defined by negative gravity anomalies	Seppelt 1 residual gravity anomaly - 0.5 mGal.  Seppelt 2 small negative residual anomaly	Pteropus 1 – - 0.6 mGal residual anomaly  Pteropus 2 – - 1.6 mGal residual anomaly	Small negative anomaly less than – 1 mGal	small

4. Ground magnetic data has shown 5 of the pipes out of 9 where magnetic surveys were used. Ashmore 4 and Seppelt 2 were not detected by ground magnetic survey.

5. Frequency domain heliborne electromagnetic surveys showed conductive areas at Ashmore, Seppelt and Pteropus but not individual pipes. Fixed wing Input EM survey at Ellendale 4 showed this pipe.

6. Ground frequency domain electromagnetic methods using Geonics EM34 system have been used at Ashmore and Seppelt and detected all 4 of the Ashmore pipes and Seppelt 1. i.e 5 out of 6 pipes in total. This system was not used at Aries or Ellendale 4 as far as is known to the author.

7. Ground gravity showed all 10 pipes.

8. Airborne gravity using the Falcon system showed targets in the areas of the pipes at Aries, Ellendale 4 and Pteropus. These results are not referred to in table 11-1. At Pteropus and Ellendale there were numerous potential targets and many of these are likely to be due to variations in regolith characteristics in these areas.

Aeromagnetic methods require close line spacing and low flying height due to the dimensions of the likely targets and the low target magnetic amplitudes.

Line spacing in the range 20 to 100 metres are required and flying heights of 40 metres or less, provided safety considerations allow this. Aeromagnetic surveying may be combined with gravity gradiometry but at much higher cost than aeromagnetism alone. Some of the pipes are shown, by ground magnetic surveys, to be either weakly magnetic or non-magnetic. This implies that lack of aeromagnetic targets does not necessarily mean no kimberlites or lamproites are present.

In the North Kimberley area, aeromagnetic surveys have helped to locate target areas for diamond exploration but have not produced really clear targets as is the case at Ellendale and Aries. Follow-up ground magnetic surveying (Ashmore and Seppelt) has shown that the kimberlite targets are variably magnetic and do not produce definitive targets for drilling without using other techniques, such as gravity. The use of gravity as a target definition tool has been successful. Where the Carson Volcanics are present, there is considerable magnetic response from these volcanic rocks which has made it hard to differentiate aeromagnetic targets due to potential kimberlites and lamproites.

In the Kimberley region, the main diamond occurrences are all on the flanks of major positive gravity anomalies. The Merlin deposit in the Northern Territory is similarly located on the flanks of a significant gravity anomaly. Locations on the flanks of major gravity anomalies have also been noted for some of the diamond deposits in South Africa.

Ground gravity has been a useful and practical exploration method and has shown that low density material found in clay weathering caps over the tops of kimberlite pipes form suitable gravity targets. Most of the gravity anomalies seen over kimberlites in the Kimberley region are negative due to the weathering that has developed over the top of the kimberlites. It would be expected that we would find some positive anomalies where weathering is either not present or thin, but this has not been seen in this study. There may be some cases where the negative anomaly due to weathered material closely balances out the gravity high from the kimberlite and leaves virtually no detectable gravity anomaly. The depth of weathering is important in

determining the gravity response. Where hypabyssal kimberlite is exposed at surface and little is seen of weathered clays, a positive gravity anomaly would be expected. No such cases were observed.

We first used gravity at Ashmore in the 1997 field program carried out for Striker Resources by honours student Sumner and the author. This work rapidly found more pipes, close to known pipes that had already been confirmed by drilling. The use of gravity was extended to other tenements held by Striker Resources and had further success. It also showed that the kimberlites were often located along linear structures which were seen in the terrain and gravity results e.g. the long fault structure that links Seppelt 1 and 2 and extends south of Seppelt 2. Gravity data were usually acquired with line spacing and station spacing of 40 metres and this was found to be satisfactory. However in some areas, line and station spacing were reduced to 20 metres. As usual there is a trade-off between resolution and cost.

Ground gravity is useful at a local scale but regional gravity datasets are also useful and have often been overlooked in company search strategies. It is important to integrate the regional data from Geoscience Australia (GA) with detailed company data. This requires that the data are tied by means of using GA 'absolute' stations that GA has established around the country. In this work with Striker Resources, a network of local gravity bases established within Striker's tenements was tied back to a GA station at Kununurra Airport.

Airborne gravity gradiometry using the fixed wing Falcon system has been used in this study, and results are shown for the Pteropus area in the North Kimberley. Results from Aries and Ellendale 4 show that the 100 m spaced Falcon surveys showed vertical gravity gradient ( $G_{zz}$ ) anomalies over pipes but produced many more similar looking targets.

In the Pteropus area, gravity gradiometry using the Falcon system showed the Pteropus 1 and 2 pipes and also located other potential targets. The Pteropus area was quite a difficult target for gravity gradiometry as the two known pipes are located in low lying ground surrounded by steep cliffs. The survey was also

flown quite late in the season with significance turbulence. The computed Bouguer gravity data were easier to use than the vertical gradient Gzz data. The latter produces many more local minima and maxima. Follow up work revealed no new kimberlite discoveries in the Pteropus area. This may be due to no further kimberlites being present or possibly a resolution issue with difficult topography. Use of a helicopter gravity gradiometer system would address this issue.

Heliborne Falcon gravity gradiometers have been developed from 2006 and have a number of advantages over the fixed wing gravity gradiometer systems. These include better ability to follow terrain, lower flying height and lower flying speed. These result in improved spatial resolution. More detail and references are provided earlier in this thesis on page 40. The rugged topography of the Pteropus area would have been better suited to the helicopter version of Falcon but was not operational then.

Results from fixed wing Falcon gravity surveys at Aries and Ellendale are included in chapters 9 and 10. These show that the vertical gravity gradient (Gzz) results are helpful in these areas. Kimberlite pipes at Aries are generally shown with negative Gzz anomalies. At Ellendale, Gzz anomalies over lamproite pipes have both negative and positive amplitudes. This is interpreted as due to whether tuffaceous (with negative anomalies) or magmatic material (with positive anomalies) dominate.

Airborne electromagnetic techniques, DIGHEM and Hummingbird helicopter borne frequency domain EM surveys were designed and implemented at Ashmore, Seppelt and Pteropus and showed locally areas of higher conductivity than the surrounding areas, but did not provide good detailed detection of weathered clays over the kimberlite pipes. Ground EM was much more successful in doing this at both Ashmore and Seppelt 1. No ground EM results were available for the Pteropus pipes.

Ground electromagnetic methods using Geonics EM 34 frequency domain EM equipment have been very effective and have worked in the Ashmore and

Seppelt areas, because there is sufficient conductivity contrast between the clay weathering caps overlying kimberlites and the surrounding host rocks. These are often sandstones with low conductivity. Had the host rocks been more conductive, this method would have been less successful. Two modes were used – horizontal coplanar and vertical coplanar – both used 20 m separation and 1600 Hz. The results are a little different and can provide information on geometry of the conductive sources.

Topography often shows fault control and this is important in controlling pipe emplacement. The kimberlites that have been studied in this thesis are located at a variety of different settings within the landscape. There do not appear to be any clear direct relationships between local topography and kimberlite occurrence, except at Aries where topographic depression is coincident with a kimberlite pipe. In work done by the author in northern Cape Province in South Africa, topography often provided clues to possible kimberlite locations as they tended to be found in low areas along subtle topographic ridges (Wilkes, 1968). This was not observed in the Kimberley region of WA except at Aries.

## **12 CONCLUSIONS AND RECOMMENDATIONS**

Airborne and ground geophysics have been used in diamond exploration in the Kimberley region with varying degrees of success. The geophysical methods have included magnetic, gravity and EM methods. SRTM topographic data are also useful in providing high resolution 90 x 90 metre data for the whole area and enable detection of some underlying faults.

Geophysical results are area specific due to the varying nature of the geology and weathering which in turn control the physical properties of the rocks and the contrasts between kimberlites and lamproites and host geology. This thesis has shown that not all the pipes studied are magnetic.

Reviewing the original project objectives:

### **1. How are suitable areas for diamond exploration recognised at regional scale ?**

Successful diamond exploration requires an integrated approach that uses multiple exploration methods in an appropriate sequence. Typically diamond exploration in the Kimberley region has used conceptual geology, field geological studies, geochemistry, airborne geophysics and ground geophysics, followed by drilling where warranted.

An important issue is recognition of deep seated geological structures and here potential field datasets are essential as has been demonstrated in this project.

### **2. How well do geophysical methods work in the Kimberley region ?**

Table 11-1 lists how the various airborne and ground geophysical methods have worked for the Ashmore, Seppelt, Pteropus study areas. This table also includes information from Aries and Ellendale 4. A combination of airborne and ground methods has been used for each area. Some of the pipes have been shown to be magnetic but not all. Close spaced aeromagnetic surveys (100 metres or less) with low flying height (40 to 80 metres) are required because of the small target amplitudes and small horizontal dimensions. It is important to recognise that the use of magnetics alone is insufficient, especially in areas

where volcanic rocks are present and where the volcanic rocks are magnetic e.g. Carson Volcanics in the area near Ashmore. Kimberlites are variably magnetic due to their varying magnetite and ilmenite content. Where the magnetic mineral content is low, the magnetic contrast with surrounding rocks can make it difficult or impossible to detect kimberlites from their magnetic response. Gerryts (1970) in his review included this factor and Wilkes (1968) did experimental ground electromagnetic fieldwork successfully in South Africa on non-magnetic kimberlites.

Airborne EM and airborne gravity have been trialled in this project at Pteropus but have not resulted in new kimberlite discoveries. This may well be due to insufficient resolution or possibly the areas surveyed included no detectable kimberlite targets. The development of heliborne gravity gradiometers addresses the resolution issue and should lead to improved detection potential. Results from 100 metre spaced fixed wing Falcon gravity gradiometer surveys at Aries and Ellendale are included in chapters 9 and 10. These show that the vertical gravity gradient ( $G_{zz}$ ) results are helpful in these areas. Kimberlite pipes at Aries are generally shown with negative  $G_{zz}$  anomalies. At Ellendale,  $G_{zz}$  anomalies over lamproite pipes have both negative and positive amplitudes. This is interpreted as due to whether tuffaceous (with negative anomalies) or magmatic material (with positive anomalies) dominate.

Ground gravity and EM methods have worked well in this area, and help to provide suitable targets due to the presence of low density and conductive clay weathering caps over kimberlite bodies. The volume and surface extent of these caps has provided good geophysical targets, and in the case of gravity, the extent of the low density clays is usually more than enough to counteract the higher density kimberlitic material in the pipes, and has usually led to small negative Bouguer gravity anomalies. If the weathering is not well developed and the magmatic kimberlite outcrops, then positive Bouguer gravity highs may be evident. This has not been seen in the work reported in this thesis. Fixed wing Falcon airborne gravity gradiometer systems and helicopter EM methods have been used in the Kimberley region but lack sufficient resolution to define kimberlite targets. For gravity exploration this could be addressed by using the

more recently developed helicopter gravity gradiometer systems with their improved spatial resolution and ability to fly lower and slower over potential target areas. This would be particularly useful in areas with significant topographic relief.

### **3. How do we optimise the use of geophysical methods within selected areas of the Kimberley region ?**

Selection of methods and appropriate survey parameters are the key here. Aeromagnetic methods have been used successfully here but do not always detect the kimberlite and lamproite targets because they are not all magnetic. Close spaced aeromagnetic surveys (100 metres or less) and low flying height (40 metres or less) are required because of the small target horizontal dimensions typically of the order of 100 metres diameter.

Ground gravity and electromagnetic methods have worked well in the Kimberley region.

This project has demonstrated that ground gravity requires stations spacing of about 20 x 20 metres to provide sufficient definition of target kimberlites with typical dimensions of about 100 metres diameter. Initial surveys may be at 40 x 20 metre spacing with infill to 20 x 20 metres where warranted. Similar spacings are required when using ground EM techniques such as Geonics EM34 frequency domain EM. This has worked well at Ashmore and Seppelt 1 because host rocks have low conductivity compared with the weathered clays over the pipes.

### **4. Which advanced processing methods are useful for defining suitable geological target areas ?**

Newly available information on variation of depth to the Moho (Aitken, 2010) has been used in this study and showed that each of the study areas are located within about 15 km of significant changes in gradient in the Moho surface. This is illustrated by Figures 5-25, 5-26 and 5-27. The 3D view is particularly useful as it shows well the major structural trends.

Table 11.1 lists the interpolated Moho depths for the six diamond occurrences used as examples in this thesis.

This project has used multiscale edge detection ('worming') of Isostatic Residual Gravity data and aeromagnetic data. This process uses upward continuation of the data which in turn relates to depth of investigation. Upward continuation to greater heights highlights deeper features. Upward continuation to lower heights highlights nearer surface features. Isostatic Residual Gravity data were used for the worming experiments as this data includes offshore as well as onshore data and it was expected that significant structures may be seen to continue offshore. These data have been corrected for variations in depth to the Moho and also variations in sea depth in the offshore data.

3D gridding of the aeromagnetic worm data has been used to produce voxel displays. These have been sliced through at various horizontal levels to highlight structures which are deep seated and potentially important for kimberlite or lamproite emplacement. The use of 3D gridding required large mesh sizes – typically 2 x 2 x 2 km, as in this thesis, in order to keep computing times reasonable. An alternative and complementary approach is to use the worm data at each level and produce more detailed 2D grids. This enables finer resolution to be used.

Upward continuation of aeromagnetic data followed by total horizontal gradient computation has been useful in identifying potential crustal scale faults. Initial tests were done with upward continuation by 1600 metres as previously published by Jaques and Milligan (2004) This continuation height is insufficient for this area, as the images still show too many near surface features. Upward continuing by 5000 m, as shown in this thesis, is more successful.

Analytic Signal computed from the Isostatic Residual Gravity is useful in identifying target areas for follow up especially in areas close to known deposits or prospects, e.g. around Aries.

All the methods used show regional geological features and localised structures which are likely to be important for emplacement of kimberlites and lamproites. The deeper features are more easily recognised in the Moho surface data and the methods that include upward continuation: horizontal gradient computation of upward continued reduced to pole aeromagnetic data and multiscale edge detection (“worming”) of aeromagnetic and gravity data.

### **5. Does present day topography provide clues to assist exploration in this area ?**

The Argyle, Aries, Ashmore, Ellendale, Seppelt and Pteropus areas are located in various topographic settings and no common features are seen between these areas. Topography is well displayed using the Shuttle Radar (SRTM) data and this has identified possible faults in or close to the study areas which may well be important for kimberlite emplacement at Seppelt 1 and Seppelt 2. The detailed topographic imaging from the Falcon gradiometry survey, using the scanning laser altimeter, shows possible structural control at Pteropus 1 and 2. The pipes studied in this thesis have a wide range of topographies ranging from flat e.g. Seppelt 2 to adjacent to hills e.g. Aries, Argyle, Seppelt 1, The author when working in northern Cape Province, South Africa, observed that often the clay weathering areas overlying kimberlite pipes were located in areas of local topographic depressions. This was not seen in this study of the Kimberley region except at Aries.

### **Recommendations**

Further work is recommended on validation and visualisation of the results of multiscale edge detection techniques using aeromagnetic and gravity data.

More data on physical properties would be advantageous (e.g. magnetic remanence, electrical conductivity and density). Downhole geophysical logging would be helpful. This should include downhole magnetic susceptibility and EM conductivity measurements. More sophisticated methods could include downhole gravity and magnetic gradiometer measurements.

Neural networks and self-organising map techniques may be useful to predict locations for potential kimberlite and lamproite pipes based on the signatures from known occurrences.

### 13 REFERENCES

- Aitken, A.R.A., 2010, Moho geometry gravity inversion experiment (MoGGIE): a refined model of the Australian Moho, and its tectonic and isostatic implications. *Earth and Planetary Science Letters*, 297, 71-83.
- Atkinson, W.J., 1989, Diamond exploration philosophy, practice and promises: a review. *Proceedings of the Fourth International Kimberlite Conference, Perth 1986 Geological Society of Australia Special Publication 14, 2*, 1075 – 1107.
- Atkinson, W.J, C.B.Smith and G.L.Boxer, 1984 The discovery and evaluation of the Ellendale and Argyle lamproite diamond deposits, Kimberley Region, Western Australia. In *Applied Mining Geology: problems of sampling and grade control*. 123-134, Society of Mining Engineers, American Institute of Mining, Metallurgical and Petroleum Engineers, New York
- Atkinson, W.J., C.B.Smith, R.V.Danchin, and A.J.A.Janse, 1990, Diamond deposits in Australia, in Hughes, F.E., (ed) *Geology of the mineral deposits of Australia and Papua New Guinea*. The Australasian Institute of Mining and Metallurgy. 69-76.
- Betts, P.G and D.Giles, 2006. The 1800 – 1100 Ma tectonic evolution of Australia in *Precambrian Research* 144 (2006) 92-125.
- Blewett, R, 2012, *Shaping a Nation. A Geology of Australia*, Geoscience Australia and Australian National University.
- Boschetti, F., F.G.Horowitz, P.Hornby, D.Holden, N.Archibald, and J.Hill, 2000, Improved edge detection in potential field maps and graphical estimation of depth to top. In *70th Annual International Meeting of the Society of Exploration Geophysicists, Calgary, Alberta: Society of Exploration Geophysics*, 406-409.
- Boschetti, F., P.Hornby, and F.G.Horowitz, 2001, Wavelet Based Inversion of Gravity Data. *Exploration Geophysics*, 32, (1), 48-55.
- Burley, A.J., and P.G.Greenwood, 1972, *Geophysical surveys over Kimberlite pipes in Lesotho*, Institute of Geological Sciences, UK, 64p.
- Carter, D., 1999, *Optimising geophysical strategies for diamond exploration in the North Kimberley Kimberlite Province of Western Australia*. B.Sc Honours Geophysics thesis, Curtin University.
- Clifford, T.N., 1966, Tectono-metallogenic units and metallogenic provinces of Africa. *Earth and Planetary Science Letters*, 1, 421-434.
- Clement, C.R., E.M.W.Skinner, and B.H.Scott-Smith, 1977, *Kimberlite redefined; Second International Kimberlite Conference, Sante Fe, Abstracts* (unpublished).

- Collins, C.D.N., 1991, The nature of the crust-mantle boundary under Australia from seismic evidence. In Drummond, B.J. (ed) *The Australian Lithosphere*. Geological Society of Australia Special Publication, 67-80.
- Cox, D.P., and D.A.Singer, 1986, Descriptive models of diamond pipes. Model 12 in *Mineral Deposit Models*. United States Geological Survey Bulletin 1693. <http://pubs.usgs.gov/bul/b1693/html/bull9fhv.htm>
- De Wit, M. 2010. Identification of global diamond metallogenic clusters to assist exploration. *Diamonds Source to Use 2010*. The South African Institute of Mining and Metallurgy. 15-38.
- Dransfield, M.H. 2010. Advances in airborne gravity gradiometry at Fugro Airborne Surveys. Abstract in EGM 2010 International Workshop – Adding new value to Electromagnetic, Gravity and magnetic Methods for Exploration, Capri, Italy, April 2010.
- Drew, G.J., and D.R.Cowan, 1994, The geophysical signature of the Argyle lamproite pipe. In *Geophysical signatures of Western Australian mineral deposits*. University of Western Australia, and Australian Society of Exploration Geophysicists Special publication 7, 393-402.
- Farr, T.G., et al., 2011, The Shuttle Radar Topography Mission. *Reviews of Geophysics.*, 45, RG2004. Also in <http://www2.jpl.nasa.gov/srtm>.
- Ferguson, J., 1977, Predicting the existence of diamonds in kimberlite from their inclusions. *BMR Journal of Australian Geology and Geophysics*, 2, 236.
- Fitzgerald, D and P.Milligan, 2013, Defining a deep fault network for Australia, using 3D “worming”. Presented at Society of Exploration Geophysicists Annual Meeting, Houston 2013.
- Fullagar, P.K., G.A.Pears and B.McMonnies, 2008. Constrained inversion of geologic surfaces – pushing the boundaries. *Leading Edge (Society of Exploration Geophysicists)* 27(1) 98-105.
- Garton, G., 2000, Investigating the relationship between regional geophysics and kimberlites of the North Kimberley province in Western Australia. B.Sc Honours Geophysics thesis, Curtin University.
- Gellatly, D.C., and J.Sofoulis, 1969, Explanatory notes for 1:250,000 scale map sheets of Drysdale and Londonderry, WA. Geological Survey of Western Australia, 20p.
- Geoterrex, 1996. Logistics and Interpretation Report of a Dighem survey for Striker Resources N.L over the Ashmore prospect, Job No. 7-763, unpublished, 20p.
- Gerryts, E., 1970, Diamond prospecting by geophysical methods – a review of current practice, in *Mining and Groundwater Geophysics*, Geological Survey of Canada, 439-446.

- Glover, J.E., and P.G.Harris, 1985, Kimberlite occurrence and origin: a basis for conceptual models in exploration. Publication No 8, University of Western Australia.
- Griffin, T.J., and K.Grey, 1990, The Kimberley Basin in Geology and Mineral Resources of Western Australia, Geological Survey of WA Memoir 3, 293-304.
- Gunn, P.J., and A.J.Meixner, 1998, The nature of the basement to the Kimberley Block, North Western Australia. *Exploration Geophysics*, 29, 506-511.
- Gurney, J.J, H.H.Helmstaedt, A.P.le Roex, S.H.Richardson, and K.J.Westerlund, 2005, Diamonds: crustal distribution and formation processes in time and an integrated deposit model. *Economic Geology* 100 th Anniversary Volume, Society of Economic Geologists, 143 - 178.
- Haggerty, S.E., 1986, Diamond genesis in a multiply-constrained model. *Nature*, 320, 34-38.
- Hassan, L.Y. 2004, Mineral occurrences and exploration potential of the West Kimberley. Geological Survey of WA Report 88.
- Hawthorne, J.B., 1975, Model of a kimberlite pipe. *Physics and Chemistry of the Earth*, 9, 1-15.
- Helmstaedt, H.H., and J.J. Gurney, 1991, Geotectonic controls on the formation of diamonds and their Kimberlitic and Lamproitic host rocks: applications to diamond exploration. *Proceedings of the fifth international Kimberlite Conference*, 2, 237-250.
- Helmstaedt, H.H., and J.J. Gurney, 1995, Geotectonic controls of primary diamond deposits: implications for area selection. *Journal of Geochemical Exploration*, 53, 125-144.
- Hillis, R.R., and R.D.Muller, editors, 2003, Evolution and dynamics of the Australian Plate. Geological Society of Australia Special Publication 22 and Geological Society of America Special paper 372.
- Hillis, R.R., and S.D.Reynolds, 2003, In situ stress field of Australia. Geological Society of Australia Special Publication 22 and Geological Society of America Special paper 372, 49-58.
- Hoffman, P., 1991, Did the breakout of Laurentia turn Gondwanaland inside-out? *Science*, 252, 1409-1412.
- Hornby, P., F.Boschetti, and F.G.Horowitz, 1999, Analysis of potential field data in the wavelet domain. *Geophysical Journal International*, 137(1), 175-196.

Hornby, P., F.G.Horowitz, and F.Boschetti, 2002, A physical interpretation of the Poisson wavelet transform of potential fields. In *Proceedings, EGS XXVII General Assembly*. European Geophysical Society.

Holden, D.J, N.J.Archibald, F.Boschetti, and M.W.Jessell, 2000, Inferring geological structures using wavelet-based multiscale edge analysis and forward models. *Exploration Geophysics*, 31, 617 – 621.

Isles, D., and I.Moody, 2004a, Falcon airborne gravity gradiometry – resolution and ground gravity comparisons. In AIG seminar “Leading edge geophysical technologies for mineral exploration geologists”, Perth, 6 September 2004.

Isles, D., and I.Moody, 2004b, Examples of Falcon data from diamond exploration projects in Northern Australia. In *Geoscience Australia Record 2004/18 Airborne Gravity*, 2004, 121 – 124.

Janse, A.J.A., 1985, Kimberlites – where and when, in Glover and Harris (ed), *Kimberlite Occurrence and Origin*, Published jointly by The Geology Department and University Extension, The University of Western Australia, Publication No 8, 19-61.

Janse, A.J.A., 1991, Is Clifford’s rule still valid? Affirmative examples from around the world. *Proceedings of the fifth international Kimberlite Conference*, 2, 215-235.

Jaques, A.L, J.D.Lewis, C.B.Smith, G.P.Gregory, J.Ferguson, B.W.Chappell, and M.T.McCulloch, 1984, The diamond bearing ultrapotassic lamproitic rocks of the West Kimberley region, Western Australia, in *Kimberlites 1: Kimberlites and related rocks*, edited by J.Kornprobst, Elsevier, 225-254.

Jaques, A.L, J.D. Lewis, and C.B. Smith, 1986, *The Kimberlites and Lamproites of Western Australia*. Bulletin 132, Geological Survey of Western Australia.

Jaques, A.L., 1998, Kimberlites and Lamproite diamond pipes. *Australian Geological Survey Organisation Journal of Australian Geology and Geophysics* 17(4), 153-162.

Jaques, A.L., 1994, Diamonds in Australia, in *The Geology and Origin of Australia’s Mineral Deposits*, ed M.Solomon and D.I.Groves, Oxford Science Publications, 787-820.

Jaques, A.L., and P.R.Milligan, 2004, Patterns and controls on the distribution of diamondiferous intrusions in Australia, *Lithos*, 77, 783-802.

Jaques, A.L., 2006a, Australian Diamond Exploration 2006: Where are the Greenfields?: presentation at World Diamond Conference, Perth, 2006.

Jaques A.L., 2006b, Australian diamond deposits, kimberlites and related rocks. 1:5 million scale map. Geoscience Australia, Canberra.

- Jenke, G., and D.R.Cowan, 1994, Geophysical signature of the Ellendale lamproite pipes, Western Australia in Geophysical Signatures of Western Australian mineral deposits. Australian Society of Exploration Geophysicists Special Publication no 7, 403-414.
- Jennings, C.M.H., 1995, The exploration context for diamonds. *Journal of Geochemical Exploration*, 53, 113-124.
- Johnson, S.P., 2013, The birth of supercontinents and the Proterozoic assembly of Western Australia. Geological Survey of Western Australia. 78p
- Jones, A.G., and J.A Craven, 2004, Area selection for diamond exploration using deep-probing electromagnetic surveying. *Lithos*, 77, 765-782.
- Kamara, A.Y.S., 1981, Review: Geophysical methods for Kimberlite prospecting. *Bulletin of Australian Society of Exploration Geophysicists*, 12(3), 43-51, September 1981.
- Kaminsky, F.V., A.A.Feldman, V.A.Varlamov, A.N.Boyko, L.N.Olofinsky, I.L.Shofman, and V.I.Vaganov, 1995, Prognostication of primary diamond deposits. *Journal of Geochemical Exploration* 53, 167-182.
- Katsube, T.J., and N. Scromeda, 1994, Physical properties of Canadian Kimberlites, Somerset Island, North West Territories and Saskatchewan. In *Current Research, Part E*, Geological Survey of Canada, Paper 1E, 171-175.
- Katsube, T.J., and B.A.Kjarsgaard, 1996, Physical characteristics of Canadian Kimberlites: in *Searching for diamonds in Canada*. Geological Survey of Canada Open File 3228, edited by LeCheminant et al., 241-242.
- Kennett, B.L.N., 2003, Seismic structure in the mantle beneath Australia. Geological Society of Australia Special Publication 22 and Geological Society of America Special paper 372, 7-23.
- Kovesi, P. 1997 Symmetry and asymmetry from local phase. AI'97 Tenth Australian Joint Conference on Artificial Intelligence. 2-4 December 1997.
- LaFehr, T.R and M.N.Nabighian, 2012. *Fundamentals of Gravity Exploration*, Geophysical Monograph No 17, Society of Exploration Geophysics.
- LeCheminant, A.N., D.G.Richardson, R.N.W.DiLabio, and K.A.Richardson, editors, 1996, *Searching for Diamonds in Canada*. Geological Survey of Canada Open File 3228, 268p.
- Lee, J.B, D.B.Boggs, M.A.Downey, R.A.Maddever, R.J.Turner and M.H.Dransfield, 2007, First test survey results from the FALCON Helicopter-Borne Airborne Gravity System. Australian Society of Exploration Geophysicists, *Preview*, 126, 26-28.
- Lewis, J.R., 1990, Diatremes, chapter 5 in *Geology and Mineral Resources of Western Australia*. Geological Survey of WA Memoir 3, 567-589.

- Li, Z.X., S.V.Bogdanova, A.S.Collins, A.Davidson, B.de Waele, R.E.Ernst, I.C.W.Fitzsimons, R.A.Fuck, D.P.Gladkochub, J.Jacobs, K.E.Karlstrom, S.Lu, L.M.Natapov, V.Pease, S.A.Pisarevsky, K.Thrane, and V.Vernikovskiy. 2008. Assembly, configuration, and break-up history of Rodinia: A synthesis. *Precambrian Research* 160 (2008) 179-210.
- Lockwood, A.M., 2004, Western Australia: Isostatic Residual Gravity anomaly and depth to basement model. Geological Survey of WA Report 2004/14, 31p
- Macnae, J., 1979, Kimberlite geophysics for exploration. *Geophysics*, 44, 1395-1416.
- Macnae, J., 1995, Applications of geophysics for the detection and exploration of kimberlites and lamproites. *Journal of Geochemical Exploration*, 53, 213-243.
- McChesney, R., 1998, Geophysics and diamond exploration in the North Kimberley Province, WA. B.Sc Honours Geophysics thesis, Curtin University.
- McMonnies, B., 1993, Stockdale annual combined report for Forrest River tenements, unpublished report.
- Meixner, A.J. and P.J.Gunn, 1997, Three-dimensional kinematic modelling of the magnetic field of the Southern Joseph Bonaparte Gulf. *Exploration Geophysics*, 28, 160-264.
- Milligan, P.R., P.Lyons, and H.G.Direen, 2003a, Spatial and directional analysis of potential field gradients – new methods to help solve and display three-dimensional crustal architecture. Extended Abstract, Australian Society of Exploration Geophysics, Sixteenth Geophysical Conference and Exhibition, Adelaide.
- Milligan, P.R, P.Petkovic, and B.J.Dummond, 2003b, Potential field datasets for the Australian region: their significance in mapping basement architecture. Geological Society of Australia Special Publication.22 and Geological Society of America Special Paper 372 (2003), 129-139.
- Morgan, P., 1995, Diamond exploration from the bottom up; regional geophysical signatures of lithospheric conditions favourable for diamond exploration. *Journal of Geochemical Exploration*, 53, 143-165.
- Mitchell, R.H., 1975, Geology, Magnetic Expression, and Structural Control of the Central Somerset Island Kimberlites, *Canadian Journal of Earth Science*, 12, 757-764.
- Mitchell, R.H., 1986, page 30. Kimberlites: mineralogy, geochemistry and petrology. Plenum Press, New York.
- Morgan, P., 1995, Diamond exploration from the bottom up; regional geophysical signatures of lithospheric conditions favourable for diamond exploration. *Journal of Geochemical Exploration*, 53, 143-165.

Muggeridge, M.T., C.B.Smith, and J.P.Jenke, 1978, Report for the yearending 30 June 1978. Temporary Reserves 6573H-6577H, Kimberley Goldfield, Western Australia; CRA Exploration P/L Report 130030, (unpublished).

Nixon, P.H., 1973, Lesotho kimberlites: Maseru, Lesotho National Development Corporation.

O'Neill, C.J., L.Moresi, and A.L.Jaques, 2005, Geodynamic controls on diamond deposits: Implications for Australian occurrences. *Tectonophysics*, 404, 217-236.

Parasnis, D.S., 1997, *Principles of Applied Geophysics*, page 232. Chapman and Hall.

Pidgeon, R.T., C.B.Smith, and C.M.Fanning, 1989, Kimberlite and lamproite emplacement ages in Western Australia, in *Proceedings of the Fourth International Kimberlite Conference*, Perth, WA. Geological Society of Australia Special Publication 14, 369-381.

Pisarevski, S.A., M.T.D.Wingate, C.M.Powell, S.Johnson and D.A.D.Evans, 2003, Models of Rodinia assembly and fragmentation. In *Proterozoic East Gondwanaland: supercontinent assembly and breakup*. Geological Society of London Special publication 206, 35-55.

Plumb, K.A., 1979, The tectonic evolution of Australia. *Earth Science Reviews*, 14, 205-249.

Power, M., G.Belcourt, and E.Rockel, 2004, Geophysical methods for kimberlite exploration in northern Canada. *The Leading Edge* 2004, 23, 1124-1129.

Pretorius, D.A., 1979, The crustal architecture of Southern Africa, *Geological Society of South Africa*, 76, Appendix, 1-60.

Rajagopalan, S, J.Carlson and D.Wittuik, 2008 Kimberlite exploration using integrated geophysics. *Preview*, 132, 35-37.

Raiche, A., 2000, Choosing an AEM system to look for Kimberlites – a modelling study. Paper presented at Australian Society of Exploration Geophysicists Conference, 2000, in Perth.

Ramsay, R.R., D.Edwards, W.R.Taylor, N.M.S.Rock, and B.J.Griffin, 1994 Compositions of garnet and spinel from the Aries diamondiferous kimberlite pipe, central Kimberley Block, Western Australia – implications for exploration. *Journal of Geochemical Exploration* 51 (1994), 59-78.

Ramsay, R.R, 1997 personal communication

Ramsay, R.R., 2000, Masters course notes at UWA.

Reddicliffe, T.H, J. Jacimowicz, A.J.Hell, and J.A.Robins, 2003, The geology, mineralogy and near surface characteristics of the Ashmore and Seppelt kimberlite clusters, North Kimberley, Extended Abstracts of the Eighth International Kimberlite Conference, Victoria, British Columbia, Canada.

Reed, L.E., and K.E.Witherly, 2007, 50 years of Kimberlite Geophysics, a Review in Proceedings of Exploration 07: Fifth Decennial International Conference on Mineral Exploration, 670-689.

Register of Australian Mining 2013/14. Resource Information Unit, Perth Western Australia

Reid, A.B., J.M.Allsop, H.Granser, A.J.Millett, and I.W.Somerton, 1990, Magnetic interpretation in three dimensions using Euler Deconvolution. Geophysics, 55(1), 80-91.

Reid, A.B. 1997 Euler deconvolution, Past, Present and Future: A Review in proceedings of Exploration 97: Fourth Decennial International Conference on Mineral Exploration, 861-864.

Roest, W.R, J.Verhoef and M.Pilkington, 1992. Magnetic interpretation using the 3-D Analytic Signal. Geophysics 57(6), 116 – 125.

Ruddock, I., 2003, Mineral occurrences and exploration potential of the North Kimberley. Geological Survey of Western Australia Report 85.

Sanders, T.S, 1999, Mineralization of the Halls Creek Orogen East Kimberley region Western Australia Geological Survey of WA Report 66, 44p.

Schissel, D and R.Smail, 2001. Deep-mantle plumes and ore deposits. In Mantle Plumes: Their Identification Through Time. Geological Society of America Special Paper 352.

Shaw, R.D., P.Wellman, P.Gunn, A.J.Whitaker, C.Tarlowski, and M.Morse, 1996, Guide to using the Australian Crustal Elements Map. Australian Geological Survey Organisation Record 1996/30.

Shaw, R.D., T.J.Meixner, and A.S.Murray, 2000, Regional geophysical setting and tectonic implications of the multi-ultramafic intrusions in Hoatson, D.M., and D.H.Blake (eds) Geology and economic potential of the Paleoproterozoic layered mafic-ultramafic intrusions in the East Kimberley, Western Australia, Australian Geological Survey Organisation Bulletin, 246, 63-98.

Shaw, W.J., M.Kelly, A.C.Moore, and S.Chapman, 1985, Pteropus Creek area, east Kimberley Region, WA, annual report to 25 Jan 1985, exploration licences E80/102 and E80/103: BHP Minerals Division (unpublished).

Simons, F.J, A.Zielhuis, and R.D.Van der Hilst, 1999, The deep structure of the Australian continent from surface wave tomography. Lithos 48, 17-43.

- Skinner, E.M.W., and C.R.Clement, 1979, Mineralogical classification of southern African kimberlites in Kimberlites', diatremes and diamonds: Their geology, petrology and geochemistry, edited by F.R.Boyd and H.O.A.Meyer. American Geophysical Union, 129-139.
- Smith, C.B., 1984, The genesis of the diamond deposits of the West Kimberley, WA, in The Canning Basin WA edited by P.G.Purcell: Geological Society of Australia and Petroleum Exploration Society of Australia; Canning Basin Symposium, Perth, WA, Proceedings, 463-473.
- Smith, T.W., and B.J.McClenaghan, 1994, Stockdale annual combined report for Forrest River tenements, unpublished report.
- Snyder, D.B, S.Rondenay, M.G.Bostock, and G.D.Lockhart, 2004, Mapping the mantle lithosphere for diamond potential using teleseismic methods. Lithos 77, 859-872.
- Spratt,J., M.C.Dentith, S.Evans, A.R.A,Aitken, M.Lindsay, J.A.Hollis, I.M.Tyler, A.Joly, and J.Shragge, 2014. A magnetotelluric survey across the Kimberley Craton, northern Western Australia.. Geological Survey of Western Australia Report 136.
- Sumner, J., 1997, Exploration geophysics in the North Kimberley Kimberlite province of Western Australia. B.Sc Honours Geophysics thesis, Curtin University.
- Sumpton, J.D.H., and T.W.Smith, 1997, Discovery of Kimberlite pipes in the Forrest River area, Kimberley region, Western Australia. 1049 - 1052 in Proceedings of Exploration 97: Fourth Decennial International Conference on Mineral Exploration, edited by A.G.Gubins.
- Thompson, D.T. 1982 Euldph: A new technique for making computer-assisted depth estimates from magnetic data. Geophysics 47(1) 31-37.
- Towie, N.J., M.D.Bush, E.R.Manning, M.R.Marx, and R.R.Ramsay, 1994, The Aries diamondiferous kimberlite pipe, Central Kimberley Region, Western Australia; Exploration, setting and evaluation. Proceedings of the Fifth International Kimberlite Conference, 2, 319-328.
- Van der Hilst, R.D., B.Kennett, D.Christie, and J.Grant, 1994, Project Skippy explores the mantle and lithosphere beneath Australia. EOS 75, 177-181.
- Wellman, P, 1972 Early Miocene potassium-argon age for the Fitzroy lamproites of Western Australia. Geological Society of Australia Journal, 19, 471-474.
- White, S.H., H. de Boorder, and C.B.Smith, 1995, Structural controls of kimberlite and lamproite emplacement. Journal of Geochemical Exploration, 53, 245-264.

Wilkes, P.G., 1968, The construction and operation of an EM prospecting instrument using natural and artificial magnetic fields in the audio frequency region. MSc thesis (unpublished) Imperial College, London.

Wingate, M.T.D, S.A.Pisarevsky, and D.A.D.Evans 2002. A revised Rodinia supercontinent, no SWEAT, no AUSWUS. *Terra Novus* 14, 121-128.

Every reasonable effort has been made to acknowledge the owners of copyright material. I would be pleased to hear from any copyright owner who has been omitted or incorrectly acknowledged.

**APPENDIX: PAPER SUBMITTED TO GEOPHYSICAL  
RESEARCH LETTERS**

***DEEP CRUSTAL GEOMETRY AND DIAMOND BEARING PIPES IN  
THE KIMBERLEY REGION OF WESTERN AUSTRALIA***

Paul Wilkes<sup>1,2</sup>,

<sup>1</sup>Curtin University and <sup>2</sup>CSIRO

**Submitted to: *Geophysical Research Letters***

Corresponding author: Paul.Wilkes@csiro.au

Current address: CSIRO, P.O Box 1130, Bentley WA 6102, Perth, Australia

Keywords: Mohorovičić Discontinuity, Moho, Gravity, Diamonds,  
Kimberlite pipes, Lamproite pipes, Magnetic fields, “Super-plumes”,  
Supercontinents, Rodinia

## **Abstract**

Structural control is important in identifying potential sites for the intrusion of kimberlite and lamproite pipes that may or may not contain diamonds. This paper presents some new results on the geometry of the Mohorovičić Discontinuity (hereon referred to as the Moho) in the Kimberley region of Western Australia and the use of gravity and aeromagnetic data in diamond exploration in this region. The Moho geometry results show major structures controlling the Moho surface and the location of kimberlite and lamproite pipes are shown to be related to these structures.

Some of the pipes in the Kimberley region have been dated between 800 and 820 Ma and this is now known to be close to the timing of superplume activity that peaked at 780, 800 and 825 Ma. Reconstructions of Rodinia (Li et al, 2008) show major continental movement and rifting at these times. These age and structural relationships are important in the localisation of kimberlite and lamproite pipes.

## **1. Introduction**

Diamond exploration uses multiple datasets and multiple lines of investigation. Gravity, magnetic, shuttle radar (SRTM) and Moho geometry data are used to illustrate how these have been used in diamond exploration in the Kimberley region of Western Australia. Many lamproite and kimberlite pipes have been discovered in the Kimberley region. The most productive of these discoveries is the Argyle deposit on the eastern edge of the Kimberleys. The only other diamond commercial diamond production has come from Ellendale. Production at Argyle and Ellendale are from lamproite pipes. Diamonds have also been found in kimberlite pipes but not yet in sufficient quantities and qualities to be commercially viable. e.g. at the Aries, Ashmore, Pteropus and

Seppelt prospects. Other diamond bearing pipes have been discovered in the Ellendale area and also in the Northern Kimberley close to Ashmore and Seppelt. Pipes close to Ellendale 4 are included in Figure 1. Pipes close to Ashmore and Seppelt are too close to these pipes to be included in this Figure.

Diamond exploration in the Kimberley region of Western Australia has made extensive use of geochemistry and geophysics. Pipes are often magnetic due to their magnetite content and this has led to aeromagnetic surveys being a primary exploration method. Pipes have higher densities than the country rocks but often weather to clays in the top part of the pipes. These clays have low densities (typically less than 2.0 g/cc) and gravity surveys over the pipes usually show gravity lows as the low gravity effect of the clays more than cancel out the gravity highs that result from the unweathered high density parts of the pipes. The clays are also often conductive and this makes them suitable targets for airborne and ground electromagnetic surveying.

Regional aeromagnetic and ground gravity datasets have been used to look for major linear structures which may indicate deep structures suitable for pipe emplacement. Regional aeromagnetic and gravity datasets, from Geoscience Australia, have been used in this way. Free-air gravity data have also been used by Aitken (2010) to help compute the Moho boundary between crust and mantle. This is described in more detail in the methodology section.

## **2. Methodology and results**

Six diamond bearing pipes have been selected for this study. Key parameters are listed in the following table.

Table 1 – Summary results for individual study areas

<b>Pipe</b>	<b>Location MGA zone 52</b>	<b>Surface elevation metres ASL</b>	<b>Moho depth in km</b>	<b>Geophysical response</b>	<b>Comments</b>
Argyle	434450 E  8152080 N	260	43.1	Subtle. About 5 nT in helimag data.. Small ground EM response.	Lamproite host.  Major international producer.
Aries	194300 E  8129600 N	436	40.0	Bouguer gravity less than -0.1 mGal. Small aeromagnetic anomaly.	Kimberlite host. Non- commercial.
Ashmore 1	315800 E  8425650 N	190	34.7	Pipe detected by ground EM, gravity and magnetic responses.	Kimberlite host. Non- commercial.
Ellendale 4	67490 E  8042070 N	163	33.7	Aeromagnetic response clear but less than 10 nT. Small ground gravity response.	Lamproite host.  Some production.

<b>Pipe</b>	<b>Location</b> <b>MGA</b> <b>zone 52</b>	<b>Surface</b> <b>elevation</b> <b>metres</b> <b>ASL</b>	<b>Moho</b> <b>depth</b> <b>in km</b>	<b>Geophysical</b> <b>response</b>	<b>Comments</b>
Pteropus 2	331000E  8382200 N	152	35.1	-1.6 mGal residual ground gravity response.	Kimberlite host.  Non- commercial.
Seppelt 1	325915 E  8403600 N	210	34.8	Defined by aeromagnetic, and ground EM, gravity and magnetic responses	Kimberlite host.  Non- commercial.

### **Geometry of the Mohorovičić Discontinuity**

Aitken (2010) modelled the Moho geometry using inversion of Free-air gravity data and seismic constraints for the Australian continent. Free-air gravity for the onshore and offshore Kimberley region are shown in Figure 1. The Aitken model consists of six layers: ocean, sedimentary basins, upper crust, lower crust, eclogitised crust and mantle. The Australian continental model covers 4695 x 3825 km with 15 x 15 km vertical prisms extending down to 99 km. Aitken computed the initial Moho surface by Delaunay triangulation using 230 estimates of crustal thickness derived from seismic reflection and refraction data (Collins, 1991) and used this to constrain three-dimensional gravity inversion used VPmg software (Fullagar et al, 2008). This uses density optimisation and geometry optimisation independently. Further detail on

variations in Moho depth across Australia as computed from seismic studies are provided by Kennett et al (2011).

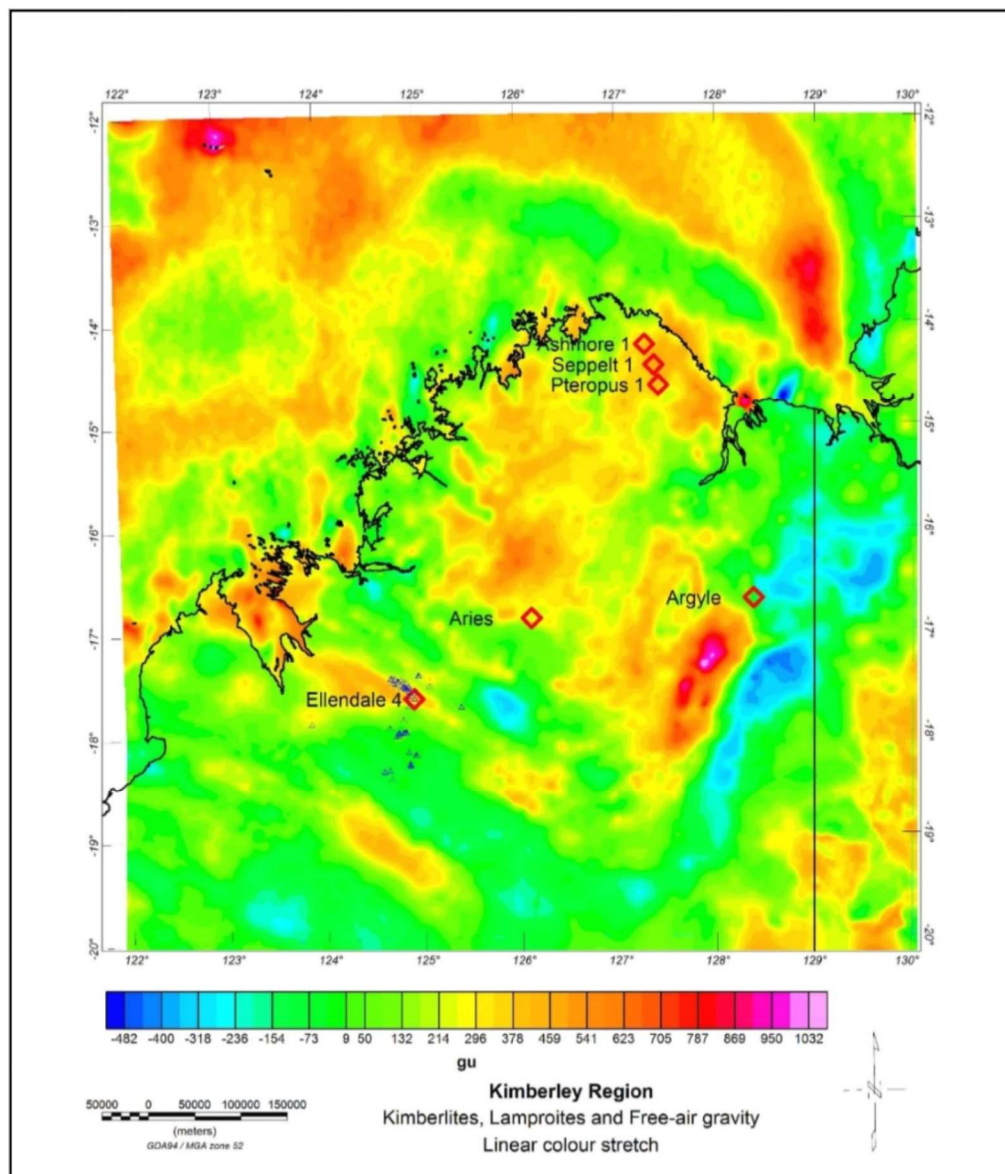


Figure 1: Kimberlites, lamproites and Free-air gravity. Red diamonds show locations of Argyle, Aries, Ashmore, Ellendale 4, Pteropus and Seppelt pipes. Other pipes in the Ellendale area are shown with small blue triangles. Free-air gravity has been computed with a 2 km grid mesh onshore and 907 metre mesh offshore. The onshore gravity station coverage is shown in Figure 2. There are clear correlations between the Free-air gravity and the Moho geometry which is shown in Figures 3 and 4. The diamond occurrences are located close to marked gradients in the Free-air gravity.

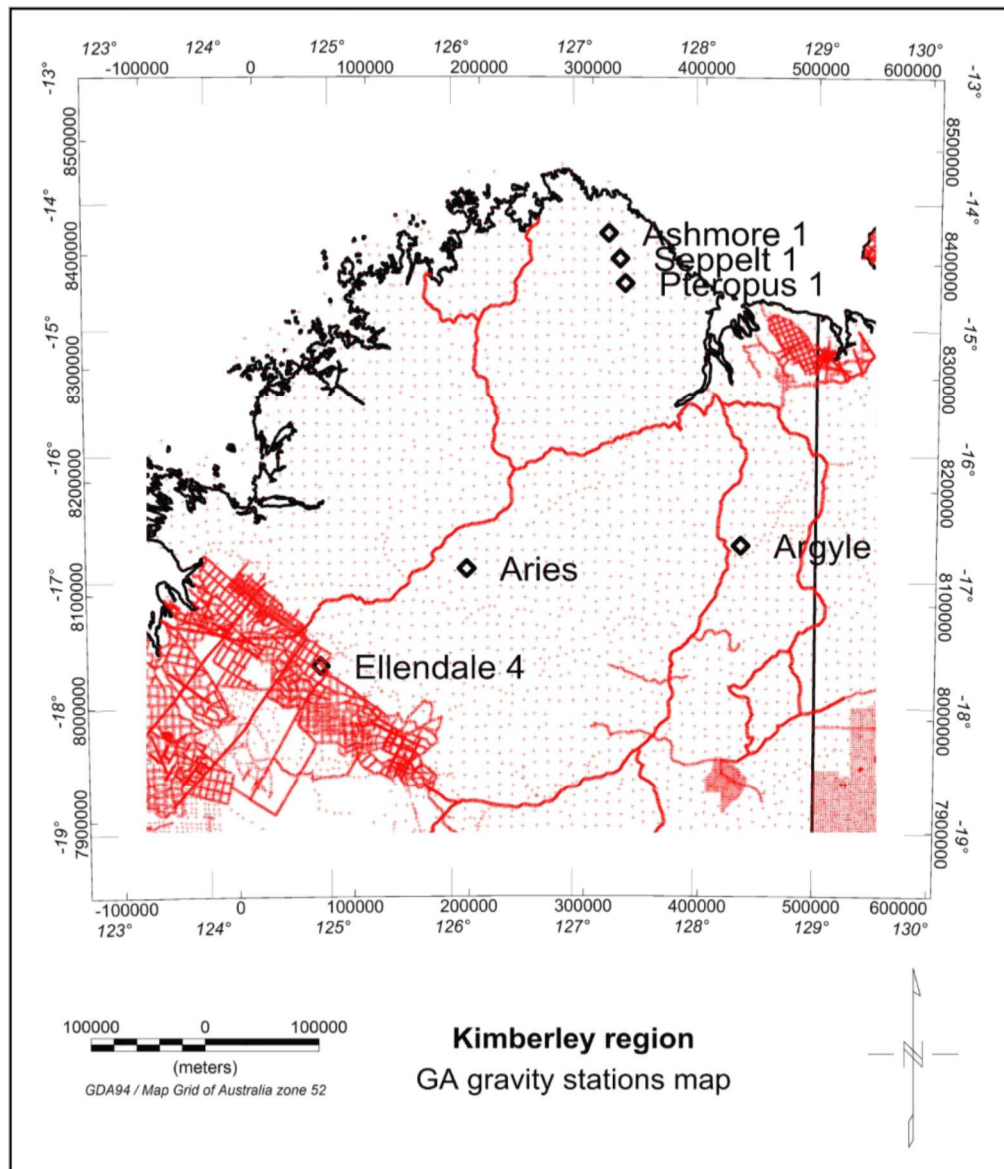


Figure 2. Geoscience Australia gravity stations map for Kimberley region. Regional coverage is 11 x 11 km supplemented by road traverses with 400 metre station spacing and more detailed traverses with approximately 800 metre spacing in the Ellendale 4 area.

For this study a subset of 3412 data points with 15 x 15 km spacing from the Aitken inversion, was extracted to cover the Kimberley region and surrounding onshore and offshore areas. This subset was further processed using Geosoft Oasis Montaj and ARC/GIS software packages. Pipes occur at significant locations relative to the Moho surface in the Kimberley region of Western Australia.

### **Processing of potential field data**

Aeromagnetic, digital terrain and gravity data for the Kimberley area have been processed and interpreted to define geological structures that may be important in recognising suitable locations for the emplacement of kimberlite and lamproite pipes. Processing of the potential field data has included Euler deconvolution and multiscale edge detection to assist in defining structural trends. This provides more detailed information on geological structures which may be important for pipe emplacement.

### **Ages of pipes and continental breakups**

Diamond bearing pipes in the Kimberley region have been dated with a wide range of ages :

Argyle at about 1178 Ma (Pidgeon et al, 1989)

Aries at about 820 Ma (Towie et al, 1991)

Ashmore at about 800 Ma (unpublished)

Ellendale at about 20 - 22 Ma (Wellman, 1972),

Pteropus 1 and 2 at about 805 Ma (Pidgeon et al, 1989)

Seppelt at about 800 Ma (unpublished)

It is significant that these ages of these pipes are close to the timing of continental breakups and also the occurrence of super plumes at about 780, 800 and 825 Ma (Li et al, 2008)..

### **3. Results**

Moho depths in the study area range from -47.9 km to -15.9 km with a mean value of -33.8 km, relative to sea level. The shallowest depths are in the northern offshore part of the study area. Figure 2 shows depth to Moho as an

image with contours superimposed and the locations of the six pipes used in this study.

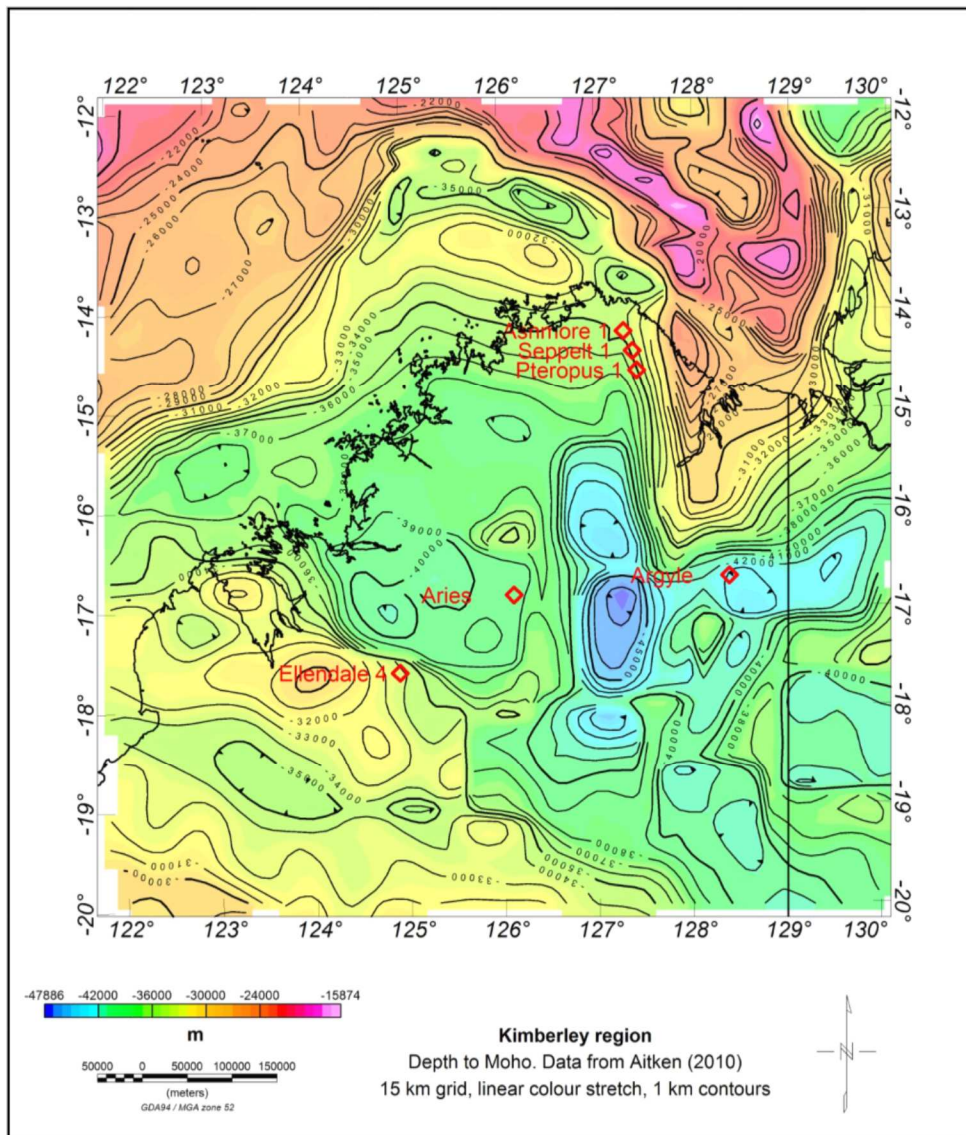


Figure 3: Image and contours of the Moho surface. This shows the locations of the Argyle, Aries, Ashmore, Ellendale 4, Pteropus and Seppelt pipes used in this study. The pipes occur close to marked gradients in the Moho surface.

Figure 4 shows a 3-dimensional view of the Moho surface together with topographic and coastline data and also shows the locations of six diamond

bearing pipes. This figure shows that all these pipes are located close to major extended gradients in the Moho surface.

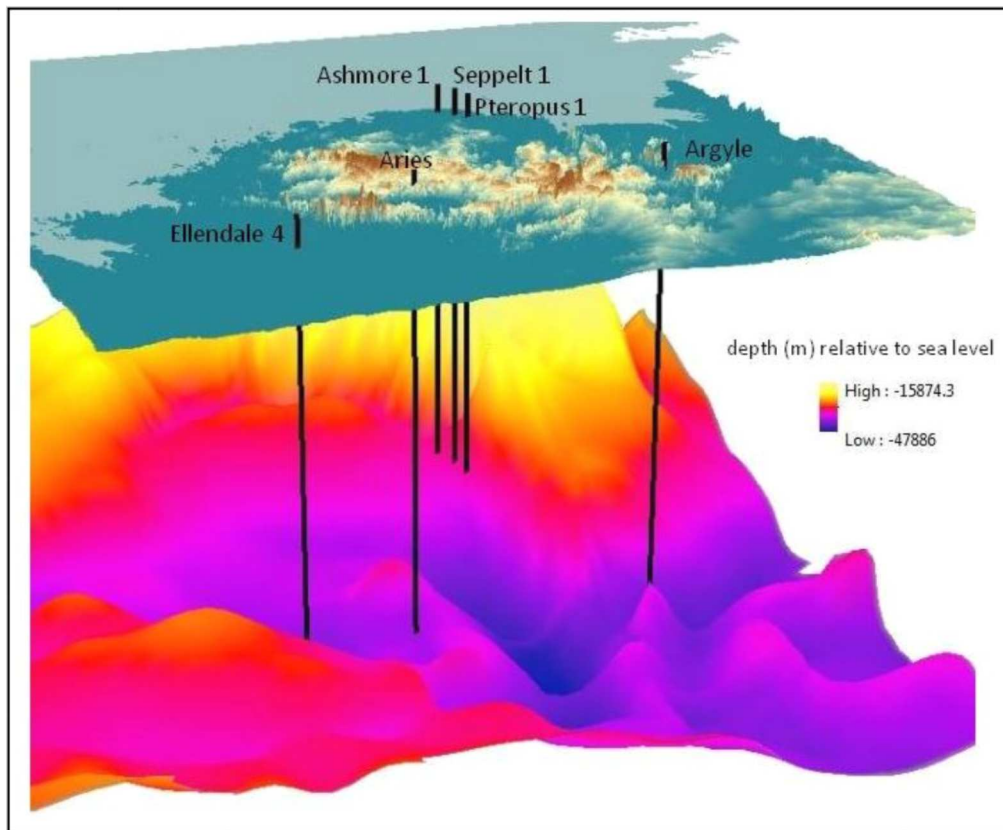


Figure 4: 3D view of Moho surface looking from the south. Top surface is digital elevation data from Shuttle Radar Topographic Mission (SRTM) data. The six vertical black lines shows the locations of the Argyle, Aries, Ashmore, Ellendale 4, Pteropus and Seppelt pipes projected vertically down from known positions at surface. Moho depth scale is in metres relative to sea level. Vertical exaggeration is 10:1.

A summary of key observations along with interpretations and caveats are provided in the following table 2.

**Table 2. Key observations related to “deep” features and Pipe locations**

<b>Key observation</b>	<b>Interpretation and caveats</b>
1. The Moho geometry is interpreted from geophysical data.	Moho geometry is derived from inversion of regional Free-air gravity data. Seismic control is used where available to reduce ambiguity in the derived results.
2. Pipes are located close to marked gradients in the Moho.	All six pipes studied here are located adjacent to marked gradients in the Free-air gravity and Moho surface. See Figures 1 ,3 and 4.
3. Temporal relationships between age of pipes and continental movements and superplumes..	The ages of emplacement of the pipes are close to ages of continental breakup and of superplume activity. This is not true for the Ellendale pipes (20 – 22 Ma).
4. Relationships between location and topographic settings.	The pipes studied in this work occur in a variety of topographic settings. Aries has a local topographic depression associated with that pipe. The other pipes studied in this project occur in gentle terrain or near hills.  Some structural control is seen in topography.

#### 4. Discussion and Conclusions

Table 2 summarises some key observations about the locations of kimberlite and lamproite pipes in relation to geometry of the Moho and age of emplacement relative to significant geological events – Superplume activity and continental breakup. The locations of pipes close to major gradients in the Moho surface and in the Free-air gravity provides a guide as to where further pipes may be found. More localised geological structures can be found using detailed aeromagnetic and gravity surveys.

#### References

- Aitken, A.R.A., 2010. Moho geometry gravity inversion experiment (MoGGIE): a refined model of the Australian Moho, and its tectonic and isostatic implications. *Earth and Planetary Science Letters*, 297, 71-83.
- Collins, C.D.N., 1991. The nature of the crust-mantle boundary under Australia from seismic evidence. In Drummond, B.J. (ed) *The Australian Lithosphere*. Geological Society of Australia Special Publication p 67-80.
- Fullagar, P.K., G.A.Pears and B.McMonnies, 2008. Constrained inversion of geologic surfaces – pushing the boundaries. *Leading Edge (Society of Exploration Geophysicists)*, 27(1) 98-105.
- Hassan, L.Y. 2004, Mineral occurrences and exploration potential of the West Kimberley. Geological Survey of WA Report 88.
- Kennett, B.L.N., M.Salmon, E.Saygin, and AusMoho Working Group, 2011, AusMoho: The variation of Moho depth in Australia. *Geophysical Journal International*, 187 (2), 946-958.
- Li, Z.X., S.V.Bogdanova, A.S.Collins, A.Davidson, B.de Waele, R.E.Ernst, I.C.W.Fitzsimons, R.A.Fuck, D.P.Gladkochub, J.Jacobs, K.E.Karlstrom, S.Lu, L.M.Natapov, V.Pease, S.A.Pisarevsky, K.Thrane, and V.Vernikovskiy. 2008. Assembly, configuration, and break-up history of Rodinia: A synthesis. *Precambrian Research* 160 (2008), 179-210.

Pidgeon, R.T., C.B.Smith, and C.M.Fanning, 1989. Kimberlite and lamproite emplacement ages in Western Australia. in Proceedings of the Fourth International Kimberlite Conference, Perth, WA. Geological Society of Australia Special Publication 14, 369-381.

Wellman, P, 1972. Early Miocene potassium-argon age for the Fitzroy lamproites of Western Australia. Geological Society of Australia Journal, 19, 471-474.